UNIVERSITY OF SOUTHAMPTON

FACULTY OF ENGINEERING AND THE ENVIRONMENT

INSTITUTE OF SOUND AND VIBRATION RESEARCH

COCHLEAR IMPLANT MODELLING: STIMULATION AND POWER CONSUMPTION

BY

RAMI SABA

THESIS FOR THE DEGREE OF DOCTOR OF PHILOSOPHY

NOVEMBER 2012

Como, Italy. 200 years ago

"At the moment when the circuit was completed, I received a shock in the head, and some moments after I began to hear a sound, or rather noise in the ears, which I cannot well define: it was kind of crackling with shocks, as if some paste or tenacious matter had been boiling... The disagreeable sensation, which I believe might be dangerous because of the shock in the brain, prevented me from repeating this experiment."

Volta, A (1800)

Alessandro Volta, inventor of the battery, describing his observation during an experiment where he placed one of the two ends of a 50-volt battery in each ear. Brilliant.

I suppose it had to start somewhere...

UNIVERSITY OF SOUTHAMPTON

ABSTRACT

FACULTY OF ENGINEERING AND THE ENVIRONMENT

INSTITUTE OF SOUND AND VIBRATION RESEARCH

Doctor of Philosophy

COCHLEAR IMPLANT MODELLING: STIMULATION AND POWER CONSUMPTION

By Rami Saba

Cochlear implants have been shown to successfully restore hearing to the profoundly deaf. Despite this achievement, issues remain concerning the power consumption and the accuracy of stimulation. This thesis is mainly concerned with investigating the spread of stimulation voltage within the cochlea. The power required to generate the stimulus is also investigated, as is the feasibility of powering a fully implanted cochlear implant by harvesting energy from head motion.

Several different models have been used to study the voltage distribution within the cochlea due to electrical stimulation from individual electrodes of a cochlear implant. A resistive cable model is first used to illustrate the fall-off of the voltage with distance at the electrode positions along the cochlea. A three-dimensional finite element model of the cochlea is then developed to obtain the voltage distribution at positions closer to the site of neural stimulation. This model is used to demonstrate the way that the voltage distribution varies with the geometry of the cochlea and the electrode array. It was found that placing the return electrode of the implant within the modiolus, as opposed to outside the cochlea, resulted in higher stimulation for the same current input, which reduces the power requirements.

The model has also been used to investigate the consequences of a current-steering, or stimulation focussing, strategy that has previously been proposed. A generalisation of this strategy is suggested, whereby impedance information at the neural level, along the path of the spiral ganglion, was used to optimise the focussed voltage distribution at the target neurons.

The power consumption of various stimulation strategies is then estimated in order to assess their energy efficiency. Strategies are defined by parameters such as stimulation rate and number of active channels. The feasibility has also been investigated of harvesting electrical energy from head motion, to power a fully-implanted cochlear implant. It was demonstrated that more power could be harvested from higher harmonics but that this would be sensitive to walking speed. The practical approach is to have a heavily damped device that is insensitive to walking speed and is able to respond to all frequencies in head motion.

Contents

List of Figures

List of tables

Academic Thesis: Declaration Of Authorship

I, Rami Saba, declare that this thesis and the work presented in it are my own and has been generated by me as the result of my own original research.

COCHLEAR IMPLANT MODELLING: STIMULATION AND POWER CONSUMPTION

I confirm that:

1. This work was done wholly or mainly while in candidature for a research degree at this University;
2. Where any part of this thesis has previously been submitted for a degree or any other qualification at this University or any other institution, this has been clearly stated;
3. Where I have consulted the published work of others, this is always clearly attributed;
4. Where I have quoted from the work of others, the source is always given. With the exception of such quotations, this thesis is entirely my own work;
5. I have acknowledged all main sources of help;
6. Where the thesis is based on work done by myself jointly with others, I have made clear exactly what was done by others and what I have contributed myself;
7. Either none of this work has been published before submission, or parts of this work have been published as:

Elliott, S.J., Saba, R. and Baumann, O.N. (2008) Vibration power harvesting from head motion [E192]. In, Brennan, M.J. (ed.) *Proceedings of EURODYN 2008, 7th European Conference on Structural Dynamics, Southampton, UK, 7- 9th July 2008.* , University of Southampton, 12pp.

Ni, G., Elliott, S. J., Lineton, B. and Saba, R. (2011) Finite element modelling of fluid coupling in the coiled cochlea. In Shera, C.A. and Olson, E.S., editors, *What Fire is in Mine Ears: Progress in Auditory Biomechanics*, pp 350-355. (DOI: 10.1063/1.3658164)

Saba, R., Elliott, S.J., Baumann, O.N., 'Vibration power harvesting from head motion', 2012. TM 998, ISVR, University of Southampton.

Signed: ……..

Date: ……..

Acknowledgements

No one said it would be easy, but the guidance of a number of colleagues and staff has been invaluable in the progress of this thesis. First and foremost, one person was there from the first day, conducting my interview for the undergraduate course, right up to the concluding day of my education, the viva. Professor Stephen J. Elliott was my personal tutor, supervisor and mentor and has been the most influential person throughout the years. I would like to thank both Professor Elliott and Dr Shouyan Wang for their invaluable supervision, support and advice throughout the PhD, both at an academic and personal level. I extend my profound gratitude to a number of staff members that have been supportive and critical of my work, including Dr. David Simpson, Dr. Gary Farrell, Prof. Paul White, Dr. Oliver Baumann, Dr. Stefan Bleeck, Prof. Mark Lutman, Dr Carl Verschuur, Dr Rachel van Besoux, ISVR technicians, SOECIC and Cochlear.

I have been lucky to have embarked on this PhD alongside many great colleagues, whom I would like to thank for their friendship, support, motivation and for making the journey rewarding and exciting. Thanks to my office colleagues for making it an enjoyable place to work. I would especially like to thank Guangjian Ni, Kiran Konde, Tony McDonald, Dr. Cristobal G. Diaz, Hessam Alavi, Andrew Causon, Dr. Niamh O'Meara, Laurence Wilmshurst, Guido Zarini, Vinay Thanki, Hector Georgiou and others in Southampton and around the world for their encouragement and support.

Finally, and more notably, I would like to thank my parents, Manolly and Hana, my siblings, Dimitri and Dima, as well as the rest of my family, in particularly, Dolly Audeh, Gebran Karam and Maro Karam Sabe. A PhD has its highs and lows, a rollercoaster of failure and triumph, throughout which my family stood by me. Their love and unconditional support holds the responsibility for developing the person I am today, and I dedicate this thesis to all of them.

List of Acronyms

3D	Three Dimensional
BKB	Bamford-Kowall-Bench
BM	Basilar Membrane
CI	Cochlear Implant
CID	Central Institute for the Deaf
CIS	Continuous Interleaved Sampling
CNC	Consonant-Nucleus-Consonant
CSR	Channel Stimulation Rate
EAS	Electro-Acoustic Stimulation
FFT	Fast Fourier Transform
FIR	Finite Impulse Response
FS	Fine Structure
FSP	Fine Structure Processing
FTM	Frequency-Time Matrix
LGF	Loudness Growth Function
MP	Mono-Polar
NF	Neural Focussing
NMT	Nucleus Matlab Toolbox
OoC	Organ of Corti
RM	Reissner's Membrane
SM	Scala Media
SPeak	Spectral Peak
ST	Scala Tympani
SV	Scala Vestibuli
TSR	Total Stimulation Rate
VN	Vestibular Nerve

Symbols

∇	Vector spatial derivative operator
J	Current density in the medium
Q_j	Current density of the source
σ	Electrical conductivity of the material (S/m)
v	Voltage (Volts)
i	Current (Amperes)
R	Impedance (Ω)
$\boldsymbol{R}$	Impedance matrix
E	Electric field (V/m)
R_1	Impedance between electrodes (Ω)
R_2	Impedance between the electrode and fluid (Ω)
G_1	Conductance, Reciprocal of R_1 (1/Ω)
$\boldsymbol{G}$	Conductance matrix
$\mathbf{v}$	Vector of voltages of the electrode positions
$\mathbf{Z}$	Square impedance matrix along the electrode array
$\mathbf{Z}_N$	Non-square neural impedance matrix
$\boldsymbol{i}$	Vector of input currents to each electrode
i_{en}	Input current to each electrode
$\boldsymbol{i}_{en}$	Input current matrix
$\mathbf{v}_d$	Vector of desired voltages at the electrode positions
$\boldsymbol{i}_d$	Vector of desired input currents to each electrode
β	Regularisation coefficient
$\mathbf{I}$	Identity matrix

n	Position in resistance network in chapter 2 and appendix A, or Number of selected active electrodes in chapter 4
m	Electrode number in chapter 4 or mass (Kg) in chapter 5
a	Pulse number in channel
CSR	Channel stimulation rate (Hz)
TSR	Total stimulation rate (Hz)
T'	Individual period (s)
T	Total period (s)
CL	Current Levels
$c.u.$	Clinical units
$\overline{P}_m$	Average power per channel (Watts)
E_T	Energy in each pulse (Joules)
a_T	Total number of potential pulses in a specified channel
b_T	Total number of potential pulses in the entire sequence
$\overline{P}_{av}$	Average total power in a sentence (Watts)
t_{tot}	Total time of the sentence (s)
τ	Phase width (s)
T	Threshold level (CL)
C	Comfort level (CL)
l	Length (m)
s	Dimensionless shape factor
ω_d	Angular frequency (radians)
A	Peak displacement of sinusoidal input motion (m)
B	Peak displacement of inertial mass (m)
m	Mass (Kg)
c	Damping (Kg/s)
W	Power dissipated (Watts)
k	Stiffness (N/m)
j	Imaginary unit
I	Moment of inertia (Kg m^2)

ρ	Density (Kg/m^3)
θ	Angular displacement (radians)
ζ	Damping ratio
f	Force (Kg m/s^2)
u	Velocity (m/s)
Z_M	Mechanical impedance
Z_E	Electrical impedance
$T_{1,2}$	Transduction coefficients
B	Magnetic flux density (Wb)
L	Length of wire in the coil (m)
W_H	Power harvested
W_S	Mechanical power supplied
R_L	Load resistor
Re	Real part
e	Efficiency of the harvesting device
F	Non-dimensional coupling factor
Δ	Peak throw of the inertial mass (m)
α	Angle (degrees)
r	Radius (m)
ρ	Resistivity (Ωm)
x	Forward and aft
y	Side to side
z	Vertical

Chapter 1

1 Introduction

The cochlea is one of the most intricate structures to be found in the human body. Its function is to bridge the gap between acoustic sound and the brain so that the brain can make sense of the acoustic environment. It does this by converting acoustic energy into electrical pulses, which are sent to the brain via the auditory nerve. There are several conditions, pathological or trauma, which result in damage to the cochlea and lead to hearing loss. Different conditions lead to different types of hearing loss and in mild cases an external hearing aid could be sufficient to restore some of the functionality of the auditory system. In cases where the damage is extreme and hearing loss is profound, a cochlear implant has been proven to restore hearing to a reasonable degree, provided that the auditory nerve is fully or substantially intact (Wilson and Dorman, 2006). A cochlear implant works by direct electrical stimulation of the auditory nerves. This thesis is concerned with investigating the voltage distribution within the cochlea due to this stimulation, estimating the power required to process an acoustic input and generate the stimulus, and investigating the feasibility of powering a fully implanted cochlear implant by harvesting energy from head motion. Chapter 1 introduces the anatomy and physiology of the ear, as well as the functionality of the cochlear implant. An outline is then presented of the research undertaken in the chapters that follow, together with a summary of the contributions of the thesis.

1.1 The Cochlea

1.1.1 Anatomy

The inner ear lies within the temporal bone, enclosed in the petrous portion. The outer portion is the mastoid portion, enclosing the outer ear (Clark et al., 1975). The outer ear and middle ear consist of the tympanic membrane and auditory ossiciles. The inner ear consists of the cochlea which has a typical length of 35 mm (Wilson and Dorman, 2008). The position of the cochlea is shown in Figure 1.1.

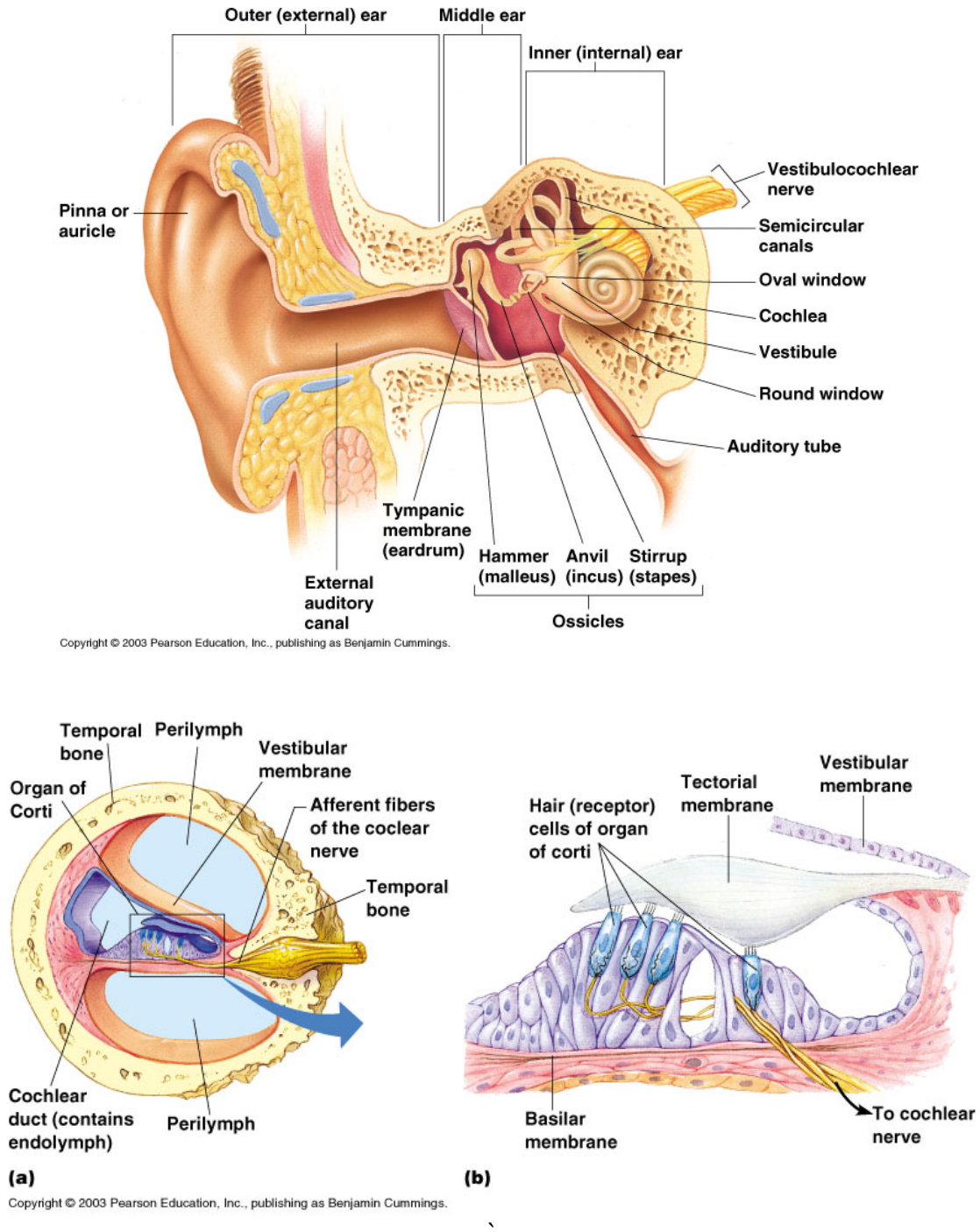

Figure 1.1: The cochlea (Marieb, 2008)

Inside the cochlea, Reissner's membrane and the basilar membrane (BM) separate the cochlear structure into three compartments; the scala tympani, scala media and scala vestibuli (Dallos et al., 1996). The scala media is filled with endolymph fluid and houses the organ of Corti, within which the inner and outer hair cells are found. The scala tympani and scala vestibuli are filled with perilymph fluid. Parts of the hair cells are also

bathed in perilymph. The hair cells along the basilar membrane in the cochlea are tonotopically organised, as illustrated in Figure 1.2. High frequencies activate hair cells near the base and low frequencies are perceived nearer to the apex of the basilar membrane. The perceivable range of frequencies is estimated to be within 20Hz to 20kHz (Everest, 2000).

The hair cells are responsible for generating electrical stimulation of the auditory nerve, which runs through the centre of the cochlea through the bony modiolus within which the spiral ganglion cells of the auditory nerves are found. The auditory nerve then delivers the stimulus to the cochlear nuclei, which is the first step in the auditory pathway. This leads to the higher auditory processing centres of the brain: the inferior colliculus, the medial genticulate nucleus and primary auditory cortex. The eighth cranial nerve houses the auditory and vestibular nerve (referred to as the cochleovestibular nerve in Rauschecker and Shannon (2002) and the lateral recess of the fourth ventricle of the brain is adjacent to the VCN. This system is shown in Figure 1.3.

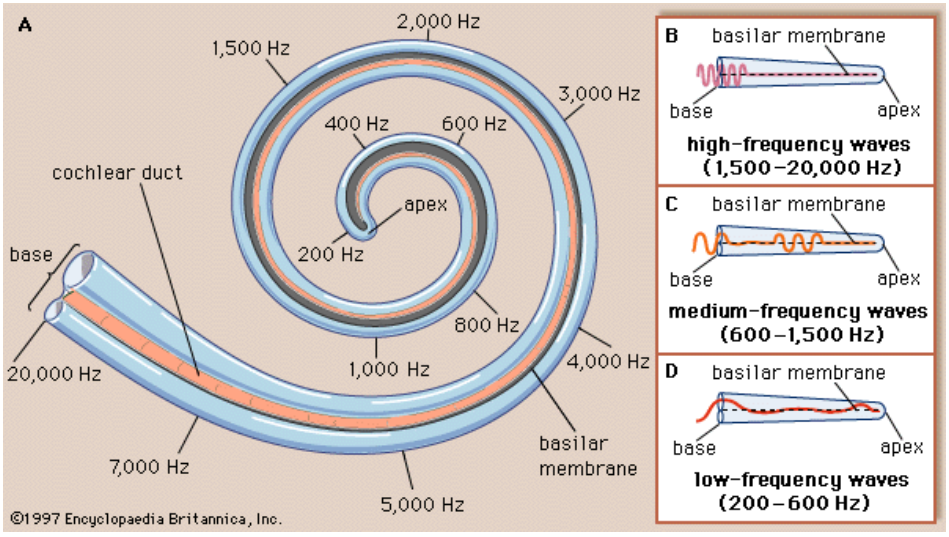

Figure 1.2: Tonotopically arranged basilar membrane (Encyclopaedia Britannica, 1997)

When hearing loss occurs, the auditory cortex is malleable and can recruit nearby neurons to form new neural connections. This is found to be far more efficient if started at an early age rather than at an older age, so that young children learn to use cochlear

implants very quickly. This is also true with music, the younger you learn the greater the sensitivity of the auditory cortex to complex sound (Zeng et al., 2004).

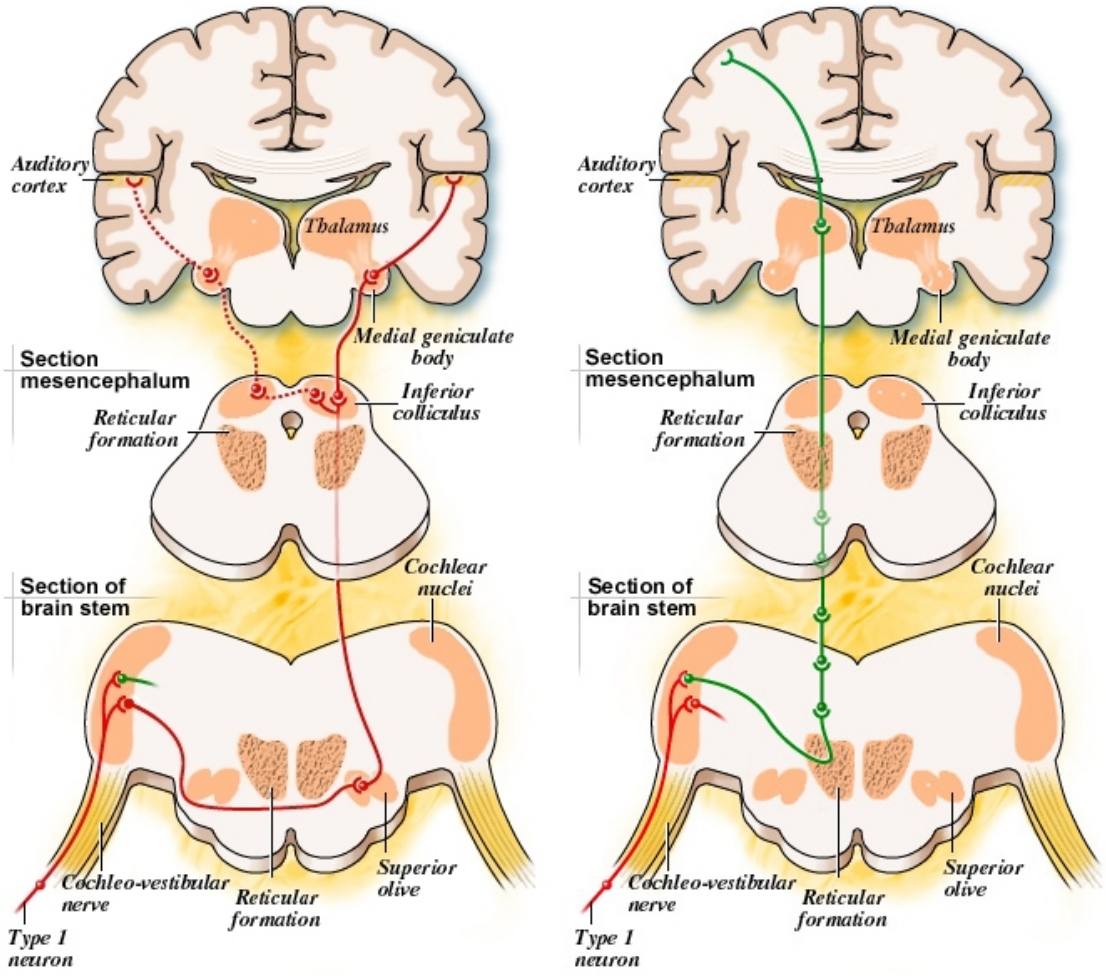

Figure 1.3: Complete auditory system (Blatrix, 1999)

1.1.2 Physiology

The auditory system is a transduction mechanism, converting acoustic energy into mechanical and finally into electrical energy. Sound waves hit the tympanic membrane causing it to vibrate. This vibration is transferred to the three bones in the middle ear; the Malleus, the Incus and Stapes, whose function is mainly to match the impedance of sound in air, at the ear canal, to sound in fluid, in the cochlea. The footplate of the stapes is attached to the oval window, a flexible membrane in the bony shell of the cochlea. Inward and outward movement of the oval window causes pressure fluctuations in the cochlear fluid, which sends a travelling wave of displacement along the BM. At the base end of the

BM, closest to the oval window, it is stiff and narrow and at the apex end it's wider and more flexible so that its natural frequency decreases from base to apex. Travelling wave moves from the base to the apex. For a sine wave excitation, the magnitude of the travelling wave increases as it moves from the base to the apex, until it reaches the point on the basilar membrane most sensitive to that frequency and it then drops quickly. High frequencies are detected towards the base whereas low frequencies are detected towards the apex (reflected in the change in stiffness across the basilar membrane).

The cochlea converts mechanical vibrations into electrical impulses by transduction at the inner hair cells. The inner hair cells activate the fibres of the auditory nerves, which project to the cochlear nucleus of the auditory brainstem where further processing takes place. The inner hair cells are attached to the top of the BM in a matrix of cells called the organ of Corti. There are two types of hair cells, arranged in 4 rows along the cochlea, such that the innermost row consists of the inner hair cells and the others are outer hair cells, of which there are three rows. There are small stereocilia projecting from the top of each hair cell, and it is the deflections of these stereocilia, due to the movement of the basilar membrane, which opens ion channels that allow K+ (potassium) and Ca+ (calcium) positive ions to flow into the hair cell body causing the cell to depolarize. In the case of the inner hair cell, this triggers the release of a neurotransmitter at the basal end of the hair cell body into the synapse. The neurotransmitter binds to the receptors of the neuron, and triggers an action potential in the auditory nerve, which travels through the rest of the auditory pathway. It is the change in potential "at the neurons" that triggers an impulse in the nerve, provided the threshold is surpassed (Wilson and Dorman, 2008). Deflections of the stereocilia of the inner hair cell in the opposite direction reverse the process, and inhibit the release of the neurotransmitter.

Outer hair cells serve as highly sensitive biological amplifiers. Deflections of the stereocilia also open ion channels allowing positive ions to flow inside and depolarize the cell. This results in a rapid variation (or vibration) in the length of these outer hair cells, causing a sharpening in the tuning of the cells to the frequency of the acoustic input. This vibration increases the movement of the basilar membrane, thus increasing the deflections at the inner hair cells, and consequently increasing the response at that frequency (Manley and Fay, 2008).

1.1.3 Hearing loss

Hearing loss in the cochlea is mainly due to the inner hair cells becoming damaged, from over-exposure to loud sounds, diseases, genetic defects and drugs. It is usually the outer

hair cells in the high frequency region that become damaged first, with the inner hair cells only being destroyed in the case of profound deafness. In the case of outer hair cell damage, threshold levels are increased and clarity of sound degrades due to decreased frequency discrimination. This is more common in hearing loss with age. In this case, a hearing aid would suffice to increase acoustic input levels received at the eardrum.

In total or profound deafness, the outer and inner hair cell count is usually close to zero and neural processes such as dendrites (peripheral to ganglion cells) rarely survive. Ganglion cells and central processes (axons) can exist in either sparse or substantial numbers. The survival of hair cells and neural systems can be quite different from patient to patient. The distribution of neural survival is also not uniform, in general. Often there are sharply reduced numbers in certain cochlear regions (Wilson and Dorman, 2008).

Hearing loss can be congenital, and this would have an effect on the normal development of the auditory pathway. Once such abnormal development occurs, a cochlear implant might not be successful in returning the sense of hearing to the patient. The pattern of neural damage can influence the type of cochlear implants that are used, so that different implant systems are designed to work with different levels or types of neural damage. One example of this is in the case of electroacoustic stimulation (EAS) where lower frequency neural survival is substantial and the implant is only used in the basal section of the cochlea. This is discussed in more detail in chapter 6. The implant considered in this thesis is a full length electrode.

1.2 Cochlear Implant

1.2.1 How they work

Cochlear Implants have been proven to reinstate the sense of hearing in the case of profound deafness, i.e. with over 60 dB loss (Rauschecker and Shannon, 2002).

Several corporations currently manufacture cochlear implants, of which three are dominant in the industry: Cochlear Corporation, Advanced Bionics Corporation and MeDel. All manufacturers share the same blueprint on the basics of the design of a cochlear implant. A cochlear implant consists of two parts, an external processing part responsible for analysing and processing an acoustic input, and an internal stimulation part responsible for direct stimulation of the neurons. The internal part of the implant is shown in Figure 1.4.

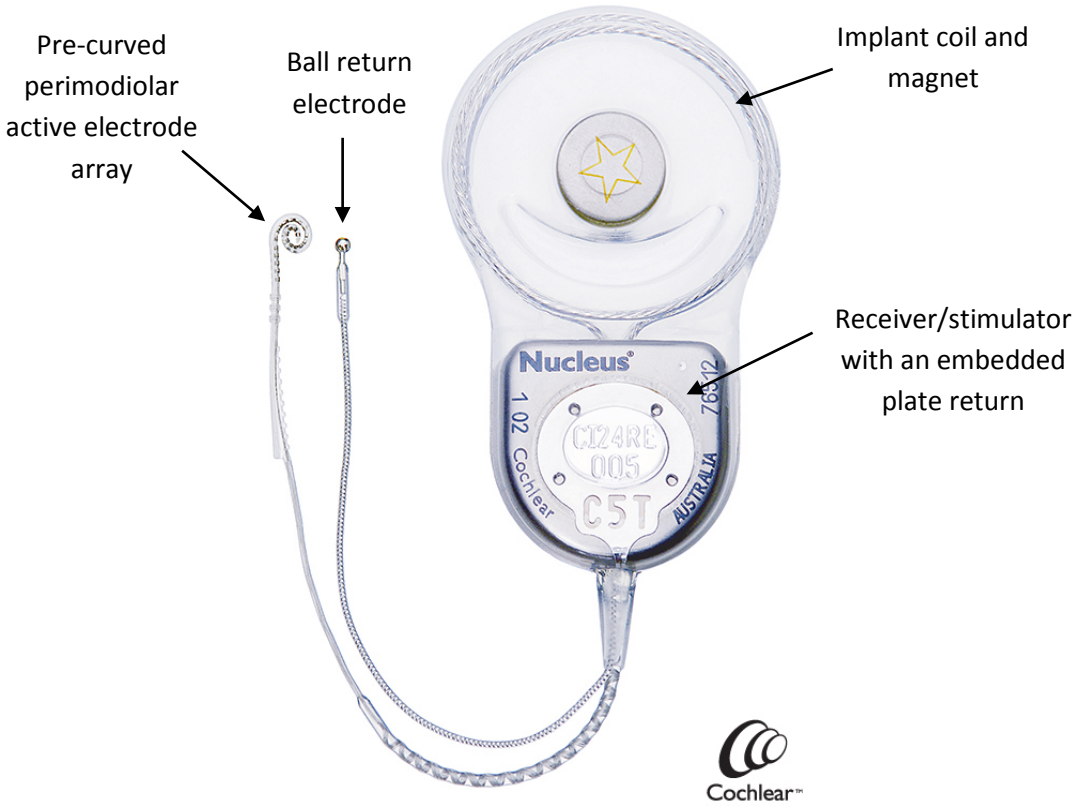

Figure 1.4: Cochlear implant device: Cochlear Contour Advance. The electrode array is the small coiled structure and the reference electrodes are on the body of the receiver stimulator (plate), and the ball electrode at the end of the other lead. Adapted from Cochlear (2012)

A microphone in the external part of the implant receives sound and converts it into an electrical signal that is analysed by a microprocessor, which samples and processes the sound to give an electrical signal that is designed to portray frequency and amplitude information. The sound is processed based on pre-programmed strategies that analyse the acoustic input using a filter bank or FFT, and process the signal to generate a sequence of equally spaced interleaved pulses that are destined to stimulate the neurons in the cochlea. Each pulse is described as having a positive current phase followed by a negative current phase separated by a phase gap. The generation of this pulse sequence is described in detail in chapter 4. The external part of the implants also houses an on-board battery that powers both the processor and, via induction, the internal part.

The pulse sequence is transmitted through the skin (transcutaneous link) to a receiver/stimulator, by means of a radio frequency signal produced by the transmitter via a coil, which relays it to the appropriate excitation sites via electrodes for each frequency

region (Somek et al., 2006). Each electrode is separately supplied with a given current and so can be controlled individually. The transcutaneous link needs to have enough bandwidth to transmit all the information (Rauschecker and Shannon, 2002).

The implanted part of the cochlear implant system is an array of microelectrodes that are threaded into the scala tympani (ST) within the cochlea. The depth of insertion of the electrode into the ST is limited by the decreasing width of the canal of the ST in the direction of the apex, and the curvature of the cochlea. The lumen of the ST is also an uneven and unsmooth canal, especially at the apical region, which limits the maximum insertion depth to about 30mm (Wilson and Dorman, 2008). The active electrodes are placed in a silicon matrix along the basilar membrane such that in the first turn, the electrodes correspond to higher frequencies whereas further into the first or second turn of the cochlea, these correspond to the lower frequencies. The degree to which the implant is inserted would dictate what sites on the basilar membrane could be reached for stimulation, consequently defining the range of frequencies that could be portrayed by the implant. Most frequencies are accessible by the CI but it becomes a lot harder to simulate the really low frequency regions, as this is in the thinnest and narrowest winding part of the cochlea, which cannot be penetrated by the electrode array. Fortunately, speech is typically within the frequency range from 100 Hz to 4 kHz (Loizou, 1998) and some of the inaccessible part of the frequency spectrum, below 1kHz, is not vital for speech perception. The brain (auditory cortex) can reconstruct the fundamental frequencies that are governed by the regions of the basilar membrane that the CI cannot reach. Much of the information outside of the range for speech is more useful for music, sound quality and identification of objects. The postlingually deaf have an established understanding of language before the onset of hearing loss, and re-connect almost immediately after implantation (Rauschecker and Shannon, 2002).

The insertion of the active electrode array into the cochlea is known as a cochleostomy, and this is achieved by drilling a large hole in the bony shell of the cochlea, near the round window, so that the electrodes enter through the round window into the scala Tympani. Sometimes, only shallow insertions of the electrodes into the cochlea can be performed. This is because of the bony obstructions in the lumen (Wilson and Dorman, 2008). The placement of the cochlear implant within the ear is shown in Figure 1.5.

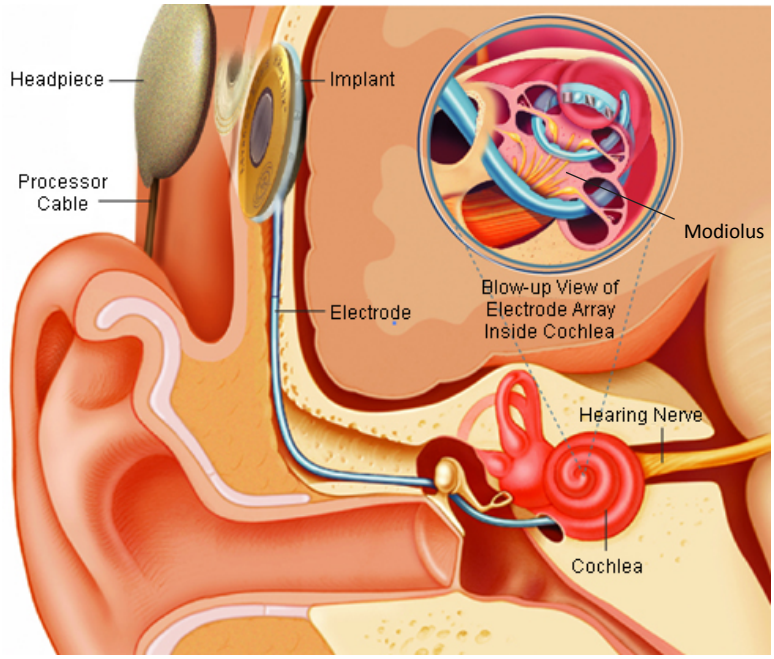

Figure 1.5: Implanted cochlear implant (adapted from The University of California San Francisco, Medical Centre, 2012)

The placement of the reference or return electrode depends on the configuration of the implant. With a monopolar configuration, described in more detail in chapter 2, there is a reference (ground) electrode outside the cochlea, usually placed under the temporalis muscle. In some configurations of the implant there is also a reference electrode embedded in the receiver stimulator, in the form of a metallic band around the outside of the receiver, which is also placed under the temporalis muscle. In bipolar configurations, the reference electrode is one of the nearby electrodes to the active electrode on the electrode array (Drennan and Pfingst, 2005). Current systems use a monopolar stimulation configuration, which uses less power but is reported to perform similarly to bipolar stimulation (Wilson and Dorman, 2008).

The active electrode array delivers electrical stimulation to the cochlea by applying a current, of the order of 100μA, between the active electrode and the reference electrode. This creates a voltage distribution throughout the cochlea. The change in potential across the neurons triggers the action potential in the auditory nerve. The degree to which stimulation is spatially specific is governed by the orientation of electrodes, the proximity to target neural structures, and the condition of the implanted cochlea (Wilson and Dorman, 2008).

As mentioned before, for an action potential to be generated at the neuron, a threshold must be surpassed. This threshold varies depending on the degree of neural survival at different position in the cochlea, and is subject to significant inter-patient variation. Each cochlear implant has to be calibrated according to the patient's sensitivity. The patient is subjected to an increasing level of stimulation at each electrode or stimulation site until two limits are found. The first is referred to as the Threshold level (T-level), which is the lowest level of current required to successfully stimulate the cochlea to give the quietest hearing sensation. The second is referred to as the Comfort level (C-level) and this represents the highest level of current that can be used to stimulation a sensation in the cochlea beyond which the sensation is no longer comfortable and ultimately painful. Tuning these levels ensures that the patient will always receive an appropriate level of current stimulation (Pfingst and Xu, 2004).

1.2.2 How they can be improved

Although current cochlear implants have restored hearing to the extent that users can have a normal conversation, the variations in user experience with cochlear implants is so vast that it suggests that the process of converting sounds into an electrical signal is not fully understood (Graeme, 2003). Most cochlear implant users are unable to perceive music or hold a conversation in noise (Wilson and Dorman, 2008). There are several factors that contribute to the variation in user experience with cochlear implants. From person to person, the cochlea can naturally vary anatomically in height, width, and length of individual turns by as much as 40% (Erixon et al., 2009). Nerve survival is also a key aspect of cochlear implant function and the distribution of surviving nerves will vary from user to user. The placement of the electrode within the cochlear chamber is not consistent from person to person. Placement can be affected by misplacement during surgery, the type of electrode array used, and the shape of the individuals cochlear curvature (Zeng et al., 2004). Excitation spread is also an issue, whereby stimulation power is not sufficiently focussed at the target neural region, resulting in unintended stimulation of neighbouring neurons. It is suggested by Wang et al. (2008) that the electrode array is where the largest power losses occur in the implants power distribution.

In order to propose suggestions that would improve user experience in the use of a cochlear implant, some of the above mentioned factors that influence the effectiveness of the implant must be addressed. There is also an increasing interest in fully implanted devices, with no external part to house the battery, so that power consumption will be an even more important aspect of the cochlear implant (Wise et al., 2002, Saba et al., 2008).

1.3 Power Required

Cochlear implants are powered by an on-board battery which could be either disposable or rechargeable (SOECIC, 2011). This requires regular daily recharging or replacing and on-going research is taking place in order to achieve an independent power source and free the patient from having to constantly recharge the implant.

In comparison, the efficiency of the neural system in the human body is said to be spectacular (Sarpeshkar et al., 2005). The inner ear requires just 14 μW of power which could theoretically be run for 115 years using one AA battery (Sarpeshkar et al., 2005).

An estimated breakdown of the power requirements of a current cochlear implant is shown below, based on discussions with a cochlear implant manufacturer. The total power requirement is around 40 mW and most of this is taken up in the processor, about 5 mW is required for electrical stimulation (Ji-Jon and Sarpeshkar, 2008, Cochlear, 2011). There is only around 30% efficiency in the transmission phase through the transcutaneous link so about 15 mW is dissipated in transmission (Cochlear, 2011). The breakdown is demonstrated in Figure 1.6 below.

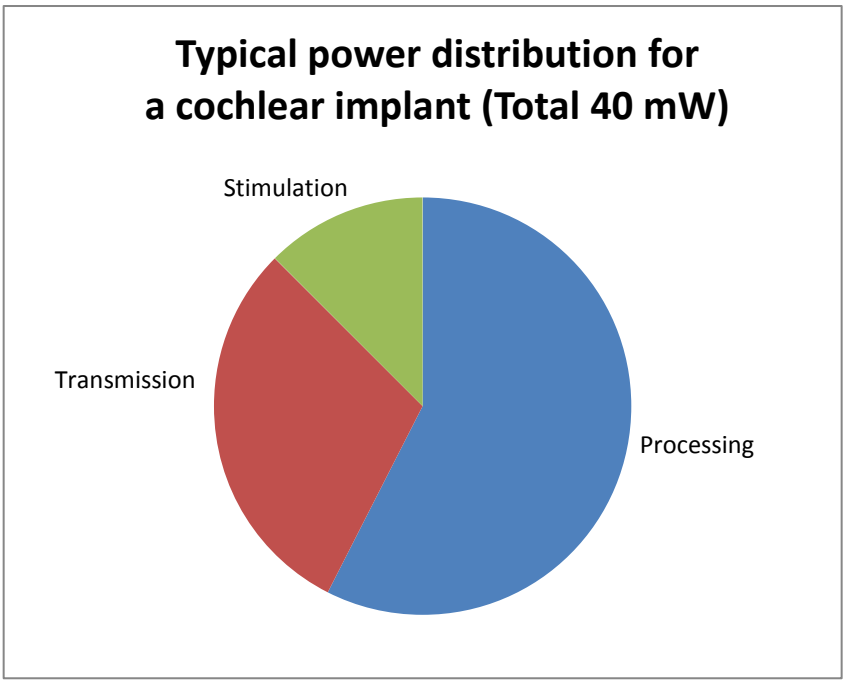

Figure 1.6: Estimated power distribution for different processes in current cochlear implants

Germanovix and Toumazou (2000) proposed a full implantable cochlear implant that would only require a total of 7 mW as a worst case scenario and 150 μW in the average case. This uses a processor that is also fully implanted but having parameters that can be adjusted using a wireless external device.

Wang et al. (2008) also investigate redesigning the cochlear implant. They report that if the transmission link is optimised with their proposed design, the transmission efficiency will increase to 40%. They apply other optimization techniques on other parts of the implant and report a decrease of 25% to 30% in power consumption on average.

The processing power requirements are subject to the competing influences of technological advancement and increasing capability. As modern signal processing devices are developed they become more powerful, but could also be made with lower power requirements for the same processing capability. Koomey (2011) reports that computations per kilowatt-hour double approximately every one 1.5 years. Cochlear implant manufacturers, however, are always seeking to increase the capabilities of their devices and to introduce new features. This tends to absorb the additional processing capability of new devices, so that the overall power requirements are similar.

1.4 Outline of the thesis

Figure 1.7 below identifies the general processes involved in the function of a cochlear implant.

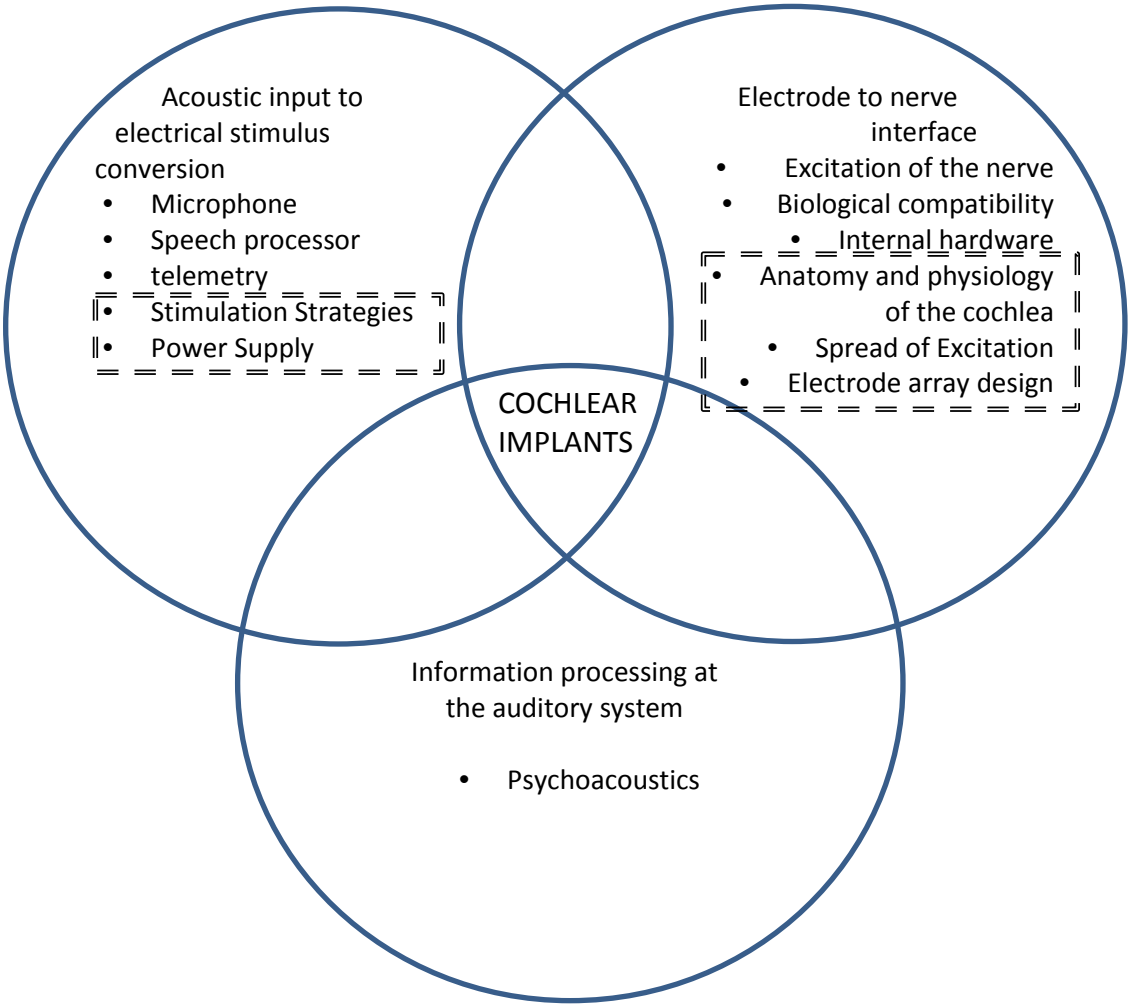

Figure 1.7: Representation of the general processes that take place in a cochlear implant. The dashed boxed indicate the processes or issues addressed in this thesis.

This thesis considers power consumption issues, stimulation efficiency and power harvesting possibilities in the application of cochlear implants. The stages within the cochlear implant process addressed in this thesis are outline with a dashed box in Figure 1.7. In general, the issues addressed include the power supply, a study on the effect of stimulation strategy selection against the power consumption, and the efficiency of stimulation of the nerves within the cochlea due to cochlear and electrode array geometric variation and configuration.

1.5 Contributions of the thesis

The main contributions of the thesis are:

- The calculation of the voltage distribution around the electrodes in a realistic, three dimensional, model of the cochlea, and the variation of this distribution with electrode position and anatomical variation.
- The use of this model to investigate the consequences of a current-steering, or stimulation focussing, strategy that has previously been proposed, and the suggestion of a generalisation of this strategy.
- The estimation of the power consumption of various stimulation strategies in order to assess their energy efficiency.
- An investigation of the feasibility of harvesting electrical power from the movement of the head, and the parameters identified that determine the power that can be generated in this way

1.6 Structure of the thesis

A brief description of each chapter of the thesis is now provided.

Chapter 2 – This chapter discusses the method by which a three-dimensional finite element model of the cochlea was developed. It demonstrated varying levels of complexity and presents several different simulations to validate the integrity of the model.

Chapter 3 – This chapter presents several studies involving the finite element model of the cochlea presented in chapter 2. The placement of the electrode array was varied in the coiled model of the cochlea. A focussing strategy was developed using impedance information at the neural level to improve stimulation accuracy. The effect of placing the return electrode within the modiolus on power consumption was also investigated.

Chapter 4 – This chapter investigate the effect of stimulation strategies on power requirements of the resultant pulse sequence. Key parameters are identified and varied individually to investigate their effect on power requirements. The effect is also investigated of patient threshold and comfort levels on power requirements. Finally, the most common strategies are compared.

Chapter 5 – This chapter investigates the feasibility of powering a fully implanted cochlear implant by means of an energy harvesting source implanted under the skin, which takes advantage of the motion of the head during walking. The investigation

focuses on optimal tuning of an inertial electromagnetic device by investigating optimal axis of head movement, stiffness and damping parameters and having a lightly damped sharply tuned device in comparison with a heavily damped device with a broader response.

Chapter 6 – This chapter concludes the contributions of the thesis to the relevant areas of research addressed and suggests potential areas of further work.

Chapter 2

2 Modelling the voltage distribution in the cochlea

2.1 Introduction

2.1.1 Issues with current stimulation strategies

Current cochlear implant devices have been developed over several decades of research, but electrical stimulation is still the subject of much research, especially in the case of controlling current spread and channel interaction. Channel interaction occurs when stimulation from one electrode spreads to other nerve sites not intended for stimulation, resulting in spatial overlap and so frequency resolution is lost and information received in the brain is distorted.

Although current cochlear implants have restored hearing to a degree where users can have a normal conversation, increasing the frequency resolution would more beneficial in being able to understand more complicated sounds, such as musical pieces or conversation in noise. Cochlear implant manufacturers are always developing their devices to try and tackle these issues and one such company, Advanced Bionics, have released a new device entitled 'HiRes', and this cochlear implant is programmed to convert the 22 physical electrodes into a 128 virtual stimulation site. This uses current steering and is effective in giving more frequency resolution. While these strategies are useful, it is far better to improve the delivery of the acoustic signal to the nerves.

This improvement could be achieved using better stimulation strategies or different electrode configurations and improved electrode geometry design. One way to test new electrode array configurations is to physically measure the response in the cochlea. Instead, a computer model could be used to simulate the stimulation in the inner ear which can allow any electrode configuration to be tested. The purpose of the work

presented in this chapter is to explore the spread of current during stimulation by developing such a model that describes the voltage distribution along the length of the cochlea. The voltage distribution can be modelled for several variations of electrode geometry, spacing, position and sequence of stimulation but the first step is to model the spread of current due to the geometry of the cochlea. A range of models is considered. These models include a uniform uncoiled model and a coiled three-dimensional non-uniform model of the cochlea and the electrode array.

The voltage distribution along the electrode array in the cochlea varies greatly from person to person Examples of the impedance distributions in a real cochlea are shown in Figure 2.1 A) and B). The figures show the impedance distribution at each electrode in response to the stimulation of the electrodes individually along the length of basilar membrane, measured by injecting a known current into each electrode in turn and measuring the resulting voltage at the other electrodes. The measured diagonal terms of the patient impedance matrix have an extrapolated value, rather than a measured one, due to polarisation of the electrode being excited. The figures represent the data for two patients, as published by van den Honert and Kelsall, (2007).

The pattern of the distribution is different between the two patients, due to the natural variation in cochlear geometry and implant position. The common features between them are that they share similar peak values and have a similar decay rates for each of the individually stimulated electrode distributions. The voltage distributions that are predicted from the cochlear models described in this thesis can thus be compared to the patient distributions in terms of peak values and decay rates.

2.1.2 Benefits of modelling and previous studies

Building a three dimensional model of the voltage distribution in the cochlea allows the evaluation of theories on the response of the cochlea due to an electrical input, without having to use the cochlea of a real life patient. Given this ability, research is able to expand in the area significantly allowing for simulations that may not even be possible in the real life cochlea. If the model is built in a flexible manner, that is to say that geometrical and electrical parameterisation is available, this gives the ability to look at specific cases or states of the cochlea (pathological or natural variation) and test for their response to specific electrical and mechanical conditions.

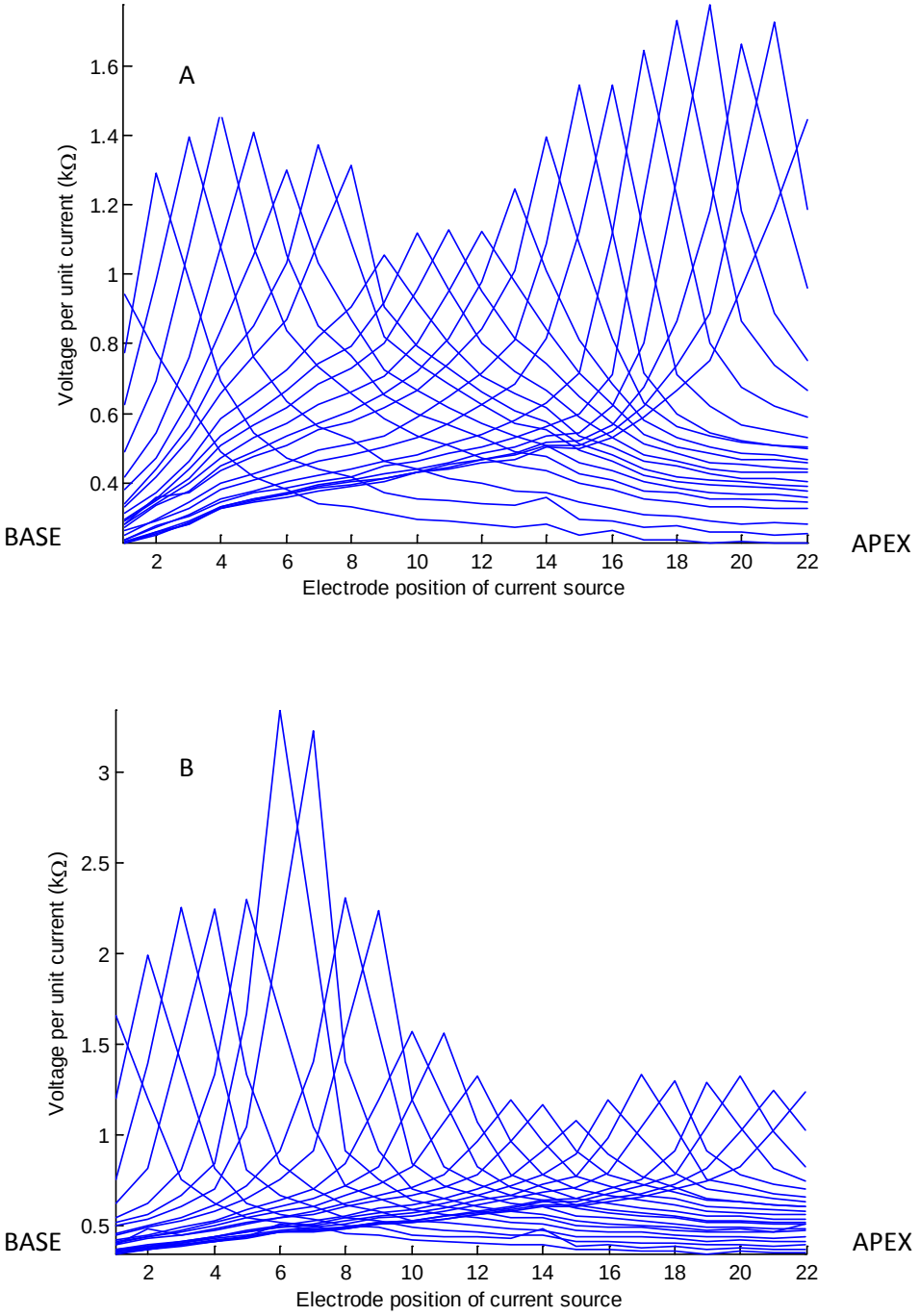

Figure 2.1: Measured voltage spread against position of current source for patient 1(A) and 2(B). Patient data from (van den Honert and Kelsall, 2007)

The modelling of the electric field has been considered by a number of authors with varying degrees of complexity up to 3 finite element models. Lai and Choi (2007), proposed a new method to model an electrode tissue interface by combining it with a 3D model of the cochlea and electrode using the finite element method. The authors tested

the model under three conditions; the model of the electrode without the interface, the electrode model with the interface effect using an equivalent circuit and finally the model of the electrode that incorporates a thin layer between the electrode and the scala tympani. Monopolar stimulation was used. By looking at the electrode potential of the equivalent circuit compared to that of the finite element model, it was confirmed that the methods give almost identical results thus validating the finite element approach. This method also demonstrates flexibility as one is able to remove the layer from the model if required. The paper also investigates the effect of using different types of electrode; planar, half banded, banded and ball. It was found that the planar electrode was the most efficient at stimulation which is in agreement with published results (Lai and Choi, 2007).

Tognola et al. (2007) conducted a study whereby a finite element model of the cochlear implant was generated with the intention of investigating the pattern of excitation as a result of changing various electrical parameters of the cochlea. The expectation is that a better understanding of the relationship between the parameters and the electric field could be reached so that an increase in efficiency and spatially localised excitation are realised. The numerical results were compared to experimental results using a water tank. A comparison of results confirmed the validity of the model used to generate the electrical potentials. It was found that monopolar stimulation generated higher values of electric potential compared to bipolar stimulation. This is due to the increase in impedance seen between the active electrode and the reference electrode external to the cochlea in the monopolar configuration. The bipolar configuration only meets the impedance of the volume in between the two nearby electrodes.

Briaire and Frijns (2000) pointed out that the human cochlea is very complicated and cannot be modelled by simply using information from a cross section of one turn as well as a scaling parameter, the reason for this being that the cochlea varies significantly along its length.

Rattay et al. (2001) modelled the cochlea in 3D using the finite element method. The purpose of the method is to test the influence of a 3D cochlea model on neuron excitability using a simplified model that takes into account the spiral shape and dimensions of the cochlea. Rattay tests the sensitivity of the parameters in the finite element model by comparing it to a 2D simplified model. Conductance of different types of tissue was tested for their effect on the voltage across the neurons. It was found that doubling the conductance had little effect on the shape of the extracellular voltage and consequently the nerve excitation and this was the same for both models for a specific case. Rattay also

notes that the electrical properties of the tissue within the cochlea are hard to evaluate and that there are large differences between different published results.

Rattay also finds that electrical stimulation of the nerve is different for laboratory animals and humans. Human nerves have a longer peripheral axon compared with laboratory animals and so excitation is different. Their simulations show differences for different polarities of stimulation for nerves near the electrode. Also, it was found that the human geometry of the nerve allows for easier excitation. With strong stimuli, both the peripheral and central axons can be stimulated, leading to confusion in timing where the excitation at the peripheral axons will have a delay. This delay, however, does not occur when fibres are degenerated, whereby fibred are physically deteriorating.

Rattay concludes that their simple model is sufficient to simulate excitation adequately and shows similar results for the voltage profile of the neural pathway near to the electrode to those of a fine structured rotationally symmetric model (Poznyakovskiy et al., 2008). He goes on to discuss that if a better model was to be designed, the two main aspects to focus on are the detail on the neural pathway and on the design and testing of focusing electrodes.

Frijns et al (2009) numerically investigated the effect of sequential and simultaneous stimulation on the loudness and place pitch. A three dimensional finite element model was used to simulate the different types of stimulation, and the results were validated with psychoacoustic measurements. Frijns found that there are two possible solutions to dual electrode stimulation. The first is that when two electrodes are stimulated together, especially in the case of simultaneous stimulation, can be used to excite an intermediate neural region and that position can be steered by adjusting the ratio of the currents. In some cases, dual simultaneous stimulation would excite an intermediate neural region that would not have been excited at all by each individual electrode. The other solution, which uses sequential stimulation, is that an intermediate neural region could not be stimulated by dual electrode stimulation because overlap of the electric fields is not significant.

Van den Honert and Kelsall (2007) describes a method whereby an array of electrodes is used to produce a focused stimulation in order to obtain a way to stimulate more than one electrode without spatial overlap. This was generally done by measuring the spread functions of the electrodes in the array resulting in a matrix of transimpedance values in between idle and stimulating electrodes. The matrix is inverted to give transadmittance values using a procedure that is explained in more detail in section 3.3 of chapter 3.

Results confirm that with this method the voltages at the electrodes due to excitation spread can be cancelled. It also finds that the inverse matrices of 22 electrodes can generally be calculated with adequate accuracy and are stable over time.

Van den Honert and Kelsall (2007) state that a perimodiolar array of electrodes, where the electrodes are placed as close as possible around the modiolus, is essential to minimise spread of excitation. The closer the electrodes are to the modiolus, the higher the impedance due to this proximity and so the less current is shunted longitudinally along the cochlea towards the apex.

There are several disadvantages of such a method to cancel excitation spread. Any focussing on the end electrodes of the array will fail because there are no flanking electrodes to cancel out the excitation spread beyond the array. The nature of the method implies that higher currents will be required to power all the flanker electrodes to produce the cancelling effect. This is a disadvantage for fully implantable cochlear implants that require reduced power consumption. The author states that future designs of this cancelation method must measure impedances and current regulation precisely to limit the error.

Ho et al. (2004) investigate the effect on power efficiency of placing the return or reference electrode within the modiolus of the cochlea. Since the target spiral ganglion neurons are within the modiolus, then it is suggested that the return electrode should be placed deep within the modiolus, so that these target neurons lie in between the active and reference electrode. With this configuration, the current flow through the target neurons is increased, which suggests that if the same current flow is assumed through the modiolus then less current is required to achieve the same level of stimulation, and consequently, less power is required overall. Placing the reference electrode away from the target pushes the stimulus away from the neurons, as discussed further in chapter 3.

A plexiglass model was used for this investigation and different positions of the return electrode were tested. Measurements clearly showed that the current passing through the target neurons was around 2.8 times higher than if the return electrode was placed outside the temporal bone. This was confirmed with tests performed on preserved temporal bone with agar, where results were compared with the return electrode placed within the modiolus and within the agar.

Other advantages of placing the return electrode within the modiolus include the reduction of side effects due to levels of electrical stimulation in the cochlea as well as an

increase in spatial selectivity due to lower current amplitudes and current spread. Disadvantages include possible damage to the auditory nerve while implanting the return electrode within the modiolus, as this would be a difficult surgery. There is also the possibility of cerebrospinal fluid leakage due to the opening of the modiolus thus increasing the risk of meningitis. This is why insertion into the scala tympani was preferred over the modiolus. It is also possible that the tissue around the return electrode in the modiolus would be easy to excite and hence non-intended excitation of neighbouring neurons would occur. This can be addressed by reducing the current density around the neighbouring neurons by increasing the electrode contact surface area. This can also be done by increasing the distance between the return electrode and the nerve fibres. Further work includes the study of changing the position of the electrodes in vivo.

The models mentioned above are all limited in various ways such as the lack of any coiling in the model or it may have an unsmoothed curvature, the lack of detail of the variation in cross-sectional areas along the length of the cochlea, constraints on modelling possibilities due to the choice of meshing algorithm. In most cases it appears that the model is not flexible for fast geometric variation.

2.1.3 Method of Analysis

Several different methods have been used in this thesis to model the electrical interaction between the electrode array of a cochlear implant and the target neurons in the auditory nerve. These different approaches are described below.

Lumped parameter models:

This method involves the use of resistors and capacitors to build an electrical network to represent geometric properties of a model. Capacitive effects are easy to integrate into this kind of approach due to the nature of the structure. According to Briaire and Frijns (2000) this method is not refined enough to be used to develop a neural model. This method has been used for cochlear implants, for example, Black et al. (1983), however it is limited to an unrolled model of the cochlea. This method predicts an exponential decay for the current and potential in cochlear implants due to electrode stimulation. This method is not recommended for detailed modelling of the cochlear implant and nerve fibres.

Boundary element method (BEM)

This method calculates the potential due to a current in a piece-wise homogenous volume conductor (Briaire and Frijns, 2000). It is different from the finite element method and finite difference method with regards to meshing. In the boundary element method, only the boundaries in between different volumes with different conductivity parameters are meshed, whereas in the finite element and difference methods, the entire model is meshed. There are thus fewer elements with this method as there is less to mesh and adding different meshes together is possible without having to re-generate the mesh. This is especially easy for applications like adding the mesh of an implant to an existing mesh of the cochlea. A major disadvantage is the computational effort required to solve and implement the method, due to surface integrals and finding the inverse solution of the matrix. The advantage however is that once this inverse solution is calculated, minimal effort is required to calculate the potential distribution of any electrode combination. If anisotropy is required, then the BEM can be combined with the FEM.

Finite difference method (FDM)

The finite difference method uses a taylor expansion of Poisson's equation to compute the potential along a fixed structure of points and this is solved iteratively (Briaire and Frijns, 2000). This method is best suited for modelling simple structures, as the grid is fixed and cannot handle complex detail such as the cochlea. This method requires a lot of memory and computational effort if smaller mesh elements are used to represent smaller structures accurately.

Finite element method (FEM)

This method computes the potential by minimisation of the energy in a volume. Briaire and Frijns (2000) state that for an electrical volume conduction problem, the minimisation of the power dissipated is required. This method operates by splitting the model into many small volumes. This method benefits from the ability to incorporate a neural model and the ability to include capacitive and anisotropic effects without the need for heavy computation. This method differs from the boundary element method in that generation of the mesh is more difficult because for every change in the model i.e. adding an electrode, the entire model has to be discretised.

2.2 Definition of the model

The model assumes a conductive media and solves for the electrical potential. The equations that govern the calculation in the finite element process are as follows:

$$\nabla \cdot \mathrm{J} = Q_j \tag{2.1}$$

where ∇ is the vector spatial derivative operator, Q_j is the current density of the source and J is the current density in the medium, defined using the Ohms law.

$$\mathrm{J} = \sigma \mathrm{E} \tag{2.2}$$

σ is the electrical conductivity of the material in the model (S/m) and E is the electric field (V/m).

Once J is known, the electric field E can be calculated from Ohms law throughout the model. The electric field is described by the equation,

$$\mathrm{E} = -\nabla v \tag{2.3}$$

where v is the voltage. In practice E is calculated as the difference between the voltage at two points divided by the distance between those points, so,

$$\mathrm{E} = \frac{\delta v}{\delta x} \simeq \frac{v_1 - v_2}{\Delta} \tag{2.4}$$

Therefore if we know the electric field we can calculate the voltage at different points.

2.3 Cable model

To begin with, a simple cable model can be used to describe the voltage spread in a uniform straight cochlea, due to a given input current. This is a network of resistors set up to represent the two main resistance paths between the electrodes and the fluid within which they are implanted. This may not entail the level of detail on impedance as present in a real cochlea but it focuses on achieving an idea of what the excitation spread may look like. The spread of excitation is then represented using an impedance matrix derived from the resistance network. This can be compared to the impedance matrix measured in patients, by van den Honert and Kelsall (2007), for example. The network used here is also comparable to Rohr (2011).

An electrode array of 22 electrodes was assumed and this was modelled with an electrical network of resistors as shown below in Figure 2.2, with ground representing the return electrode:

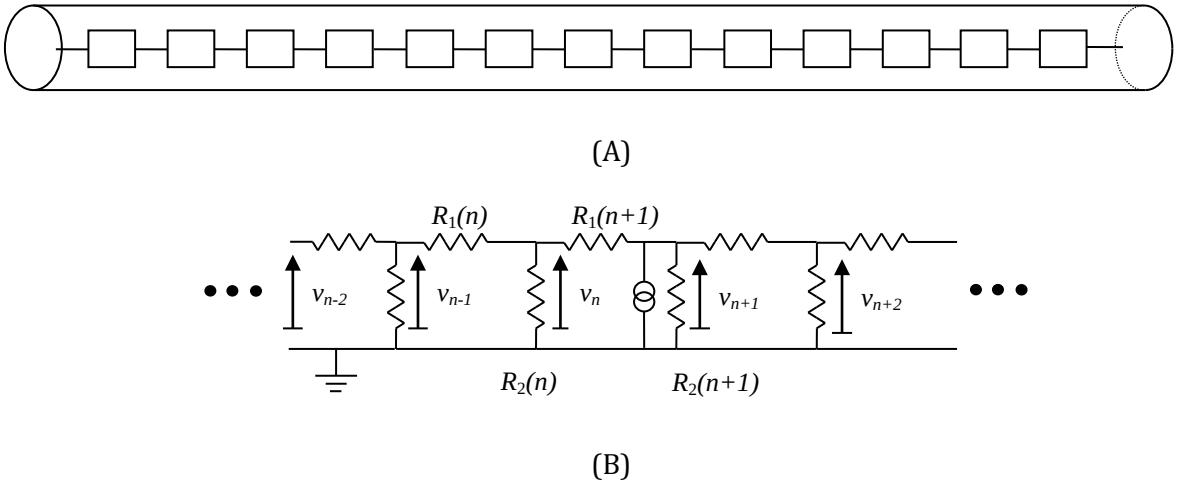

Figure 2.2: A) shows the electrode array within the scala tympani, B) shows the equivalent circuit network or cable model of the electrode array.

This network is analysed in Appendix A, and the predicted voltage distribution at the 22 electrodes, when excited by a current source at each of the electrodes in turn, is shown in Figure 2.3 when R_1 (impedance in between electrodes) and R_2 (the impedance in between the electrodes and the perilymph fluid) are 1 kΩ and 2 kΩ respectively, and are uniform along the length of the model.

This shows that at either end of the cable model the resistance is highest and so the voltage is highest. As you go towards the middle, the overall effective resistance decreases, decreasing the peak of the voltage at the point of excitation. This is due to the fact that at the ends of the array no resistance exists beyond the array. In the cochlea, the end of the array meets the tissue and fluid of the scala tympani and so it meets a large resistance.

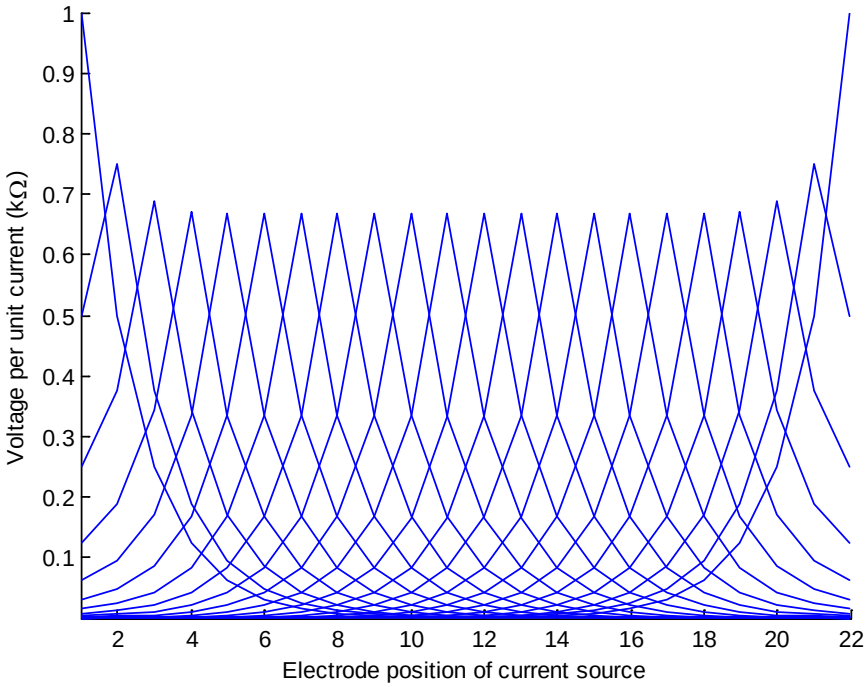

Figure 2.3: Estimated voltage spread against position of current source

The predicted impedance matrix is comparable in general structure and characteristic to the impedance matrix published by (van den Honert and Kelsall, 2007) as shown in Figure 2.1 in section 2.1.1 although it is more uniform.

The attenuation rate is a measure of the spread of excitation and is defined as the voltage at one electrode divided by the voltage at the neighbouring electrode nearer the stimulation. Stimulating at one electrode, the attenuation rate along the length of the array can also be calculated for the measured impedance matrices in Figure 2.1 and Figure 2.3.

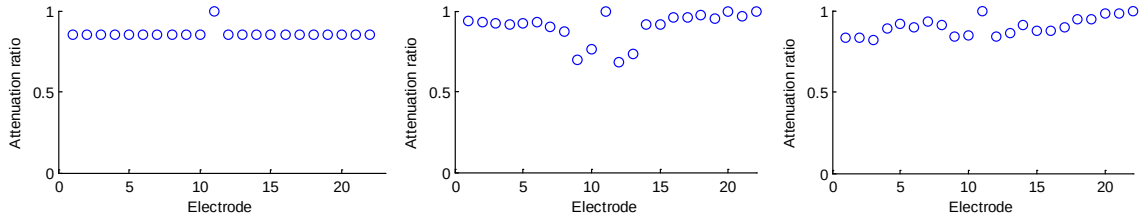

(A) (B) (C)

Figure 2.4: A) the attenuation rate curve for the simulated uniform spread for ratio $R_1 / R_2 = 1/40$, B) the attenuation rate curve for patient 1, C) the attenuation rate curve for patient 2. The patient results are calculated based on data from (van den Honert and Kelsall, 2007).

The magnitudes of the predicted voltages will depend on the assumed magnitudes of R_1 and R_2, and the rate of fall-off of voltage with longitudinal position will depend on the ratio R_1 to R_2, as discussed in the Appendix A. The values of R_1 and R_2 will depend on the relative geometry of the fluid chambers and the cochlear implant. In particular as the ground electrode is moved further away from the implant array, R_1 will remain substantially unchanged whereas R_2 will be increased, so that the ratio R_1 / R_2 will fall. These impedances are constant, away from the ends, in a uniform model, but will vary with longitudinal position with more realistic geometries. In order to investigate this, a three dimensional finite element model is used, as discussed in the next section.

2.4 Three dimensional modelling

A one-dimensional cable model can give an idea of what the voltage spread is like at the electrodes but cannot take into account the excitation at the nerves and have difficulty incorporating the geometrical changes that would affect this spread. To calculate the effect of geometrical (and electrical) changes a three-dimensional model is required. There are a wide variety of issues in the building of this model, which include software selection and geometry data collection and geometrical building techniques. The final selection of software is listed in Appendix B. Throughout the project there have been many issues that caused problems in the geometrical solid generation phase. Some of these issues are dealt with in detail in Appendix G. The following sections will outline the method finally used that works for all software involved.

2.4.1 Cochlear Geometry

The geometry used in the model was either calculated or assumed based on previous literature on geometric modelling of the cochlea. The two primary sources for the anatomical details and their measurements are two images of a mid-modiolar section of the cochlea taken in the form of an electron micrograph. These were extracted from (Zakis and Witte, 2001) Figure 2.5 and (Rattay et al., 2001) Figure 2.6. The remaining measurements were taken from various publications listed later in this section.

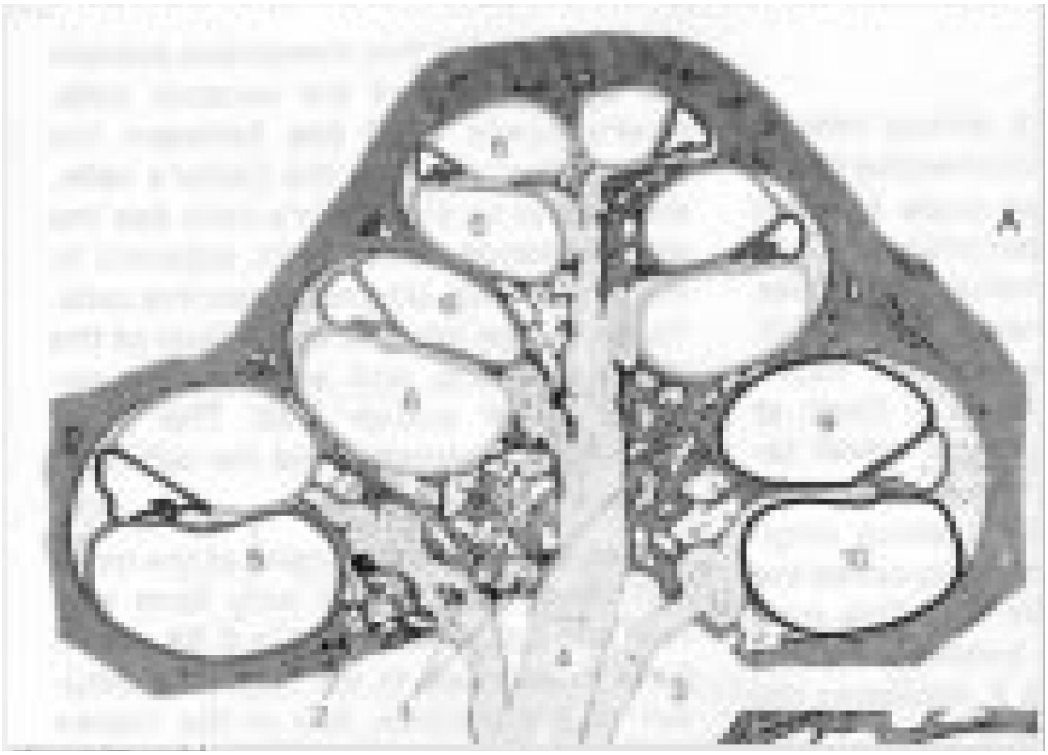

Figure 2.5: The human cochlea (Zakis and Witte, 2001)

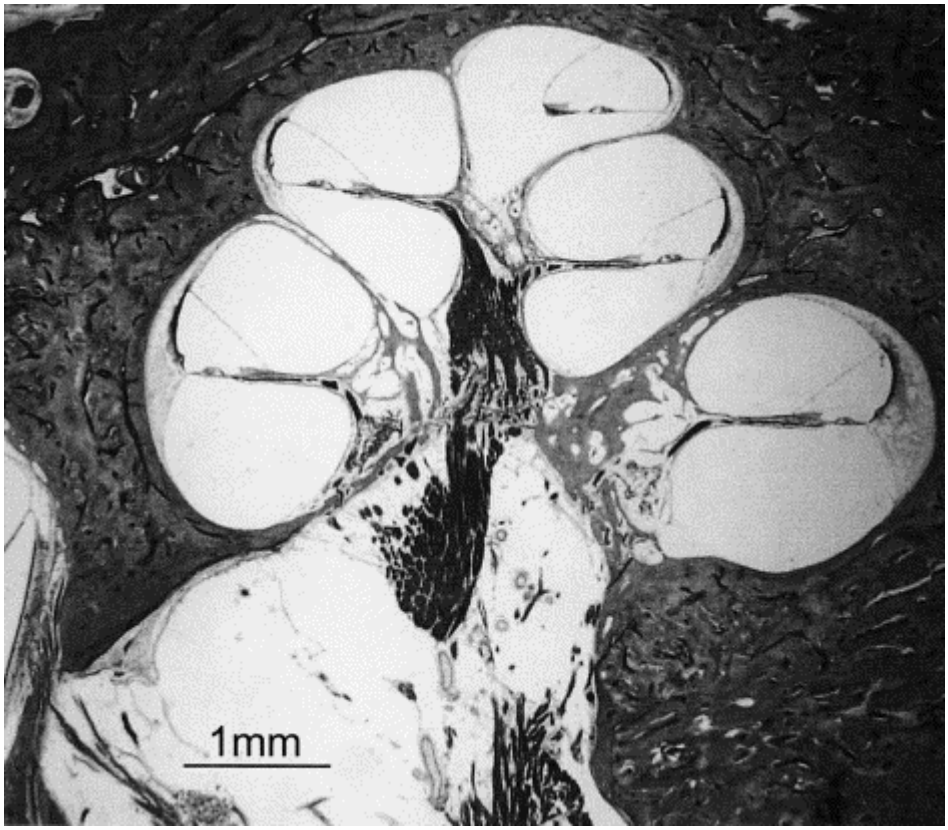

Figure 2.6: The human cochlea (Rattay et al., 2001)

The two images represent a mid-modiolar section of the human cochlea. Figure 2.5 shows the majority of the cochlea with two and a half turns of the spiral visible in the image. In Figure 2.6, slightly less of the cochlea is visible but with far more detail for the finer structures. Figure 2.6 shows a reference length of 1 mm allowing for measurements of the structures in relation to that reference, whereas Figure 2.5 does not. Hanekom (2001) reported that an average height of the spiralled cochlea is approximately 5 mm and so Figure 2.5 was rescaled and resized to fit that height. This enables measurements to be taken reliably from Figure 2.5. Therefore, Figure 2.5 was used rather than Figure 2.6 as the primary source for structural dimensions because it showed more of the cochlear turns which is necessary to establish the variation in cross-sectional areas. Figure 2.6 was used as a reference to validate the measurements from Figure 2.5.

Corel Paint Shop Pro X2 was used to import the images from the source papers and saved as a separate high-resolution image file. This was then imported into AutoCAD as a Raster Image reference. The image was scaled to the correct size by measuring the overall height of the cochlea in the image, and using a ratio of measured to required height to scale the image to the required height.

When the image is scaled correctly, measurements of lengths and widths can be taken, using the distance tool within the inquiry toolbar, such as the cochlear partition width. The images were not reliable enough for certain measurements, including the basilar and Reissner's membranes thickness, as well as the overall spiralled length of the cochlea. The basilar membrane and Reissner's membrane measurements were taken from Skrodzka (2005a). Skrodzka reports that the basilar membrane thickness varies from 0.03 mm at the basal end to 0.01 mm at the apical end. According to Figure 2.5 and Figure 2.6, it appears that Reissner's membrane is similar in thickness to that of the basilar membrane and so it is assumed to be the same.

When measuring the area of a structure, the outline was traced using the spline function in Autocad. The spline approximates the shape of the structure, and built-in functionality calculates the area of the surface created by the spline. The full trace of all the important structures (scala vestibuli, scala tympani and scala media) is shown below in Figure 2.7. The figure also shows how the trace was obtained.

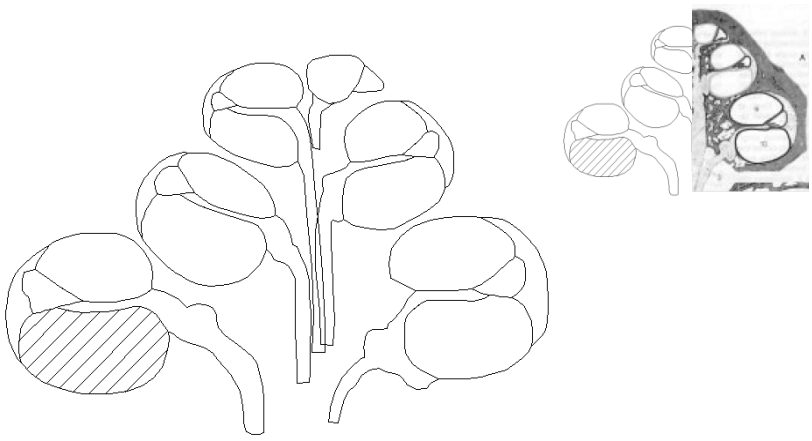

Figure 2.7: The trace of each chamber in the cochlear cross-section

The length of the cochlea was approximated by a helix going through the cochlear partition, through each cross-section in the image. The length was defined as being along the centre of the basilar membrane, as is conventional in modelling the mechanics of the cochlea. The length was around 32 mm so this was extended by 3mm at the base to make the length equal to 35 mm, the usually quoted length of the basilar membrane (Hanekom, 2001). Note that in section 2.7, the length measured along the inner curve at the spiral ganglion in Figure 2.37 is 11.05 mm and it is this which is important in defining excitation sites. This is discussed further in that section. The areas of the various fluid chambers and the width of the cochlear partition, obtained from the trace in Figure 2.7, are shown in Figure 2.8 and are in agreement with (Thorne et al., 1999).

These areas were used to calculate the equivalent segment of a circle to represent the top chamber and bottom chamber, while the chord that subtends these segments is equal to the cochlea partition width at that point along the length of the cochlea, as described in Appendix C.

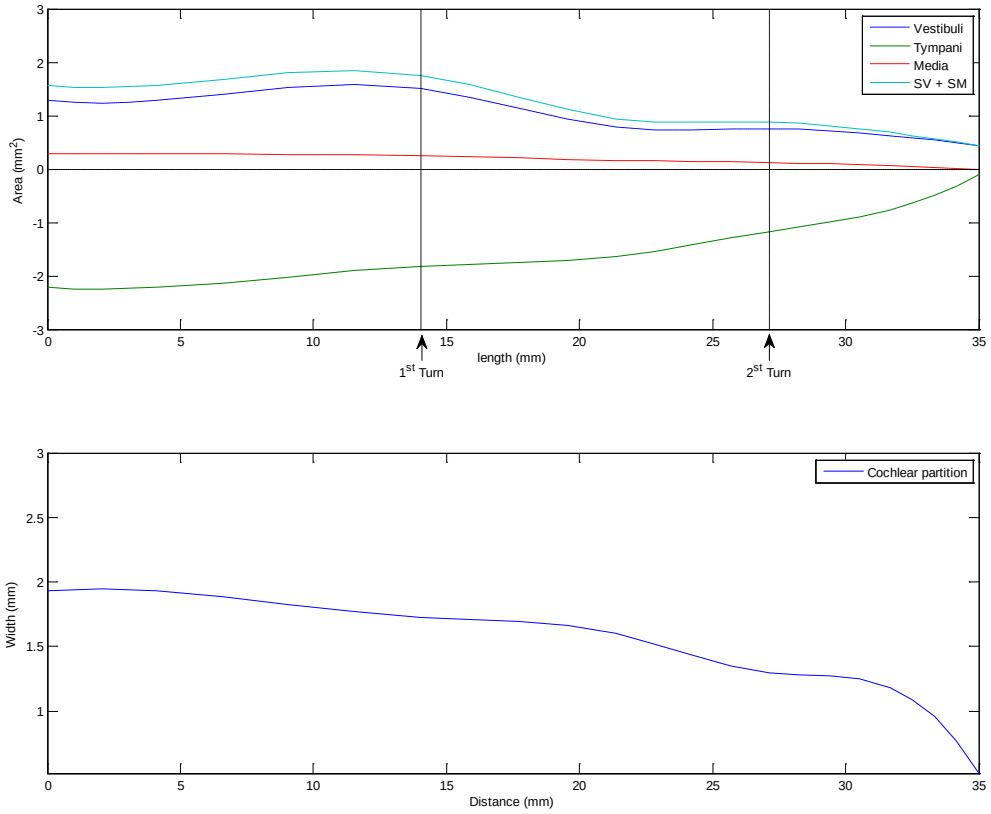

Figure 2.8: Plot of varying cross-sectional areas of the fluid chambers and the width of the cochlear partition along the cochlear length, taken as the length along the centre basilar membrane – light vertical lines correspond to end of the 1st and 2nd turn in the spiral structure.

The result is a set of numbers describing several cross-sections along the length of the cochlea which can be used to build the model. However, further detail is required to give better shaping of the curvature of the cochlea in both the straight and coiled model. This is achieved using a spline function, implemented in Matlab, to estimate the values for cross-sections at quarter intervals to those already calculated above, which gives 4 times the resolution. This extra data is applied differently in the straight and coiled models during the modelling phase, but is mostly useful in the coiled cochlea. The spline calculation is described in Appendix D.

The structures in the cochlea are characterized by resistivity values that describe the resistance of the material. Resistivity values were obtained from Finley et al (1990),

Hanekom (2001), Briaire and Frijns (2000) and Rattay et al. (2001) and the final selection is listed in Table 2.1. The basis on which the selection was made is discussed in appendix E.

Material	Resistivity (Ωm)
Electrodes	0.001
Silicon	10.1
Endolymph	0.6
Perilymph	0.7
Basilar membrane	37.5
Reissner's membrane	500
Bone	6.41
Organ of corti	83
Stria Vascularis	188

Table 2.1: Resistivity values for the cochlear structures. Sources: (Finley et al., 1990, Hanekom, 2001, Briaire and Frijns, 2000, Rattay et al., 2001)

2.4.2 Electrode Array Geometry

The main varieties of cochlear implants include a standard length electrode array (approximately 22 electrodes) for complete hearing loss, and a short electrode array for high frequency hearing loss. The latter is usually referred to as electro-acoustic stimulation.

As well as different types of electrode arrays, there are several cochlear implant manufacturers that have their own configurations involving the number of electrodes, their size and positioning.

The cochlear implant array considered in this thesis is manufactured by Cochlear Corporation and is based on the Nucleus 24 Contour & Contour Advance electrode array, as shown in Figure 1.5. The electrode array geometry used in this thesis is shown in Figure 2.9.

The datasheet for the Nucleus 24 electrode array is reproduced in Appendix F, but some measurements were either unclear or missing. Any missing geometrical data was extracted in similar way to that of the cochlear structures, by measuring a large feature of the real implant, such as the magnet, then taking a picture of the cochlear implant on a flat surface. This was imported into AutoCAD and scaled using the large feature as a reference. Once resized correctly, measurements of any missing dimensions were taken. The main

dimensions of the implant are listed in Table 2.2 and illustrated in Figure 2.9. The point at which the cochlear implant is at maximum insertion length is referred to as the insertion point, and this is represented by three small bumps on the silicon carrier, as shown in Figure 2.9.

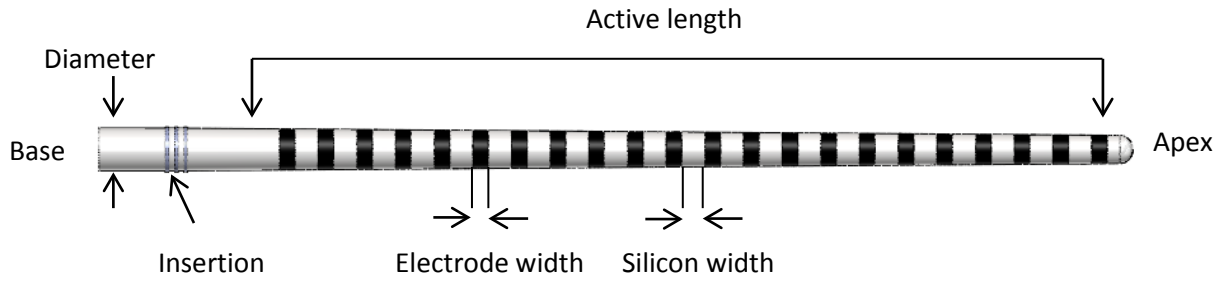

Figure 2.9: Electrode array geometry

Parameter	Length (mm)
Overall Active Length	16.5
Electrode Width	0.3
Silicon Width	0.45
Diameter of Silicon Carrier	0.8 – 0.5 (Base – Apex)

Table 2.2: Electrode array geometry.

2.4.3 Method of construction

This section will discuss the general method used to build the cochlear models. The target is to construct a reasonable model of the cochlea using Solidworks with a reasonable level of detail, while ensuring that the model can then be exported into Comsol for analysis. The cochlear model was constructed using a combination of solids and surfaces. These solids and surfaces were generated using tools that refer to a combination of sketches and guide curves. The sequence used is to create a solid by drawing the cross-section of the solid and using a function to extrude that cross-section into the third dimension. This can also be guided by a guide curve if further control of the direction of the extrusion is required. The sketch is not always the cross-section of the solid, but can be anything that relates to a part of the solid. Complicated structures are usually created using several sketches and guide curves.

It was decided that the best way to model the structures present in the cochlea was to construct the outline first, as a whole solid along the length of the cochlea, and then to split this into the relevant sections using surfaces. This is the cleanest, most error-free way, to achieve the structures in the cochlea that meet perfectly at the boundaries and follow the outline shape exactly. The sketches consisting of the cross-sections, as a result of the spline calculations, were calculated for every quarter of a turn. The guide curves were generally constructed by linking corresponding points on each of these cross-sections using a curve function. The positioning of these cross-sections depends on whether it is a straight or coiled model. The different cases are discussed in sections 2.5, 2.6 and 2.7 for the uniform, non-uniform and coiled models respectively.

The outline solid was generated using the loft function, which requires input features such as sketches and guide curves. The surfaces used to split the outline structure can be created in two ways. One way is much the same as lofting solids, but instead, a surface is lofted based on the sketches and guide curves. The sketches used here are usually lines as opposed to cross-sections. In cases where this does not work or is not reliable enough, the second way is to use existing edges in the model to create a surface. This uses the boundary surface tool which requires identification of the edges that bound the surface in two directions. The loft of the outline and surfaces are demonstrated in Figure 2.10.

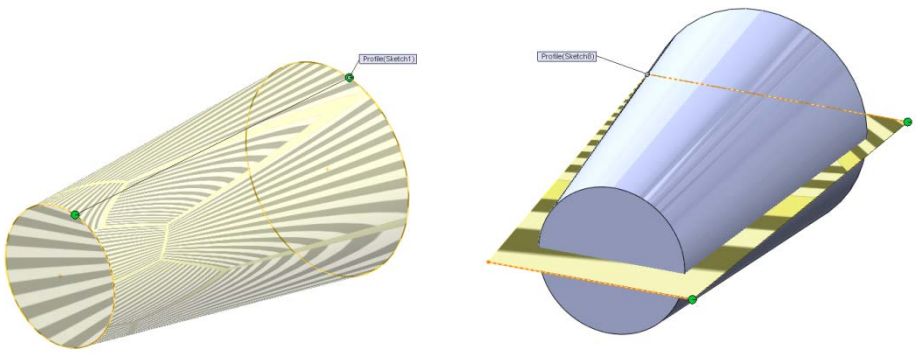

Figure 2.10: Examples of lofting and using a surface to split a solid.

Different relations are used in sketches depending on what is being constructed. In this thesis there are two types of models, one which requires defining the curvature along the length and one which does not. For the latter case, constructing the cross-section and simply extruding this is all that is needed. In this case coincident relations are sufficient to lock the cross-section of the structure in position relative to the origin. In the former case, pierce relations are required. There is a specific order of build for this to work. First the

guide curves that define the curvature must be produced based on a series of reference points or sketches. The cross-section sketches can then be constructed and linked to the curve on their respective planes using pierce relation. This means that the point on the cross-section within which the curve passes through is strictly paired with the curve at that point on that plane. Therefore, when the solid is lofted from cross-section to cross-section along the guide curves, the solid generated will strictly adhere to the guide curves. If this relation is not applied then it can cause miss-alignment issues between the outline solid and the surface that will split it.

The electrode array was also built using sketches, guide curves and solids. The technique is similar to how the cochlear structures were created. The exact method of construction depends on whether the model is straight or coiled, but any differences are described in the relevant sections later in this chapter. In general, a number of planes and therefore sketches were constructed along the length of the cochlea. These cross-sketches included a single point, which were joined by means of a curve function to create the central line of the cochlear implant. At the start of the curve, a circular cross-section representing the implant was created with the starting thickness of the implant. From this a surface was created. This surface was then repeated using the pattern tool, one at a time, at a specified distance depending on whether it was to represent an electrode or silicon partition or otherwise. A plane was created on that new surface, on which the next circular cross-section of the implant was created. This cross-section had slightly altered geometry to represent the variation of the implants silicon carrier thickness. This was used to create a new surface and the cycle was repeated itself until you have enough cross-sections and surfaces to represent the full electrode array. A lofting function was then used to create a solid through all the circular cross-sections. This gives a long tube with a continuously varying thickness. The surfaces that were created in the process can now be used to split the tube into sections representing the electrodes and silicon partitions. This procedure is demonstrated in Figure 2.11.

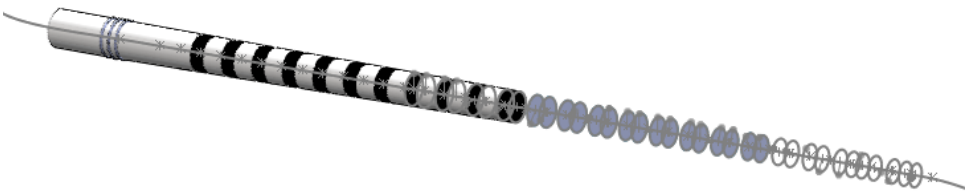

Figure 2.11: Electrode array modelling procedure

Once the geometry is created, the next step is to transport the model to Comsol Multiphysics for finite element meshing and simulation. The above techniques have described the general method of generation of cochlear and implant geometry. The next few sections will discuss in further detail how the techniques were used in building different types of models.

2.5 Straight uniform model

2.5.1 Building the model

The first model constructed to model the spread of current due to an electrode array was of a uniform uncoiled cochlea. The model is simplified by using a cylinder to represent the cochlea. The simplicity of this model allowed the efficient investigation of several effects, as discussed in the subsections below. This cylinder includes the scala vestibuli, scala tympani and the basilar membrane. The width of the basilar membrane was assumed to be uniform along the axis and equal to the measured cochlear partition width at the basal end of the cochlea. The scala vestibuli and scala tympani were assumed to have the same area, equal to half the total of the cross-section area of the cochlea at the basal end. The area is represented by a semicircle. The cross-sectional areas of the scala chambers are uniform along the length of the basilar membrane.

The model is built using the technique outlined in section 2.4.3. A template sketch was drawn according to the dimensions calculated from the measured geometry represented in Figure 2.8 consisting of the cross-sectional areas of the three structures. On the same plane, a sketch of the outline is constructed. The sketch was then extruded to form the outline solid. Two surfaces were extruded along the length of the basilar membrane to split the outline solid into three separate structures that will now represent the three structures in the cochlea. The outer bony shell of the cochlea is represented by a cylindrical solid within which lie the three solids. The size of the outer bony shell is such that the total volume is $1cm^3$, which is equivalent to the volume of bone within which the cochlea exists. The resulting cochlear geometry is shown in Figure 2.12.

The electrode array was constructed using similar techniques are mentioned in section 2.4.3. This was based on the Cochlear Nucleus Implant. Since this is a straight model, the planes and sketches containing the points that represent the centre line of the electrode array were constructed in a straight line. Sketches and planes were then

constructed along the length of that centre line, defining the cross-section of the array's silicon carrier. Once the outline of the array was lofted, planar surfaces were created using these sketches, and these surfaces were used to split the outline into the respective electrode and silicon solids. The electrode array was positioned near the centre of the scala tympani with the centre line positioned at a fixed distance from the basilar membrane along the length of the model. The resulting electrode array is shown in Figure 2.12.

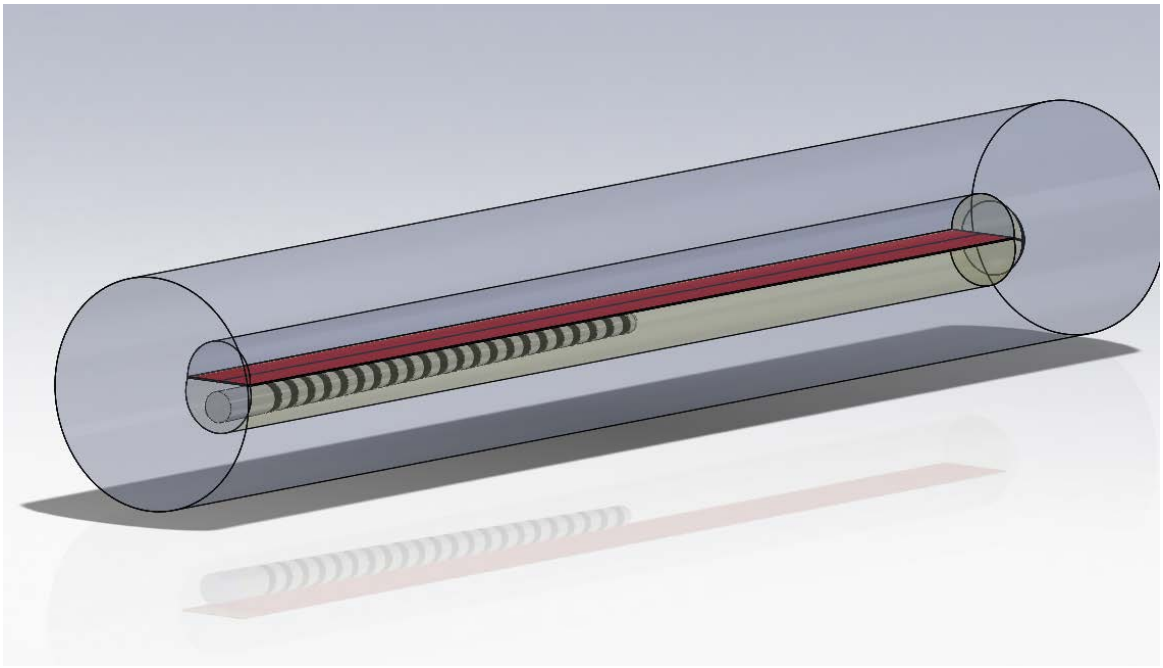

Figure 2.12: Uncoiled uniform model. The outer blue cylinder represents the extent of the bone.

The solids are now imported into Comsol Multiphysics. In Comsol, the solids can now be meshed and a physics environment can be applied with certain boundary conditions. The boundary conditions and material properties will reflect the particular case. The mesh is usually unchanged for a particular geometrical state of the cochlea. The material properties are defined as resistivities, using the values in Table 2.1.

The boundary conditions define where the current source is (the electrode), the grounded surfaces (reference electrode) and any other boundary conditions required for a particular situation, such as electrical insulation between the silicon sections and the electrode. The boundary conditions used in this model are listed below in Table 2.3. Results for the voltage distribution along the electrode array are shown in Figure 2.13.

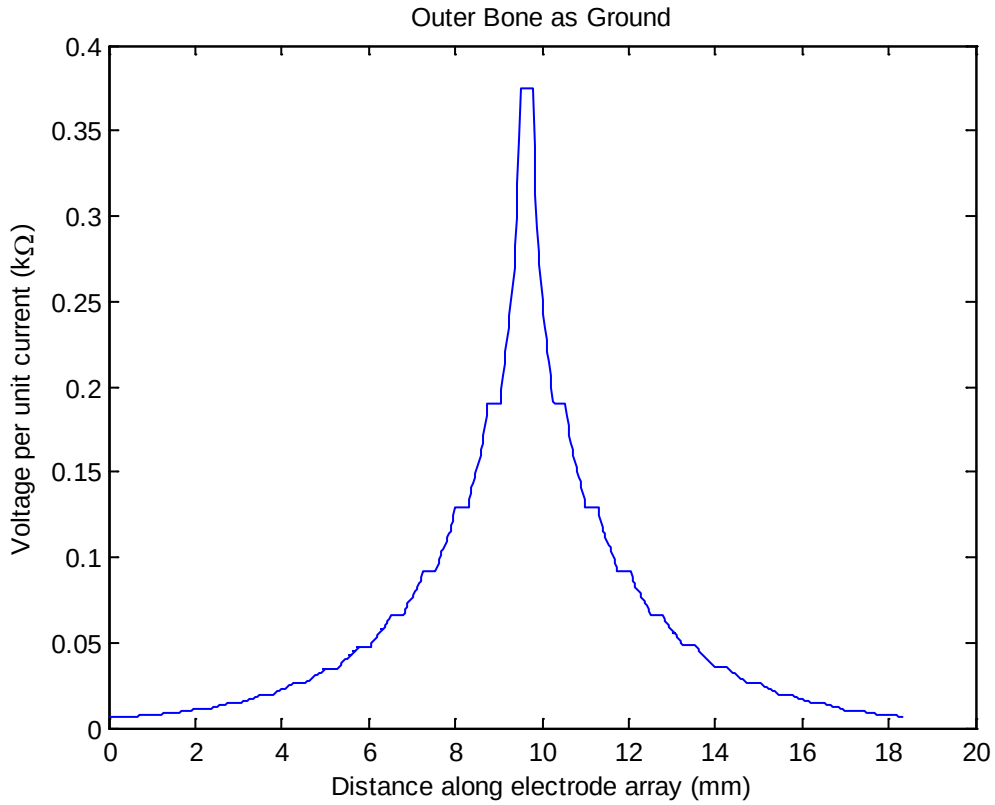

Figure 2.13: Voltage distribution when exciting the 11th electrode for outer bone ground boundary condition.

Boundary condition	Location
Reference Ground	Outside surface of the bone compartment
Current Source	A current density is set for the curved surfaces of the electrode being stimulated.
Insulation	The circular surfaces enclosing the electrode being stimulated
All other surfaces	Set to continuity

Table 2.3: Boundary condition setup in the finite element software Comsol MultiPhysics.

2.5.2 Effect of reference electrode position

In general, the reference electrode is positioned some distance away from the cochlea and provides a return path for the current. In the case of the Nucleus Contour Advance electrode array, there are two reference electrodes. One is a plate electrode built into the

receiver stimulator and the other is a much smaller ball electrode (1mm diameter) attached to the end of a lead from the receiver stimulator, as shown in Figure 1.4 in chapter 1. Both the ball electrode and the receiver stimulator are placed under the temporalis muscle on the outside of the temporal bone, but their exact position is variable but the average distance that the current travels from active to reference electrode is estimated to be approximately 4 cm, as measured from a skull replica, biased to one side of the cochlea. The other side of the cochlea is separated from the rest of the brain by thin bone. Figure 2.14 below demonstrates the bone compartment suggested. In the case of the Contour Advance electrode array, the most common type of stimulation configuration is to have both reference electrodes active as ground. This is referred to as monopolar stimulation, MP(1+2), where 1 refers to the ball electrode and 2 refers to the plate electrode. This configuration of reference electrodes is modelled using the configuration shown in Figure 2.14. Figure 2.15 demonstrates the voltage per unit current (impedance) distribution due to this configuration for the stimulation of the 11th electrode.

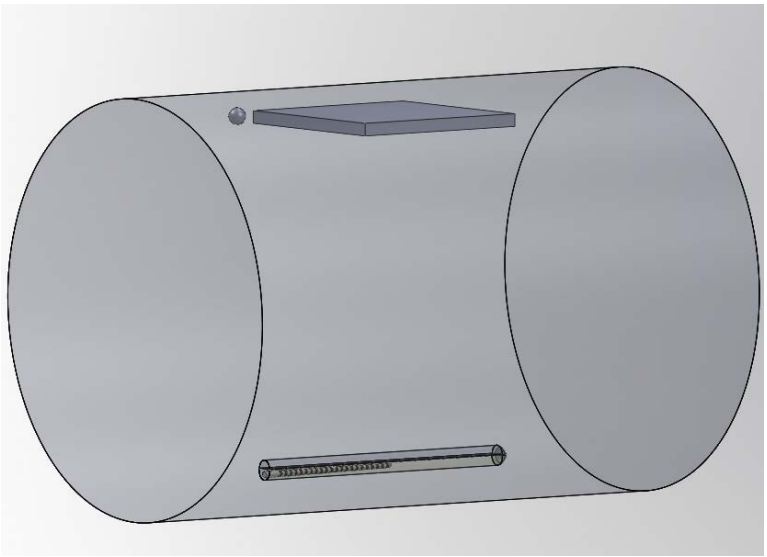

Figure 2.14: Alternative bone compartment geometry with reference electrodes.

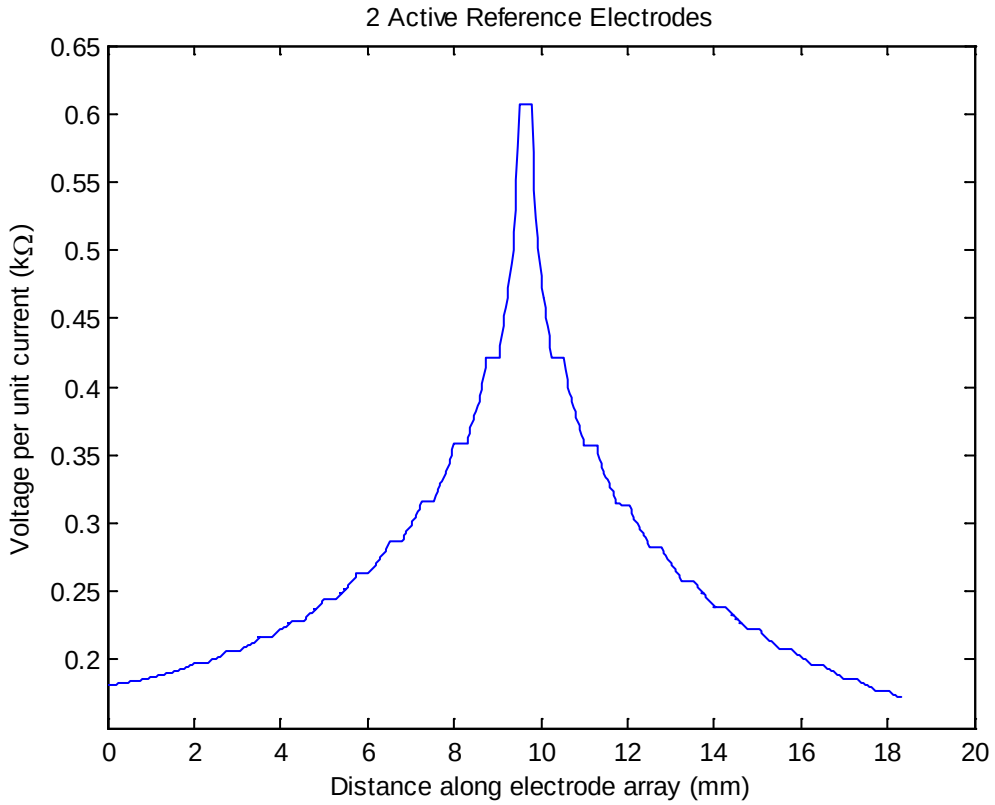

Figure 2.15: Voltage distribution when exciting the 11th electrode for 2 activated reference electrodes.

The voltage distribution in Figure 2.15 is very similar to that in Figure 2.13, apart from a change of scale.

It is, therefore, possible to represent the two reference electrodes by setting the external surface of the bone compartment to ground, rather than defining a reference electrode in later variations of the model in the thesis.

2.5.3 Effect of mesh size

The effect of the mesh size on the predicted results can now be investigated. Standard mesh configurations, built into Comsol, were used and adapted where necessary to ensure that the minimum element size was compatible with the geometry of the model. The free tetrahedral mesh type was used as in Figure 2.16. Three meshing resolutions were initially tested: coarse, average and fine. The resulting geometry meshes consisting of approximately 240000, 480000 and 770000 elements and the detail at the end of the electrode array is shown for these in Figure 2.17.

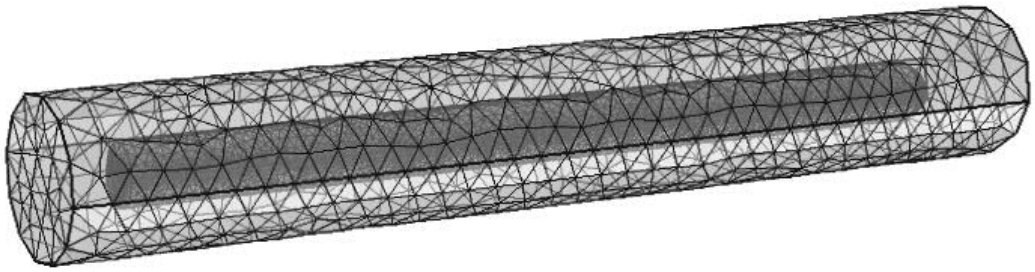

Figure 2.16: The complete mesh of the uniform uncoiled model with an average mesh size.

Basilar Membrane view

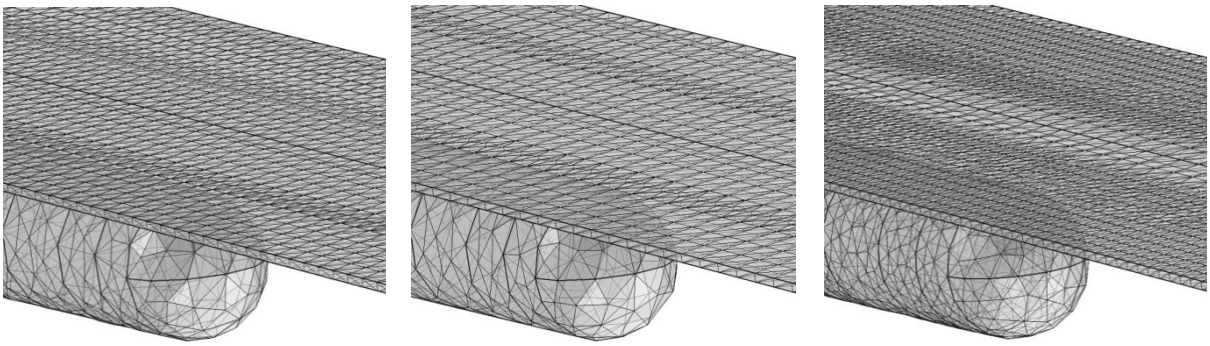

240,000 Coarse

400,000 Average

770,000 Fine

Figure 2.17: An enlarged view of the basilar membrane mesh for the three mesh sizes respectively to illustrate the difference visually.

The model was solved using a linear stationary solver. The electrode array is stimulated one electrode at a time and a solution for the voltage field is plotted for this stimulation. The overall excitation for one such electrode stimulation is shown in Figure 2.18. The excitation spread along the length of the basilar membrane is also measured at the centre of the basilar membrane.

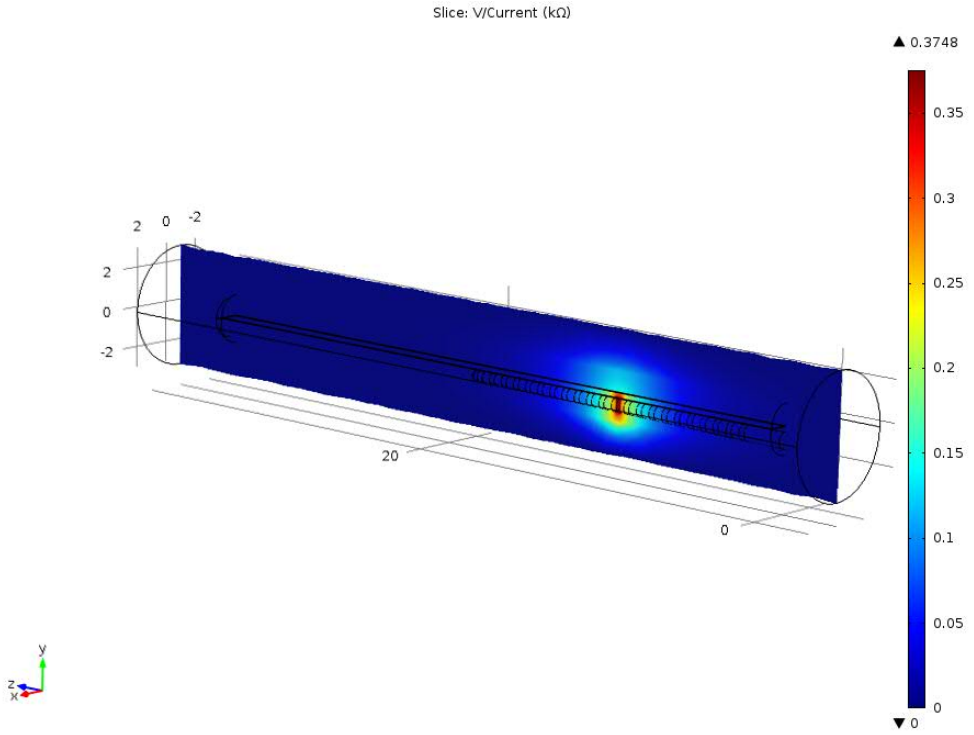

Figure 2.18: Overall voltage spread due to central electrode stimulation

The resulting voltage distribution is plotted in Figure 2.19 for the three mesh sizes, in ascending order. The results in Figure 2.19 are very similar to the uniform distribution shown in Figure 2.3, however, the electrode array is not symmetrically placed and does not give such a uniform spread as the uniform cable model. The voltage distributions are almost identical in all three cases, implying that a variation in the resolution of the mesh has negligible effect on the outcome. This conclusion holds as long as the resolution is not reduced to a value significantly lower than the coarse mesh resolution. In general, the greater the mesh resolution is, the smaller is the element size, which would increase the calculation accuracy. At some point, however, for the very fine mesh resolution the computing time increases significantly, and there is the danger of numerical ill conditioning. For all models presented in this thesis, a mesh resolution is chosen such that it is fine enough to give accurate results but still only requires reasonable computation time.

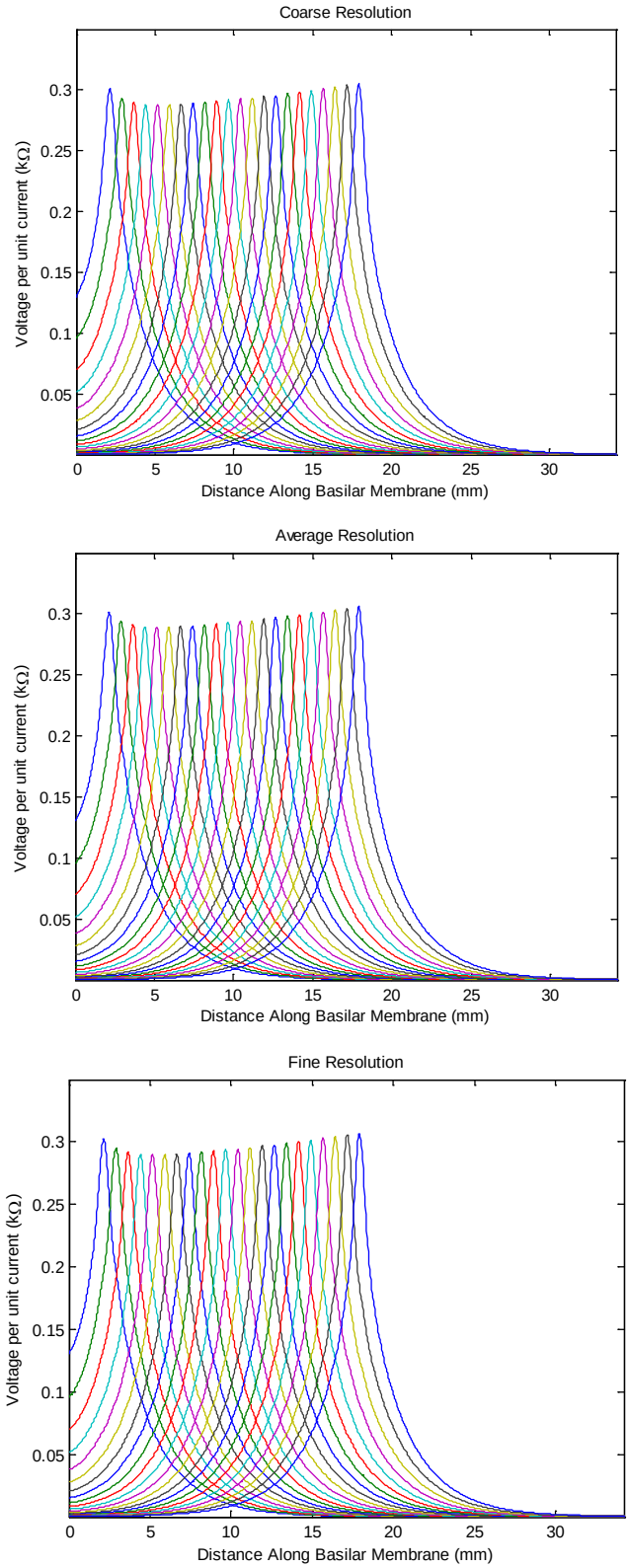

Figure 2.19: Voltage distribution along the basilar membrane with varying mesh resolution

2.5.4 Prediction of the impedance matrix at the electrodes

Figure 2.20 below shows the impedance matrix, measured only at the array electrodes, for this uniform uncoiled model.

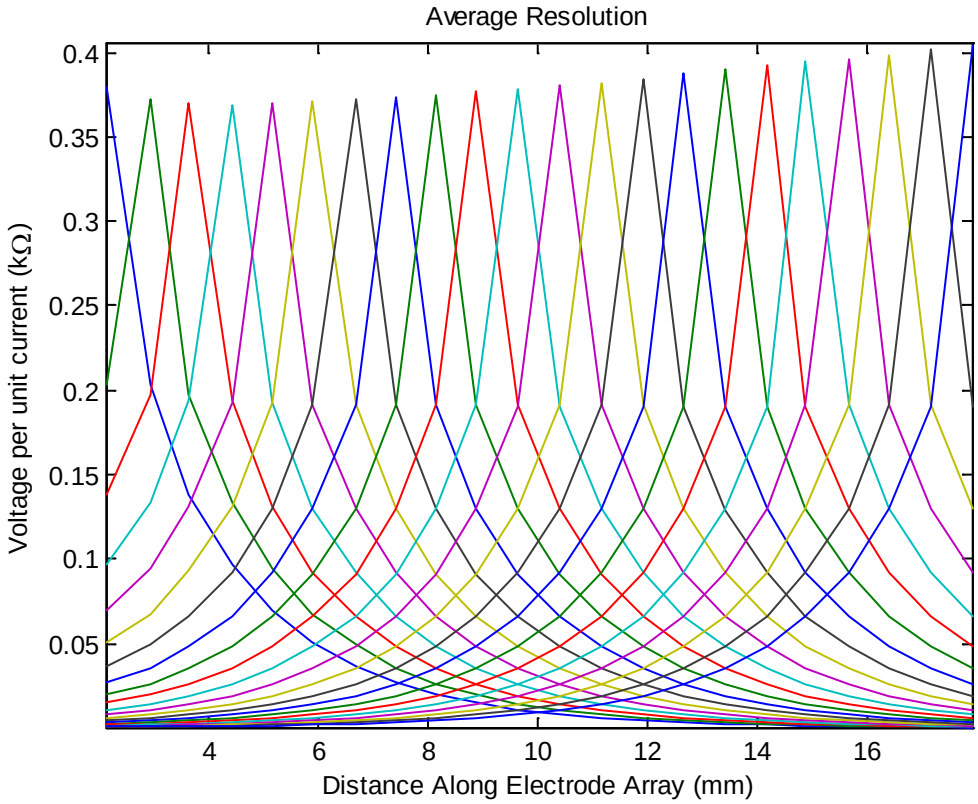

Figure 2.20: Electrode impedance matrix (kΩ)

This can be compared to the impedance matrices for both the experimental results published by van den Honert and Kelsall (2007), shown in Figure 2.1 and the theoretical matrix calculated from the cable model, shown in Figure 2.3.

Patient data presented in chapter 4, reports an impedance for monopolar stimulation within the range of 6 to 12 kΩ. This is in agreement with (Tognola et al., 2005, Hanekom, 2005, deSauvage et al., 1997, Rohr, 2011, Dorman et al., 1992). The impedance values presented in this thesis, as in Figure 2.20, peak at around 0.4 kΩ and are within the order of magnitude reported by van den Honert and Kelsall (2007). The reason for this difference in the impedance magnitude is thought to be the omission of the electrode-tissue interface, which is not taken into consideration in this thesis or in the investigation by van den Honert and Kelsall (2007), as acknowledged in section C of their paper, and in

the investigation of the encapsulation layer impedance by Hanekom (2005), as acknowledged in section 4 of that paper.

This interface impedance may be due to a number of factors, including, one factor as reported by Hanekom (2005), the encapsulation tissue that surrounds the electrode array. Fibrous scar tissue growth and ossification (bone growth) can occur in the first few months after implantation, resulting in a layer encapsulating the electrode array, contributing a resistance in the order of hundreds of ohms. This impedance also forms part of the electrode-fluid interface impedance discussed by deSauvage (1997) and Aran and Erre (1977). The electrode-fluid impedance was measured using non-invasive extracochlear stimulation in a guinea pig, and this study gave an average impedance of approximately 12.5 kΩ ranging between 10 to 20 kΩ.

The effect of such an interface could be represented in the model in this chapter by surrounding the electrode array with a thin highly resistive sheet, the geometry and the effect of which are demonstrated in Figure 2.21 and Figure 2.22 respectively. In this case, the layer is assumed to be uniform, of thickness 0.5 mm and resistivity 1000 Ωm giving a resistance of approximately 20kΩ in agreement with Hanekom (2005) and deSauvage (1997). The results in Figure 2.22 have a very similar shape to those predicted without this thin interface, as in Figure 2.20.

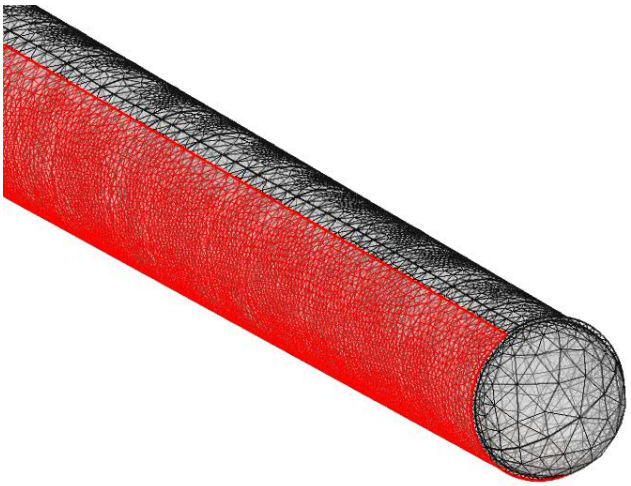

Figure 2.21: Thin electrode tissue interface layer, represented by the red surface. The layer is semi-visible to show the electrodes.

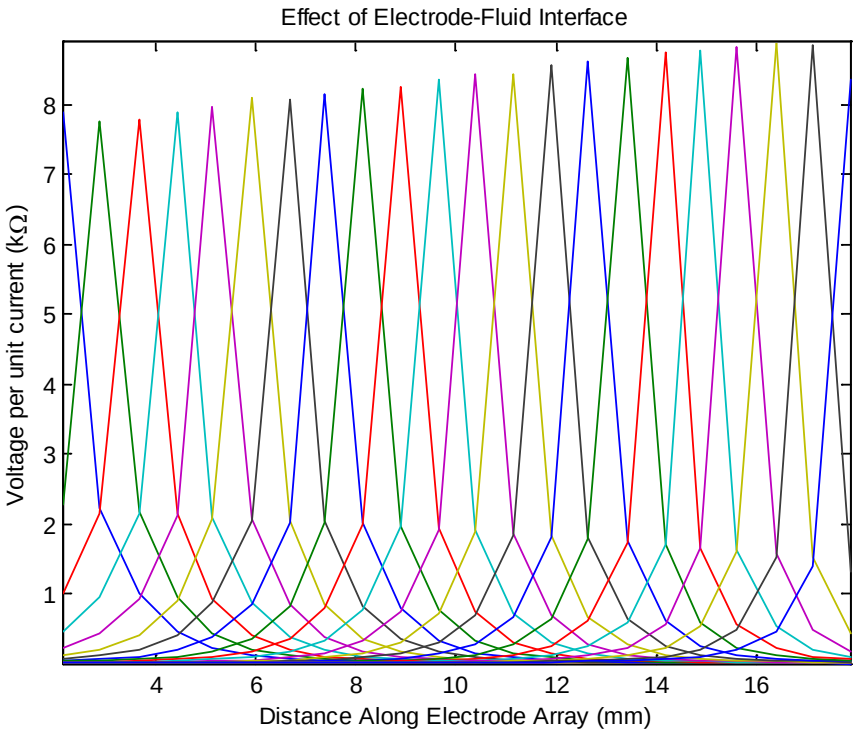

Figure 2.22: Effect of electrode-fluid interface on the impedance distribution

Therefore, the model presented in this thesis can be used to reasonably predict the geometric properties of the impedance distribution through the cochlea, even though the

resulting magnitudes are somewhat lower, and so this complication is omitted from the models described below.

2.5.5 Voltage distribution away from the cochlear implant

The model can also be used to calculate the excitation spread along any line, across any surface or indeed for the entire domain or sub domains of the model. Figure 2.23 shows the overall spread along the cochlea, zoomed in to show the stimulating electrode and the effect on the surrounding structures and fluids, namely the resistive basilar membrane.

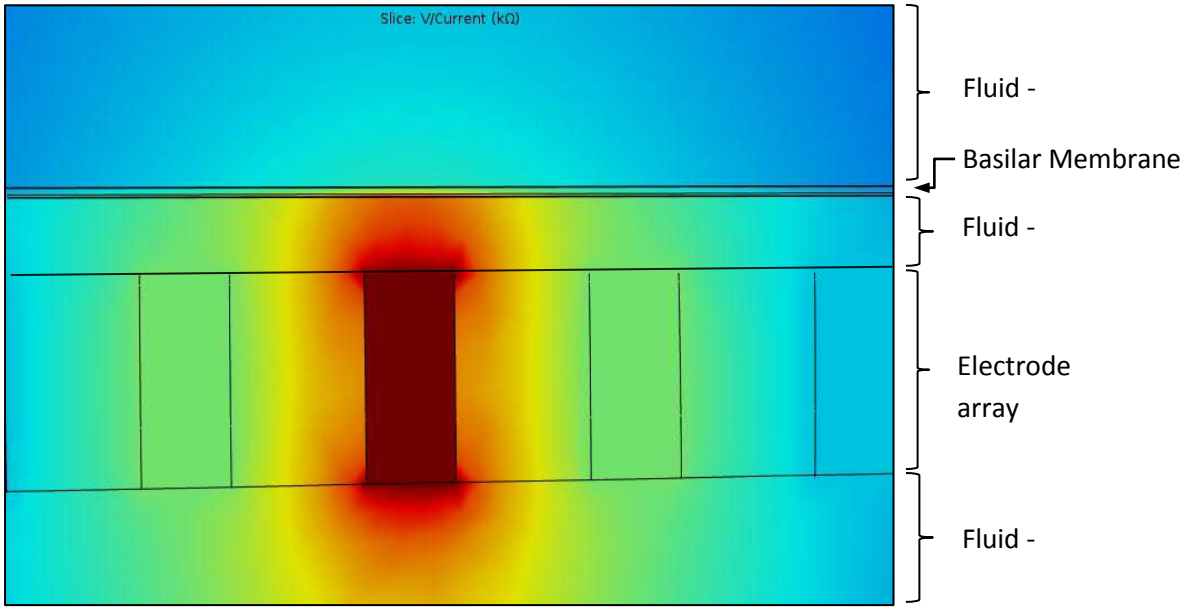

Figure 2.23: Spread of excitation perpendicular to basilar membrane zoomed close to the electrode array (v / i (kΩ)).

It is apparent that as the excitation passes through the basilar membrane, the voltage drops dramatically. This is because the resistivity of the basilar membrane is much higher than that of the fluid. The effect can also be illustrated if the excitation spread is plotted along a line down the middle of the basilar membrane on the scala tympani side or the scala vestibuli side, when each electrode is individually stimulated, as shown in Figure 2.24 and Figure 2.25.

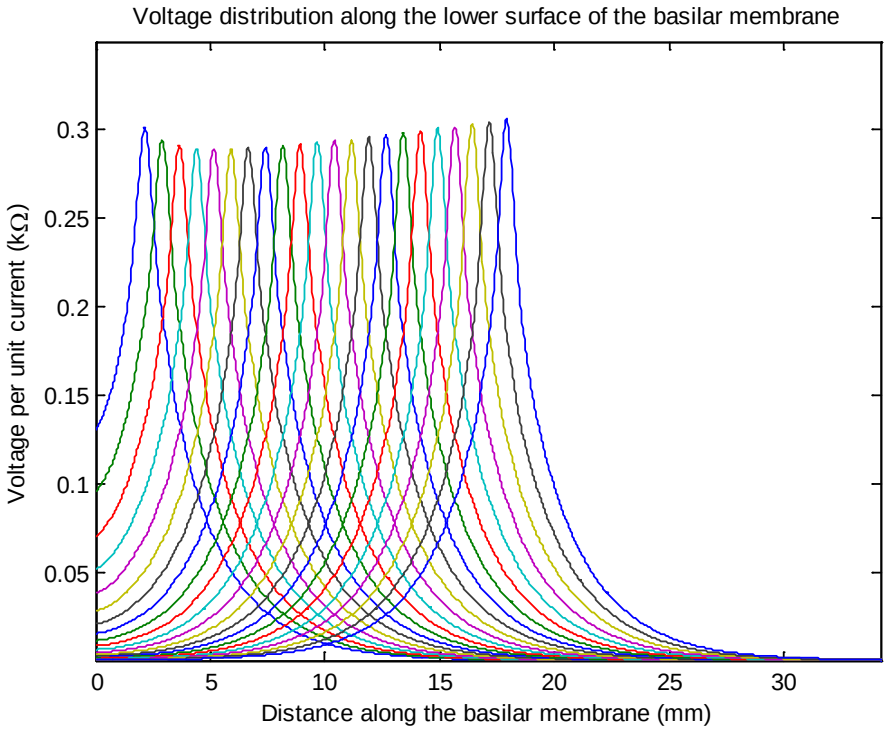

Figure 2.24: Excitation spread on the *lower* surface of the basilar membrane when each electrode is activated separately.

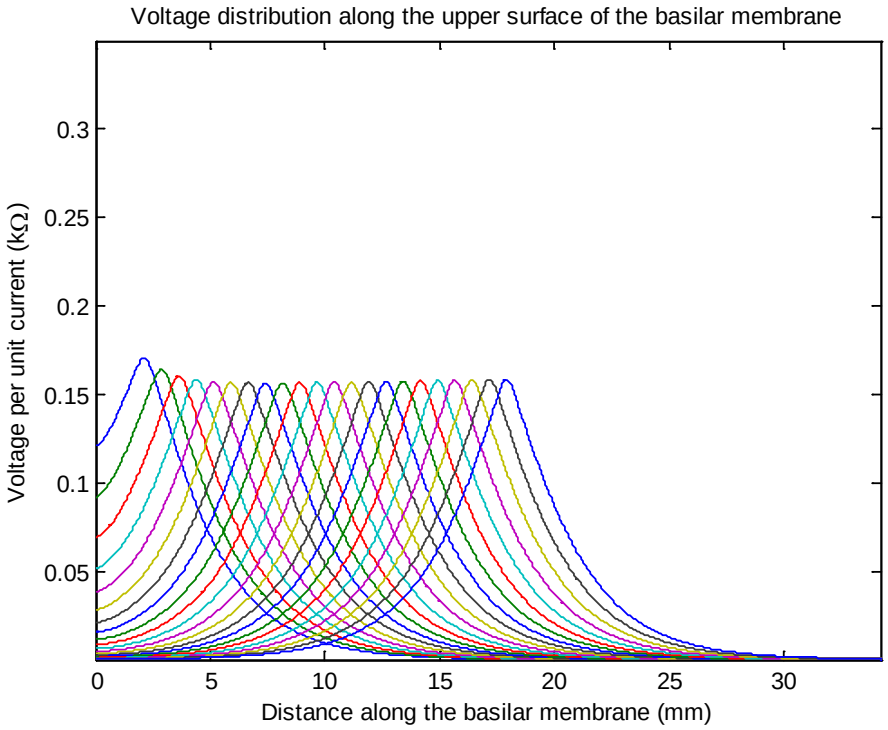

Figure 2.25: Excitation spread on the *upper* surface of the basilar membrane when each electrode is activated separately.

Figure 2.25 shows a similar pattern to Figure 2.24, but the peak values are approximately halved, and the peaks are wider. This effect is due to the relatively high basilar membrane resistance discussed above.

2.5.6 Effect of implant position

The position of the cochlear implant can play an important role in the spread of excitation, especially at the point of excitation. This was investigated by bringing the surface of the electrode array closer to the basilar membrane, from a distance of 0.3 mm to a distance of 0.04 mm, as demonstrated in Figure 2.26 below.

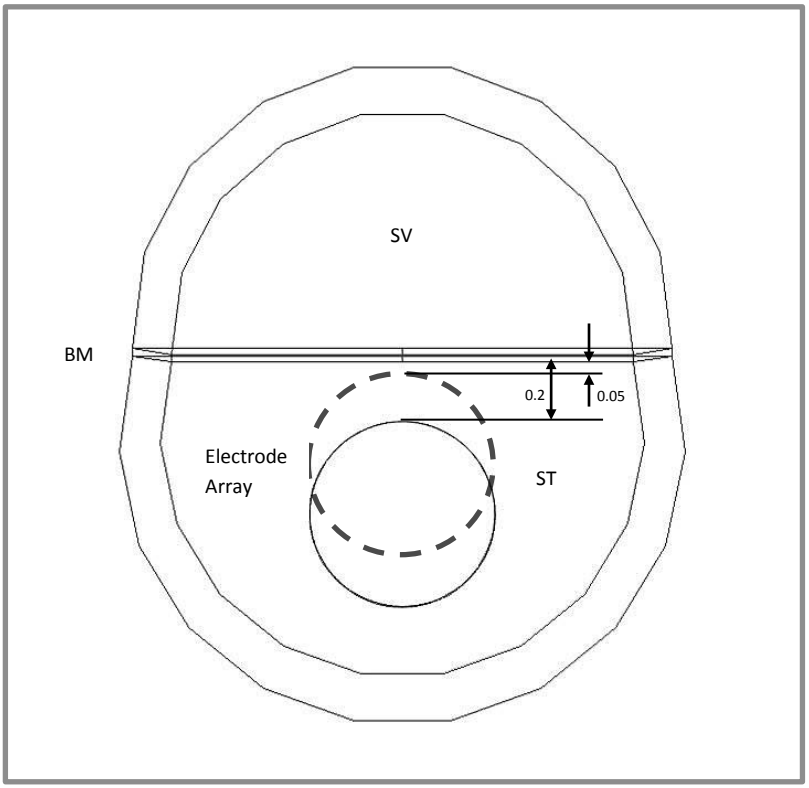

Figure 2.26: Change in distance from electrode array to basilar membrane

All material properties and boundary conditions were kept the same. The effect of stimulating closer to the target region, shown in Figure 2.27, results in a flattened excitation at the peak, where the target nerves lie, but the spread of the excitation at the other electrode positions along the basilar membrane remains similar. The flattening of the excitation is predominantly due to the fact that the excitation current is the same

across the entire surface of that electrode and the close proximity of the electrode surface to the basilar membrane translates this pattern over to the excitation measured at the basilar membrane.

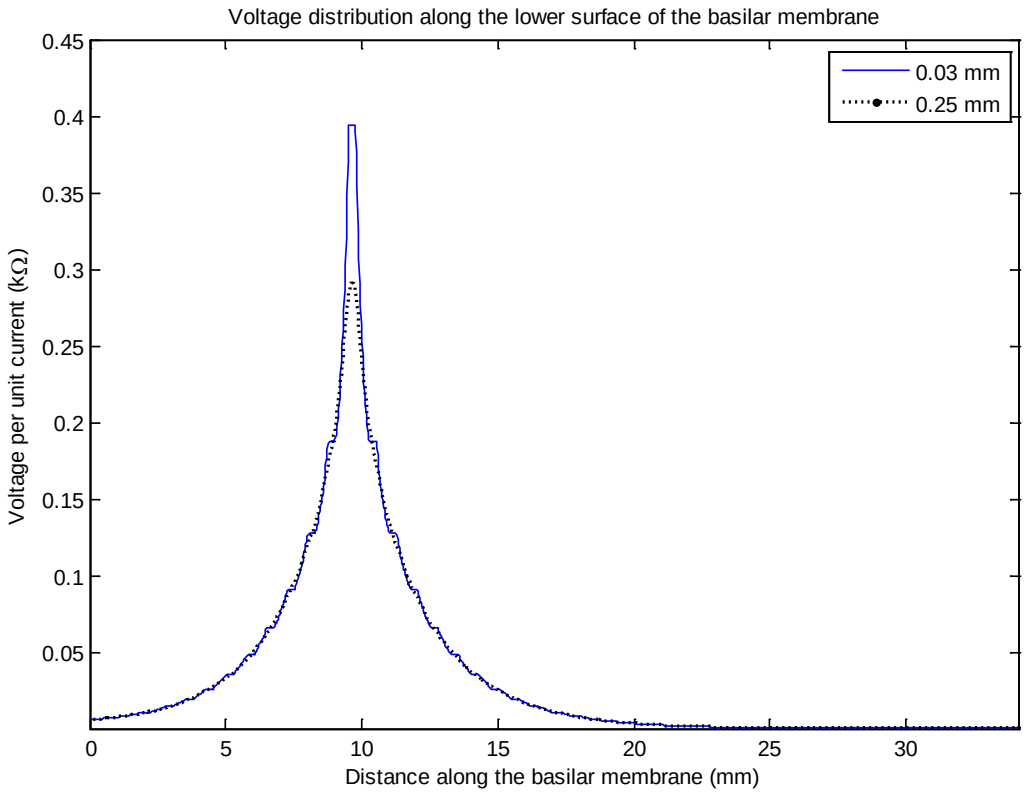

Figure 2.27: Comparison of voltage distribution along the basilar membrane with changing distance between the electrode array and the basilar membrane.

The next model to be analysed is the same as above in terms of structure detail however this time the structures are defined by non-uniform cross sectional areas for the scalae and basilar membrane.

2.6 Straight non- uniform model

The next model investigated remains uncoiled but now the cross sectional area of the scalae and basilar membrane were varied along the length of the cochlea. All other geometries remained the same. The purpose of this simulation is to demonstrate the effect of geometric variation on the variation in resistance in the cochlear structures which ultimately affects the voltage distribution. Resistivity parameters remained unchanged so any resistance variation is solely dependent on the geometry. The cross-sectional areas were measured using Figure 2.5. The method by which this was constructed is discussed in section 2.4.3. The cross-sections representing the cochlear structures were separated at distances equivalent to half a turn in a coiled model. These cross-sections were positioned in a straight line and the centre of the basilar membrane is then centred on that line. The sketches that make up the cross-sections of the cochlear structure are not the direct trace of the image. The cross-sections are represented using segments of a circle for the scala tympani and scala vestibuli, with the chord of both segments equal to the width of the cochlear partition. Calculation and generation of such a sketch is dealt with in Appendix C.

The outline solid was constructed by using a solid loft function from cross-section to cross-section. Surfaces were also created using a surface loft function and were used to split the outline section into the three structures. The electrode array was built in exactly the same way as in the straight uniform model. The basilar membrane was varied in thickness from 0.03mm (base) to 0.01mm (apex) (Skrodzka, 2005a). The model was again embedded in a cylinder of bone, grounded on the outer surface and the model was meshed with approximately 330,000 elements. The geometry of the model is shown below in Figure 2.28 to Figure 2.30.

This was solved using the same mesh and material settings and the same boundary conditions as the previous model and the results are plotted below in Figure 2.31 and Figure 2.32.

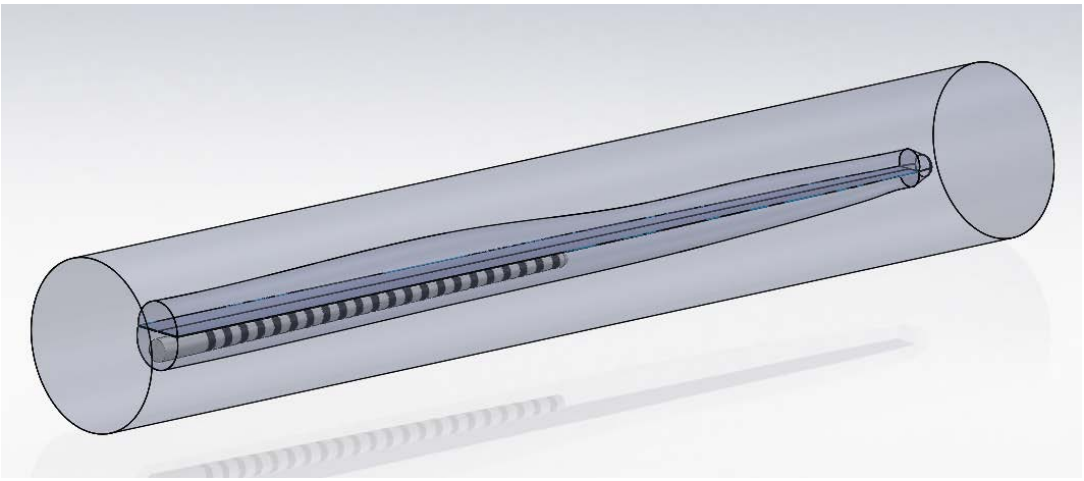

Figure 2.28: Simple geometry of the uncoiled cochlea with non-uniform area cross-sections, where the outer cylinder denotes the bone, with the reference electrodes as the outer surface.

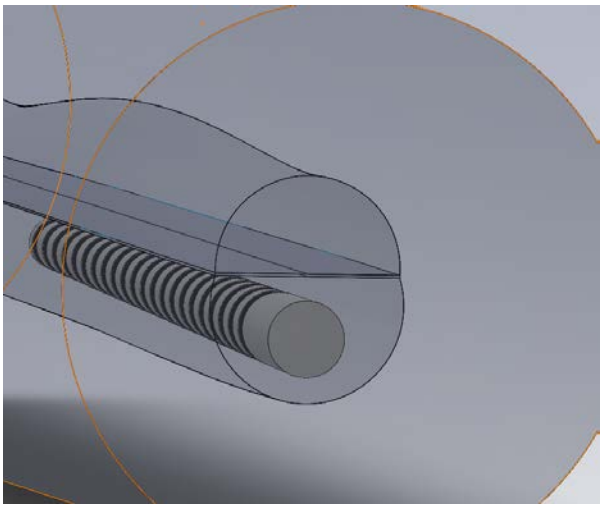

Figure 2.29: A more detailed cross section of the model at the middle showing the scala, the basilar membrane and the electrode array within the bone chamber.

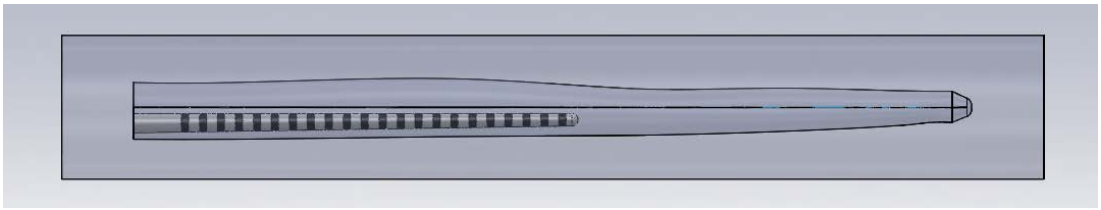

Figure 2.30: Side view of the non-uniform model.

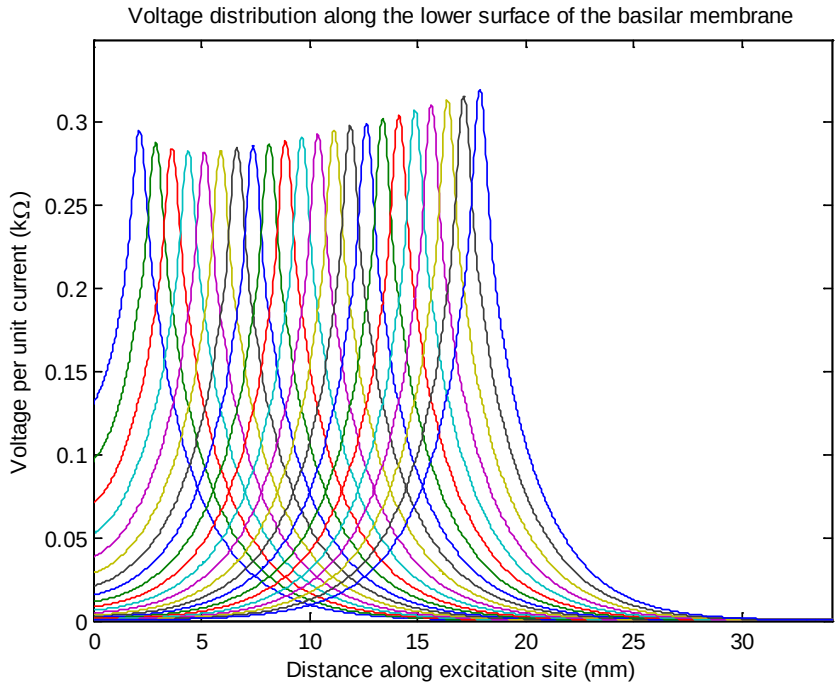

Figure 2.31: Excitation spread on the *lower* surface of the basilar membrane when each electrode is activated separately.

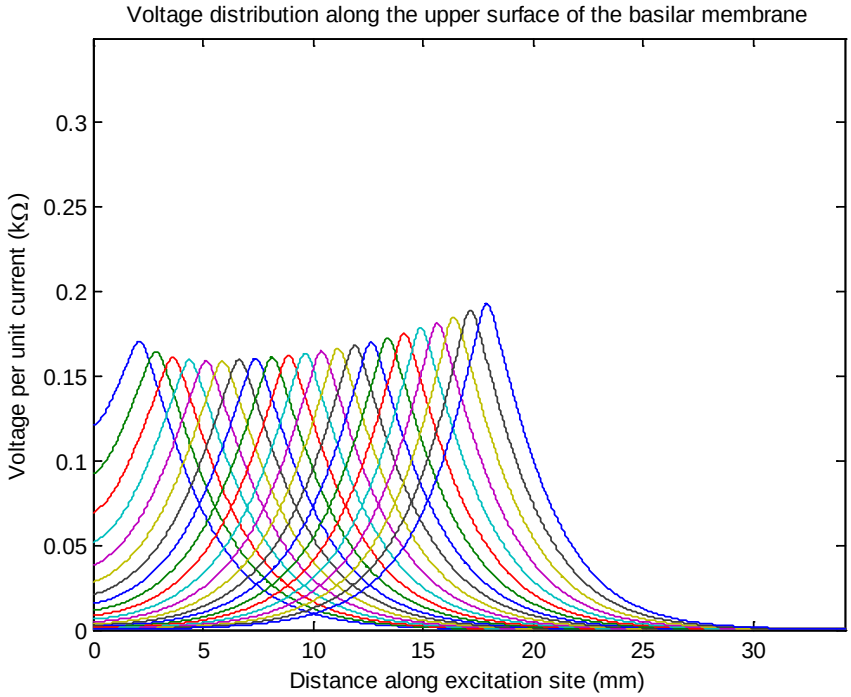

Figure 2.32: Excitation spread on the *upper* surface of the basilar membrane when each electrode is activated separately.

The two results above are similar to what was achieved using the uniform uncoiled model, except that this time the voltage peaks increase along the length of the cochlea, where there is a decrease in cross-sectional area. As the cross-sectional area decreases, the resistance increases and so less current is shunted in the longitudinal direction resulting in higher voltages along the basilar membrane. This is less apparent in Figure 2.33 because the impedance matrix along the electrode array is less sensitive to changes in geometry in the cochlea. The non-uniformity of the peak voltages along the array would lead to non-uniformities in the degree of neural excitation, and consequently implant performance, due to the increased proximity of the electrode to the target neurons.

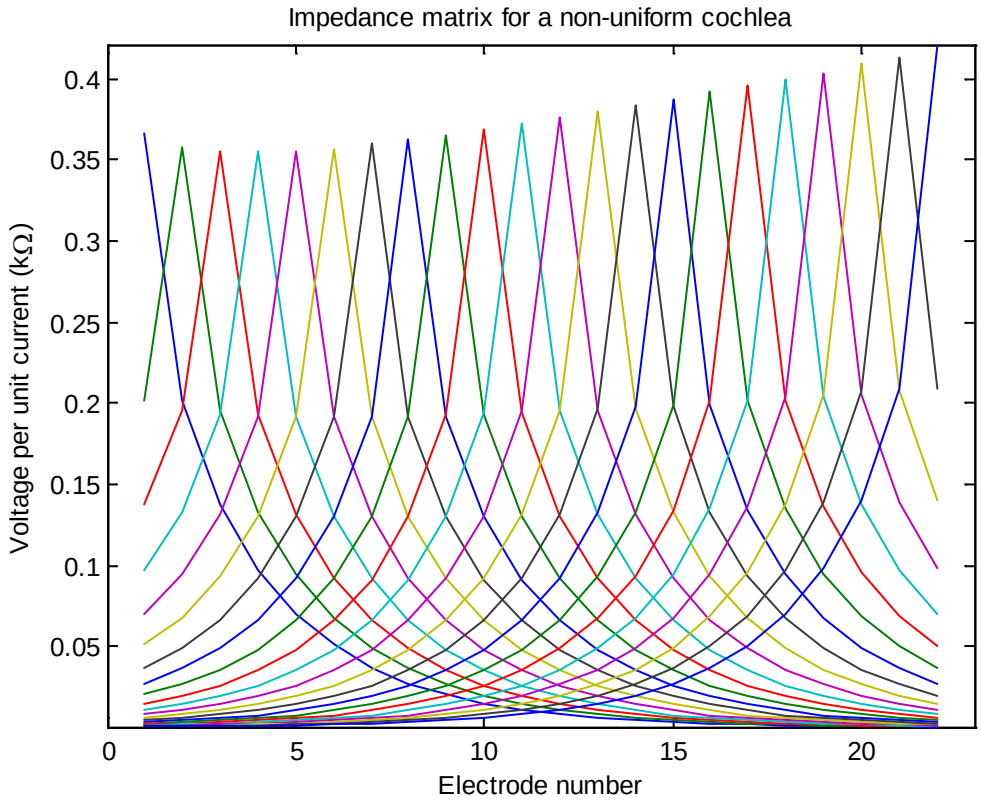

Figure 2.33: Impedance matrix at the electrode position of the non-uniform uncoiled model (kΩ)

2.7 Coiled model

When building a model with a non-uniform cross-sectional area along the length of the cochlea, the geometry could be constructed by drawing a sketch of the cross-section in one plane and extruding this along a set of spiralled curves. This gives rise to two issues.

One is that the spirals would have to be constructed separately and the direction of the curvature in this method is difficult to estimate from cochlear scans. A symmetrical helix could be used, but this would not represent the real curvature of the cochlea. Secondly, the cross-sectional area of the cochlea will vary along the length as in the non-uniform straight model in section 2.6 above. This means that several sketches containing the cross-sections are needed to define the change in cross-sectional area, as in the non-uniform straight model. The sketches would also be used to better define the spiral. `The spiral direction of the coil was constructed based on the positions of these cochlear cross-section sketches. These cross-sections all exist in the same plane, where the plane is defined as going through the centre of the cochlea. This is because the image from which the cross-section information is taken is a mid-modiolar cross-section image. The cross-sections were not spaced at equal distances in the longitudinal direction along the length of the cochlea, because the coil diameter decreases towards the apical end giving a decreasing length for every consecutive half length.

In the non-uniform straight model of the cochlea, the cross-sections were represented within the model by sketches at irregularly spaced intervals in a straight line, whereas in the spiral model, they were represented by sketches that are positioned according to their corresponding positions in the cochlear scan.

The position of each cross-section was found by measuring the horizontal distance from the centre of that cross-section to the centre of the cochlea (modiolus). The vertical distance is the relative distance between each consecutive cross-section. The resulting plane and profiles in Figure 2.34 look similar to Figure 2.7 in the previous section, except that the plane does not include profiles for the nervous system or other structures in the cochlea in Figure 2.7. The sketches that make up the cross-sections of the cochlear structures are not the direct trace of the image as discussed in section 2.6. These sketches also used the pierce relation discussed 2.4.3 to ensure that the solids lofted using these sketches will strictly follow the guide curves that direct the path of the spiral.

The curvature of the model requires more than the single plane available. A guide curve could be created using two perpendicular planes giving 4 reference points per turn, but Appendix D explains why having just 4 points per turn is not accurate enough. Section 2.4.1 and Appendix D discuss the use of spline functions to calculate the estimated areas for every quarter of a turn. This gives 4 planes and 8 reference points per turn in total. Using these four planes a curve was generated by driving a curve through corresponding points from sketch to sketch. This was done by creating a three-

dimensional sketch. A spline curve function was used to create a curve that goes through the corresponding points on each sketch. This is demonstrated in Figure 2.35.

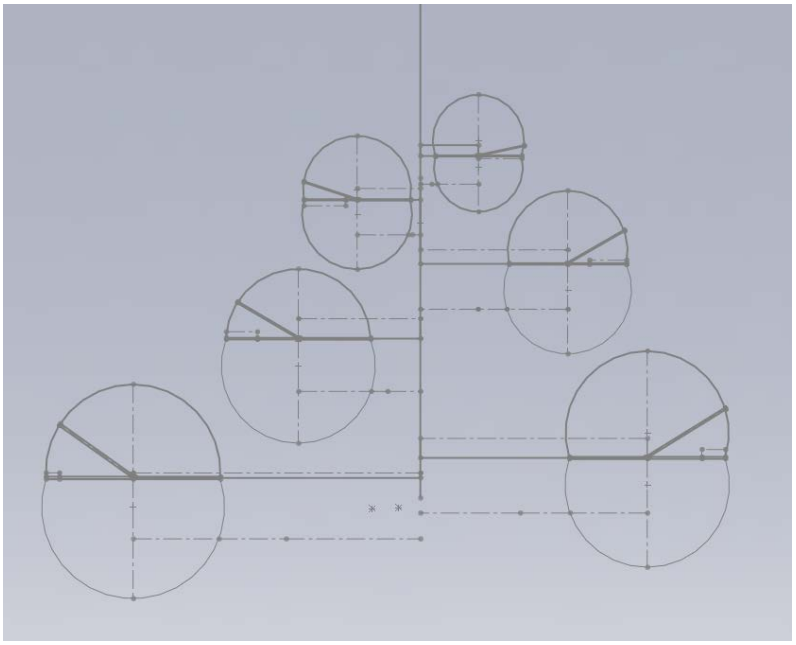

Figure 2.34: Profiles for each structure along the central cross-section of the cochlea

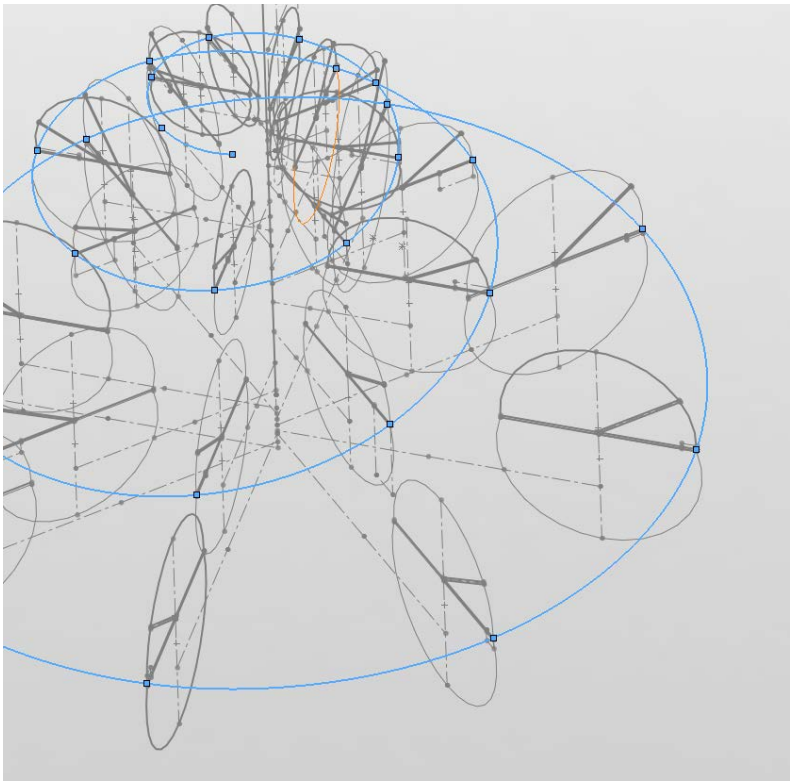

Figure 2.35: Spline curve through corresponding reference points

The guide curves were then used to generate the outline solid using a solid loft. Surfaces were also created using the surface loft and used to spit the outline solid to achieve three cochlear structures as before. The result of the split is shown in Figure 2.36.

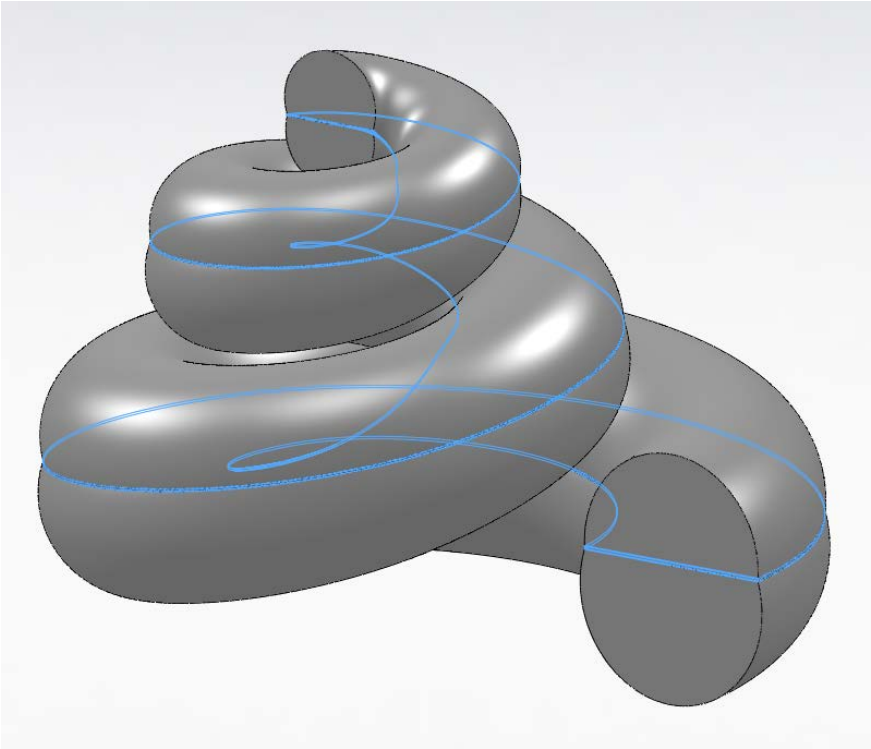

Figure 2.36: The split function generates the scala vestibuli, scala tympani and the Basilar membrane.

The electrode array was created in much the same way, as mentioned in section 2.5.1. Several sketches were created on the same planes on which are the cross-sections of the cochlear geometry. These sketches contain points that indicate the centre line of the cochlear implant. Changing the position of these points will alter the direction of the electrode array. A curve function was used to create a curve connecting these points together. Once this curve was generated, planes and sketches were created along the curve representing the cross-section of the implant at each position. The planes and sketches were made perpendicular to the direction of the curvature of the curve. These sketches were used to make a planar surface at each position. The outline of the implant was created by lofting a solid through the cross-sections using the curve as a centreline. The surfaces were then used to split the outline solid into the electrodes and silicon separators. The final resulting cochlear and electrode geometry is shown in Figure 2.37, which corresponds to the "tightly coiled" model in the next chapter.

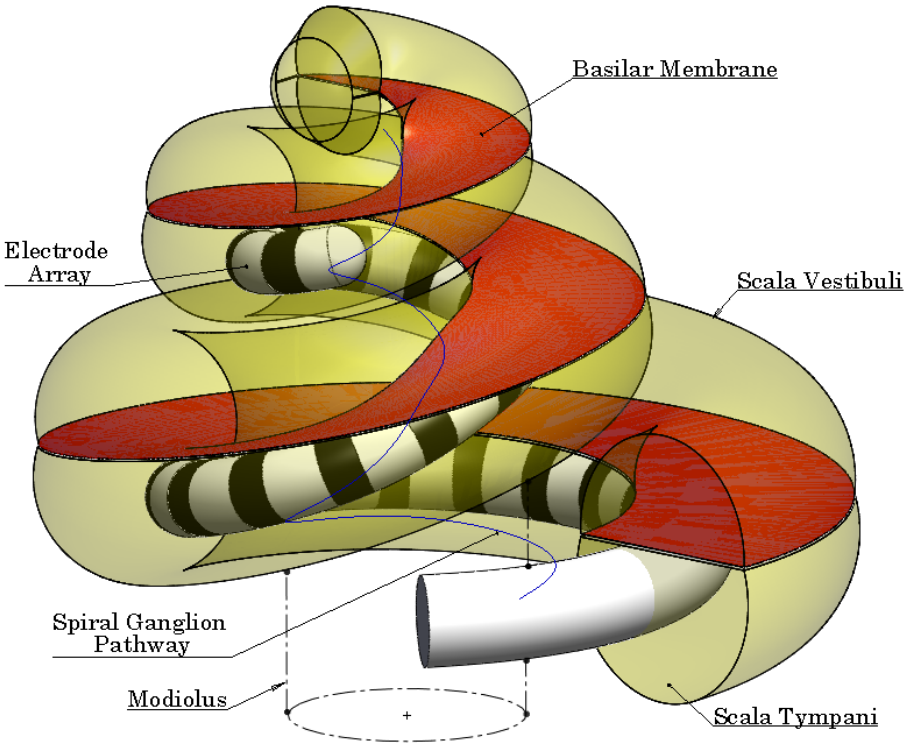

Figure 2.37: The cochlear structures and the full Cochlear Contour Advance electrode array.

The image also shows a blue curve representing the predicted position of the spiral ganglion, where stimulation is predicted to occur. This is where the nerve endings that are stimulated by the cochlear implant are predicted to exist. The neural excitation is assumed to be dependent on the voltage level at the spiral ganglion, although the exact mechanism of neural excitation is not well understood (Frijns et al., 2009, Tognola et al., 2005, Hanekom, 2005). The nerve dendrites that lie within the organ of Corti are assumed to be damaged or degenerating. Stimulation is thus more likely at the cell body or nucleus of the nerve in the spiral ganglion. The approximate position of the curve running through the spiral ganglion was estimated from the cochlear image in Figure 2.5.

Once the geometry was generated, this was transferred to Comsol Multiphysics as before. Due to the complexity of the model, the number of elements required in the mesh is now around 1.4 million. A free mesh of tetrahedral elements was again used and material properties and boundary conditions were set in the same way as before, with the outside of the bone set to ground. The finite element mesh of the coiled cochlea is shown in Figure 2.38 and the overall voltage spread, calculated for the coiled cochlea, is shown in

Figure 2.39. Figure 2.40 shows the voltage distribution at the spiral ganglion pathway due to stimulation of each electrode using the geometry shown in Figure 2.37. Figure 2.41 shows the impedance matrix at each electrode position.

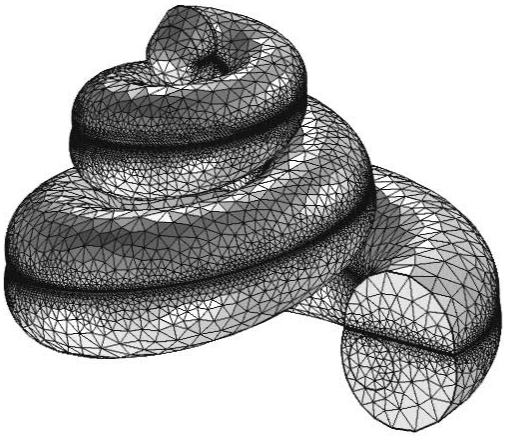

Figure 2.38: Finite element mesh of the coiled cochlea

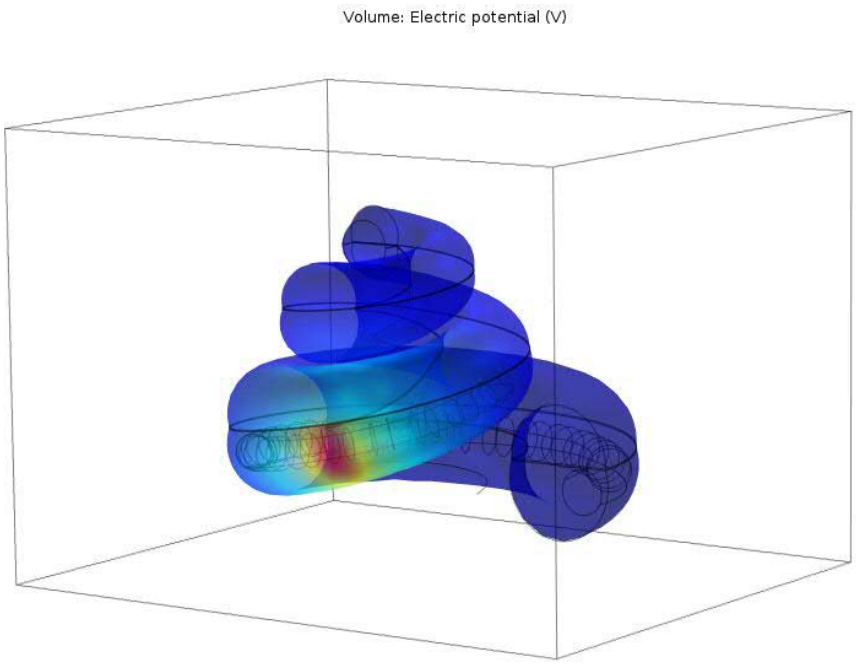

Figure 2.39: General spread of excitation in the cochlea

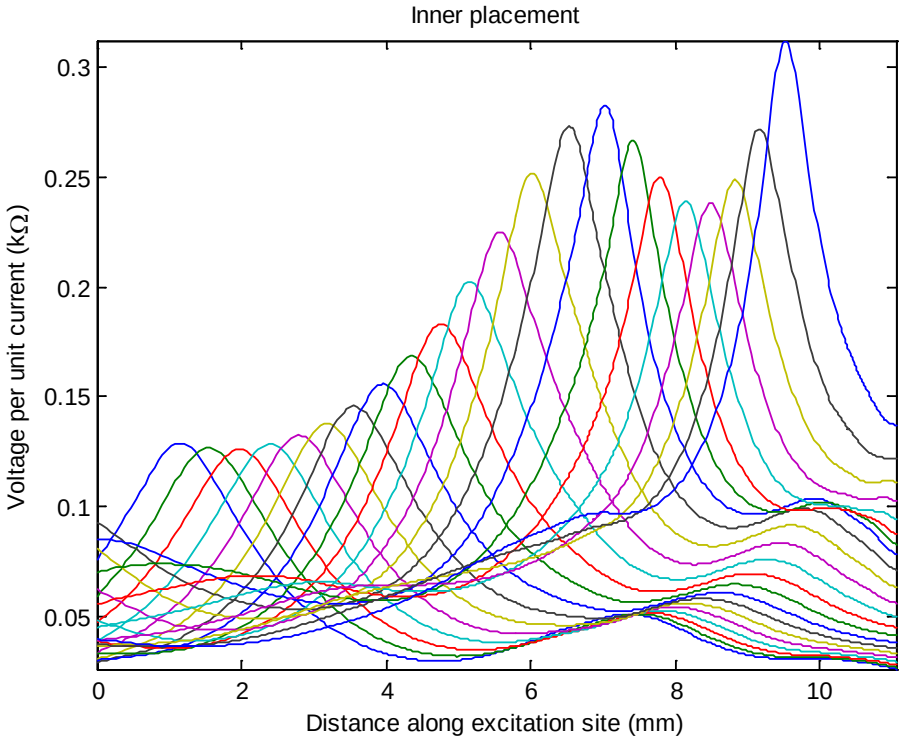

Figure 2.40: Excitation spread along the spiral ganglion path when each electrode is activated separately.

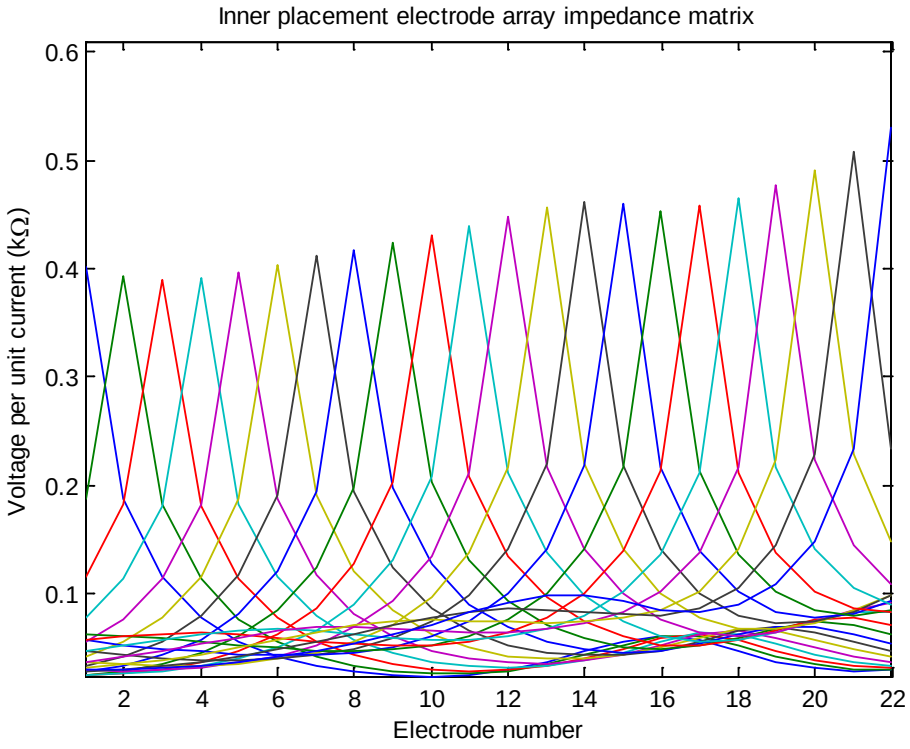

Figure 2.41: Impedance matrix at the electrode positions of the non-uniform coiled model.

Figure 2.40 shows that the voltage peaks increase along the spiral ganglion path in the direction of the apex, in agreement with the previous non-uniform straight model. The added effect of the coiling of the cochlea is that when each electrode is stimulated individually, a secondary peak in the voltage distribution is observed, suggesting that excitation in one turn of the cochlea spreads to the neighbouring turn, which is near to the stimulating electrode. This peak occurs at about 6.5mm from the main peak for the first 8 or so electrodes, which is the circumference of the first turn in the pathway along the spiral ganglion, corresponding to the first turn of the cochlea. This effect is also evident in the impedance matrix at the electrode positions in Figure 2.41.

2.8 Sensitivity Analysis

The purpose of the sensitivity analysis is to understand which material properties most affected the voltage distribution. The materials used in the model were defined in Table 2.1 as; the electrode metal, the Basilar membrane, the bone, the perilymph fluid and the silicon insulator and carrier.

Each material property was varied by increasing or decreasing the resistivity value by a factor of ten. Each material resistivity was varied individually and for each simulation no other changes were made. The voltage spread was calculated along the spiral ganglion for the 11th electrode, and these are plotted in Figure 2.42 to Figure 2.46.

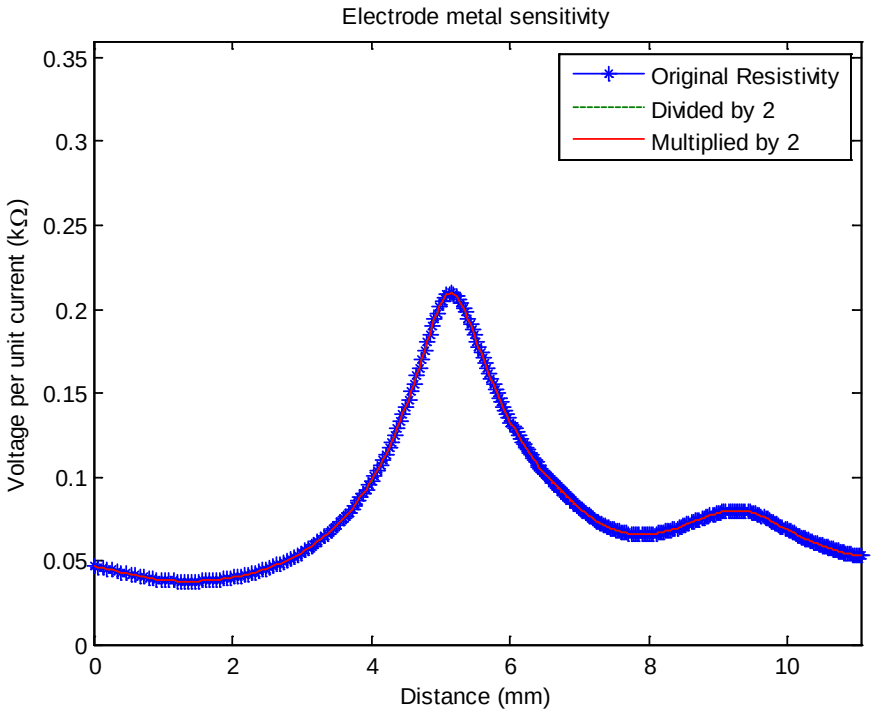

Figure 2.42: Sensitivity analysis for electrode metal resistivity

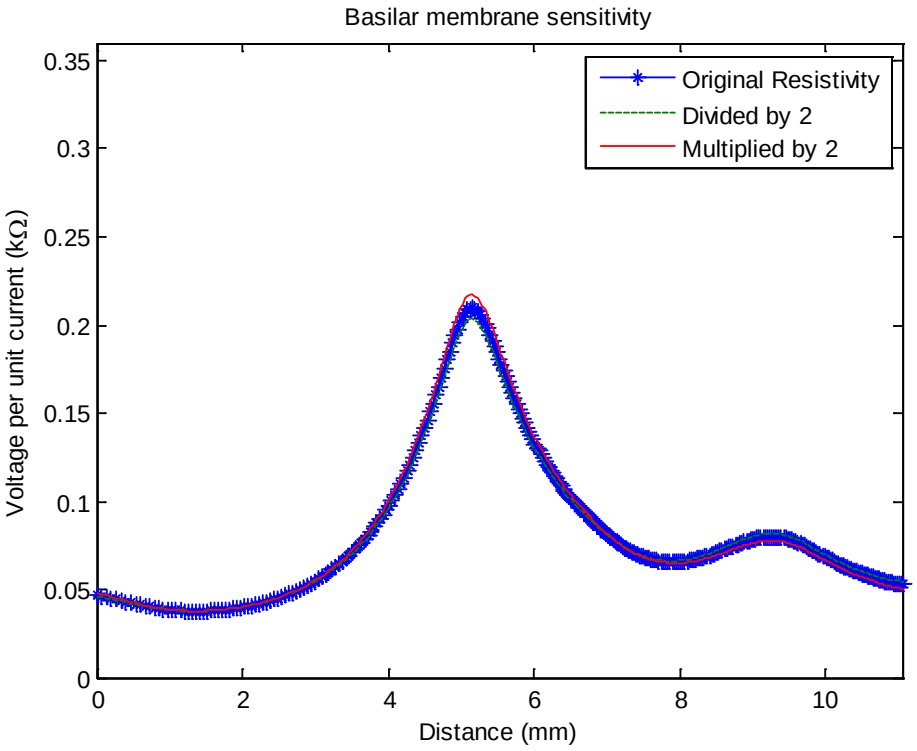

Figure 2.43: Sensitivity analysis for basilar membrane resistivity

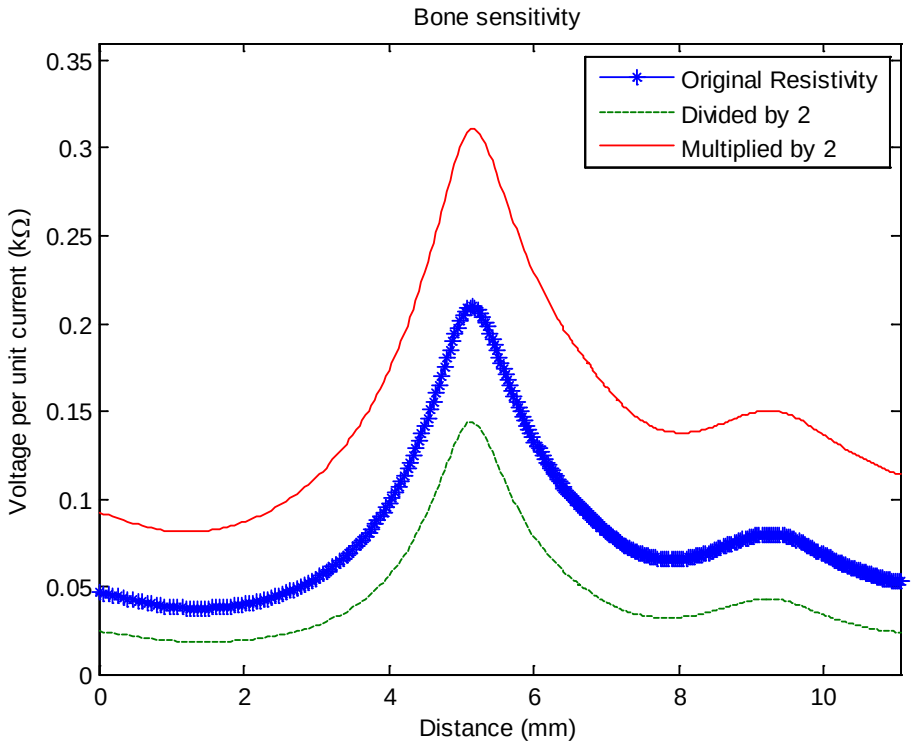

Figure 2.44: Sensitivity analysis for bone resistivity

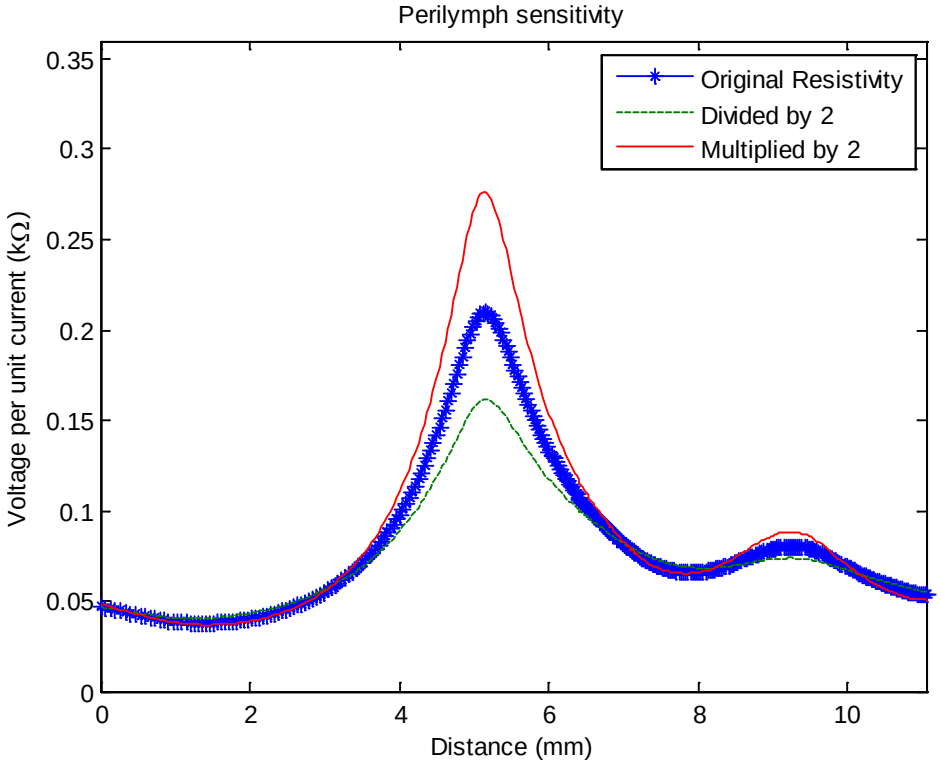

Figure 2.45: Sensitivity analysis for perilymph resistivity

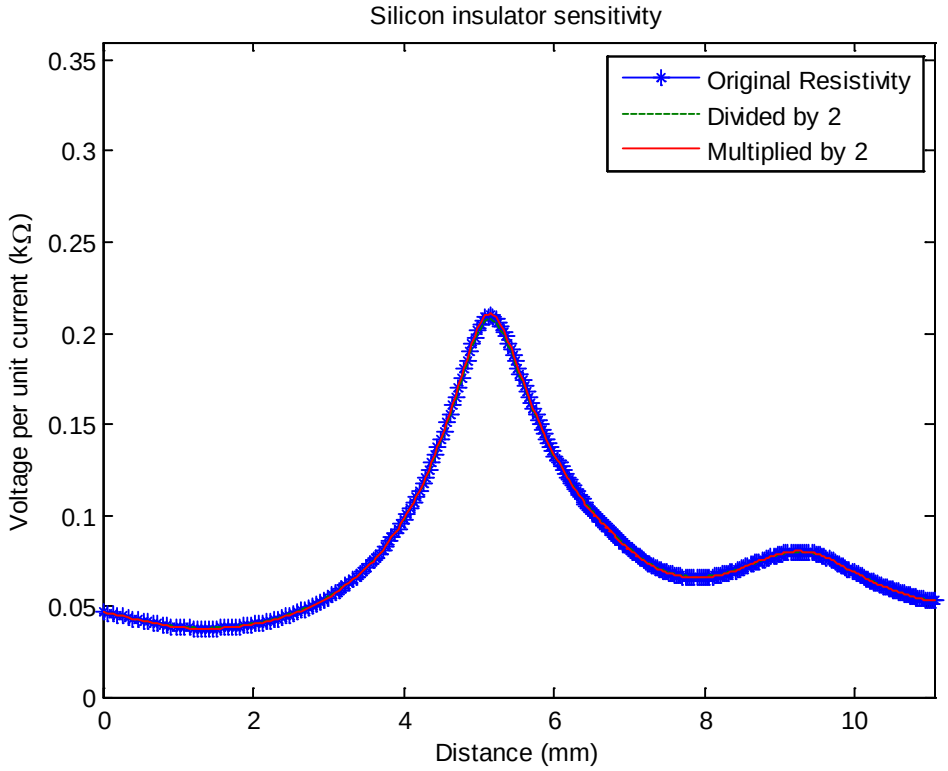

Figure 2.46: Sensitivity analysis for silicon resistivity

Some material properties have more effect on the voltage spread than others, depending on their size and geometric position in relation to the active electrode and the spiral ganglion.

The electrode metal resistivity has almost no effect on the levels of stimulation as long as it is reasonably conductive. The basilar membrane has little effect on the levels of stimulation, since the membrane does not intersect the pathway between the active electrode and the spiral ganglion. The membrane is also not in the vicinity of the spiral ganglion and so has little effect on the resistive environment local to the spiral ganglion.

Stimulation levels are most greatly affected by the resistivity values of the bone enclosure, the perilymph fluid. Varying bone resistivity has the largest effect on the impedance of the model. Generally the resistivity would not be divided by ten as this would imply that it has a similar resistivity to that of perilymph fluid which is not physically practical. On the other hand, multiplying by ten has a significantly large increase on the impedance. This would correspond to a resistivity value reported (Rattay et al., 2001) however this was not an accurate value for the purposes of this thesis due to the method in which the value was calculated. This is discussed in Appendix E. The large effect is not unexpected due to vast presence of bone around the cochlea and at the modiolus, and causes impedance levels to rise by about 4.5 times that of the original resistivity.

Perilymph fluid has a moderate effect on the impedance levels. Increasing resistivity of the fluid means that less current can be shunted through the fluid away from the nerves. This leads to higher voltages at the site of stimulation.

Finally, the resistivity of the silicon insulator is assumed to be an order of ten higher than that of the fluid, as the silicon carrier is designed to hold the electrodes in position but also to provide some insulation in between electrodes to focus stimulation to some degree. Increasing the resistivity has little effect. This implies that although in reality the silicon used in cochlear implants could have a much higher resistivity than that used in this model, its effect is negligible.

This sensitivity analysis shows that the results of the model are fairly robust to reasonable variations in electrode metal and basilar membrane resistivity values, but with moderately sensitive to the fluid and silicon resistivity values and a relatively highly sensitive to the bone resistivity.

2.9 Conclusion

Chapter 2 has demonstrated the effect of coiling in the cochlea on the voltage distribution, as well as the effect of varying material parameters. It was shown that the geometry of the cochlea has a significant effect on the voltage distribution, implying that with the same electrode array configuration, inter-patient variability will result in varied voltage distributions. In particular, this research showed that variation in geometry of the cochlea will affect voltage distribution which consequently would affect neural stimulation resulting in varied performance of the cochlear implant. Chapter 3 investigates the effect of varying positions and configurations of the electrode array on voltage distribution within the cochlea. In the future, the model could be used to test the effect of geometric variability, for example, height of the cochlea or radius of the cochlear turns from the centre of the modiolus.

Chapter 3

3 Investigation of excitation spread under varying conditions

3.1 Introduction

Different patients who receive a cochlear implant will have varying performance levels with their implant. These variations of performance are due to several factors, including the variation of cochlear anatomy, electrode position and electrode configuration.

In this chapter, the model developed in chapter 2 is used to investigate the effect of varying some of these factors on the spread of excitation. A variation on the general pattern of excitation will alter the degree to which different nerve sites are excited, which in turn affects pitch perception due to place pitch coding of the cochlea and hence affects speech recognition. It is therefore important to understand these effects in a bid to improve understanding of which configurations would work best and in what anatomical circumstances they apply.

3.2 Electrode placement

During implantation, the placement of the cochlear implant greatly varies. Originally, straight electrodes were used and when implanted these tended to followed the outer wall of the cochlear chamber. More recent developments such as the Nucleus 24 system are pre-coiled prior to implantation, and hence tend to be closer to the inner wall of the cochlear chamber (Zeng et al., 2004).

During implantation, a stylet is used to aid the insertion of this implant into the cochlea by straightening it temporarily. Once the implant is fully inserted the stylet is removed and the implant returns to its naturally coiled state, in close contact with the inner wall of the

cochlear chamber i.e. hugging the modiolus wall. The point of nerve excitation during implant stimulation is at the spiral ganglion cells, which lie within the modiolus. This means that pre-coiling the implant should bring the electrodes into a closer proximity to the target area. In practice, this is not necessarily the case, since the implant is not always inserted in the same way and the variation of implant placement within the scala tympani can be large.

To test the effect of implant position on the distribution of excitation, several versions of the cochlear model were constructed. These included an inner placement along the inner modiolar wall, as in chapter 2, an outer placement along the outer scala wall, a mid-placement along the centre line of the scala tympani and finally a kinked placement demonstrating the random nature of the final resting position of the implant during surgery. This is due to inherent difficulties in positioning the implant correctly during implantation. In all cases, the outer surface of the bone was grounded to represent the reference electrode as in the monopolar configuration.

Figure 3.1 demonstrates the effect of placing the electrode along the outer wall, resulting in a shorter penetration of the cochlea, wider peaks and lower excitation levels. Figure 3.2 demonstrates the effect of placing an electrode along the inner wall, as is the ideal placement with a pre-coiled cochlear implant, resulting in a tighter fit of the electrode array around the modiolus, giving further penetration into the cochlea, narrower peaks and higher levels of excitation. Figure 3.3 demonstrates a more realistic case in which the electrode array is not ideally placed close the modiolar wall resulting in a kinked placement of the electrode array. This results in a combination of the inner and outer placement.

A

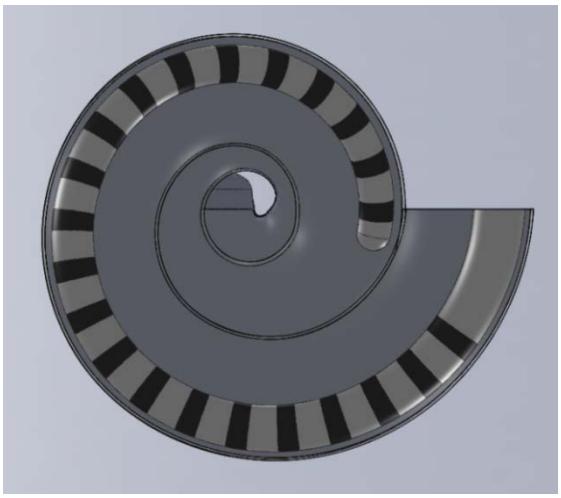

B

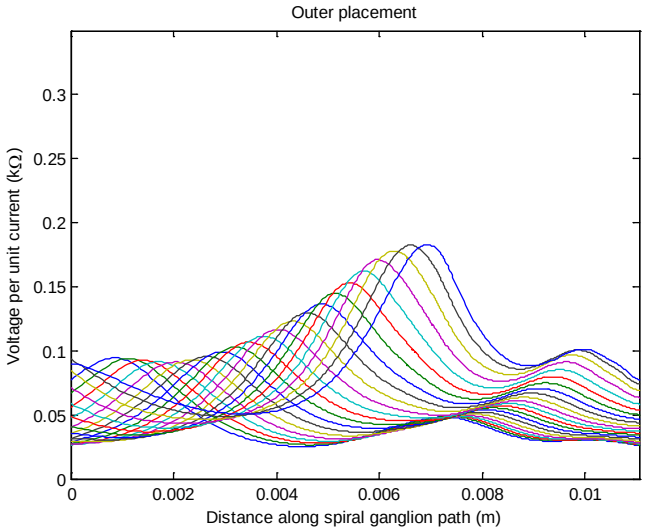

C

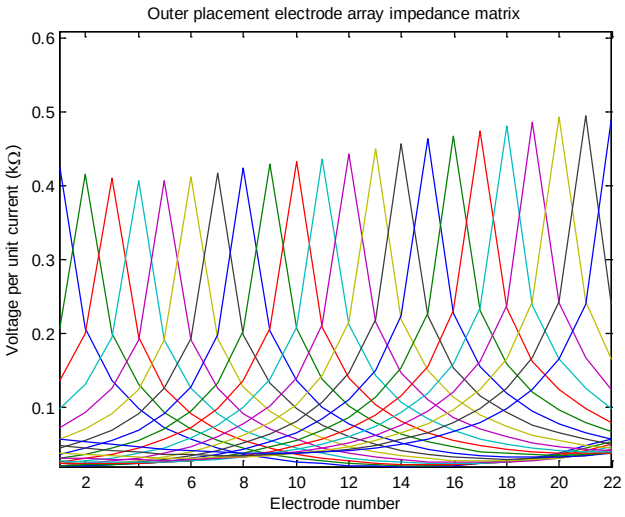

Figure 3.1: Position of the loosely coiled electrode array within the cochlear model (A) and the resulting voltage distribution for unit current input into each of the electrodes along the spiral ganglion (B) and electrode array (C).

A

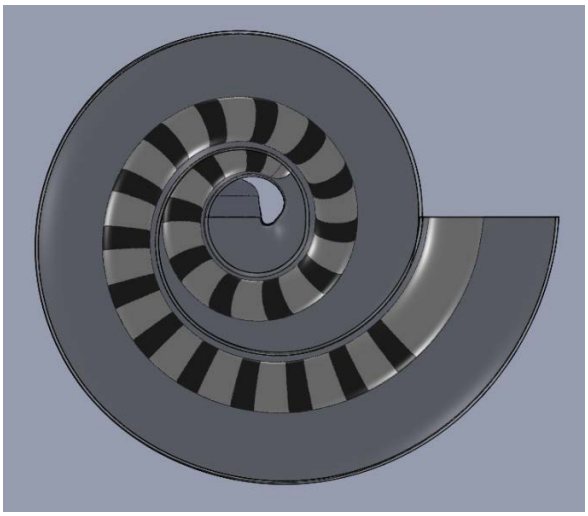

B

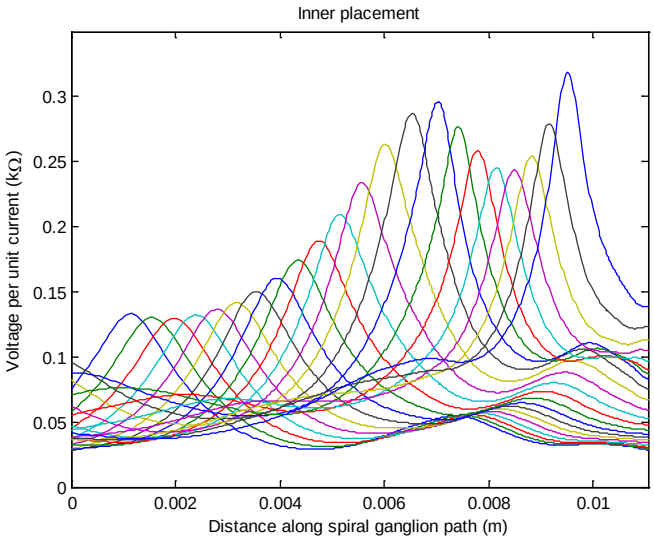

C

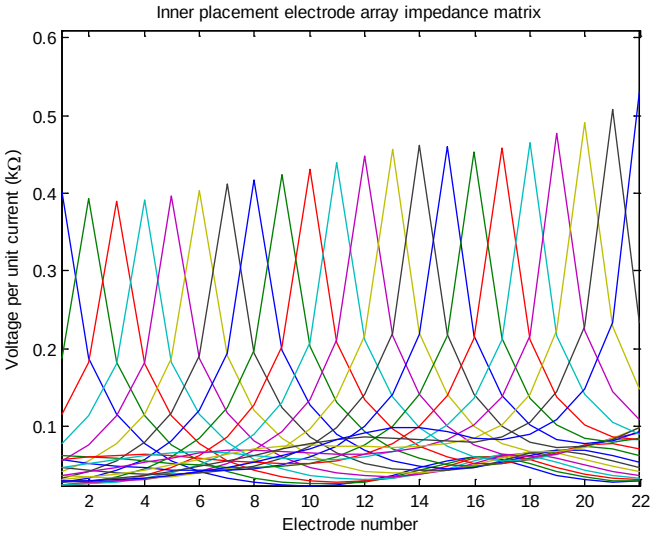

Figure 3.2: Position of the tightly coiled electrode array within the cochlear model (A) and the resulting voltage distribution for unit current input into each of the electrodes along the spiral ganglion (B) and electrode array (C).

A

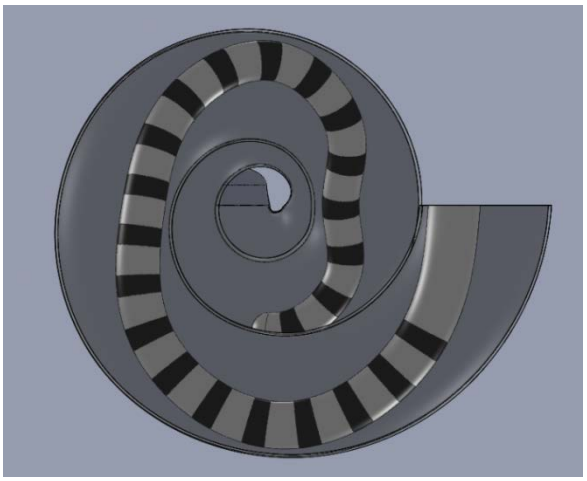

B

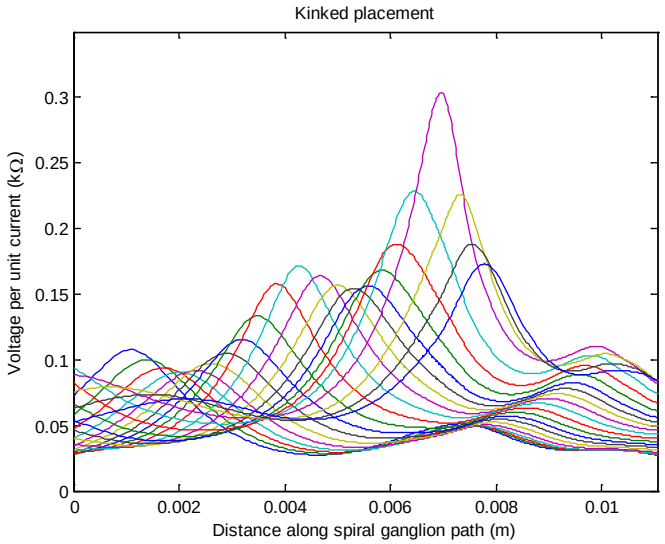

C

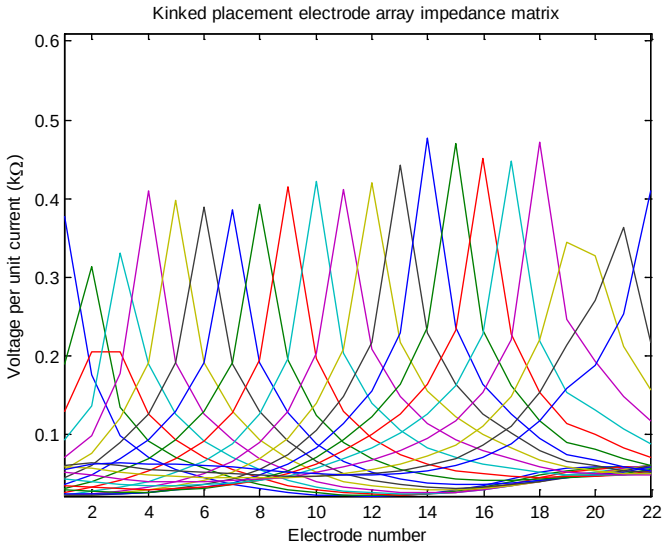

Figure 3.3: Position of the kinked electrode array within the cochlear model (A) and the resulting voltage distribution for unit current input into each of the electrodes along the spiral ganglion (B) and electrode array (C).

3.2.1 The effect of electrode array placement on Voltage distributions

In the outer placement of the electrode array, the distribution of the voltage per unit current input is fairly broad as shown in Figure 3.1 (B) with peaks of around 0.17 kΩ. The voltage distribution is affected by the geometry to some extent in that there is a secondary peak due to the overlapping turns of the cochlea as discussed in chapter 2. An outer electrode placement means that the electrode array penetrates less of the cochlea, therefore the region covered that would be stimulated directly by a specific electrode is fairly short covering approximately half of the spiral ganglion pathway according to the model. These effects are less evident when measuring along the electrode array as in Figure 3.1 (C), as this is generally somewhat insensitive to geometrical changes along the length of the cochlea.

The voltage distribution shown in Figure 3.2 (B) indicates that an inner placement of the electrode array will significantly increase the voltage per unit current along the spiral ganglion. This is because an inner placed electrode array would be positioned significantly closer to the target nerves and so current flow is increased through the spiral ganglion. The levels increase to approximately double that of the outer placement. This implies that lower currents would be required to achieve the same stimulation as that in the outer case. The distribution also has narrower peaks, implying that the accuracy within which nerves are targeted is improved, improving frequency discrimination and ultimately, most probably, speech perception.

This inner placement also means the electrode array penetrates further into the cochlea covering a much larger length of the spiral ganglion. Resistivity along the length is not consistently increasing, however, as it decreases at around the 15th electrode before it rises again. This is because the cross-sectional area of the chambers in this model breaks away from the general decreasing trend, as described in chapter 2, and increase slightly between the 15th and 21st electrode. This effect is not seen in Figure 3.1 (B) because the array is not spiralled to the same degree due to being positioned nearer to the outer wall. Figure 3.2 (C) indicates similar levels of impedance along the electrode array due to the fact that this measurement is still taken at the current source which is fairly insensitive to the change in the resistive environment.

When the electrode array is surgically implanted, the final resting position of the implant is never consistent from patient to patient (Finley et al., 2008). The first two cases demonstrated above show a smooth inner and outer placement of the electrode array, but in practice the electrode array will tend to be more crooked in random places along the

length of the cochlea. This inaccurate placement of the electrode array leads to further variation of the spread of excitation, as shown in Figure 3.3. The distribution is a combination of the previous 2 cases. At some points where the electrode is near to the modiolar wall, it behaves in a similar manner to that of an inner placed electrode in that peaks generally become sharper. In places where the electrode is further away from the modiolar wall, closer to the outer wall, then it behaves more similarly to an outer placed electrode array, in that the peaks are broader. This implies that after implantation the final position of the implant within a specific patient's cochlea will affect threshold and comfort levels as well as the general performance of the implant for that patient.

Figure 3.3 (C) indicates that impedances levels along the electrode array are similar to the two previous cases, but since the array is kinked the peaks do vary slightly in accordance to the pathway of the electrode array.

Figure 3.1 (C), Figure 3.2 (C) and Figure 3.3 (C) plot the impedance along the implant, at the positions of the 22 electrodes, in the same way as van den Honert and Kelsall (2007). These impedances could, in principle, be directly measured for an implanted patient and so give a guide as to the placement of the array. The impedance matrix that most resembles the impedance matrix plots of patients measured by van den Honert, as shown in Figure 2.1 is that of the kinked position of the electrode array. They are in a similar order of impedance as well as exhibiting a variation of the peaks along the electrode array, which is dependent on the exact position of the implant as well as the variation in cochlear geometry and neural survival.

These differences in the electrode impedances with position, however, are far smaller than the differences in excitation at the spiral ganglion, and are thus seen to be a poor indicator of ultimate cochlear implant performance.

3.3 Electrode focussing

The voltage distribution due to stimulation of one electrode is quite broad and consequently stimulates whole groups of neurons. This is particularly evident in Figure 3.1 (B), where in the outer placement of the electrodes, the peaks are quite broad. One way to control this is to implement a focussing strategy that uses other nearby electrodes with a configuration of currents that will result in a focussed pattern of excitation peaking at the desired position at the spiral ganglion pathway with reduced stimulation levels everywhere else.

Previously, van den Honert and Kelsall (2007) have suggested a focussing strategy at the electrode positions. They assume that the voltages at the electrode positions can be calculated from

$$\boldsymbol{v} = \mathbf{Z}\boldsymbol{i} \tag{3.1}$$

Where $\boldsymbol{v}$ is the vector of the voltages of the electrode positions, $\mathbf{Z}$ is a square impedance matrix along the electrode array and $\boldsymbol{i}$ is the vector of input currents to each electrode. It is the columns of this $\mathbf{Z}$ matrix that are plotted in figures Figure 3.1 (C), Figure 3.2 (c) and Figure 3.3 (C). Although the elements of $\mathbf{Z}$ are strictly impedances we have seen in practice these are mainly real and can be accurately represented by resistances.

Van den Honert and Kelsall (2007) then defined an ideal focused voltage distribution represented by

$$\boldsymbol{v}_d = \begin{bmatrix} 0 \\ \vdots \\ 1 \\ \vdots \\ 0 \end{bmatrix} \tag{3.2}$$

Where the voltage is unity at one selected electrode and is zero at all the other electrodes. The input current vector $\boldsymbol{i}_d$ required to achieve this distribution of voltages at the electrode positions is obtained by inverting the impedance matrix in equation (3.1), assuming it is not singular, to give

$$\boldsymbol{i}_d = \mathbf{Z}^{-1}\boldsymbol{v}_d \tag{3.3}$$

Once this ideal current is calculated it can be used for stimulation in the cochlea to achieve the desired result of focussing at one point, while reducing the stimulation levels everywhere else. Figure 3.4 shows the voltage distribution at the electrodes before and after the focussing strategy, suggested by van den Honert, was implemented at electrodes 2 (A) and 11 (B), assuming the impedance matrix for the tightly coiled cochlear implant, with the inner placement, as shown in Figure 3.2 (A). Figure 3.5 shows the currents driving the individual electrodes before and after this focussing strategy is applied, as given by equation (3.3), to focus the voltage distribution at electrodes 2 (A) and 11 (B). These results are based on an initial input current to one electrode at 125 μA giving an initial target voltage of about 0.05 V.

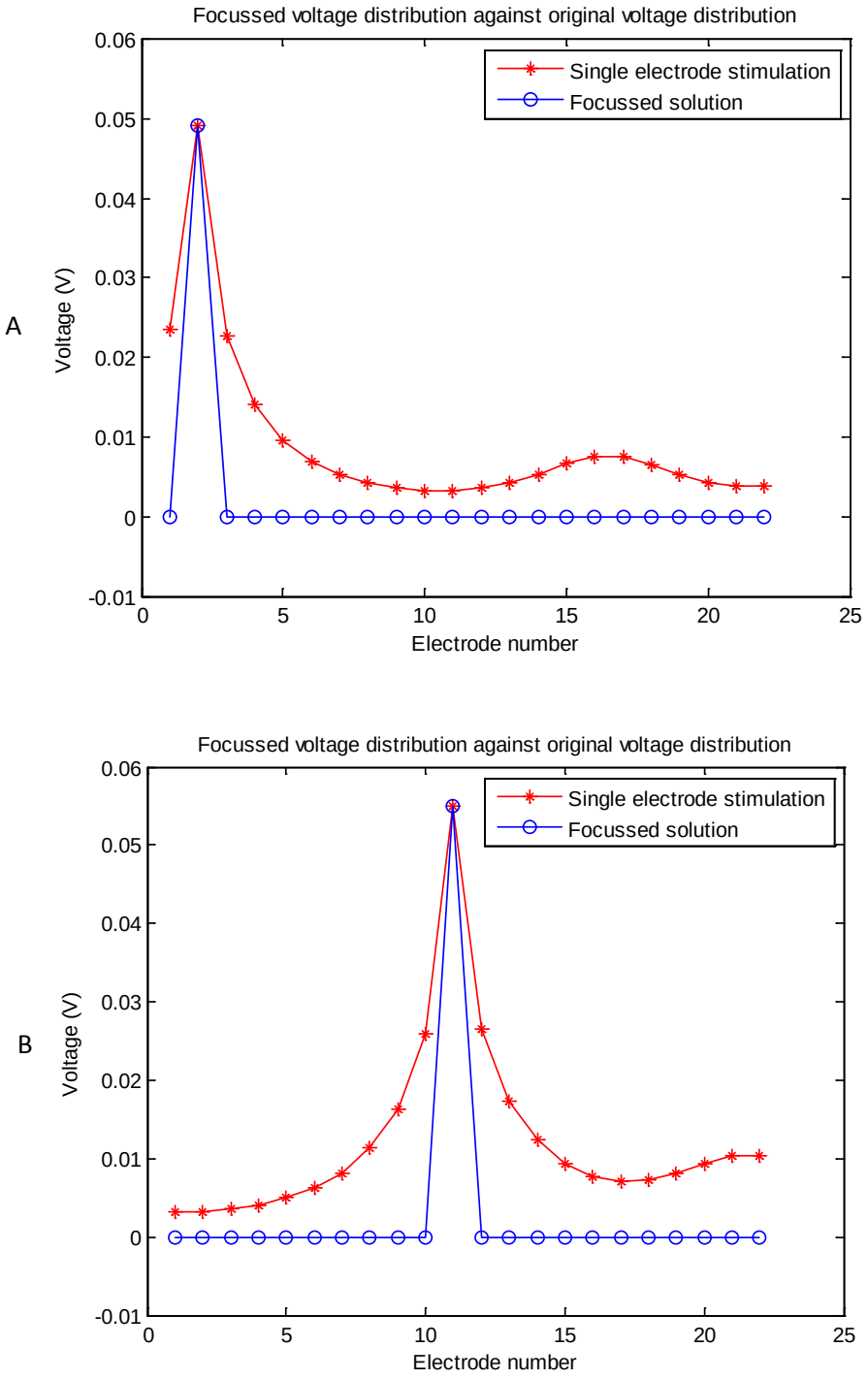

Figure 3.4: Voltage distribution along the electrode line before and after Implementing the focussing strategy, electrode 2 (A) and 11 (B), for an *inner* electrode placement.

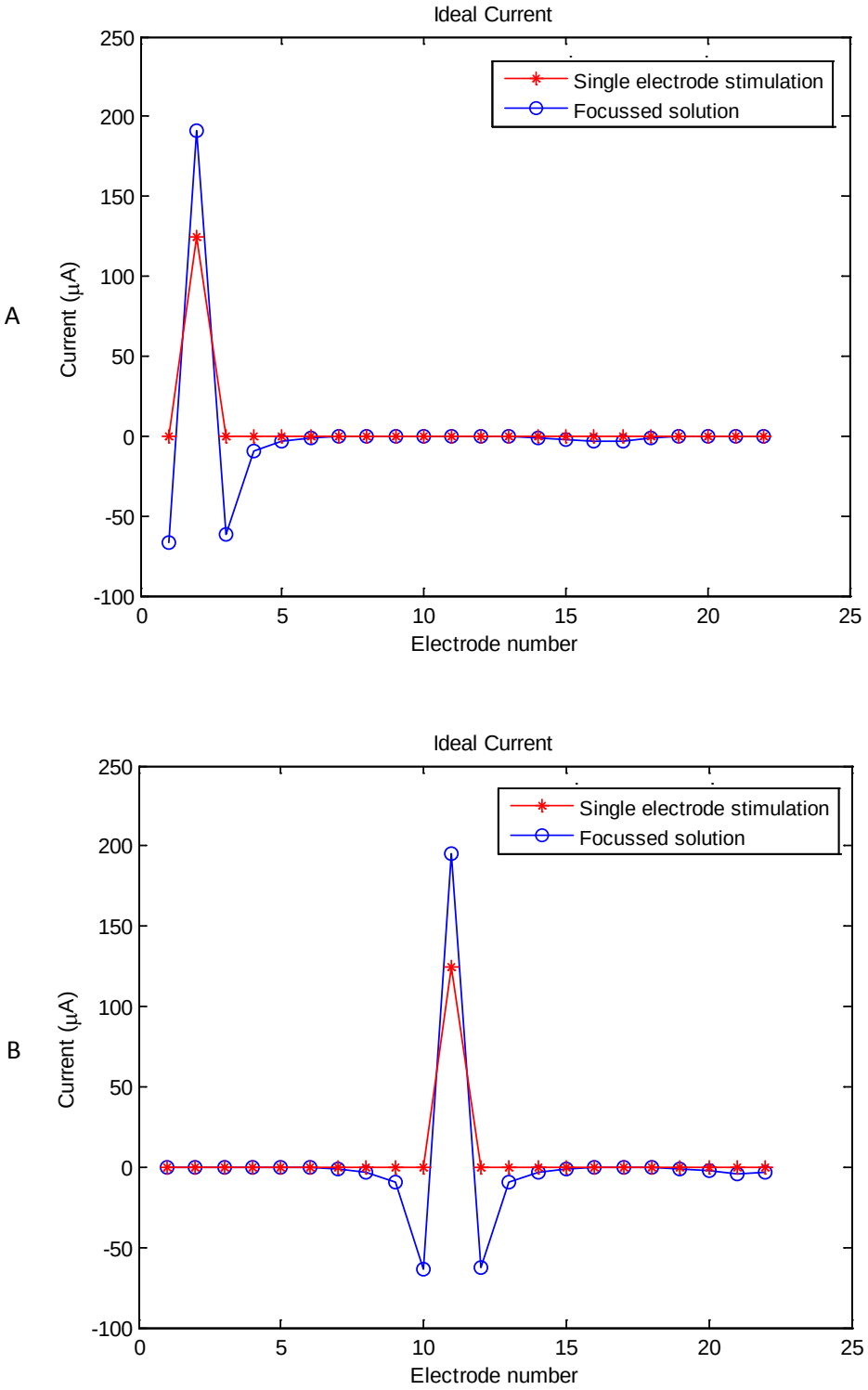

Figure 3.5: Current required before and after implementing the focussing strategy, electrode 2 (A) and 11 (B), for an *inner* electrode placement.

.

Figure 3.4 (A) and (B) show that the voltage distribution is perfectly focussed along the electrode array at the specified electrode. To achieve this, for focussing at electrode 11 as shown in Figure 3.5 (B), a total current input of 364 μA is required, calculated as the sum of the modulus of the currents to all electrodes, in comparison to the 125 μA originally used. This represents a 290% increase in current input total required, with a 60% increase at electrode 11. The ultimate target for stimulation, however, is at the pathway through the spiral ganglion cells, as opposed to along the electrode array. The calculated ideal current can be used to calculate the voltages along the pathway of the spiral ganglion cells using the impedance matrix of that pathway from the finite element model in chapter 2. The results for this voltage distribution due to stimulation at either the 2nd or 11th electrode are shown in Figure 3.6 (A) and (B) respectively.

Figure 3.6 (A) and (B) show that perfect or near perfect focussing cannot be achieved at the neural level using the ideal currents calculated along the electrode array. There are some positive outcomes of the focussing strategy in that the voltages everywhere other than the region of interest are mostly cancelled, but in the region of interest, rather than focussing, the peak is simply reduced by about 50% to 60%. The outcome is even less convincing when looking at the voltage distributions at the spiral ganglion when focussing the voltages in an outer placement of the electrode array, as shown in Figure 3.8. The electrodes are obviously further away from the spiral ganglion in this case.

This result is vital in demonstrating the limitations of the methods proposed by Van den Honert and Kelsall (2007). These limitations are largely due to the inability to measure the impedance matrix along the spiral ganglion using an electrode array. The model presented in this thesis, on the other hand, has the ability to measure the impedance matrix anywhere in the three dimensional geometry, allowing for such conditions to be investigated.

A

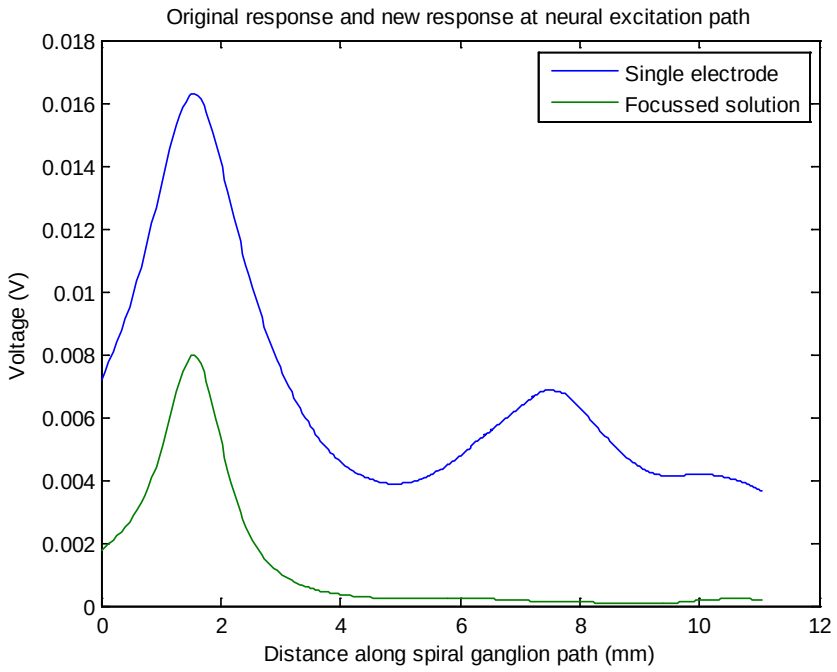

B

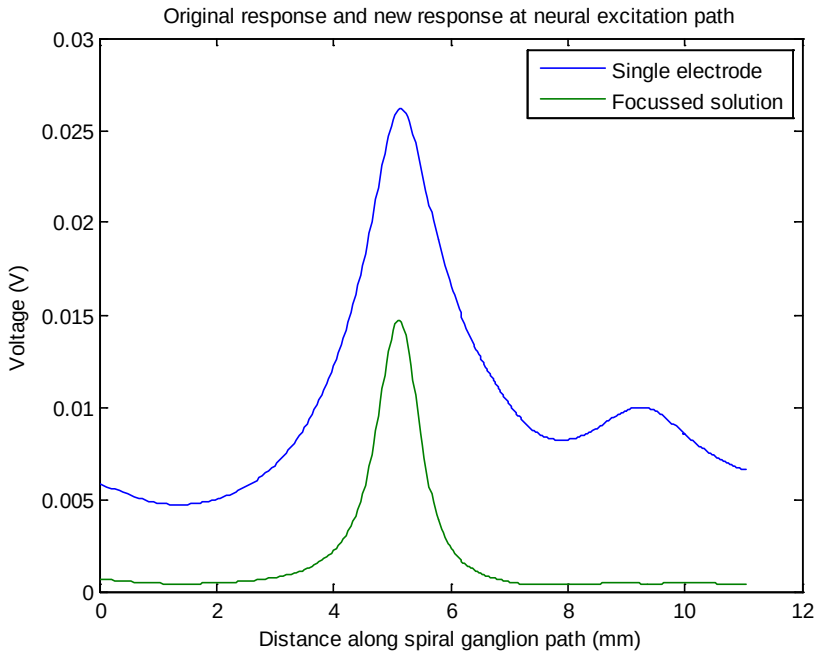

Figure 3.6: Voltage distribution at the spiral ganglion pathway before and after implementing the focussing strategy, electrode 2 (A) and11 (B) with the *inner* electrode placement.

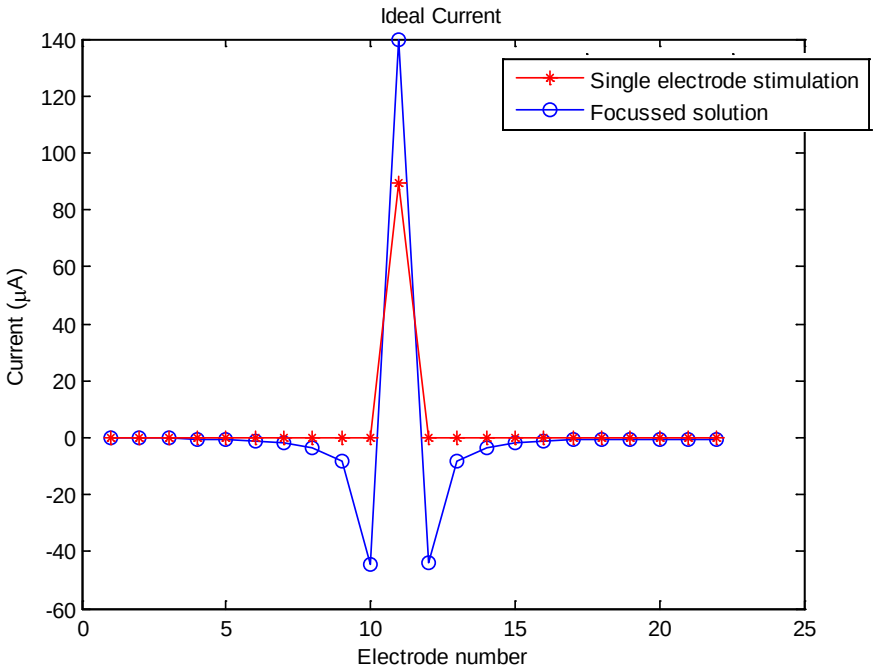

Figure 3.7: Current required before and after implementing the focussing strategy at electrode 11, for an *outer* electrode placement.

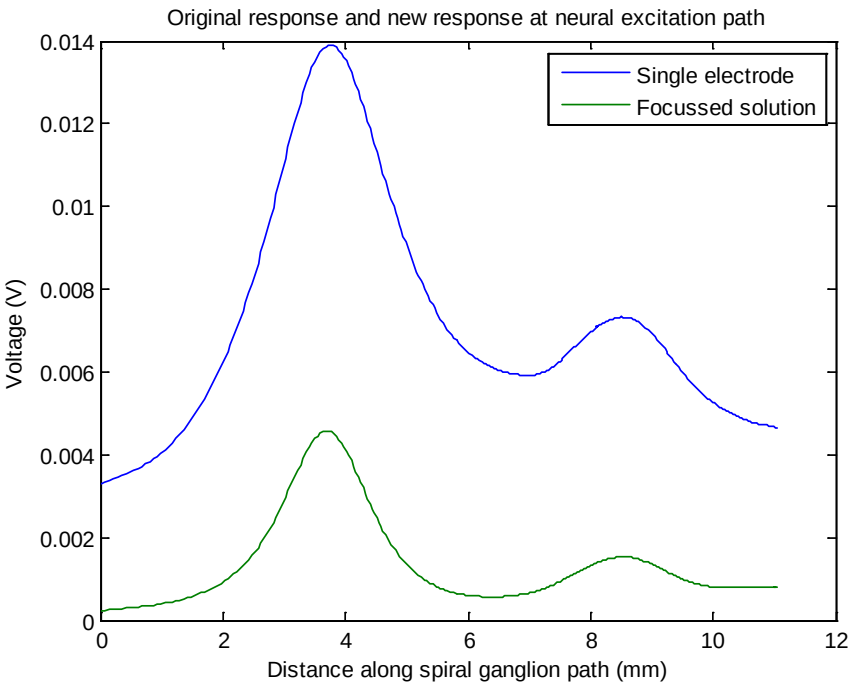

Figure 3.8: Voltage distribution at the spiral ganglion pathway before and after implementing the focussing strategy, at electrode 11 for the *outer* electrode placement.

The total input current required to focus at the 11th electrode in this case is 290% higher than that stimulating a single electrode, with a 60% increase at the peak electrode. The peak voltage at the neural pathway is, however, reduced by about 70% as a result of focussing at the electrode array. In order to maintain the same voltage level at about 4 mm along the spiral ganglion, the total current would need to be about six times greater than that when not using this focussing strategy, and yet the voltage distribution at the spiral ganglion position, at least in the case of an outer placed electrode array, is not significantly improved, as shown in Figure 3.9 and Figure 3.10. Large input currents increase battery requirements significantly and could potentially cause damage to cochlear structures and the auditory as mentioned by deSauvage et al. (1997).

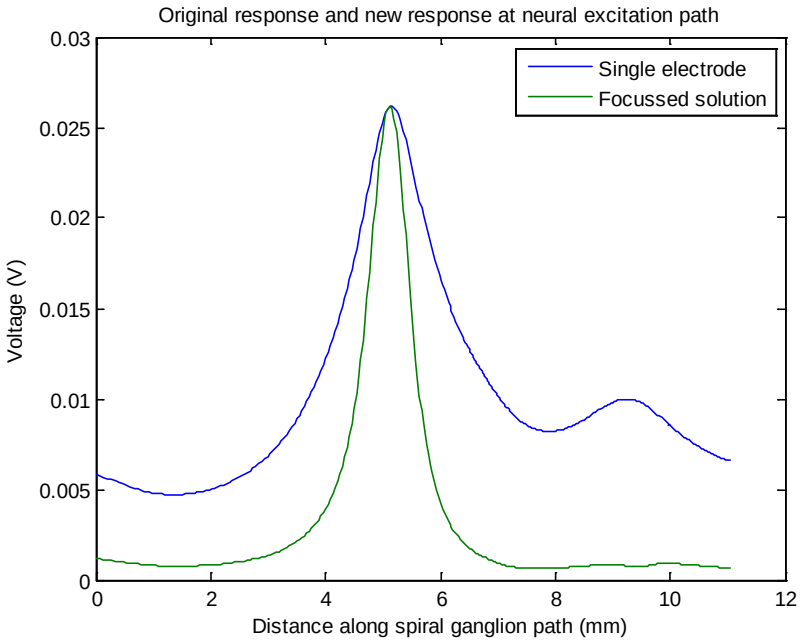

Figure 3.9: Voltage distribution at the Spiral Ganglion, for the *inner* placement at electrode 11, before and after focussing at the electrodes but using the current level required to give the same peak voltage at the Spiral Ganglion as a single electrode.

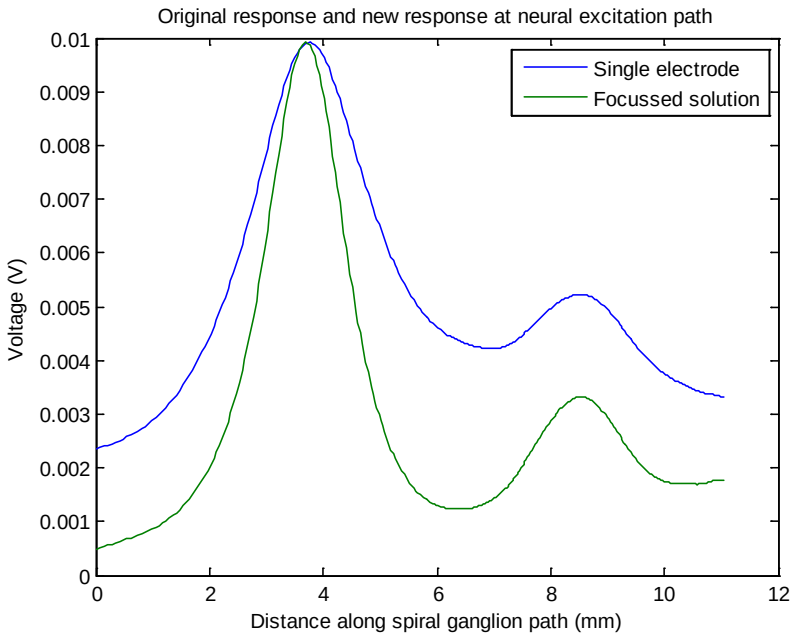

Figure 3.10: Voltage distribution at the Spiral Ganglion, for the *outer* placement at electrode 11, before and after focussing at the electrodes but using the current level required to give the same peak voltage at the Spiral Ganglion as a single electrode.

3.4 Neural Focussing

The focussing study presented by van den Honert and Kelsall (2007) is based on the impedance matrices measured at the electrode position. This limits the ability to investigate the effect focussing has throughout the cochlea as mentioned earlier. Figure 3.6 and Figure 3.8 clearly show that focussing in this way is not very useful at the spiral ganglions. Honert notes that impractically high currents will be required to reach the target voltage at the target neurons.

Focussing at the neural pathway was further investigated by developing the focussing method suggested by van den Honert and tailoring it to an impedance matrix measured along the pathway of the spiral ganglion. The impedance matrix along the spiral ganglion pathway is available here because of the finite element model of the cochlea presented in chapter 2. It is not clear how something similar to this matrix could be measured in practice, so for now, this study is limited to an estimation of the fundamental effects of such a neural focussing strategy if this impedance matrix was available. Equation (3.1) was first extended to take into account a non-square impedance matrix, since the number

of measuring points along the Spiral Ganglion is much larger, i.e. 391, than the number of electrodes, 22. The neural impedance matrix $\mathbf{Z}_n$ is thus a 22 x 391. To be able to calculate the required current for neural focussing, the equations have to be developed as follows:

$$\boldsymbol{v}_n = \mathbf{Z}_n \boldsymbol{i} \tag{3.4}$$

Where $\boldsymbol{v}_n$ is the voltage distribution at the 391 points along the spiral ganglion and $\boldsymbol{i}$ is the 22 electrode currents, as before. The optimum current that minimises the difference between $\boldsymbol{v}_n$ and a desired distribution $\boldsymbol{v}_d$ is equal to the generalised or pseudo inverse of the impedance matrix at the spiral ganglion pathway multiplied by the desired voltage distribution.

$$\boldsymbol{i}_d = pinv(\mathbf{Z}_n)\boldsymbol{v}_d \tag{3.5}$$

The pseudo inverse of the non-square impedance matrix can be written as:

$$pinv(\mathbf{Z}_n) = (\mathbf{Z}_n{}^T \mathbf{Z}_n)^{-1} \mathbf{Z}_n{}^T \tag{3.6}$$

where $\mathbf{Z}_n{}^T$ is transpose of the non-square impedance matrix.

Equation (3.5) was used to calculate another configuration of current inputs, which were optimised to achieve focussing at a single point along the neural pathway, with the inner electrode placement. The peak voltage achieved with this optimised current distribution is lower than that in the desired distribution and this is a consequence of using a linear least square method, as opposed to an exact matrix inversion. This method of optimising the vector of currents uses a larger number of measurement points, and therefore equations, to optimise a smaller number of variables, and therefore the result is over-determined and is the optimal solution, as discussed by Elliott (2001). The peak is lowered significantly (10% of the original peak voltage) and although areas away from the region of interest have been significantly cancelled out, the region of interest remains only marginally focused. Once again, higher currents are required to achieve the desired voltages at the desired locations. Figure 3.11 shows the current distribution and Figure 3.12 shows the voltage distribution when the levels of currents were increased to achieve the desired voltage at the target location. Figure 3.12 shows that neural focussing results in a sharper peak at the target area, whilst the voltages elsewhere are greatly reduced, but this requires far more current than focussing using the electrode array matrix. The total stimulation current is 56 times that for single electrode stimulation in this example of neural focussing (1000 μA/ 125μA), which is about a factor of 10 greater

than required for electrode focussing. The neural focussing strategy uses a great deal of current in achieving the very sharp excitation pattern seen in Figure 3.12, which results in the oscillating "sidelobe" behaviour of the voltage away from the target position.

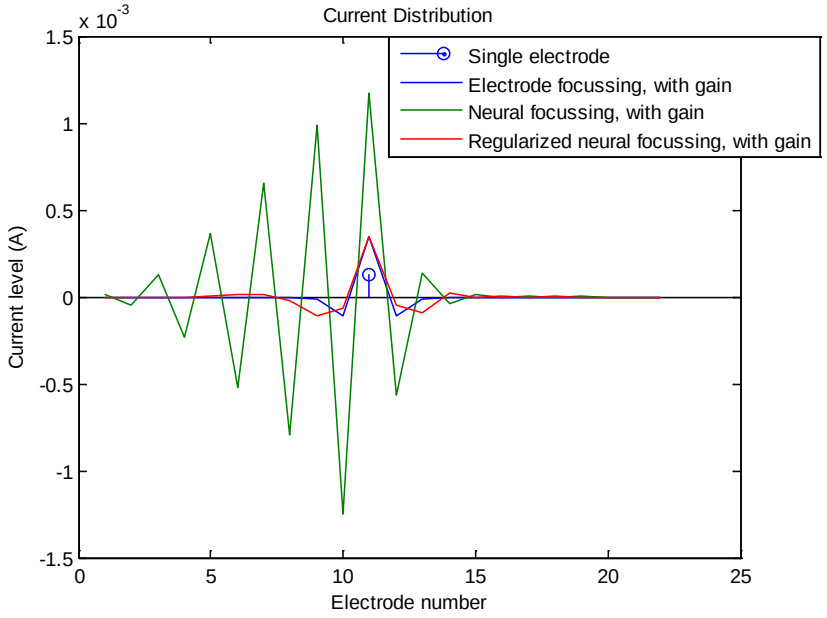

Figure 3.11: Current required when focussing using the neural impedance matrix, with the *inner* electrode placement.

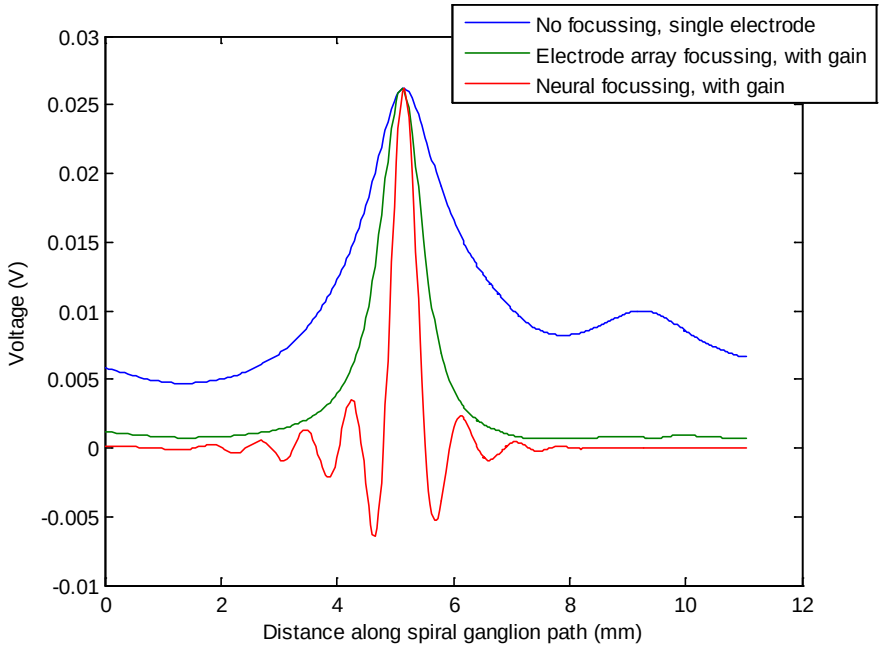

Figure 3.12: Voltage distribution at the spiral ganglion pathway before and after implementing electrode array and neural pathway focussing in the *tightly* coiled model, all normalised to give the same peak voltage.

Different compromises between focussing of the voltage distribution and the current requirements can be obtained by including a regularisation coefficient in the generalised inverse matrix.

$$pinv(\mathbf{Z}_n) = (\mathbf{Z}_n{}^T\mathbf{Z}_n + \beta \boldsymbol{I})^{-1}\mathbf{Z}_n{}^T \tag{3.7}$$

Where β is a regularization coefficient that weights the sum of squared currents, and $\boldsymbol{I}$ is the identity matrix.

Equation (3.7) was calculated with a variety of arbitrary values for the coefficient β, resulting in a variation of performance with respect to undulation level (and consequently current requirements) and focussing width. The results, in Figure 3.14, show that for the inner placement of the electrode array, at a certain coefficient of regularization, which in this case is the 3rd step, the current required is similar to that when focussing at the electrode array. The width of the peak at the focussed region is still significantly sharper than that achieved with electrode focussing, however, as seen in Figure 3.14 . This implies that neural focussing with some form of regularization would perform better than regular focussing at the electrode array surface. Figure 3.14 shows that with further regularization the strategy performed similarly to focussing at the electrode array, but the current required was reduced below that which was required for electrode array focussing, as in Figure 3.13.

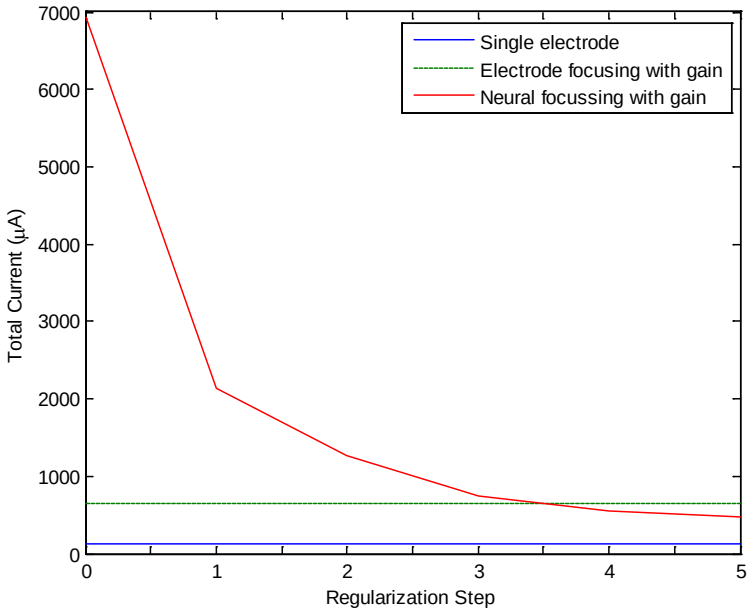

Figure 3.13: The total current at each regularization step, using the *tightly* coiled model.

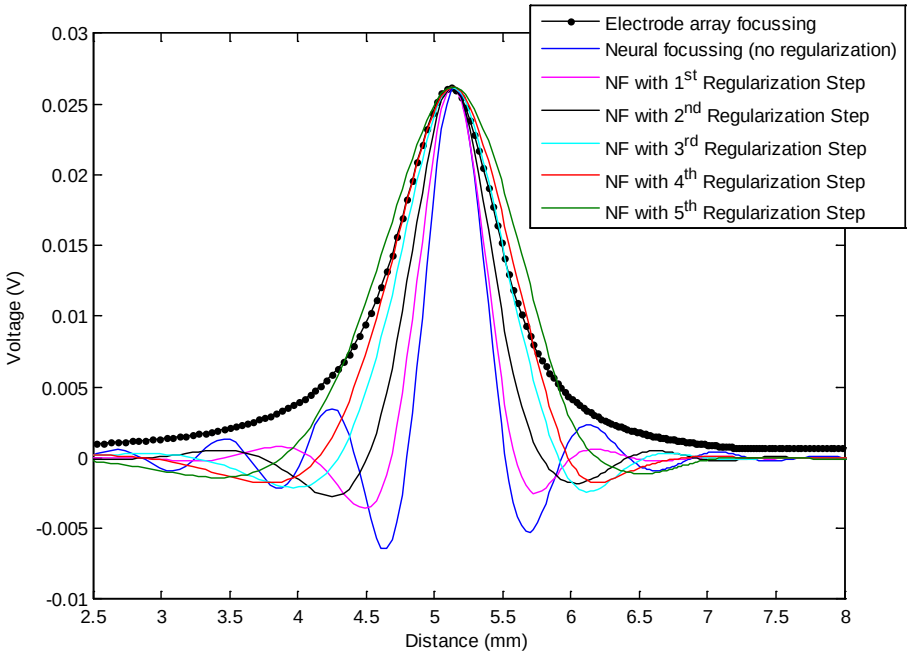

Figure 3.14: The effect of varying the regularization parameter in 5 steps on the voltage distribution at the spiral ganglion, using the *tightly* coiled model.

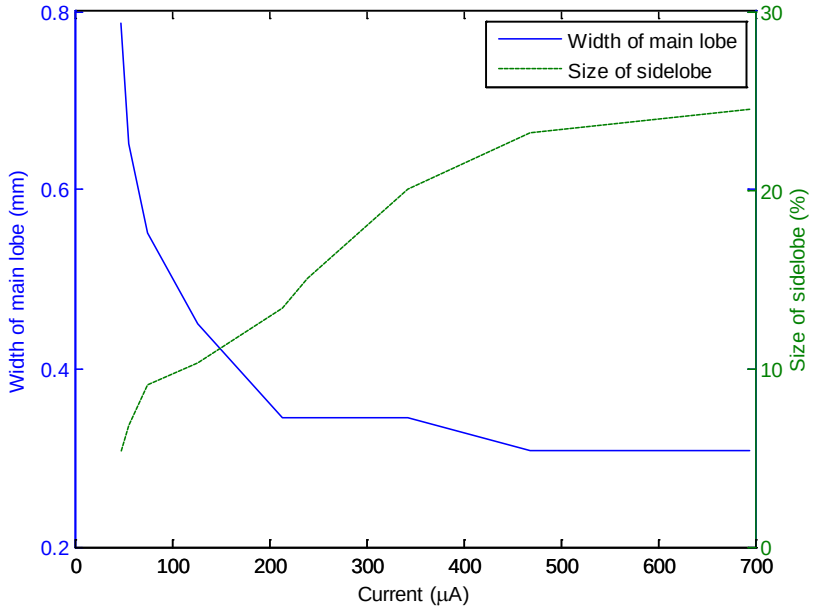

Figure 3.15: Variation of the width of the main lobe and the size of the largest side lobe with total current requirements.

Figure 3.15 shows that adding regularization could lead to a reduction in the total current by about a third, the size of the largest side lobe can be reduced to about 15%, and only result in small increase in the width of the main lobe compared to the unregularized

solution. Therefore, current requirements can be reduced to some extent without greatly compromising the degree of focussing.

The relevance of neural focussing required becomes apparent when taking into account measured threshold ('T') and comfort ('C') levels of each patient in different scenarios, as described in the chapter 1 and chapter 4. The T and C levels dictate what degree of focussing, if any, is required. T and C levels vary greatly depending on several factors, including inter-patient anatomical variation of the cochlea, electrode array model and manufacturer, electrode array placement, variation over time after implantation and variation from basilar to apical electrodes.

As it is difficult to find an average T and C level. Instead, eight examples are demonstrated in appendix H, two of which are shown below. There are two groups of subjects, four with an inner placed electrode array, and four with an outer placed electrode array. The T and C levels, measured for each patient at each electrode, were adapted from threshold currents into threshold voltages using the cochlea model, as described in appendix H.

Figure 3.16 and Figure 3.17 demonstrates the difference in focussing strategies for an inner and outer placement of the electrode array, when stimulating at the C-level of the particular subject for the 11th electrode, along with measured patient T levels. The subject threshold levels were obtained from (Pfingst and Xu, 2004).

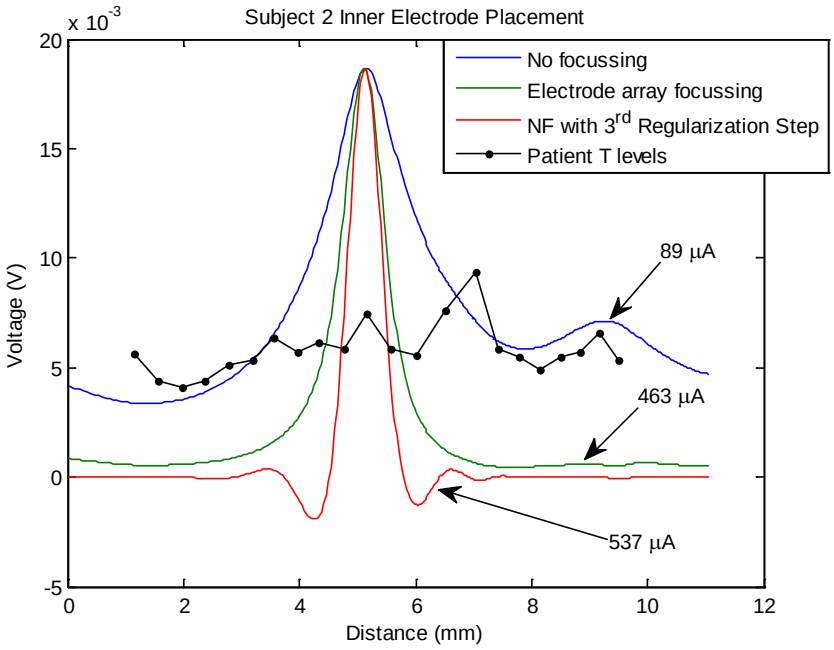

Figure 3.16: Focussing using different strategies. T levels are for subject 2 with an *inner* electrode placement.

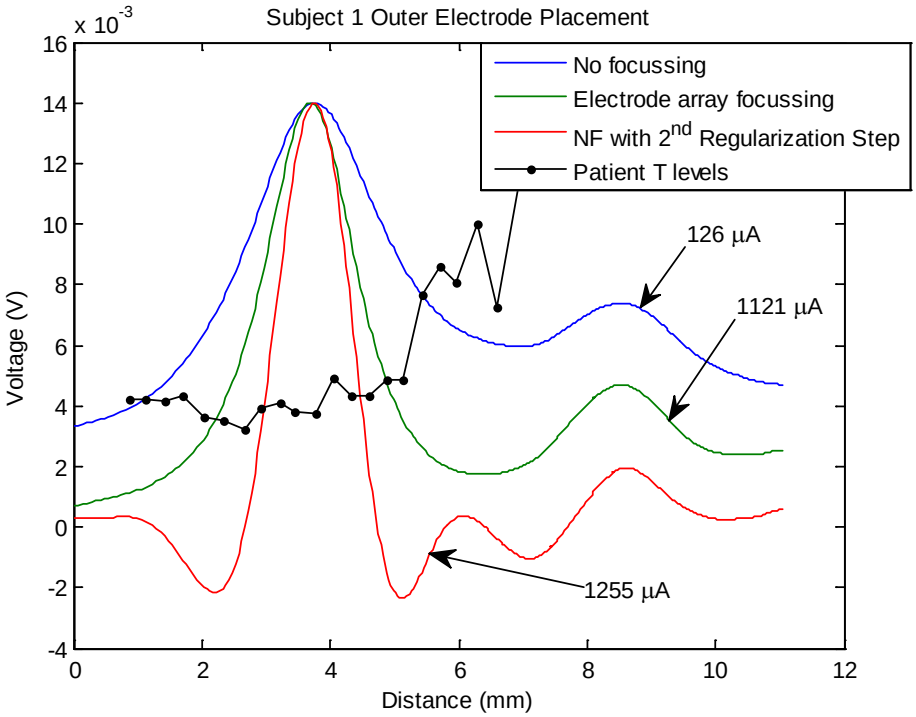

Figure 3.17: Focussing using different strategies. T levels are for subject 1 with an *outer* electrode placement.

Figure 3.16 and Figure 3.17 demonstrate the trade-off between the total current required and the focussing width with respect to subject thresholds. At a certain level of regularization, shown in Figure 3.16 and Figure 3.17, the resultant voltage spread is sharper using focussing at the neural level as opposed to at the electrode array for a similar total current requirement. In the case of subject 2 with an inner placement of the electrode array, in Figure 3.16, it is clear that neural focussing has a significant impact on narrowing down the region of nerves that could be potentially excited, at the T level from 8 electrode positions without focussing, to 3 with electrode focussing, to 1 with regularised neural focussing. In the case of subject 4 (Appendix H) for the same inner placement, the subject is less reliant on the neural focussing method for the narrowest region of excitation. In the case of an outer placed electrode array, the threshold levels for subject 1, in Figure 3.17, clearly indicate the benefit of using the neural focussing method whereas in the case for subject 2 (Appendix H), the benefit is marginal.

Results for other subjects are also shown in Appendix H. These results show that from across subjects, threshold and comfort levels differ as well as the difference between them. When the difference between T and C levels is large, this implies that when stimulating at

the C level, the threshold level is significantly lower along the spiral ganglion and so more of the spiral ganglion is excited. This therefore implies that better focussing is required to focus the voltage towards the desired target area on the spiral ganglion. If the difference between T and C levels is smaller, then less of the spiral ganglion is potentially excited and so neural focussing is not necessary.

Conclusion

This section has shown that whilst electrode array focussing is a viable option, this strategy is much less effective at the spiral ganglion position. Figure 3.16 and Figure 3.17 show the effect of neural focussing in achieving a better focused voltage spread than focussing at the electrode array, for both the inner and outer placement cases respectively in relation to varying subject thresholds. It was also found that some patients may not benefit from neural focussing depending on the threshold levels across the spiral ganglion.

In the interest if conserving power, regularization could be introduced at the electrode array level but aside from reducing current requirements, it widens the voltage spread further, resulting in a broader excitation across greater area of neurons, which hinders performance, and so this is considered to be an impractical option. Future cochlear implant designs may reduce power requirements of other components, such as the processor and reduction of power loss with a full implantable design. These reductions in power requirements could lead to flexibility in selecting an appropriate level of focussing at the neural level to achieve the desired result.

3.5 Modiolus reference electrode test

The nucleus 24 implant uses two return electrodes, a plate and ball electrode. The plate electrode is embedded within the stimulator casing away from the cochlea. The ball electrode is connected via a thin wire and is placed beneath the temporalis muscle closer to the cochlea (Pfingst and Xu, 2004). An alternative way to reduce stimulation power requirements, could be to place the return ball electrode nearer to or within the modiolus, as suggested by Ho et al. (2004). It is expected that by placing a return electrode nearer to the target nerves, as well placing the nerves in between the active and return electrodes, current requirements would reduce dramatically, as discussed in chapter 2 section 2.1.2. This theory was tested using the spiral model of the cochlea, using the inner placement of the electrode array, with a ball electrode of width 1 mm introduced within the modiolus.

Four cases were tested:

1 – A control case with both the plate and ball electrodes activated

2 – Only a single outer surface of the bone enclosure set equal to ground.

3 – Only the outer surface of the return ball electrode set equal to ground.

4 –Both the return ball electrode and the single outer surface of the bone enclosure set equal to ground.

These four cases were compared using a simulation using a tightly coiled cochlear implant as in Figure 3.2.

3.5.1 Control Case

The control case considers that both plate and ball return electrodes are on the outside of the cochlea. This is represented by setting all outer surfaces of the bone enclosure to ground. The result is shown again in Figure 3.19.

The resulting geometric and boundary condition changes are outlined in Figure 3.18.

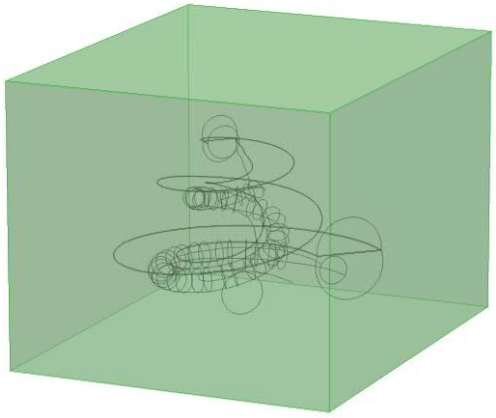

Figure 3.18: Wireframe of the modified geometry of the cochlear model for the control case. The green surfaces indicate where the boundary condition is set to ground, representing both the ball and plate return electrodes outside the cochlea.

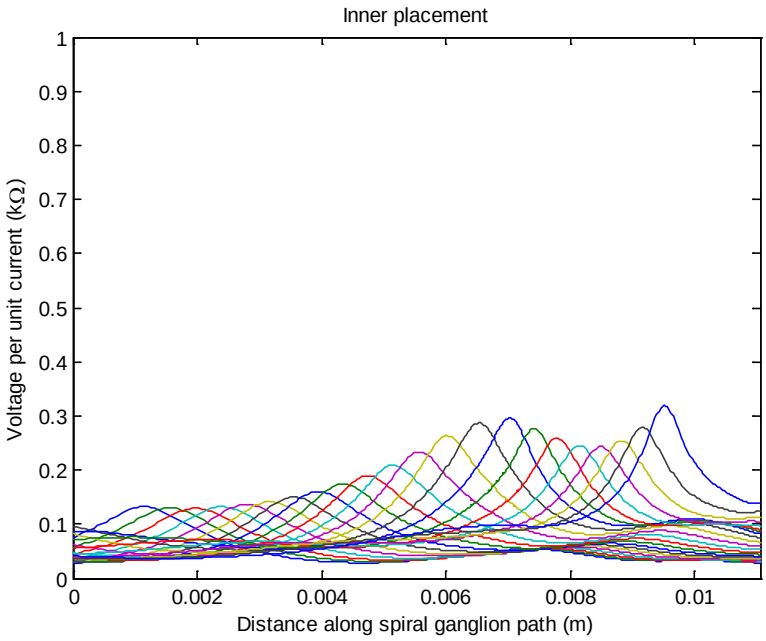

Figure 3.19: Resulting voltage distribution at the spiral ganglion pathway for unit current input into each of the electrodes, using both return electrodes placed outside of the cochlea.

3.5.2 Second Case

The second case takes into account possible "directionality" to the ground boundary condition due to the plate electrode. In this simulation, the ground boundary condition is applied to the single outer surface of the bone enclosure that best corresponds to the direction of the plate electrode in relation to the rest of the model. This is shown in Figure 3.20. All other parameters and boundary conditions were left unchanged as before and the voltage spread was calculated alone the electrode array. The result is shown in Figure 3.21.

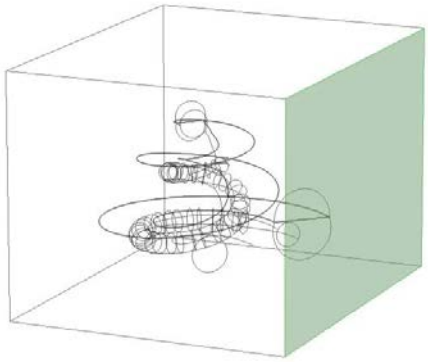

Figure 3.20: Wireframe of the modified geometry of the cochlear model for case 2. The green surface indicates where the boundary condition is set to ground, representing only the plate return electrode outside the cochlea.

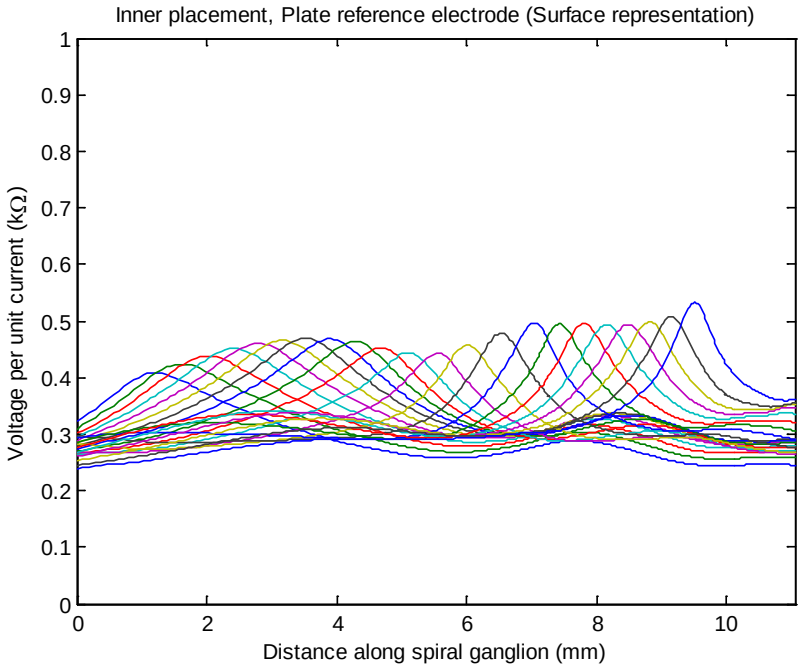

Figure 3.21: Resulting voltage distribution for unit current input into each of the electrodes, using only the plate reference outside of the cochlea as ground.

It is clear from Figure 3.21 that the general pattern of the distribution is similar to that of the control case, but the voltage levels are much higher in this case than the control and are sustained throughout the cochlea with a floor impedance of about 0.25 kΩ. This is due to the much smaller surface area of the ground boundary condition. It is assumed here that the neural excitation is dependent on the voltage level but in fact, the exact mechanism is not yet well understood. It is probably important to increase the voltage difference between different places on the spiral ganglion, not just the magnitude of these voltages.

3.5.3 Third Case

In this case, only the outer surface of the return ball electrode in the modiolus is set to ground. This implies that the plate electrode is not being used.

The resulting geometric and boundary condition changes are outlined in Figure 3.22.

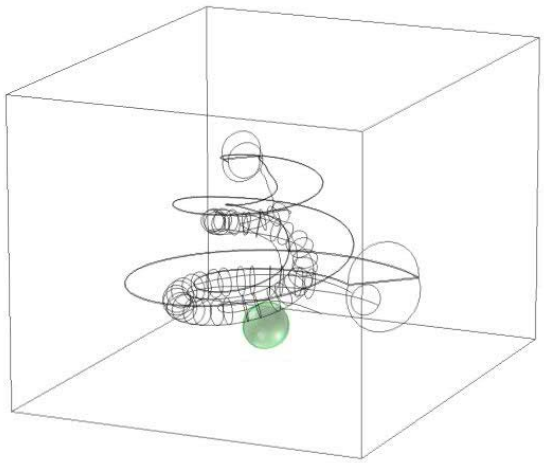

Figure 3.22: Wireframe of the modified geometry of the cochlear model for case 3, with the ball electrode placed within the modiolus. The green surfaces indicate where the boundary condition is set to ground, representing the ball return electrode within the cochlea.

All other parameters and boundary conditions were left unchanged and the voltage spread was calculated along the electrode array. The result is shown in Figure 3.23.

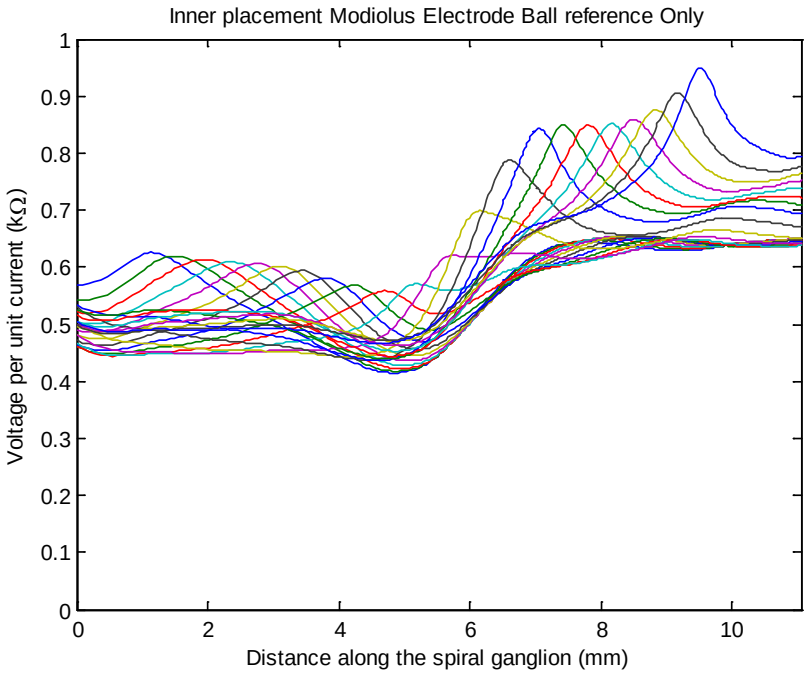

Figure 3.23: Resulting voltage distribution at the spiral ganglion pathway for unit current input into each of the electrodes, using only the ball return electrode within the modiolus.

Figure 3.23 shows that the result with the ball return is very different from that with the return as the outer surface of the bone (plate), as in Figure 3.1. The return ball electrode has an even smaller outer surface compared with that of the control case and case 1, which would increase the impedance, although the ground boundary condition has been moved closer to the implant array, which would decrease the impedance. The net effect is an increase in the stimulation voltage. The nerves now sit in between the source electrode and ground allowing more current to flow through. The expected result, demonstrated in Figure 3.23, is that voltages are much higher throughout the model, implying that higher voltages are achieved for the same excitation current input as expected. Hence, lower currents could be used to achieve similar voltage levels compared with the control shown in Figure 3.19 and the result in Figure 3.21.

The nature of the position of the return electrode with respect to the spatial orientation of the spiral ganglion path, along which measurements are taken, would also result in higher resistance towards the apical end of the pathway and a dip in the resistance at about the 10th electrode where the pathway runs closest the ball return electrode.

3.5.4 Fourth Case

The final case considered is where the surface representing the plate electrode and the ball electrode surfaces within the modiolus are both set equal to ground.

The resulting geometric and boundary condition changes are outlined in Figure 3.24.

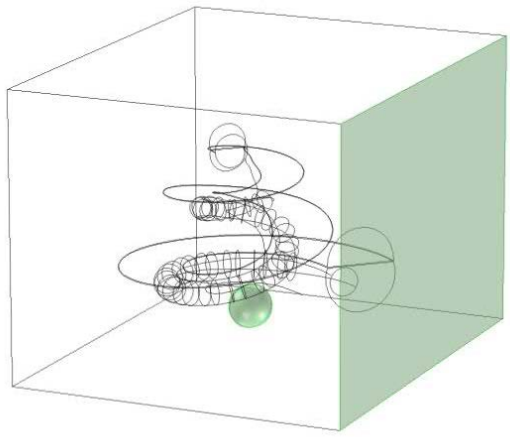

Figure 3.24: Wireframe of the modified geometry of the cochlear model for case 3, with the ball electrode within the modiolus. The green surfaces indicate that the boundary condition is set to ground representing both the plate and ball return electrodes.

All other parameters and boundary conditions were left unchanged and the voltage spread was calculated along the electrode array. The result in Figure 3.25 shows that when the directionality of the plate electrode is introduced, the benefit of a modiolus return electrode becomes clear. The general shape of the voltage spread is largely unaffected in comparison to the result in Figure 3.19, but the impedances are higher such that if the same current is applied, higher voltages would be achieved at the spiral ganglion. This in turn would once again imply that for a lower current input, similar voltages could be achieved as in Figure 3.1. On average, the impedance along the spiral ganglion is increased by approximately 0.1 to 0.2 kΩ which at some electrodes, in particular at the basal end of the cochlea, represents a doubling or tripling of the voltage for the same current.

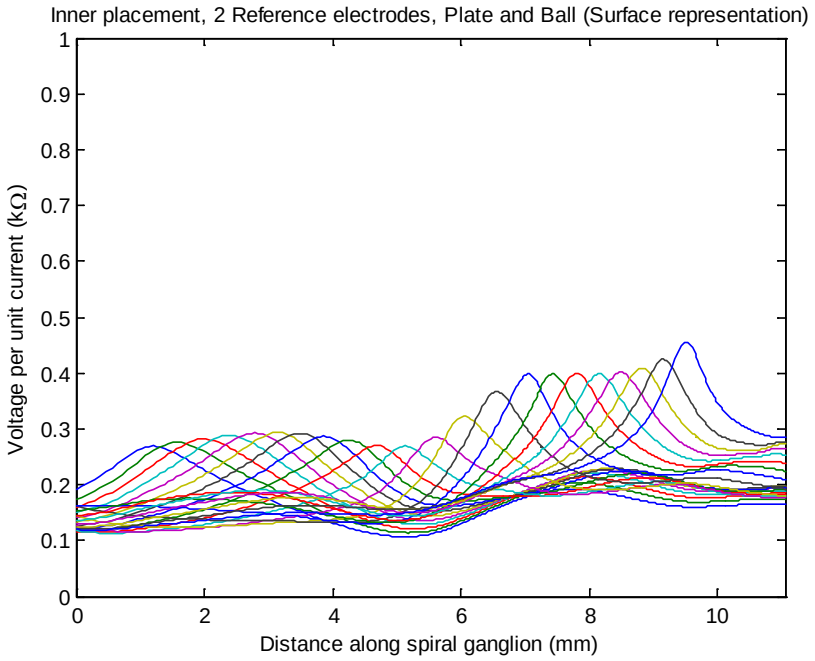

Figure 3.25: Resulting voltage distribution at the spiral ganglion pathway for unit current input into each of the electrodes, using both the ball return, within the modiolus, and plate return electrode, outside of the cochlea.

In case three, it was shown that placing the ball electrode within the modiolus increases the stimulation voltage. This was only true when the ball electrode was the only active ground. When the outside of the bone enclosure was set to ground, the source electrode is placed in between the ground electrode and the target nerves. This discourages current to travel to the nerves. When the ball electrode is placed within the modiolus and is individually activated as the ground, then the nerve is now effectively positioned in between the source electrode and the ground. This implies that when only the ball electrode is active, higher voltages could be achieved at the spiral ganglion for the same current input but this consequently implies high voltages throughout the cochlea which may not be practical. When activating both the ball electrode within the modiolus and plate electrode outside the cochlea as ground, however, as shown in Figure 3.24, it was found that this combination resulted in a more similar distribution to that of the conventional control case, but still resulted in higher impedances at the peaks than the control case.

3.6 Discussion

The spread of voltage excitation was investigated in order to better understand the different ways in which the current can be controlled to improve neural excitation, as well as addressing the issue of power loss. The focussing study in section 3.3 and 3.4 shows that focussing at the electrode array does not in fact have the desired effect at the neural level along the positions of the spiral ganglion. The method of using an electrode array to test the strategy proposed by van den Honert and Kelsall (2007) is limited in that the electrode array cannot be used to measure the impedance along the spiral ganglion and so focussing performance at the neural level cannot be measured. This impedance is possible to measure in the model presented in this chapter, and it was also shown that the voltage spread can be better focussed using a neural level focussing method, although a balance between the degree of focussing and the current requirements must be taken into consideration. Also, placing the ball reference electrode within the modiolus was found to increase the voltages achieved at the spiral ganglion for the same current input compared with more remote reference electrode placements.

The study of the focussing strategies and reference electrode position could lead to two improvements in cochlear implant design: One is that the presence of the ball electrode within the modiolus could lead to reduced power requirements resulting in longer battery life or increased flexibility in designing smaller batteries for a fully implanted device. The second is to use the extra power available to improve the focussing effect at the neural level, resulting in more accurate stimulation and consequently probably improving speech recognition. The impedance of the electrodes at the basal end is doubled or tripled with a modiolus electrode, this therefore means that the current required to achieve the results in the focussing study are greatly reduced. This trade-off between current requirements and focussing strength could be optimised such that some power reduction is achieved while improving the degree of focussing during stimulation. Alternatively, the extra power could be used elsewhere in the cochlear implant process.

Chapter 4

4 Stimulation strategies in the cochlear implant

4.1 Introduction

As discussed in chapter 1, cochlear implants have been shown to reinstate the sense of hearing to the hearing impaired, although, power consumption is still a major issue. There are many aspects of power consumption, including processor efficiency, transcutaneous link power loss and the interaction between the electrode and nerve ganglion cells. Wang et al. (2008) has suggested that the electrode array is where the largest losses occur in the implants power distribution. This chapter explores the power required to trigger the nerve fibres when the electrodes are driven using different strategies generated by the cochlear implant processor.

The acoustic input from the implants microphone is digitally sampled, and then processed according to the particular processing strategy. The first stage of processing is to split the signal up into different frequency bands for each channel, which can be achieved using either a filter bank or Fast Fourier transforms. In recent years the latter is much more widely used (Boex et al., 1996). The ultimate result of the processing chain is a generated pulse sequence that carries information with respect to magnitudes of current levels and their corresponding electrode. This is delivered to the implant chip (or receiver/stimulator), which in turn delivers the pulse to the electrode array in order to trigger an electrical interaction between the electrode and the corresponding target nerves. Each pulse in the sequence varies in amplitude to represent the energy in the channel corresponding to that pulse. The rate at which the pulses arrive at each electrode is called the Channel Stimulation Rate and this parameter defines the number of pulses per second for a specific electrode. The total number of pulses being delivered per second from the receiver stimulator is referred to as the total stimulation rate, which is the summation of all the pulses per second across all electrodes. The strategies used at the moment usually use constant rates of stimulation.

It is the total stimulation power that is of most interest. This chapter investigates some of the different stimulation strategies used in industry, and how variation in parameters that define these strategies affects the power requirements. The numerical analyses performed in this chapter are based on the Nucleus implant manufactured by Cochlear Corporation and these calculations are performed using the Nucleus Matlab Toolbox (2008) software provided by Cochlear Corporation, referred to hence forth as NMT.

4.2 Strategy

The algorithm of converting speech into a pulse sequence is referred to as a strategy (Vondrasek et al., 2008). In the case of the 4th generation implant from Cochlear Corporation, the Nucleus 24 Freedom electrode array, there are 22 electrodes requiring 22 band pass filters. Other electrode array models from different manufacturers have a different number of electrodes and consequently a different number of filter banks (MeDel electrode arrays typically have 12 and Advanced Bionics electrode arrays typically have 16).

The audio signal can be filtered in one of two methods: Digital FIR filters ((Wilson and Dorman, 2008),(Boex et al., 1996)) or FFT filters. In the case of an FIR filter bank, the bank of 22 band pass filters are used to filter the input audio wave in the time domain, resulting in 22 new filtered signals or channels containing frequencies within predefined bandwidths. They must then pass through a half or full wave rectifier to convert the filters output into a positive envelope. The signals are generally passed through a low pass filter to smooth the envelope, cutting out the high frequencies to avoid aliasing, as CI users cannot perceive fast modulation (fast temporal changes), although a half-wave rectifier has been used without a low pass filter (Wilson and Dorman, 2008, Rauschecker and Shannon, 2002). The result is a set of time varying envelopes representing how each frequency band in the signal varied with time. This process is generally referred to as envelope detection, and it is these envelopes that will be used to modulate the pulse sequence depending on the strategy deployed. Spectral information is affected by the number of filters used and their order whereas temporal information is sensitive to how smooth the resulting envelope is (low-pass filter). The stimulation rate needs to be at least twice that of the cut-off frequency of the envelope to avoid aliasing.

The FFT method analyses the entire audio wave by converting the data into a frequency spectrum and splitting the spectrum into predefined bins (a 128 point FFT gives 64 bins,

one of which is not used as it is at zero Hz) and those bins are summed and sorted into the 22 bands that correspond to each electrode. The spectral information in this method depends on the FFT length and the window applied. Temporal information is affected by the number of FFTs performed per second as well as the overlap in time. Both filter bank methods essentially generate the same result, but the FFT method is generally more efficient in terms of speed.

Frequencies in between the centre frequencies of adjacent band filters can be conveyed using the finite cut-off rate of the filters, which affect the ratio of the amplitudes of the stimulation pulse of the two corresponding adjacent electrodes (Wilson and Dorman, 2008), as is discussed in section 4.5.1.

4.3 Different Strategies using constant rates

4.3.1 CIS:

The Continuous interleaved sampling strategy (CIS) was the first strategy to use a digital filter bank and was originally used as the default strategy or processing option in all implant systems. The aim of this strategy is to deliver information about the acoustic wave by using rapid temporal changes in the waveform of the acoustic signal (NMT, 2008). The acoustic input (from a microphone or other device) is put through a pre-emphasis amplifier to attenuate strong components in the signal below 1.2 kHz. The input speech or sound is then filtered into bands of frequencies. In this strategy the number of processing bands is fixed for each individual but can vary between patients. In practice this strategy has been implemented using between 4 – 22 channels. The width of the filter bands in this strategy increases almost logarithmically, according to characteristic frequencies that correspond to the tonotopical arrangement of the basilar membrane (Vondrasek et al., 2008). This is so that it coincides approximately with the logarithmic increase of frequency sensitivity shown by the cochlea. The strategy does not discriminate between different channels based on energy levels of each band in the way that Ace and Speak strategies do (as discussed later) but rather all the information available is used for stimulation (Vondrasek et al., 2008). The variations in the envelopes in different bands are detected and later represented at the cochlea via the electrodes as modulated trains of biphasic electrical impulses (Wilson and Dorman, 2008), as discussed in section 4.7. Once the envelopes are extracted, they are compressed using a non-linear mapping function in order to compress a 100dB dynamic range into the much smaller range (10 dB) used for

electrically evoked hearing. Channel mapping then takes place, where the sequence of pulses is generated from the processed information, and it is the output sequence for each band that is sent to a single corresponding electrode (Wilson and Dorman, 2006). In most strategies, a random access memory with battery backup is used to store information needed for mapping such as thresholds and comfort levels when dictating current levels of the pulse sequence. In the CIS strategy this also stores the number of channels used (Vondrasek et al., 2008). The CIS strategy can be defined as a strategy with a high stimulation rate and a fixed low number of processing bands.

The pulse trains are interleaved in time so that they are non-simultaneous (staggered) across all the channels. This is to eliminate a component of electrode interaction which would have been produced by direct vector summation of the electric fields from different electrodes stimulated at the same time (Rauschecker and Shannon, 2002).

4.3.2 SPEAK:

Spectral Peak (SPeak) is another strategy that was developed by Cochlear Corporation and was implemented in cochlear implants with successful results. The SPeak strategy relays information about the acoustic waveform depending on the frequency content of the waveform (NMT, 2008). Therefore the number of stimulation channels is not fixed but rather varies depending on frequency. It uses either a bank of 20 filters which can be modified and programmed digitally or the FFT method described above. The signal is analysed in the frequency domain, the strategy analyses the relative amplitudes of information in each band (Staller et al., 1996). The SPEAK strategy uses a channel selection scheme such that within the *m* number of channels, the envelopes (or power in each band) are scanned before each stimulation event, and the *n* highest amplitudes of the envelopes (or powers) of the signal are sent to the corresponding electrodes only. Therefore, only *n* number of electrodes are stimulated at any one time (Wilson and Dorman, 2008). This number is adaptive, according to the level and frequency content of the signal (Staller et al., 1996). The energy of the rejected bands is not used for stimulation, in contrast to the CIS strategy (Vondrasek et al., 2008). This selection is done in order to reduce the density of stimulation while still relaying the important information for speech recognition. The reduction in the number of electrodes stimulated also helps decrease the level of interference and masking between electrodes, which in turn improves the chances for successful speech recognition. It also reduces the signal to noise ratio, as you are taking the highest amplitudes and omitting the bands that only contain noise. This channel selection method is thus designed so that channel stimulation density is reduced while maintaining a high level of important information representing the

acoustic input. Typical impulse rates are approximately 250 pulses per second per electrode. This rate of stimulation is much lower than the *n*-of-*m* (explained later), CIS, and ACE strategies (Wilson and Dorman, 2008). Therefore, the SPEAK strategy can be characterised by having a low rate of stimulation and a relatively low number of processing bands, usually around 6 to 10 channels at any one time (Vondrasek et al., 2008). The SPEAK strategy has been used with a Nucleus 24 electrode but only supports 20 bands and so the first two electrodes in the 22 electrode device are not used (Staller et al., 1996, Vondrasek et al., 2008).

4.3.3 ACE:

The ACE (Advanced Combination Encoder) strategy encodes the information on the acoustic wave in terms of both temporal and spectral changes (NMT, 2008). It uses the same selection process as the SPEAK Strategy but the number of active channels, *n*, is fixed for this strategy. Typical impulse rates are about 1000 pulses per second per electrode. This strategy is more or less identical to the CIS strategy except for the lack of channel selection (Wilson and Dorman, 2008). This strategy can be characterised by high stimulation rates while using a high number of processing bands (Vondrasek et al., 2008). It uses a 22-band filter (2 more than SPEAK). The two extra bands (bands 1 and 22) correspond to the apical and basal electrode respectively. ACE is usually regarded as the strategy that takes the benefits of SPEAK and CIS and combines them giving the high stimulation rates and the maxima selection process. A very similar strategy developed by MeDel is called the *n*-of-*m* strategy. Advanced Bionics also developed the HiResolution, which is similar to the CIS strategy but uses higher rates of stimulation and higher cut-off frequencies for the envelope detectors and is limited to using 16 channels with 16 corresponding stimulation sites (Wilson and Dorman, 2008).

4.4 Fine structure stimulation

In the last few years, more and more emphasis is being placed on relaying 'fine structure' (FS) information to the cochlear implant. This works by varying the rate of stimulation according to the envelope of the signal. The signals can be decomposed to slowly varying envelopes that can modulate the stimulation rate of high frequency carriers and this modulation is referred to as the fine structure of the signal (Riss et al., 2008). The Instantaneous frequency of the carrier varies continuously.

When tests are performed using audio stimuli that mix the envelope cues from one set of bandpass filters with the fine structure (FS) of another set of bandpass filters, it has been found that for speech, envelope information was more important for 8 channels and above whereas FS information was more useful with one or two channels. Melodies were also perceived better using FS information up to 32 channels beyond which envelope cues took over and the work by (Riss et al., 2008) is in agreement that music is the most difficult to perceive. Both cues were important for an intermediate number of electrodes in sentence recognition. Lateralization of sentences, which is when cochlear implant users could focus on a specific source in the horizontal plane, is difficult with a small number of channels, but increasing this number resulted in improved performance.

There are limitations to using fine structure for stimulation. Changing the rate of stimulation of an electrode will, in general, only be perceived as a change in pitch up to 300 Hz. Present day electrodes use envelope cues whose frequencies generally reach 200 or 400 Hz or higher for the Hires strategy and so FS information could still be perceived at these low frequency ranges. Channel balance cues also result in FS information being conveyed and arise because of simultaneous or rapid sequential stimulation of adjacent electrodes.

There is also a conflict concerning the number of channels needed for fine structure information to be conveyed. The number of effective sites of stimulation seems to be limited to a range of 4 to 8 electrodes, regardless of the number of electrodes available. The number of different sites that can be discriminated during multichannel speech recognition is not equal to the number of sites that can be discriminated in frequency when stimulated in isolation (Wilson and Dorman, 2008). This implies that if fine structure is to be implemented, then any fine adjustments as to which site should be stimulated would be limited.

4.5 Strategy improvements

MeDel introduced a new strategy called FSP (fine structure processing), with an aim to increase the amount of FS information transmitted to the ear (Riss et al., 2008) . The idea uses the timings of zero crossings in the positive direction to convey the FS information for frequency bands with the lowest centre frequencies (up to the 4th band-pass filter, ~300 Hz). These zero crossing timings are represented with a short group of pulses for the corresponding channel. The amplitude of the pulse is determined from the magnitude

of energy in that band. The rest of the channels in the system use normal CIS processing. A limitation to the quality of marking the zero crossings is the requirement to interlace the pulses of all electrodes together. This is especially true when long pulses are used for a high number of activated electrodes.

Another approach is to use multiple stimulation sites for one channel and one bandpass filter. This is similar to the HiRes strategy and it referred to as HiRes with fidelity 120 options (HiRes120). It creates virtual channels to increase the number of discriminable sites beyond the number of physical electrodes (Wilson and Dorman, 2008). Virtual channels are discussed in more detail below.

(Riss et al., 2008) investigated the number of channels required for good perception using an FSP strategy. It was found that for under the conditions of the experiment regarding number of channels activated, there was no significant advantage for the FSP strategy over the CIS strategy. It was also mentioned, however, that this could be due to the low cut-off frequency at 300Hz used in the experiment which eliminates important temporal and frequency cues found in the low frequency region. This is especially important for music perception and the ability to convey F0 (fundamental frequency) information.

4.5.1 Virtual Channels:

Adjacent electrodes may be stimulated simultaneously to effectively shift the perceived frequency in any direction. Many subjects have been able to identify an intermediate frequency when two adjacent electrodes are stimulated. If perception of a frequency lower than that of the first electrode is required (i.e. lower than the frequency position at the most apical electrode in the implant) then a smaller pulse of opposite polarity would stimulate the adjacent electrode to cause the shifting effect in the direction required. These intermediate perceived frequencies alone can provide more discriminable sites along and beyond the electrode array.

This concept can extend to creating a high number of sites by using different ratios of currents transmitted to the electrodes simultaneously. With 6 intracochlear electrodes, for example, then by adjusting the ratios of currents (e.g. 25% and 75% then 50% and 50%) 21 channels can be achieved. A study by Firszt et al. (2007) found that an average of 93 discriminable sites were available when using 16 electrodes. The HiRes 120 strategy follows the same concept and although the stimuli for each of the channels are

transmitted in a non-overlapping manner, two electrodes are stimulated at the same time, unlike the CIS strategy.

The motivation for these virtual channel based strategies is to allow patients to detect relatively small changes in frequency in all types of sound. Music perception is very poor with CIS and so virtual channels would provide more effective frequency discrimination. This could increase fine structure information delivered at the electrodes. This effect could already exist using the CIS strategy, as well as other strategies using sequential stimulation, whereby non-simultaneous impulses sequentially stimulate adjacent electrodes creating a virtual perceptual pitch. This effect would only work if the sequential pulses are close in time for adjacent electrodes.

To compare CIS and virtual channel based strategies, tests have been done on speech perception in quiet and it was found that there was no difference between the two. This was not, however, tested for a large number of subjects nor was it tested for speech in noise or for music, so the investigation is not complete (Wilson and Dorman, 2008).

4.6 Use of strategies

Different strategies are deployed by different cochlear implant manufacturers and these details are shown in Table 4.1 (Wilson and Dorman, 2008). The strategies in italics are the default setting for the corresponding manufacturers (Loizou et al., 2000).

Manufacturer	CIS	*ACE*	SPEAK	*FSP (FS4)*	*HiRes*	*HiRes 120*
Cochlear Corporation	Yes	Yes	Yes	No	No	No
MED-EL Medical Electronics	Yes	No	No	Yes	No	No
Advanced Bionics Corp	Yes	No	No	No	Yes	Yes

Table 4.1: Strategies currently in use by cochlear implant manufacturers

*CIS is no longer in use by Cochlear Corporation

ACE, CIS and HiRes and very common and can give monosyllabic words at a 50% correct average score, although there is a large individual variation. Tests could be made harder by introducing noise, in which systems with a larger input dynamic range would outperform the lower input. These sorts of issues highlight that it is not always the obvious differences (such as number of electrodes) that have an effect on performance but also how common components are hardwired together and how they are implemented. Examples of these other important features include the input dynamic range and the shape of the compression function.

It is also thought that variability in results is due to differences in cortical or auditory pathway functions. On average, patients who were deaf for a short period of time prior to using the implant scored better than patients with a longer period of deafness. This leads to the belief that the longer the period of deafness, the more neurons and ganglion cells would degenerate due to sensory deprivation and also the use of these neurons by other sensory inputs (due to plasticity of the brain).

Generally speaking, patients with an intact or nearly intact neural distribution are expected to fare much better than patients without. In fact, no correlation was found between neural and ganglion cell survival and word recognition scores. Also, a number of ganglion cells are required for cochlear implants to work but this number is in fact small. In children, it was also discovered that after the age of 4, they become less adaptive to inputs and have generally worse results than younger children due to the difficulty of reinstating normal latencies in cortical responses (Sharma et al., 2002, Wilson and Dorman, 2008). It was also shown by Lee (2001) that metabolic activity in the auditory parts of the brain decreased with an increasing period of deafness. This corresponded to a rapid decrease of sentence score over a deafness period ranging between 2 to 20 years in the test. This is also because of brain cross-modal plasticity, where parts of the brain adapt to respond to more than one type of stimulus in the event of long term sensory deprivation.

Other tests, involving the MED EL COMBI 40 implant system that uses the CIS strategy, showed that results improved over a period of 24 months from when the implant was fitted. This improvement is more obvious along the lower ranges of scores. Even more evident improvements were observed for the results for sentences over 12 months until they reached a plateau at 90% whereas word test scores asymptote at 55 %. Such results are typical of the best cochlear implant systems. These are excellent results for the top scorers as only 8 broadly overlapping sections of the auditory nerve are stimulated using

this device taking into consideration that a large number of neurons (equivalent to stimulation sites), measurable in the thousands, are used in a normal hearing ear. The test also shows the important of brain plasticity as test scores improved due to learning which is required to make the most of sparse information (Wilson and Dorman, 2008).

Coding strategies, however, are not solely responsible for the quality of the delivered signal, as the pulse sequence also influences the recognition of sound.

4.7 Pulse Sequence Theory

A pulse is defined by its amplitude, width and period and these parameters are controlled by the processor. The pulse sequence, generated by the processor following the implementation of a strategy, is a made up of series of pulses that are biphasic and equally spaced out (constant stimulation rate). Biphasic pulses consist of a phase of positive amplitude with duration equal to the parameter Phase_width, τ, a short gap defined by the parameter Gap_width, and finally a phase of negative but equal amplitude and width to that of the positive phase. This is called a charge balanced pulse.

In the case of a Nucleus cochlear implant, a typical value for phase width is around 25 microseconds whereas the phase gap is usually around 8 microseconds (NMT, 2008).

(Hartmann et al., 1984) and (Miller et al., 1998, Miller et al., 2004) have studied the effects of the different types of pulse stimuli on the auditory nerve in animals, this was done mainly using a monophasic pulse where there is only a negative phase in the pulse. Monophasic pulses are not used on humans as a monophasic pulse will result in a build-up of charge following consecutive pulses that can cause irreversible damage to the tissue or the nerves. This is because when a stimulus is delivered and the nerve cells are polarised, chemical reactions take place that are generally reversible if the nerve is subjected to an opposing polarity shortly afterwards. In the case of monophasic stimulation, the charge build up does not allow for a reversal of the chemical reaction leading to irreversible build-up of chemicals that could be dangerous to biological tissue (van Wieringen et al., 2008). A biphasic pulse and its key parameters are shown in Figure 4.1. An example of a sequence of pulses is demonstrated in Figure 4.2. A review of the development of the pulse sequence is presented in Appendix I.

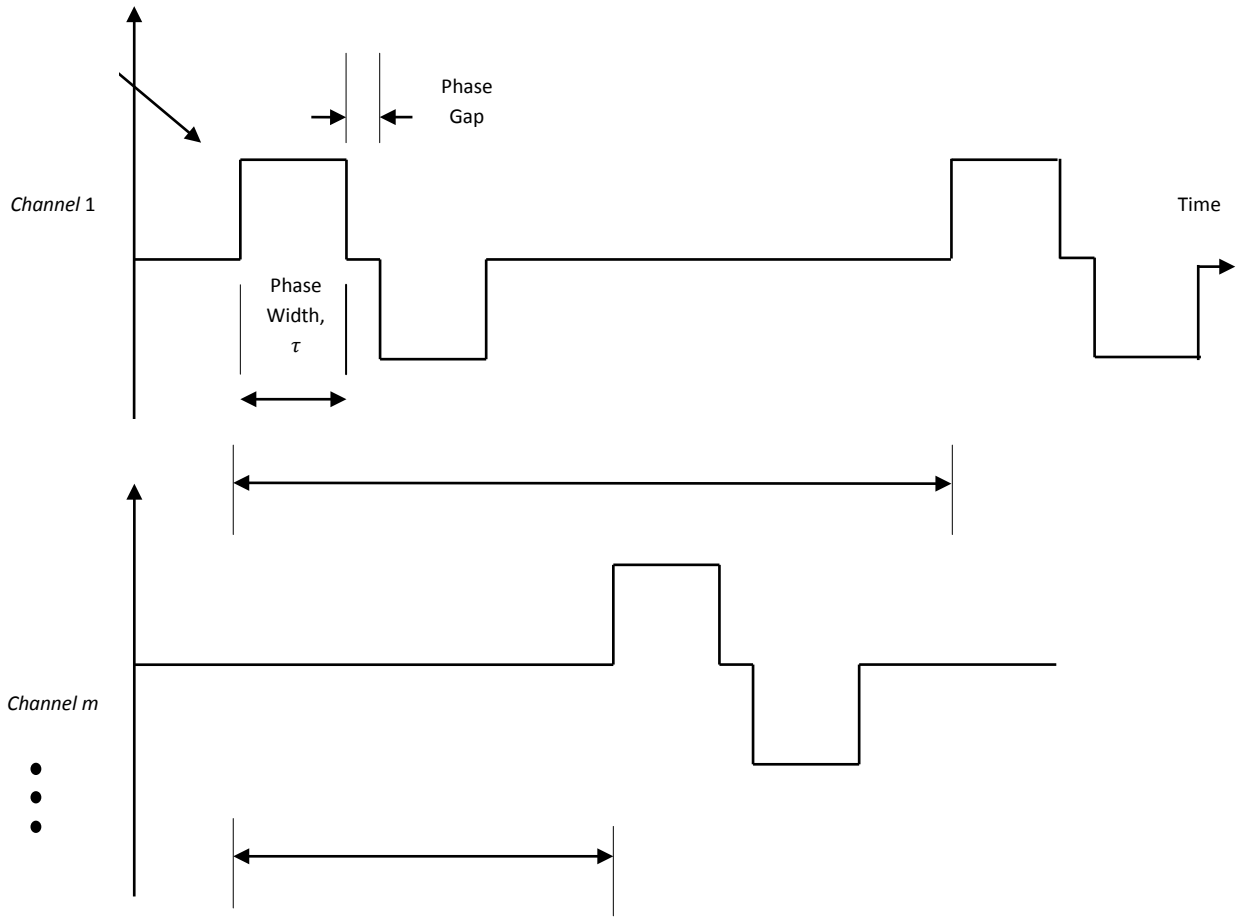

Figure 4.1: Biphasic pulse sequence with key parameters, where a is the pulse number in an individual channel, T' is the individual period, CSR is the channel stimulation rate, T is the total period, TSR is the total stimulation rate, and m is the electrode or channel number.

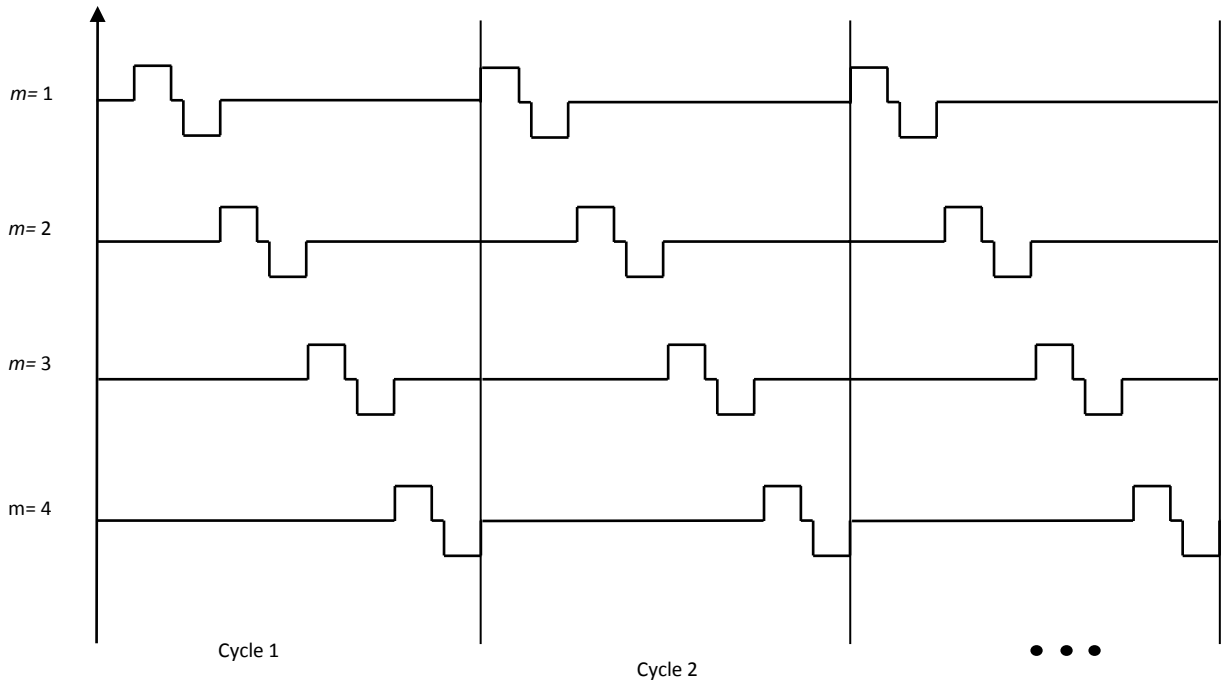

Figure 4.2: Example of a pulse sequence.

The total stimulation rate is defined by,

$$TSR = CSR \times n$$

The amplitude of the pulse is defined in the Nucleus Matlab toolbox by the parameter Current_levels and is proportional to the level of energy in the frequency band corresponding to that channel (or electrode). The units for the amplitude of a pulse are in terms of clinical units (c.u.) and they range between 0 and 255 units. Clinical units are converted to the equivalent current in amps in a way that is dependent on the type of implant chip being using. A typical value for the current is in the order of a several hundred microamps. The individual period is defined as the time between the start of one pulse to the start of the next within the same channel and this is set by the channel stimulation rate. The channel stimulation rate is the number of pulses per second delivered to a specific electrode. Simulation using the NMT toolbox, however, generates a pulse sequence for a particular input audio wave, and the pulse sequence is in fact defined as a long vector of pulses that are interlaced across all the active electrodes. Each pulse also contains information to be read by the implants chip to determine the current required and the electrode to which the pulse must be delivered. Frequency information is conveyed by driving an electrode with pulses generated from a frequency band, where

the electrode lies in the region of the basilar membrane governed by that same frequency band. This means that frequency content within that that band will be represented by one pulse at that moment in time. The amplitude of the pulse also depends on each patient's threshold and comfort levels as described in chapter 1. These two parameters define the dynamic range for each electrode to be used, and this is referred to as the loudness growth function (LGF). This function ensures appropriate levels of stimulation at all times within the patient's dynamic range for each electrode, by calibrating the amplitude of each pulse. The function is logarithmic such that the further you increase the clinical unit level, the less the increase in perceptual loudness until a perceptual loudness reaches a peak, and any further increase of clinical unit level no longer results in louder perception . The rate at which increasing the current unit level no longer has an effect on perceived loudness, varies in steepness by a parameter called the Q factor (NMT, 2008), as demonstrated in Figure 4.3.

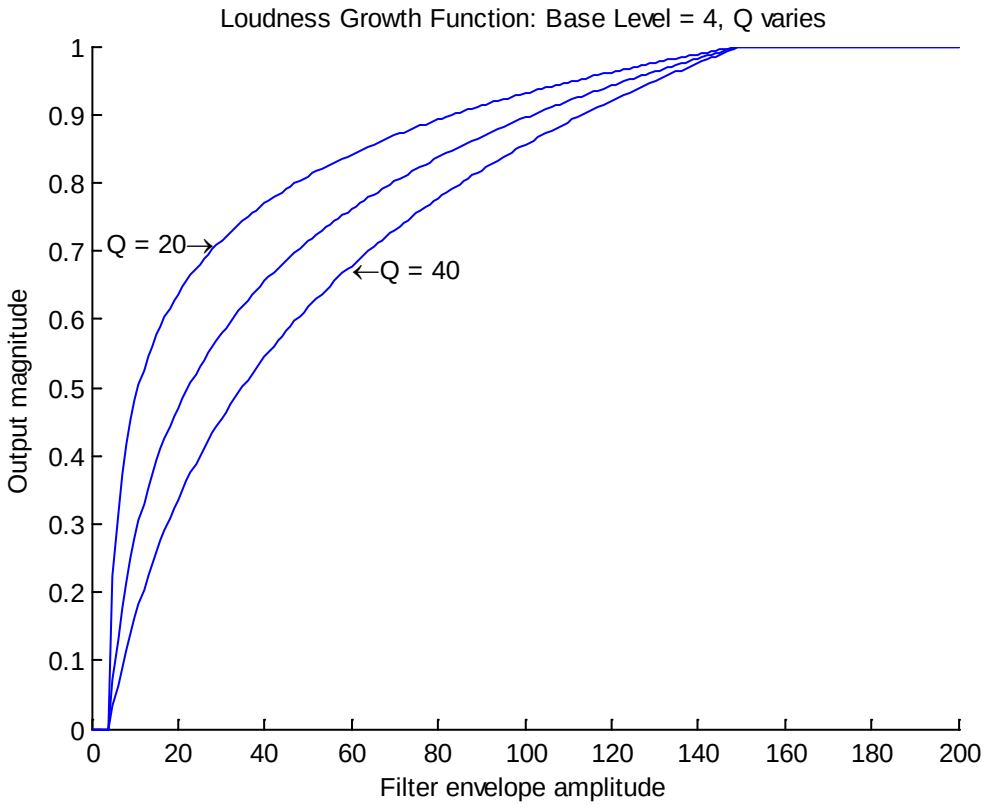

Figure 4.3: An example of the loudness growth function and how it varies with the parameter Q.

The base level is the level at which minimum stimulation occurs. The base level could be varied to control background noise by only allowing higher stimulation levels to be active (NMT, 2008). The LGF varies from patient to patient and depends on the position of the electrode array as well the mode of stimulation in use (Fu, 2005). The output magnitude in Figure 4.3 is normalised to the Comfort level of the patient whereas Threshold level of the patient is equivalent to an output magnitude of zero. For the purposes of this study, the parameter detail of a particular patient was used throughout the chapter, which was taken from the patient database of the South of England Cochlear Implant Centre (SOECIC) in Southampton, UK.

4.8 Audio Input and Power Calculation Theory

As discussed previously, the aim of this chapter is to analyse examples of a typical pulse sequence to investigate how much power is required at the stimulation phase. There are several types of speech recognition tests currently in existence. Each test is designed for a particular subject group defined by parameters such as age and whether or not they are postlingual. In the case of adults who are postlingual for example, (Staller et al., 1996) reports the use of lists of Central Institute for the Deaf (CID) sentences and lists of Consonant-Nucleus-Consonant (CNC) Monosyllabic Word Test. Most commonly used, the Bamford-Kowall-Bench (BKB) sentences are recorded open-set speech recognition test sentences for speech in noise testing. They were designed to be administered to hearing-impaired children based on their vocabulary, pre and post implantation of the cochlear device. These tests are performed pre and post implantation. BKB sentences have a large set but the length of each sentence varies within the set (Rauschecker and Shannon, 2002).

In this study, the Bamford-Kowall-Bench (BKB) speech sentences were used as the audio input to the simulation. They contain 50 key words in 16 sentences and they are usually used in assessment of more difficult speech perception skills and are linguistically complex (Staller et al., 1996). Parametric studies, discussed later in this chapter, only one sentence is used for consistency, but otherwise, all 50 sentences are used to generate an averaged result.

The first part of the simulation is to generate the pulse sequence. This is done by using a number of processes within the 'NMT toolbox' in Matlab, and the processes involved are listed in Figure 4.4 for the case of the ACE strategy:

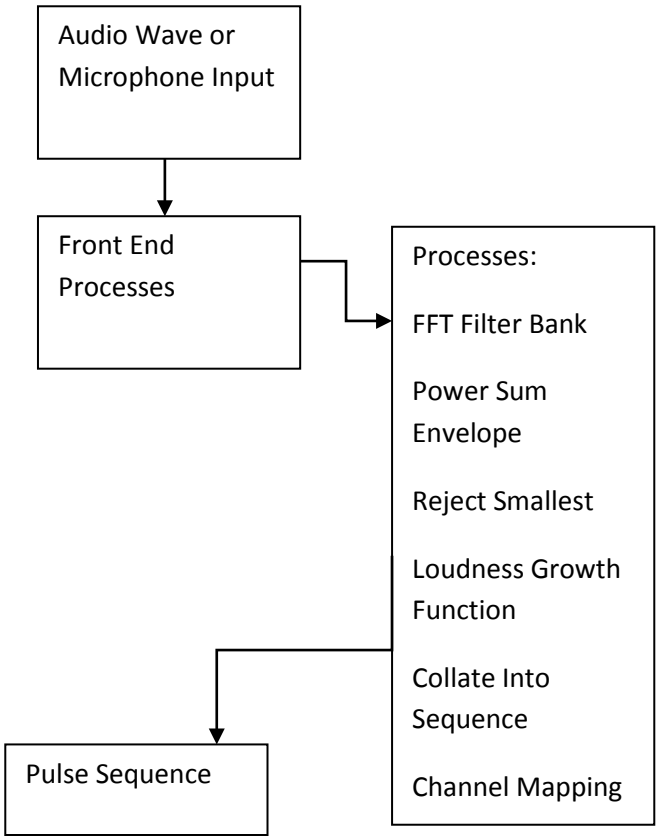

Figure 4.4: Block diagram of the process undertaken to generate a pulse sequence

The processes are initially set up and 'CIReadMap(p,'Subject.txt')' is used to set the parameter values according to a particular patient. The audio input is read within the front end processes, and an FFT filterbank is created according to the parameters set (otherwise default values are used).

At the filter bank stage the signal is split into blocks followed by the application of a window after which an FFT is performed on each block. The signal is analysed in its entirety and the resulting output is a frequency-time matrix where each row represents a frequency band (or electrode). Although the length of the FFT in this case is 128 (window length also 128), the number of useful bins is actually 64 (62 if you discard the 0 and 125Hz bins where).

The 'Power_envelope_sum' process simply sorts the bins into their correct bands and sums up the power of the signal in each band by adding the bins together to get an overall representative number.

In the ACE strategy a peak picking method is used whereby the highest *n* amplitudes or magnitudes are chosen from a possible *m* electrodes or channels (hence known as *n*-of-*m*) and this is done by the process 'Reject_smallest_proc'.

The signals then undergo amplitude compression, whereby lower amplitudes are boosted much more than higher amplitudes. This is done by calibrating the signals according to the patient's electrical dynamic range using the Loudness Growth Function ('LGF_proc') which was described earlier in this chapter. 'Collate_into_sequence_proc' then converts the output into the pulse sequence structured to reflect the strategy selected and this is the form in which the information will be delivered to the electrodes. This pulse sequence is now complete and can be delivered to the electrodes.

The power could be calculated in three ways: Instantaneous power, Average power per channel or average power over the entire sequence. All three can be calculated using one sentence or averaged over a list of sentences and they all begin in the same way. The average impedance values of each electrode for the subject is defined to be 6 kΩ, which is in agreement with (Tognola et al., 2005) and (Hanekom, 2005) and (deSauvage et al., 1997). The calculation assumes that monopolar stimulation is used (MP1+2) where current flows within the active and both reference electrodes (ball and plate). The reason for this is that MP1+2 is the most commonly used stimulation mode with the nucleus device (NMT, 2008). The amplitude of the pulses in the sequence is defined for each electrode as a current level (CL) (also referred to as clinical unit (c.u.)). This has to be converted into amps using the following equations from NMT (2008) and Hughes and Goulson (2011):

$$i(\mu A) = 10 \times e^{\frac{CL \times \ln(175)}{255}} \quad \text{for CI24M/R CIC3 based cochlear implants} \tag{4.1}$$

$$i(\mu A) = 17.5 \times 100^{\frac{CL}{255}} \quad \text{for CI24RE CIC4 based cochlear implants} \tag{4.2}$$

Where CI24M/R is a cochlear implant based on the 3rd generation implant chip (CIC3) used with the Esprit 3G processor and CI24RE is a cochlear implant based on the 4th generation implant chip (CIC4) used with the Freedom processor. Figure 4.5 below demonstrates how the current in amps varies with current level using equation (4.2).

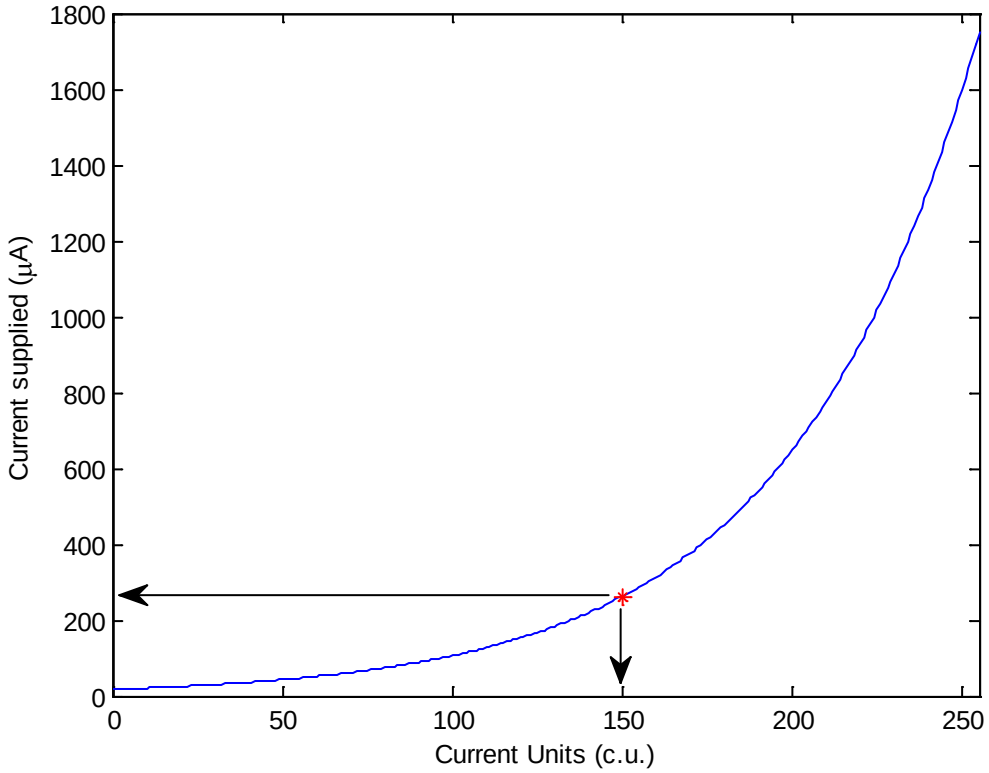

Figure 4.5: Supplied current against current level

Instantaneous power:

Once the current levels have been converted into Amps, equation (4.3) can be used to calculate the instantaneous power in a pulse.

$$Instantaneous\ Power\ = i_m{}^2 R_m \tag{4.3}$$

where i_m is the instantaneous current in the channel and R_m is the impedance of the mth electrode.

Average power per channel

This is obtained by taking the sum of instantaneous power for all pulses in one channel, and multiplying this by the duration that the power is on, and dividing by the total time. The average power for mth channel, $\overline{P}_m$, can be calculated by,

$$\frac{E_T(a,m)}{t_{tot}} = \frac{2\tau}{a_T T'} \sum_{a=1}^{a_T} i_{am}^2 R_m, \tag{4.4}$$

where E_T (a,m) is the energy for each pulse a, and electrode m, t_{tot} is the total time of the sentence, i_{am} is the input current for this pulse and electrode, T' is the individual period, τ is the phase width as defined in Figure 4.1, R_m is the electrode resistance for the mth channel and a_T is the number of potential pulses in the specified channel.

Average total power

This is obtained by calculating the instantaneous power of all the pulses in the pulse sequence regardless of channel number since channel stimulation rate is identical for all channels. The instantaneous power is then multiplied by the duration that the pulses are active and divided by the total time of the sentence. Therefore, the average total power per sentence, $\overline{P}_{av}$, is given by,

$$\overline{P}_{av} = \frac{2\tau}{b_T T} \sum_{b=1}^{b_T} i_{bm}^2 R_m \tag{4.5}$$

Where T is the total stimulation rate period, b_T is the total number of potential pulses across all electrodes for the entire sentence. Any averaging functions in these calculations only consider when the electrodes are active.

4.9 Power Calculation Estimates

The maximum instantaneous and average powers have been calculated for a sentence chosen at random from the sets of BKB sentences available and different stimulation strategies in Figure 4.6 to Figure 4.12. The sentence is represented in several different ways; the sound wave (Figure 4.6), the Frequency-Time Matrix (FTM) (Figure 4.7), and the electrodogram (Figure 4.8). The sound wave shows how the amplitude of the wave varies with time, the frequency time matrix shows how the amplitude at each frequency varies with time and finally, the electrodogram represents the FTM by displaying it as current levels of the pulse sequence in each frequency band that is sent to the electrodes using the ACE strategy. Figure 4.9 shows an electrodogram of the maximum instantaneous power of the pulses in the sequence using the ACE strategy. Figure 4.10 shows a magnified version of the electrodogram from Figure 4.9, in order to demonstrate the pulse sequence structure. Figure 4.11 shows the electrodogram for the CIS strategy

showing that only electrodes 10 to 22 are active for this strategy. Figure 4.12 shows how the average power varies over the electrodes for this sentence.

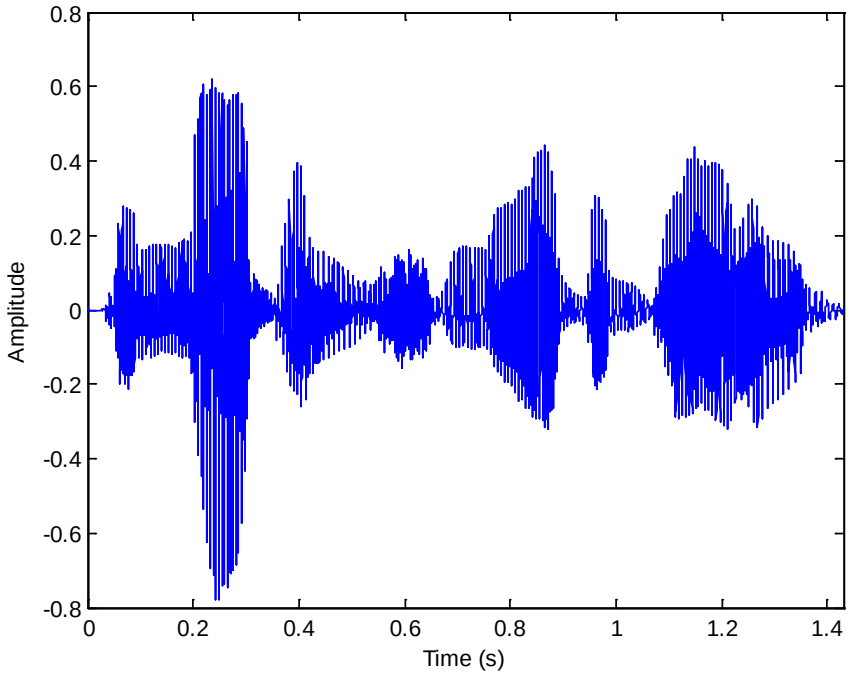

Figure 4.6: Sound wave

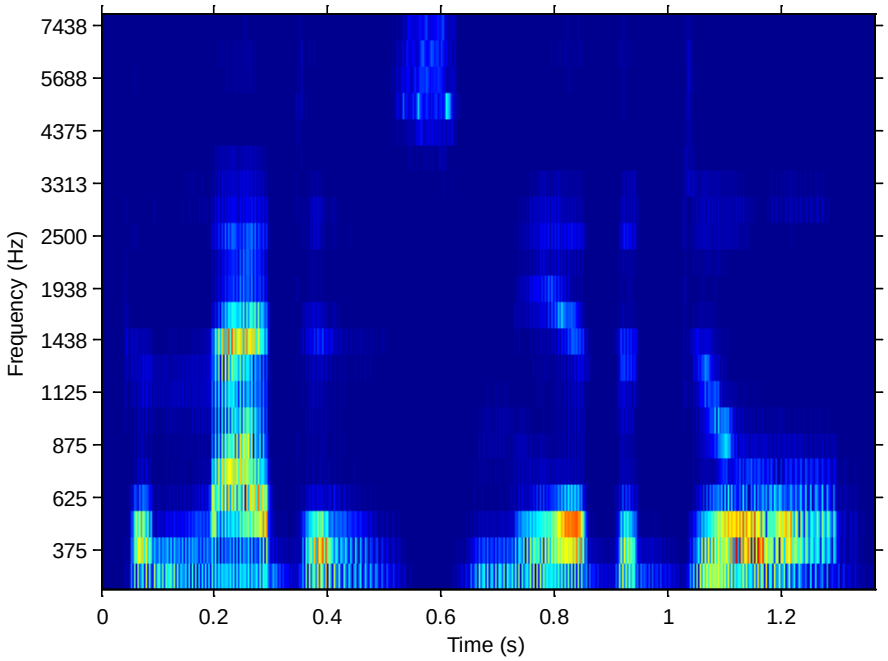

Figure 4.7: Frequency-Time Matrix

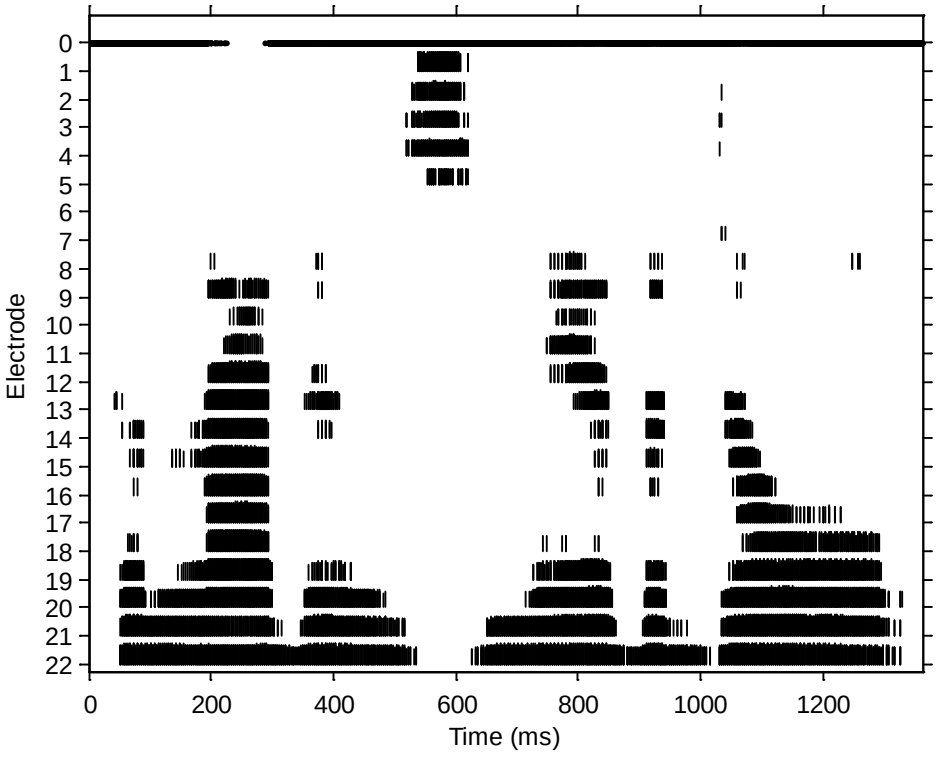

Figure 4.8: Current Levels Electrodogram using the Ace strategy

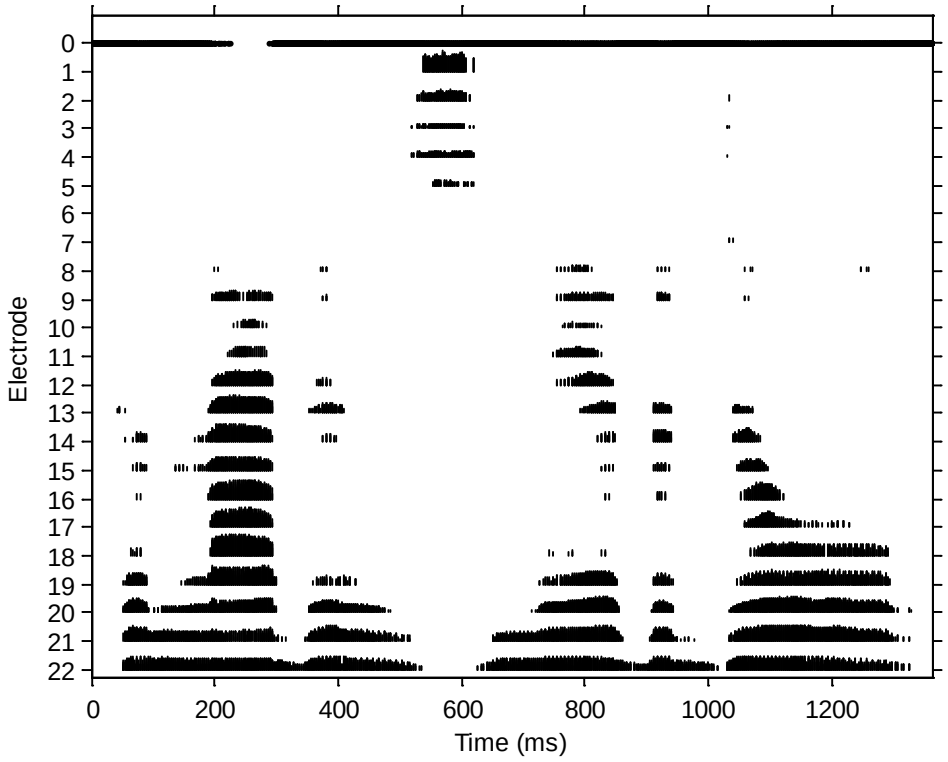

Figure 4.9: Instantaneous Power Electrodogram using the ACE strategy.

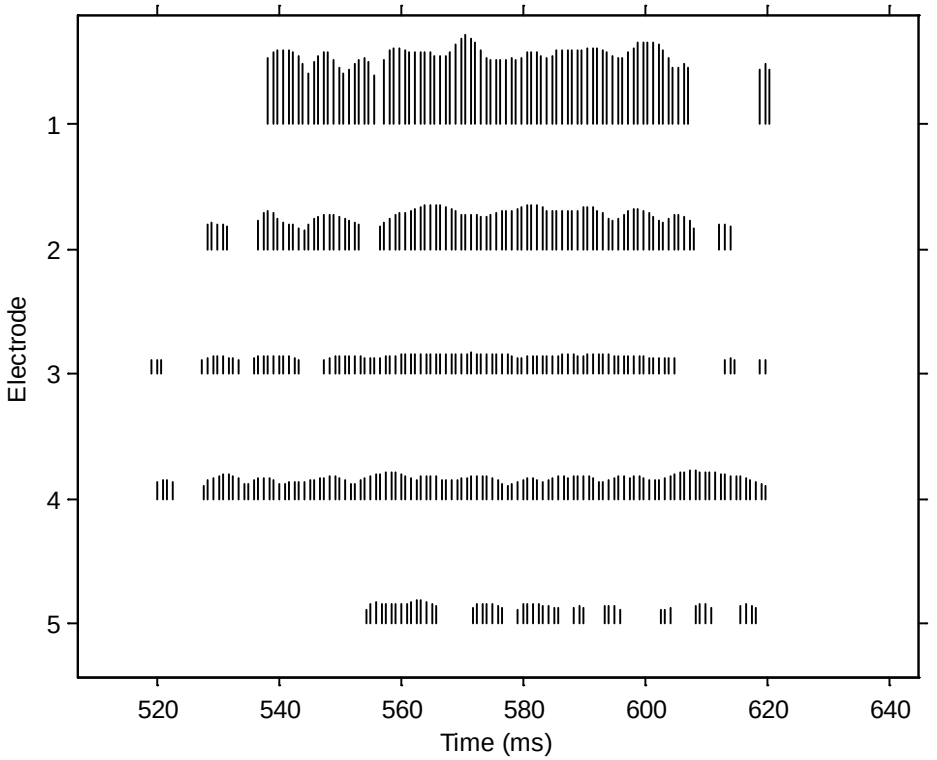

Figure 4.10: Magnified view of the electrodogram from Figure 4.9

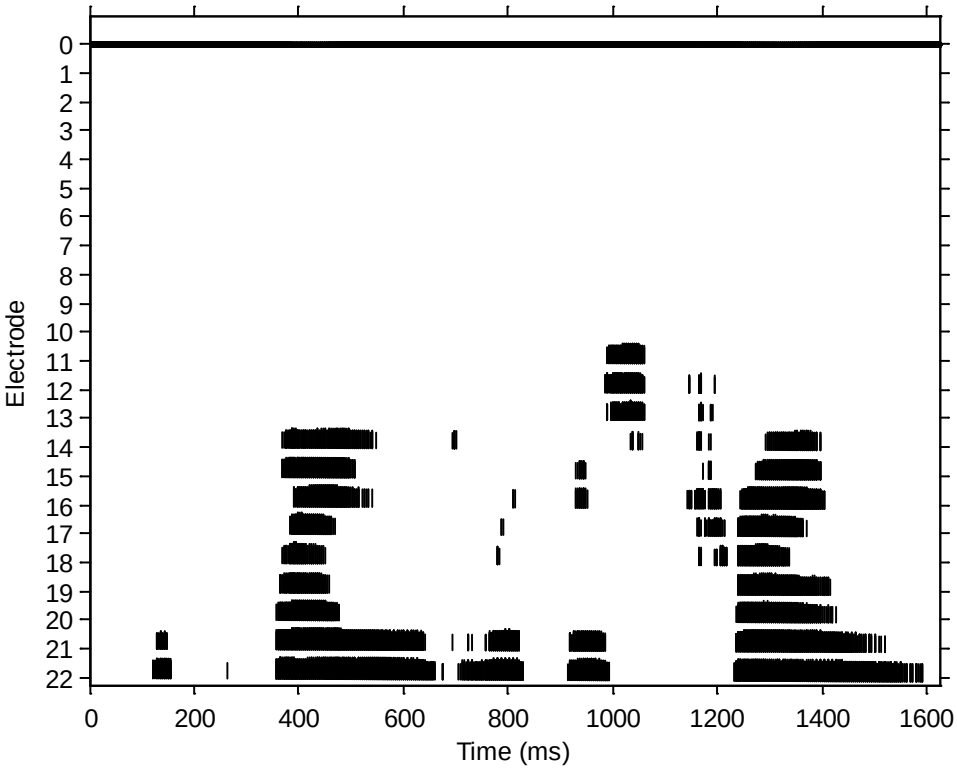

Figure 4.11: Electrodogram for the CIS strategy.

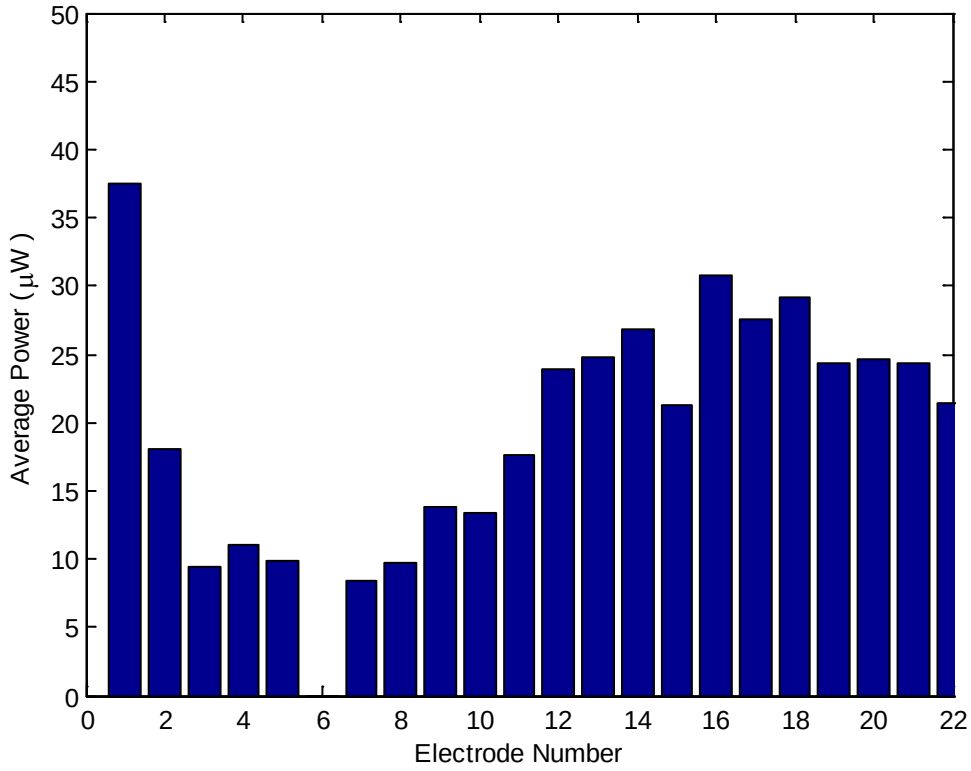

Figure 4.12: Average power against electrode number.

The average power, $\overline{P}_{tot}$, for this sentence was calculated to be about 0.28 mW. The maximum average power due to one electrode or channel for this sentence, $\overline{P}_{m}$, is around 37 μW. This corresponds to the 1st electrode. It is important to note that although electrode 1 has the highest average power, Figure 4.8 shows that it is in fact electrodes 19 through to 22 that are predominantly in use. The average power, $\overline{P}_{av}$, was also calculated across all the sentences available and this gave about 0.27 mW.

The *maximum* stimulation current that can be delivered to an electrode is 1.75 mA, and in the case where this current is used for all pulses in the sequence, at an average stimulation rate of 500 Hz, the *maximum* power required equates to 6.5 mw which is in agreement with the prediction of 5 mw required for electrical stimulation in the cochlea, as discussed in section 1.3 of chapter 1.

The power calculated for the sequence will depend on a host of parameters that should be investigated. Certain parameters would have a greater effect than others on the power consumption of the pulse and so the next section explores the effect of these parameters

on the power to define which should be monitored in the interest of reducing power requirements.

In the above calculation, the 6th electrode was switched off based on the strategy map of the patient.

4.10 Parameter Test

The main parameters investigated in this section include channel stimulation rate, the number of channels selected, T and C level adjustment and phase width. These parameters were selected as they represented the major differences between different strategies. The average power was calculated for different stimulation rates keeping everything else constant except for other parameters that are directly related to the stimulation rate and must change to maintain the validity of the strategy. The results are shown in Figure 4.13 and they are averaged over the set of BKB sentences available and presented along with the standard deviation.

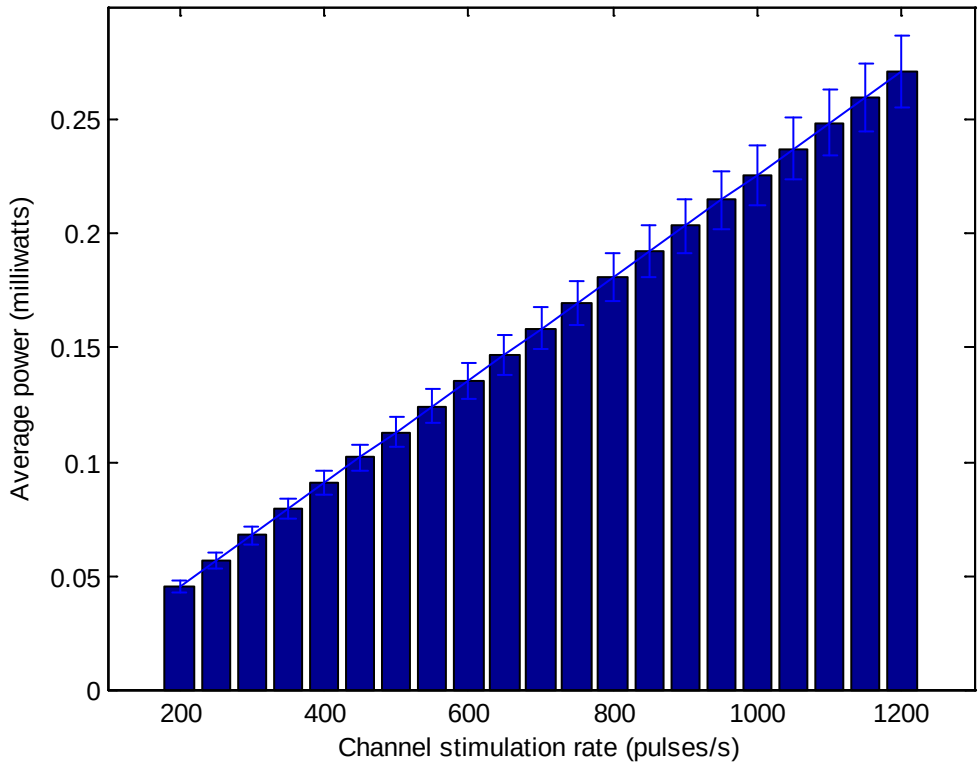

Figure 4.13: Power as a function of channel stimulation rate with standard deviation averaged over all sentences represented as error bars, using the Ace strategy.

This shows that as you increase the channel stimulation rate the power increases linearly. This is expected from equation (4.5), where the average power over a sentence is proportional to the total period, T, where T is the reciprocal of the total stimulation rate, TSR therefore, assuming that the number of channels selected is constant,

$$\overline{P}_{tot} \propto TSR \text{ and } TSR \propto CSR$$

$$\text{Therefore, } \overline{P}_{tot} \propto CSR$$

Increasing the stimulation rate up to 6 times gives you 6 times the power. The average power calculated in Figure 4.13 varies from around 0.05 mw to 0.27 mw. This calculation does not, however, take into account the necessary variation in other parameters that must take place when stimulation rate is adjusted. In practice, every time a patient is subjected to a different stimulation rate, the clinician must re-measure the patients T and C levels (SOECIC, 2011). If the T and C levels are adjusted then this implies that the current levels defining the amplitude of pulses in the sequence will also be adjusted. The relationship between the channel stimulation rate and patient T and C levels has been explored by McKay et al. (2004) and Vandali et al. (2000) and Hsiao-Man et al. (2004). Figure 4.14 shows this relationship adapted from the study by McKay et al. (2004) and reductions in comfort and threshold levels as well as the increase of dynamic range are consistent with similar measurements by (Holden et al., 2002, Vandali et al., 2000). (Saunders et al., 2002) reported that placing the electrode closer to the modiolus would also result in similar reduction in Comfort and Threshold levels as well as an increase in dynamic range but that other factors such as fibrous growth and neural survival also affect these levels.

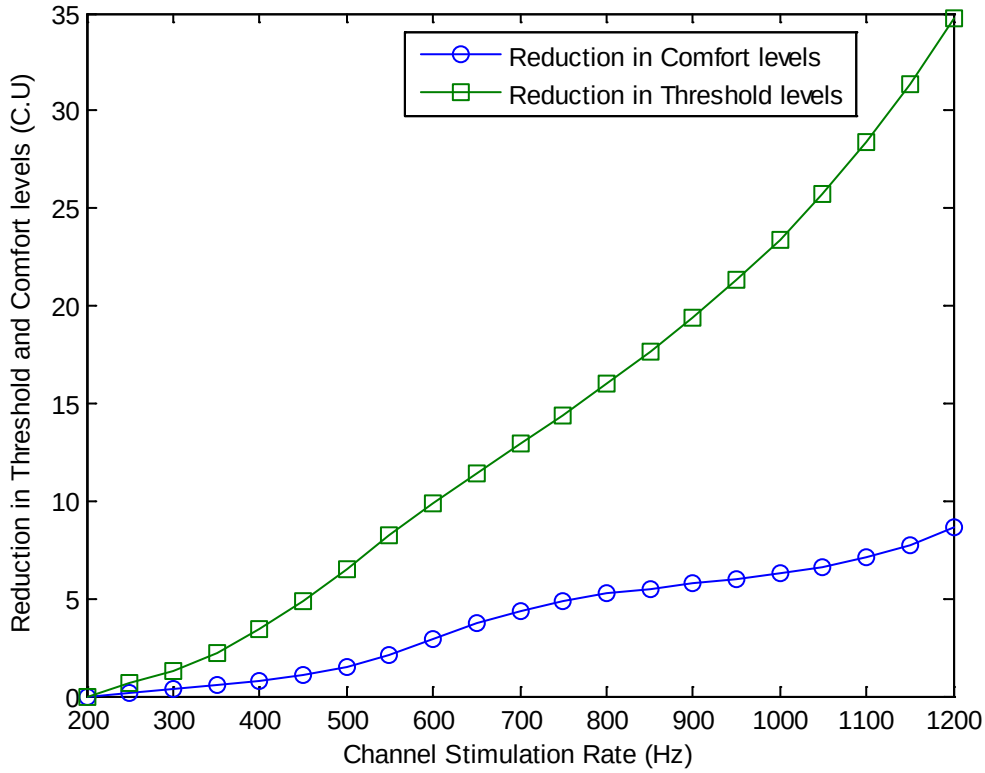

Figure 4.14: Showing how T and C levels are reduced with increasing stimulation rate, from McKay et al. (2004).

It appears that as channel stimulation rate increases, T and C levels decrease almost linearly within the range of stimulation rate under consideration in this chapter (250-1200 pulses/second), which is the range supported by the NMT software. T and C levels decrease because as stimulation rate increases, patients perceive this change as an increase in loudness. Therefore, C and T levels are seen to decrease when the patient is re-measured (SOECIC, 2011). This effect can be applied to the result in Figure 4.13 in order to investigate whether channel stimulation rate increase or the consequent decrease in T and C levels results in a larger effect on power requirements. The result is shown in Figure 4.15 below. Since the patient's data was provided at the high stimulation rate of 1200 Hz, T and C levels remained the same for this rate, and the effect is applied in reverse in that, the lower stimulation rate, the more the T and C levels were increased.

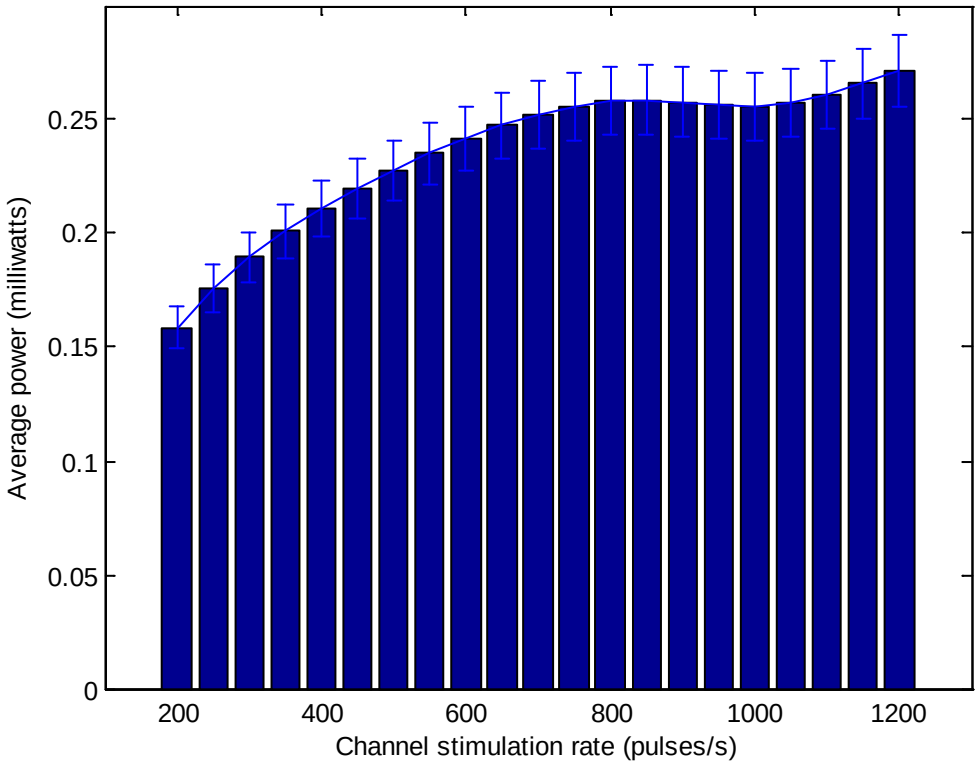

Figure 4.15: Average power as a function of channel stimulation rate and varying T and C levels with standard deviation averaged over all sentences represented as error bars.

Figure 4.15 shows that increasing channel stimulation rate has a larger effect on average power than the consequent reduction in T and C levels, and that the average power now varies from 0.16 mW to 0.27 mW.

The channel stimulation rate remains the dominant parameter but now the range within which the average power varies is much smaller. The other observation is that T and C level adjustments lead to a nonlinear increase in power requirements as opposed to the linear increase in Figure 4.13.

T and C levels depend on many other factors such as individual physiology, neural survival, type of implant and placement of the electrode array within the cochlea. T and C levels are also subjectively measured and so the same patient could be measured twice in a short space of time, and feel as though they perceive loudness differently the second time from the first. This leads to large uncertainties in quantifying the variability of T and C levels and their trend of variation.

It is also of interest to see how the effect of channel stimulation rate changes alongside a changing number of channels selected for stimulation. The average power over the sequence (or sentence) was again calculated and averaged over the set of sentences available. Figure 4.16 shows all possible combinations of channel stimulation rates against number of channels selected. The average power is an approximately linear function of the product of the number of channels and the stimulation rate.

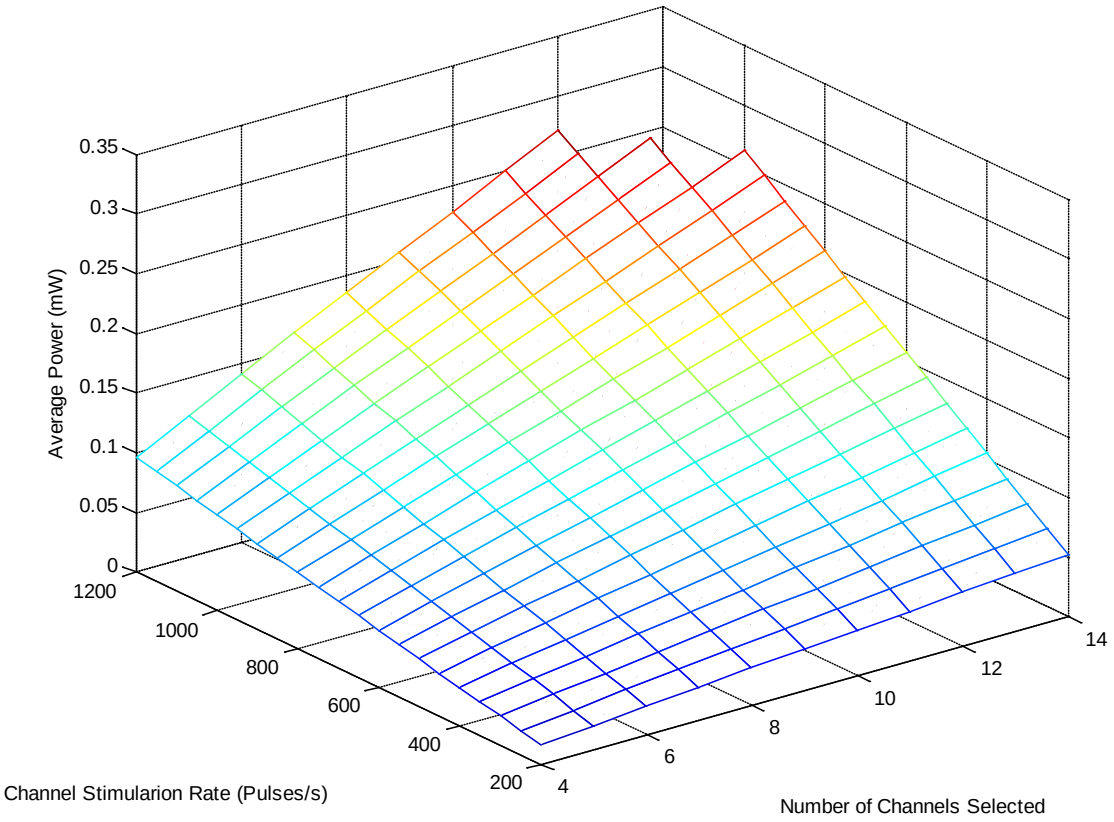

Figure 4.16: The average power is plotted against a series of combinations relating the two parameters in channel stimulation rate and number of maxima selected.

Figure 4.16 does not take into account the change in T and C levels and their effect on the average power required. This is because it is difficult to estimate this change when varying the number of active channels. Threshold and Comfort levels are always re-measured for each patient once the patient's configuration has been adjusted. T and C levels are by definition measured in isolation for each stimulation site and so do not depend on other stimulation sites. Therefore, the T and C levels are dependent on

parameters such as channel stimulation rate, phase width and current level as they all dictate the level of charge arriving at the stimulation site which affects the perception of loudness. Changing the number of active electrodes is not perceived in isolation at each individual stimulation site. Therefore, when the patient is subjected to this change and T and C levels are re-measured, initially the patient perceived no change in loudness and T and C levels remain the same. Once the full electrode array becomes active, clinicians report that patients suddenly notice a reduction in overall loudness which is corrected by the clinicians by increasing the T and C levels appropriately and collectively across the electrode array. Ultimately, it is believed that the change in the number of active electrodes has a smaller effect on T and C levels in comparison to channel stimulation rate (SOECIC, 2011).

Other parameters considered in this study were the phase width and phase gap. Phase gap was found to have no effect on the average power, provided that the overall period remained the same, as expected. A larger phase width, however, implies that a current is passed through to the electrode for a longer duration (increased charge for each pulse). This was varied in the same way as with channel stimulation rate, and the average power was calculated over all sentences. The range of phase widths for this test varies depending on the stimulation rate. For a stimulation rate of 1200 pulses per second, phase gap can vary from 25 to 28 μs and this increases the average power by approximately 5 μw. The range is small because as stimulation rate increases, the period decreases, thereby constricting the phase width range. For a stimulation rate of 250 pulses per second, the phase width can increase to 150 μs. These ranges are defined by the devices capabilities. Results for this analysis are shown in Figure 4.17.

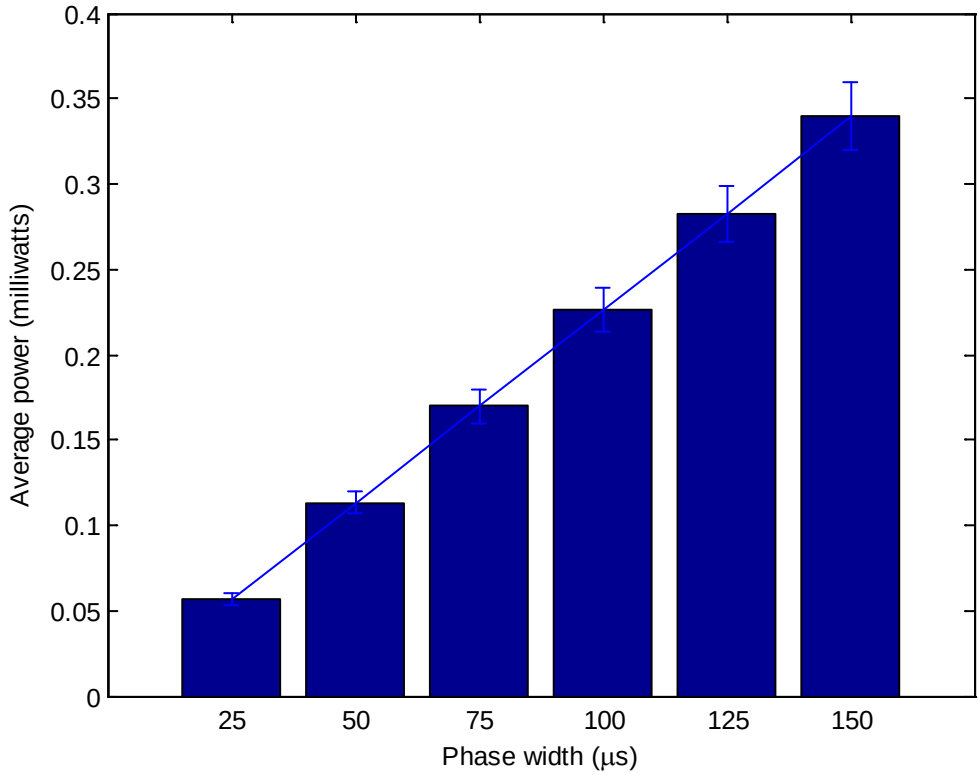

Figure 4.17: Change in average power with phase width.

Figure 4.17 shows that the default phase width, set at 25 µs, requires around 0.06 milliwatts. Increasing the phase width by to 150 µs increases the power required to around 0.34 milliwatts. This is an increase of around 0.29 milliwatts and so for a channel stimulation rate of 250 pulses per second, the effect is just as significant as increasing channel stimulation rate in Figure 4.13, but its effect diminishes as you increase the channel stimulation rate itself as this will reduce the range of pulse width selection. The above calculation also does not take into account the variation in T and C levels. Variation in T and C levels with varying phase width is not straightforward to calculate as this will depends on the patients individual loudness growth functions for each electrode and they would need to be re-measured clinically (SOECIC, 2011). The general trend is that as phase width increases, T and C levels decrease. It can therefore be deduced from the similar result in Figure 4.15, that a decrease in T and C levels will have a decreasing effect on the average power required. This would have a similar effect on Figure 4.17 as shown in Figure 4.15, where the variation in average power becomes non-linear and the range of variation would decrease. Perhaps more importantly, the phase width is only varied for a patient as a last resort when the impedance of an electrode is too high and the T and C

levels need to be reduced. These cases are rare and in general, the phase width for a nucleus implant from the Cochlear Corporation is set to a default of 25 μs.

Threshold and comfort levels of a patient also play a significant role in determining the order of magnitude of the average power required. An increase in T and C levels for the selected patient by 10% resulted in the doubling of the average power required. This, however, is not an accurate estimate of the effect of T and C levels on average power because an overall increase of 10% is considered to be a high increase and in fact, as shown in Figure 4.14, T and C level variation depends on individual electrode placement within the cochlea as well as cochlear anatomical variation from patient to patient.

4.11 Effect of stimulation strategy on power consumption

Today's cochlear implant processors use several different strategies and these will require different levels of power. In light of the previous sections, the investigations of the parameters tested previously were combined to represent and compare some of the different strategies currently used in cochlear implants. The parameters of each strategy were defined based on typical and common configurations used and where a range exists for one parameter, such as in the case of channel stimulation rate, the most representative rate is chosen. The strategies that are possible to represent in the Nucleus toolbox are ACE, CIS. SPEAK cannot be used in the toolbox directly as it uses a varying number of selected electrodes N as opposed to a fixed number of electrodes stimulated at any one time as in ACE. The Nucleus tool box has built in a map of each of the CIS and ACE strategies defined by default parameters. The individual's set of parameters used in previous calculations was also used here for all the strategies.

The Nucleus Technical Reference Manual suggests that the CIS strategy attempts to decode and send information regarding frequency to the electrodes and only utilises a fixed set of electrodes that are spaced out over the basilar membrane and stimulates only those electrodes no matter what the spectral information gives. Therefore it does not attempt to convey frequency information but rather it focuses on rapid temporal changes by using very high total stimulation rates. The channel stimulation rate for this strategy

can vary from 900 to 2400 according to the manual, which in turn dictates the number of electrodes that can be used (4 to 12) to remain within the limits of the implants total stimulation rate. For comparison to other strategies, the typical values will be used and this is 1200 pulses per second with 12 fixed channels for stimulation.

The ACE strategy takes advantage of the 22 electrodes as well as using very high stimulation rates. It conveys frequency information by selecting which *n* electrodes are stimulated but also conveys temporal information by the use of a high stimulation rate. This strategy gives a lot more flexibility to the user to adjust these parameters according to the patient's requirements but in this case for comparison the typical settings will be used giving a stimulation rate of 1200 pulses per second with 12 maxima selected at any one time. The number of channels stimulated, *n*, is fixed. The stimulation rate can vary from 250 to 2400 pulses per second while the number of channels selected can vary from 1 to 20 according to the manual (in this case the first two electrodes are disregarded as they lie in the basal region and their spatial location corresponds to frequencies above that which concerns the implant at roughly 10 kHz.

The SPEAK strategy attempts to convey information regarding frequency information and utilises 20 out of the 22 electrodes available as this strategy can only handle up to 20. A number of channels, *n*, are stimulated from 20 available channels. The specific electrodes selected for stimulation vary depending on the result of the spectral analysis of the acoustic wave at that moment in time, however, *n* can change depending on the information analysed. It generally uses very low stimulation rates and an average rate would be around 250 pulses per second as suggested by the manual. The parameter *n* is variable but in the toolbox it cannot constantly change within analysis so it would have to be set to the typical number used, 10, as recommended by the toolbox manual. This implies that the calculation for SPEAK is an even greater estimate due to the lack of complete representation of the methodology of this strategy, and so *n* is fixed in the simulation in this chapter.

The three strategies were all simulated for the sentence used above in Figure 4.6 and the results are shown in Table 4.2. It can be seen that the ACE and CIS strategies, which has the same stimulation rate and number of channels, require a similar average power, where the Speak strategy requires significantly less, partly due to the smaller number of

channels and slower stimulation rate. It should be reinforced that in light of these results, ACE and Speak have the additional benefit of selecting the channels with the most useful information.

Strategy	Channel stimulation rate (pulses/s)	Number of channels selected (*n*)	$\overline{P}_{av}$ with adjusted T and C levels (mW)
CIS	1200	12	0.274
SPEAK	250	10	0.1
ACE	1200	12	0.271

Table 4.2: Comparison of the average power requirements for the different typical strategies currently used in cochlear implants.

4.12 Discussion and Conclusion

It seems that when determining the most influential parameter, the average power is mostly sensitive to the channel stimulation rate. T and C level adjustment is the second most influential parameter, the channel number selected is the third and finally, the phase width is deemed the least influential predominantly due to its limited variation in practice. The results presented in this chapter show that ACE and CIS both required similarly high levels of power compared to SPEAK as they utilise both a high stimulation rate and a high number of active channels. Both strategies require approximately 0.27 mW. The current strategy in use is ACE and has the advantage of selecting channels with useful information and discarding channels with noise, as demonstrated in Figure 4.8, unlike CIS which has a fixed subset of channels, as demonstrated in Figure 4.11. SPEAK was found to have the least power requirements with an average of 0.1 mW. The reason or this is that the strategy uses a much lower rate of stimulation as well as a smaller number of maxima selected.

The NMT manual (NMT, 2008) reports that for power consumption purposes the CIS strategy is only used with SPRINT processor. This is presumably due to the fact that the Sprint uses an FFT filter bank whereas the ESprint uses 20 digitally programmable filters and this was found to be less efficient.

The results shown above represent trends for power requirements under certain conditions for a typical cochlear implant user. Implant parameters, such as channel stimulation rate and the number of channels selected, and other biological factors, such as

cochlear impedance and threshold and comfort levels influence the average power calculated and these parameters and factors can vary significantly from patient to patient.

Chapter 5

5 Vibration power harvesting from head motion

5.1 Introduction

A number of implanted measurement and medical devices require electrical power. While this power could be supplied by batteries, which could be replaced or externally recharged, it is of interest to consider the power that could be generated from the motion of the body (Thad et al., 2004). Of particular interest here are medical devices, such as the cochlear implant, mounted within the head and the possibility of powering them from normal head motion, while walking, for example. Clearly a person will only be moving about and thus generating power from head motion for a fraction of the time and so the average power available will be significantly less than the peak. Other head implanted measurement and medical devices include cranial pressure monitors (Ginggen et al., 2008), brain stimulators (Mogilner et al., 2001) penetrating auditory nerve array (Middlebrooks and Snyder, 2007) and are anticipated to have requirements ranging from a few μW to several mW. There is significant interest, for example, in cochlear implants or penetrating nerve arrays that have no external parts, and although a large number of technological issues need to be addressed with such devices, their powering is one particular concern.

This chapter is a development of earlier work Saba (2008), and discusses the dynamics of an inertial device for harvesting power, for both linear and angular motion and derives simple rules for the way in which this power scales with the size of the device. The proportion of this harvested power that can be converted into electrical form is then analysed, which is shown to depend on a non-dimensional coupling factor, the magnitude of which is also shown to scale with device size. The problem of using a small device to harvest power from head movement, where the excitation amplitude is much greater than the device size, is rather different from most conventional power harvesting applications (Glynne-Jones and White, 2001), where the excitation amplitude is much smaller than the

device size. It is thus important to return to the fundamental equations that govern such a device to estimate the available power.

Previous measurements of head motion in all six linear and angular directions while walking are then used to estimate the maximum electrical power that could be generated by a harvesting device of 1 cm^3, assuming power is harvested by tuning the device to the fundamental walking frequency. The scaling law for power harvesting predicts that the power available is proportional to the vibration amplitude times the excitation frequency cubed. This prompts a study of power harvesting from higher harmonics of motion, which have lower amplitudes but higher frequencies. This requires the acquisition of higher bandwidth measurements of head motion than were previously available.

5.2 Dynamics of an inertial harvesting device

Figure 5.1 illustrates the main components of an idealised inertial device for harvesting power from linear motion along its axis. The details of the transduction mechanism are set to one side for the time being and it is assumed that half the power dissipated in the viscous damper, c, is available for harvesting. This factor of two will be justified, using the example of an electromagnetic device, in the following section.

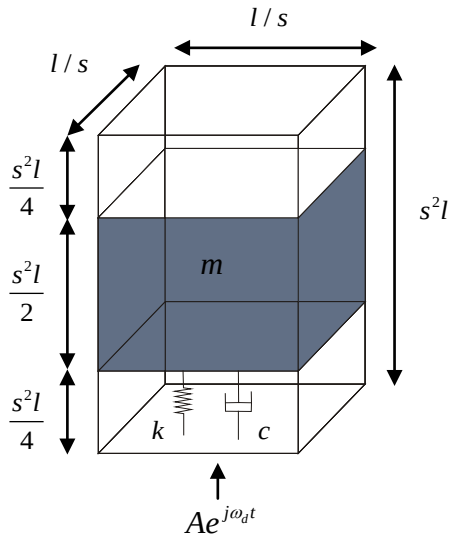

Figure 5.1: Idealised sketch of an inertial device for harvesting power from the imposed sinusoidal motion having displacement of A and angular frequency ω_d.

The device is assumed to have dimensions $l/s \times l/s \times s^2 l$, where l is a characteristic length and s is a dimensionless shape factor, so that the volume is always l^3, and s would equal unity if the device were cubic, for example. It is driven along its axis by sinusoidal motion of peak displacement A and angular frequency ω_d . The vertical displacement is thus equal to the real part of $Ae^{j\omega_d t}$, which is assumed to produce a displacement of the inertial mass, *m,* equal to the real part of $Be^{j\omega_d t}$. The complex relative displacement between the base and the inertial mass is then equal to

$$A - B = \frac{-\omega_d^2 mA}{j\omega_d c + k - \omega_d^2 m} \tag{5.1}$$

The maximum power that can be harvested from a practical device is half the power dissipated in the damper, with damping factor *c*, as discussed in section 5.3, and this is equal to

$$W = \frac{1}{4} c\,\omega_d^2 \left|A - B\right|^2 \tag{5.2}$$

which is then equal to the result by (Williams and Yates, 1996)

$$W = \frac{cm^2\,\omega_d^6\,A^2}{4\left|j\omega c + k - \omega_d^2 m\right|^2}. \tag{5.3}$$

Assuming that the system is operating at resonance, so that $k = \omega_d^2 m$, where k is the stiffness, then the power becomes

$$W = \frac{m^2 \omega_d^4 A^2}{4c}. \tag{5.4}$$

This suggests the apparently paradoxical result that an infinite amount of power could be harvested if the damper were to become negligible (Stephen, 2006). Physically the mechanical load impedance presented by the device would become infinite under these conditions, but of more importance practically, the throw of the inertial mass would also become infinite.

We thus assume that the damping in the device is adjusted so that the throw of the internal mass is limited to the maximum allowance within the enclosure, equal to $\pm\Delta$, so that using equation (5.1) with k equal to $\omega_d^2 m$,

$$c = \frac{m\omega_d A}{\Delta} \tag{5.5}$$

Note that the damping must then depend on the excitation amplitude as well as the maximum throw. Substituting this value of c into equation (5.4) gives the maximum power available for harvesting (Stephen, 2006, Yeatman, 2008, Saba et al., 2008)

$$W = m\omega_d^3 A\Delta / 4 \tag{5.6}$$

We now assume that for a power harvesting device having the linear dimensions as above, the inertial mass has dimensions of $l/s \times l/s \times s^2 l/2$ and is of density ρ, so that m is equal to $\rho l^3/2$. We also assume that the maximum throw, Δ, is equal to $s^2 l/4$, as indicated in Figure 5.1. Under these circumstances the power available for harvesting, equation (5.6), is equal to

$$W = s^2 \rho A \omega_d^3 l^4 / 32 \tag{5.7}$$

Clearly the available power is larger as the device becomes longer and thinner, so that s is greater than one. For practical reasons, however, we assume that s^2 can be no larger than 2, so that the maximum power that can be harvested will be

$$W = \rho A \omega_d^3 l^4 / 16, \tag{5.8}$$

which is in a convenient form for scaling studies. In the calculations below, ρ is assumed to be equal to 7860 kg.m-3, i.e. that of steel, since the inertial mass is often also required to supply the magnetic field in electromagnetic devices. One potential problem with using vertically-orientated inertial devices tuned to walking speeds, and so having low natural frequencies, is that if the spring is linear, it has a large deflection due to the influence of gravity on the mass. This can be avoided by using a nonlinear spring, with a high stiffness, to support the weight of the mass, and a low dynamic stiffness, to achieve the required natural frequency. A number of nonlinear mechanisms designed to achieve this for vibration isolation applications, where a similar need arises, have recently been reviewed by Ibrahim (2008).

A very similar analysis can be performed for angular excitation of a tuned rotational system (Yeatman, 2008, Saba et al., 2008). In this case, the maximum power

available for harvesting, assumed again to be half the power dissipated, is not limited by the maximum angular displacement, which could be very large in a well-designed device, but is limited by the minimum practical damping ratio of the device, ζ, so that

$$W = \frac{I\,\omega_d^3\,\theta^2}{8\zeta}, \tag{5.9}$$

where I is the moment of inertia of the mass and θ is the imposed angular displacement. In practice one would like the damping to be almost entirely provided by the electrical power harvesting mechanism, which must thus be set to be significantly higher than the inherent mechanical damping in the device. Assuming that it would be difficult to get the mechanical damping ratio below 1%, a reasonable value for the total damping ratio, ζ, may be 10%. Also, assuming that the inertial mass is a cylinder of length s^2l and radius l/2s, where s is again a dimensionless shape factor, its moment of inertia, *I*, is equal to $\pi\rho l^5 / 32s^2$. In this case the power available is increased as the device becomes thinner and flatter, i.e., *s* is smaller than one. Assuming, however, that for practical reasons s^2 can be no smaller than ½, the maximum power available for harvesting from an angular displacement of θ is thus approximately,

$$W = \rho\theta^2\,\omega_d^3\,l^5 / 4. \tag{5.10}$$

Yeatman (2008) has also estimated the power available from a non-resonant rotational device, such as those used in self-powering watches and shown it to be similar to equation (5.9) with ζ set to 1, so that the resonant device is more efficient, although more highly tuned. This author also shows that one potential method of increasing the power harvested from angular motion is to use a gyroscopic device, although this would then have to have a mechanism to maintain the speed of the gyroscope.

The dependence of the maximum power available for harvesting on l^4 in equation (5.8) and l^5 in equation (5.10), suggests that it would be far less efficient to implement multiple micro-miniaturised devices than a single device that is as large as possible. These equations are used in the following section to estimate the power that could be potentially harvested from the various axes of motion of the head.

5.3 Transduction efficiency

In order to provide an estimate of the proportion of total mechanical power supplied to the inertial harvesting device that can be converted into electrical energy, we consider a two-port representation of the electromagnetic inertial device shown in Figure 5.2. The equations linking the force applied to the device, *f*, its velocity, *u*, and the voltage generated by the coil, *v*, and current flowing, *i*, can, in general, be written as (Hunt, 1954)

$$f = Z_M u + T_1 i, \tag{5.11}$$

$$v = T_2 u + Z_E i, \tag{5.12}$$

where Z_M is the mechanical impedance of the device when the coil is open circuit, which in this case is equal to

$$Z_M = \frac{j\omega m(j\omega c + k)}{j\omega c + k - \omega^2 m} \tag{5.13}$$

where *m*, *k* and *c* are the mass, stiffness and damping of the inertial mass on its suspension.

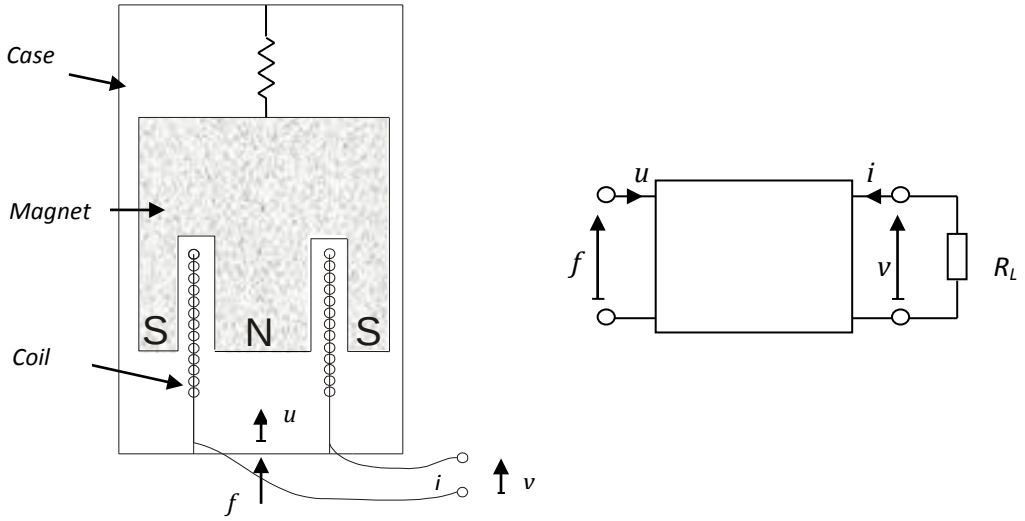

Figure 5.2: Sketch of an idealised electromagnetic harvesting device, in which the magnet also acts as the inertial mass, *m*, which is suspended by a stiffness *k* and a viscous damper *c*, and the coil is attached to the case. The equivalent two-port network is also shown, where the coil is attached to a resistance R_L.

T_1 is a transduction coefficient equal to

$$T_1 = \frac{BLm\omega^2}{j\omega c + k - \omega^2 m}, \tag{5.14}$$

where *BL* is the product of the magnet's flux density and the length of wire in the coil. Since the device is anti-reciprocal (Hunt, 1954), then transduction coefficient, T_2, is equal to $-T_1$. Z_E is the electrical impedance when the mechanical part is blocked, which is assumed to be entirely resistive and denoted by *R*.

If the electrical terminals of the device are connected to a load resistor, R_L, the dissipation within which is equal to the electrical power harvested, then the power harvested is equal to,

$$W_H = \frac{1}{2} R_L |i|^2 \tag{5.15}$$

But if *v* is equal to $-R_L i$ in equation (5.12) then

$$i = \frac{-T_2 u}{R + R_L} \tag{5.16}$$

so that

$$W_H = \frac{R_L |T_2|^2}{2(R + R_L)^2} |u|^2 \tag{5.17}$$

The mechanical impedance of the device when connected to the load resistor can also be shown to be equal to

$$Z_M(total) = Z_M - \frac{T_1 T_2}{R + R_L}, \tag{5.18}$$

and so the total mechanical power supplied to the harvesting device is

$$W_S = \frac{1}{2} \mathrm{Re}\left[Z_M - \frac{T_1 T_2}{R + R_L} \right] |u|^2, \tag{5.19}$$

where Re denotes the real part of the quantity in brackets. The ratio of the harvested power, W_H, to the power supplied, W_S, can be defined to be the efficiency of the device, which, in general, is equal to

$$e = \frac{R_L \,|T_2|^2}{(R+R_L)^2 \,\mathrm{Re}[Z_M - T_1 T_2 / (R+R_L)]} \tag{5.20}$$

If the inertial device is driven at ω_d and is assumed to be operating at resonance, so that $k = \omega_d^2 m$, then $\mathrm{Re}[Z_M]$ is equal to km/c, and $-T_1 T_2 = |T_2|^2 = (BL)^2 km/c^2$. Differentiating the resulting expression for e with respect to R_L and setting this to zero shows that the maximum power is harvested when R_L is equal to R. Under these conditions, the power harvesting efficiency can be written as

$$e = \frac{F}{4+2F} \tag{5.21}$$

where F is a non-dimensional transduction coupling factor, as derived in a different context (Nakano et al., 2007), which is given by

$$F = \frac{(BL)^2}{Rc} \tag{5.22}$$

The coupling factor will be large if the magnet is strong and the length of wire in the coil is large, so $(BL)^2$ is large, and if the electrical resistance of the coil and intrinsic mechanical damping is small. When F is much greater than unity then the efficiency, *e*, in equation (5.21) tends to ½, since negligible power is dissipated in the intrinsic mechanical damping, *c*, so all the power is dissipated by the circulation of the current, and half of this is harvested in the matched load R_L. It is this limiting condition that is assumed above.

It is also interesting, however, to estimate how this transduction coupling factor, F, scales with size, and thus see how difficult it would be to achieve this limiting condition as the device dimensions are made smaller. Assuming that B is independent of size, but that L is proportional to length scale l, R, which equals the resistivity times coil length over wire area, is proportional to l^{-1} and the intrinsic mechanical damping is proportional to l (J.Piers, 2001), then F is proportional to l^2 and it becomes progressively harder to maintain its value well above unity as the device is made smaller.

5.4 Estimates of power available from various axes of head motion

Both the linear head acceleration in all three axes and that in the three axes of angular head acceleration were measured in 12 subjects while walking by Woodman and Griffin (1996). Typical waveforms for the acceleration in all directions are shown in Figure 5.3. The amplitude in the z (vertical) direction is higher than that in the y (side to side) or x (forward and aft) directions.

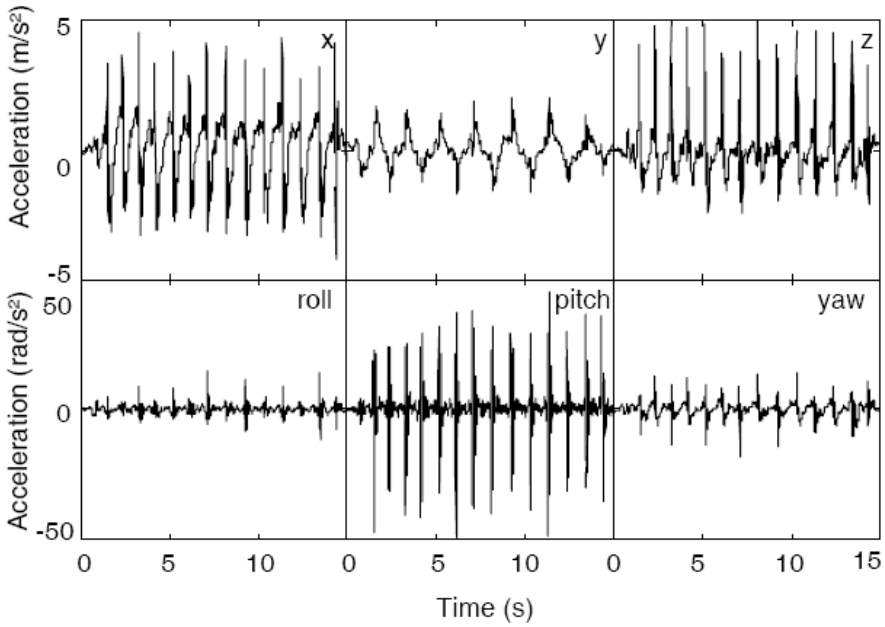

Figure 5.3: Acceleration time histories at the head in six axes for a single subject walking at 1 steps/s taken, with permission, from P.D. Woodman, M.J. Griffin, Six axes of head acceleration during ambulation, Proc. Inter-noise 96, pp.1719-1724, 1996.

From the power spectra of these waveforms, the fundamental excitation frequency and the amplitude of motion at this frequency were estimated for different walking speeds, as shown for z - axis motion in Table 5.1. Equation (5.8) from section 5.2 was then used to estimate the maximum power available for energy harvesting using a 1 cm^3 device at each walking speed, which is also listed in Table 5.1. At a normal walking speed of about 1.5 steps per second, the maximum power available from a 1 cm^3 device was calculated to be about 60 μW for the z - axis (vertical) motion. This is about twice that available from the x-axis motion at this walking speed, for example.

Walking speed (steps/second)	1	1.25	1.5	1.75	2	2.25
Fundamental frequency (Hz)	1	1.25	1.5	1.75	2	2.25
Linear amplitude (mm)	14	10	16	10	13	13
Power available from linear motion for 1 cm^3 device (μW)	17	40	64	94	125	125
Angular amplitude (radians)	0.018	0.02	0.011	0.01	0.009	0.007
Power available from angular motion for 1 cm^3 device with 10% damping (μW)	0.016	0.03	0.02	0.02	0.04	0.03

Table 5.1: Fundamental frequency (Hz), maximum linear amplitude (mm), maximum angular amplitude together with estimated power available for harvesting from the fundamental component of the translational motion in the vertical axis and the angular motion in the pitch direction, for various walking speeds, using the data from (Woodman and Griffin, 1996).

The angular acceleration of the head motion in the pitch direction is also significantly greater than that in the roll or yaw directions. The angular displacement calculated from the measured angular accelerations is also listed in Table 5.1 at each walking speed together with the associated available power calculated using equation (5.10) from section Table 5.1. The power available is significantly less than that potentially available from the vertical motion in Table 5.1, being about 0.02 μW for a 1 cm^3 device with a damping ratio of 10% at a walking speed of 1.5 steps per second, for example.

5.5 Power available from higher harmonics

The initial calculations presented in section 5.4 suggested that the most likely source of power for harvesting was from the vertical motion of the head. Bandwidth limitations in the original measurements (Woodman and Griffin, 1996), however, prevented them from being used to calculate the potential power available from higher harmonics of the fundamental head motion frequency. Equation (5.7) in Section 5.2 suggests that the

power available is proportional to $A\omega_d^3$ for a device of a given size, which is equal to ω_d times the acceleration. Thus, even if the acceleration is slightly lower at the higher harmonics, the linear dependence on frequency may make it more worthwhile to tune the inertial system to this higher frequency.

A series of measurements was thus carried out by Saba (2008) with an MIE triaxial accelerometer mounted on a headband, and attached to a portable data logger (Online, 2004). The apparatus and the experiments on a treadmill are illustrated in Figure 5.4. Figure 5.5 shows the power spectra of the vertical acceleration when walking at about 1.6 steps per second on the treadmill. Significant energy is contained in the first five harmonics and the measurements are well above the noise floor at these frequencies. Plotting the acceleration multiplied by frequency, i.e., $A\omega_d^3$, shows that the power available from the third harmonic is about three times that available from the fundamental. The amplitude of the fundamental vertical motion was in reasonable agreement with that measured by Woodman and Griffin (1996) and the predicted power available from the fundamental was comparable to the 60 μW prediction above.

Figure 5.4: Equipment used to measure head motion and its use on the treadmill.

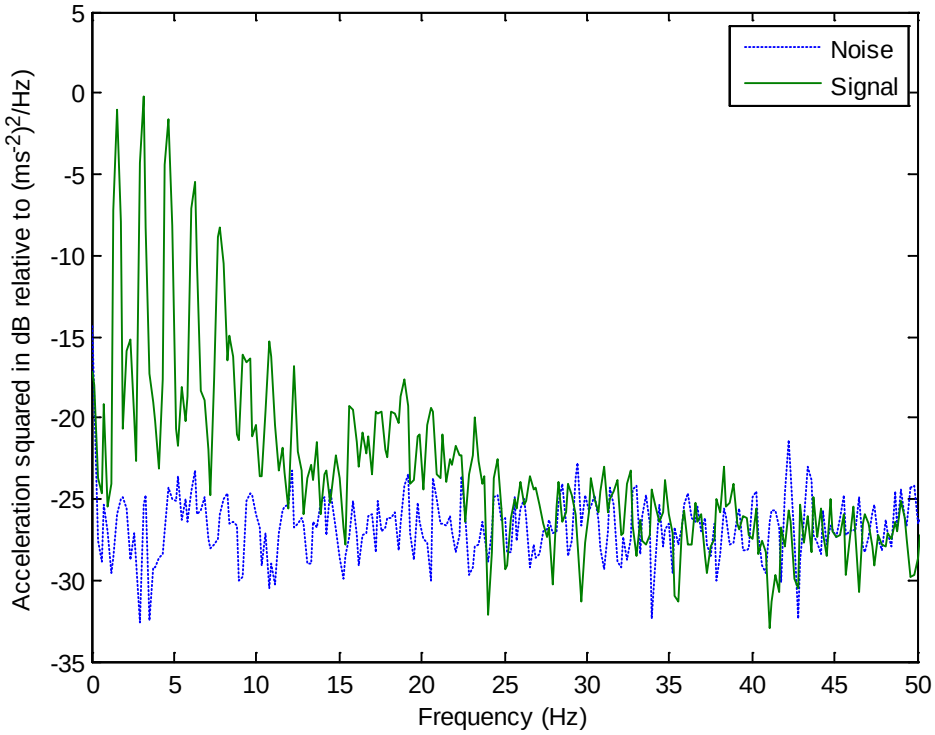

Figure 5.5: Power spectral density of vertical head acceleration at a walking speed of 1.6 steps per second on the treadmill.

Table 5.2 shows the frequency at which most power was available for various walking speeds measured by Saba (2008) on the treadmill together with the estimated power available from a 1 cm^3 device. At a walking speed of 1.6 steps per second, the potential power available from the third harmonic is about 130 μW.

Walking speed (steps/second)	1	1.4	1.6	2.1	2.7
Dominant frequency (Hz)	3	4.1	4.8	10.3	18.3
Power available, in μW, from the dominant frequency	35	116	131	206	1044
Power available, in μW, from entire waveform with a single device having a natural frequency of 1.6 Hz and a damping ratio of 2	14	41	80		

Table 5.2: Estimated power available from vertical head motion at the dominant frequency of each walking speed.

5.6 Harvesting from multiple harmonics

To constrain the motion of the inertial mass so that it does not strike the case when excited at a single frequency, the total damping has to be adjusted according to equation (5.5). The damping ratio corresponding to this value of damping is equal to

$$\zeta = \frac{A}{2\Delta} \tag{5.23}$$

which, for a typical fundamental amplitude of vibration (16 mm in Table 5.1) and size of device (7 mm x 7 mm x 20 mm, so that Δ is equal to 5 mm), is greater than unity.

An inertial device tuned to harvest power from the fundamental component of head motion would thus be very well damped and would have a significant response to several of the harmonics due to a walking motion. This is in sharp contrast to devices designed to harvest power from the high frequency motion of machines, where the driving displacement is very small compared to the device size and so the aim is to design a resonant device with as little damping as possible (Glynne-Jones and White, 2001), and the tuning becomes a significant problem. In fact, it is not clear how such a heavily damped device should be tuned since, if it is tuned to the fundamental, as in section 5.4, then it will also respond to the harmonics and if it is tuned to a harmonic as in section 5.5, it will also respond to the fundamental.

A numerical study has thus been conducted using the measured waveform of the vertical acceleration signal, in which the natural frequency of the inertial device has been varied, and for each natural frequency, the damping has been adjusted so that the peak throw of the inertial mass, Δ, was 5 mm. The total power harvested is then calculated as half the sum of the power dissipated in the damper due to each harmonic. The results are shown for a walking speed of 1.6 steps/second in Figure 5.6, together with the damping ratio required to limit the throw to ± 5mm at each assumed value of the natural frequency.

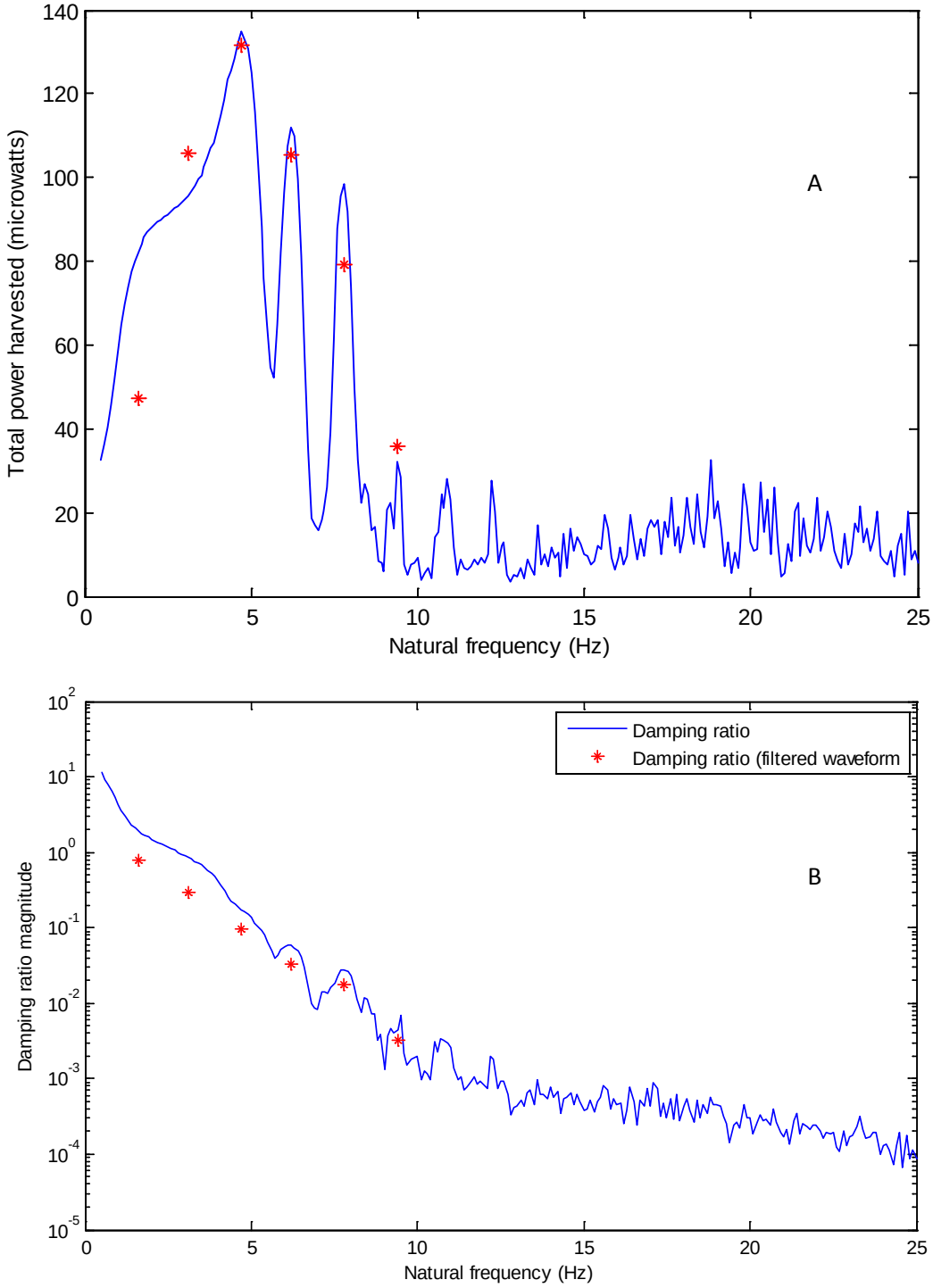

Figure 5.6: (a) The power harvested from all frequencies against the tuned natural frequency of the inertial device. The stars indicate the calculated power harvested assuming only single frequency excitation at each harmonic. The change in damping ratio with the assumed natural frequency of the harvesting device is also shown in (b), together with that required to limit the motion at each harmonic on its own.

The required damping ratio is high at low natural frequencies, so that the total power harvested when excited by all the harmonics is rather larger than harvested from the fundamental alone, as shown by a star at 1.6 Hz on Figure 5.6 (a). It should be noted however that the resonant frequency is related to the natural frequency by a factor of $\sqrt{1-\zeta^2}$ and so at high damping ratios the natural frequency at which most of the power is harvested is rather different from the excitation frequency. At the second harmonic, 3.2 Hz, the power available from excitation at this frequency alone is slightly higher than that available from excitation by the whole waveform, since the damping ratio can be allowed to be smaller when only the harmonic is present.

The power harvested is greatest, generating about 130 μW, when the natural frequency is set to the third harmonic, at about 4.8 Hz. The power generated by the individual harmonics is also largest at this frequency, as recorded in Table 5.2, and is almost the same as that generated when the device is excited by the whole waveform. The damping ratio required to achieve these power levels is about 0.2, however. Such a device would thus be quite sharply tuned, and unable to respond significantly if the walking speed changed by more than about 10%. A more practical solution may thus be to live with the slightly lower power output with the device tuned to the fundamental, for which it must be over-damped, the damping ratio being 2 in Figure 5.6 (b), in order to benefit from the very broad tuning of this device and its insensitivity to the frequency of excitation. The final row in Table 5.2, for example, indicates the power available for a single such over-damped device, with a fixed natural frequency of 1.6 Hz and a damping ratio of 2, when driven by the whole waveform at each walking speed. The results are not shown for walking speeds of 2.1 and 2.7 steps/second since the throw then exceeds 5 mm. A device with nonlinear damping could be designed to limit the throw more effectively at various walking speeds, and nonlinear springs have also been suggested as a way of decreasing the sensitivity to excitation frequency.

5.7 Discussion and Conclusions

This chapter has considered the maximum power that could be harvested from head motion in order to drive fully-implantable medical devices. The performance of an inertial power harvesting device of a fixed size was analysed, and the scaling laws for the maximum available power from both translational and angular excitation were derived.

Previous measurements of head motion in all three translational and three rotational axes while walking (Woodman and Griffin, 1996), were initially used to estimate the power available from the fundamental component of different forms of motion. At a normal walking speed of about 1.5 steps per second, it was found that harvesting from the vertical head motion gave the highest potential power output, which was about 60 μW.

Subsequent measurements of the head motion over a greater bandwidth while walking on a treadmill suggested that somewhat more power could be harvested if the inertial device was tuned to a higher harmonic of the fundamental frequency. Tuning the device to the third harmonic, for example, gave a potential power output of about 130 μW, but resulted in a lightly damped device, which was sensitive to changes in walking speed. A more practical strategy is shown to be using an over-damped device tuned to a lower frequency that is able to respond to all the harmonics in head motion, and which performs well with a wide range of walking speeds.

The maximum power harvested, about 80 μW, is far below that required for current cochlear implants, about 40 mW, as discussed in chapter 1, or even the currents required for stimulation, about 1 to 5 mW. This method of powering cochlear implants is thus not practical at the moment. It is probably not feasible to fully power a cochlear implant with such current requirements, but may become feasible in future, fully implanted, cochlear implant designs with much lower power requirements, as discussed in section 1.3 in chapter 1.

Chapter 6

6 Conclusions and Suggestions for Further Work.

This thesis investigated different aspects of stimulation power consumption in the cochlear implant. A three-dimensional cochlear model was produced with the purpose of investigating the voltage distribution in the cochlea, in order to better understand the different ways in which the current can be controlled, with an aim of improving selectivity as well as addressing the issue of power loss. The model was used to investigate variations in voltage distribution due to varying cochlear geometry and implant configurations. The model was also used to develop a previously proposed focussing strategy into a more generalized solution. The power requirements of different stimulation strategies were also assessed with respect to the parameters that govern them. This thesis also presented a feasibility study of harvesting power from head motion to power a fully implantable cochlear implant. This chapter concludes the findings of these studies and suggests areas of further work in relation to these findings.

6.1 Evaluation and Summary

A three-dimensional cochlear model was presented in chapter 2. The complexity of the model was increased throughout the chapter to take into account non-uniformity in the cochlear geometry as well as the effect of the coiling of the cochlear along the longitudinal direction. Introducing non-uniformity into the straightened cochlea resulted in variations in impedance distribution along the cochlea. The cochlear chambers generally get narrower in the direction of the apex, and consequently, the impedance increases in the same direction. This is because impedance is inversely proportional to the area of the resistive material. The coiling of the cochlea resulted in a secondary peak in the impedance distribution corresponding with the position at which one turn of the cochlea

passes over another turn at the point within which the stimulating electrode is positioned. This implies that when a current is passed through an electrode in one turn, neurons that belong to another turn which passes over the electrodes position could also be unintentionally stimulated. The non-uniformity in voltage distribution due to these geometric variations would lead to non-uniformity in the excitation of the neuron bundles leading to the implants performance becoming somewhat geometry dependant. The model presented in this thesis can estimate trends due to the effect of geometric variation and resistivity parameters on the voltage distribution, but cannot be used to predict a particular solution for an individual subject unless the geometry is optimised for that subject. Data on neural survival would also be required for the purposes of estimate neural activation. Resistivity values were taken from a variety of sources, the accuracy of which is difficult to determine. It was shown in chapter 2, however, that the model was largely insensitive to variation in resistivity values, with the exception of bone and silicon, the two most insulating domains.

It was shown in Chapter 3 that the position of the electrode array with respect to the target neurons would affect the impedance distribution within the cochlea. In the case of an inner placed electrode array, the impedance distribution was more narrowly focussed and peaked at higher impedance levels, due to the relatively close position of the electrode array to the neurons, in comparison to an outer placed electrode array. It is for this reason that a patient with an outer placed electrode array would have higher threshold and comfort levels. The nucleus contour advance implant was designed to have a pre-coiled electrode array that wraps around the modiolus in order to reduce the distance in between the electrode and the target neuron reducing threshold levels and therefore reducing power consumption as well as increasing the accuracy of stimulation.

The model presented in this thesis can be used to predict relative variations in voltage distributions due to a variation in electrode positions, but it would be important to accurately measure the final resting position of the electrode array for a particular subject if the suggested solutions are to be personalised. Inaccuracy in electrode position could possibly invalidate suggested idea current vectors and current work based on this thesis is under way to address this issue.

Chapter 3 also suggested an alternative method of stimulation to increase the current through the neurons. It was demonstrated that if the ball return electrode was placed within the modiolus, this would place the target neurons directly in the pathway of the applied current, resulting in higher currents through the target neurons and,

consequently, greater levels of stimulation. In the case that higher currents are required through the neurons in comparison to the result using a conventional return electrode, then placement of the return electrode within the modiolus could solve this issue. In the case that the conventional placement of the return electrode resulted in acceptable levels of stimulation, placement of the return electrode within the modiolus implies that less input current would be required, thus conserving power. This result assumed that stimulation depends on voltage level where in fact the exact mechanism is not well understood, and it may be that it is the voltage difference across that neuron rather than the absolute voltage that actually fires the nerve.

Alternatively, the extra power that becomes available due to the placement of the return electrode within the modiolus could be reassigned elsewhere in the cochlear implant process. Chapter 3 also investigates a focussing strategy proposed by van den Honert and Kelsall (2007) in which simultaneous stimulation could be used to focus the voltage distribution towards target neurons. The authors show that by measuring the impedance matrix of the electrode array, and by assuming a desired voltage distribution at the position of the electrodes, a vector of ideal currents can be calculated by computing the inverse of the impedance matrix. This vector could be used to stimulate the electrode array and achieve a focussed result. The limitation with such a method is that there is no way of measuring the impedance along the spiral ganglion to be able to assess the degree to which stimulation focussed is successful. Chapter 3 shows that this focussed result is only optimized along the electrode array and does not result in the same benefit along the spiral ganglion pathway. In fact, in order to achieve a focussed solution with the intended voltage at the spiral ganglion, significantly more current was required. Chapter 3 also demonstrates how the concept could be developed further by utilizing impedance distribution data within the three dimensional space of the cochlear model presented in chapter 2. Since the spiral ganglion is regarded as the primary site of stimulation, the strategy was applied using the impedance matrix along the spiral ganglion pathway. Since this was not a square matrix, as it was in the solution proposed by van den Honert and Kelsall (2007), a pseudo-inverse calculation was required to generate the vector of ideal currents. In this way, the study in this chapter shows that the focussing strategy could be optimised at the spiral ganglion and results in a significant improvement in focussing towards the target neurons. It is not clear, however, how the impedance matrix at the spiral ganglion could be measured in practice, and so although their study presented in this thesis is useful for demonstrating the potential for such methods, further development is still required.

One way to reduce the current requirements, and hence power consumption, is to include a regularization coefficient with these focussing techniques. It was shown that the greater the regularization coefficient, the less the degree of focussing. It was also shown that for a specified regularization coefficient, the power required to achieve a focussed result using the neural impedance matrix, was about equal to the power required to achieve a focussed result using an electrode array impedance matrix, but with an increased degree of focussing towards the target neurons.

Chapter 4 investigated the different strategies used by current cochlear implant processors, and the way in which the parameters that define these strategies affect the power required. The chapter demonstrates that the key parameters that define a strategy include the stimulation rate and the number of active channels. It was shown that stimulation rate was the dominant factor and an increasing stimulation rate implies an increasing number of pulses per second translating to an increase in power requirements, even when the changes in threshold and comfort levels are taken into account. Equally, an increase in the number of active channels implies an increase of pulses per second, hence an increase in power requirements.

A major issue in power consumption is the power loss due to the transcutaneous link. This could be eliminated with a fully implanted cochlear implant. Chapter 5 investigates the feasibility of powering a fully implanted cochlear implant by harvesting energy from head motion, initially using a tuned inertial device in the 6 different axes excited during walking. The study demonstrates that the power available for harvesting depends on the size of the device and the frequency of movement. The study concludes that for a 1 cm^3 device, more power could be harvested by tuning the device to higher harmonics, although this would result in a lightly damped device which was sensitive to variations in walking speed. A more practical approach is to use an over-damped device tuned to a lower frequency that was relatively insensitive to walking speed and is able to respond to all the harmonics in head motion. Even then the estimated power harvested is small compared with the current power requirements of a cochlea implant with an external processor, and therefore this approach is probably not feasible at this point unless a fully implantable cochlear implant is introduced.

6.2 Future Work

The three dimensional cochlear model used to model the voltage distribution within the cochlea includes the key structures of the cochlea, such as the scala typmani and scala vestibuli, Additional structures could be modelled to better represent the impedances in the cochlea. Chapter 2 briefly discusses the effects of an electrode fluid interface in the straightened cochlear mode. An investigation on the effects of this interface on the coiled cochlea would enhance the simulation of the distribution of impedance with the cochlea. This electrode fluid interface could represent a number of biological changes that occur post implantation, such as fibrous tissue growth that encapsulates the electrode array, and ossification (bone growth) in the scala tympani (Makary et al., 2010).

The model was varied in complexity, introducing non-uniformity, by coiling of the cochlear chambers. There is scope for an investigation into the variation of cochlear geometry in terms of the height of the cochlea, the number of turns and the cross-sectional areas of the chambers. This could provide information about the effects of inter-subject anatomical variation on the effectiveness of implant designs.

Conditions of the cochlea that result in anatomical changes due to disease could also be investigated using the model. One such condition, called Common Cavity, occurs when the bone separation between two turns erodes, effectively merging the scala vestibuli of the lower turn and the scala typmani of the upper turn (Makary et al., 2010). This could be modelled using a modification of the coiled cochlea. Another condition that could be considered for future work is known as Mondini (Mondini, 1791, Paparella, 1980) whereby the cochlea does not develop into the full 2.5 turns but rather is limited to 1.5 turns. This could have an impact on the effectiveness of current electrode array designs.

The electrode array modelled in this thesis is only one of many different designs currently in commercial use. The model could be developed to simulate different types of electrode array geometry, including electrode array length and variations in electrode type, such as full banded as assumed in this thesis, or half banded as is the case with other electrode designs such as in appendix F. Electrode array length also varies depending on the manufacturer and application. Pre-coiled electrode arrays tend to be shorter as the insertion depth is less. Med-El manufacturers longer arrays in general as these tend to follow the outer cochlear wall, resulting in increased insertion depth. The EAS electrode array (Electro-acoustic stimulation) is a short electrode array designed to have limited

insertion depth into the cochlea, covering only the high frequency regions of the basilar membrane. This is used for patients with residual low frequency hearing at more apical positions. The study could investigate the effect of electrode stimulation and voltage spread towards the apex, assessing the possibility that a short electrode array could still stimulate regions of the cochlea that that are still mechanically functional, and the effect of this unintended stimulation on residual hearing.

Probably the most important development of the model presented in this thesis would be to couple it to a neural model. This would expand on modelling the voltage distribution by simulating the excitation patterns of the neurons. Chapter 3 uses threshold levels to predict nerve excitation but does not take into account variation in nerve survival.

The neural focussing study presented in the thesis demonstrated the capability of the strategy to optimise the focussed solution at the neural pathway through the spiral ganglion. If a practical way could be found to measure or estimate the impedance matrix along the spiral ganglion in the real cochlea, significantly greater selectivity could be achieved. In a clinical application, this strategy would have to be optimised for an individual patient.

The preliminary study of power harvesting from head motion indicated that the amount of power potentially harvested was significantly less than that used in present cochlear implants. As these devices are developed and become fully implanted, however, no energy will be required to transmit the signal though the skin. It is also expected that developments in processor technology and stimulation strategy will reduce the power requirements, as discussed in section 1.3. Harvesting energy from head motion could then play a part, perhaps along with re-chargeable batteries, in the power management strategy of these future devices.

Appendix A: Cable Model Calculation

This appendix describes the analysis performed on the cable model to generate an excitation spread.

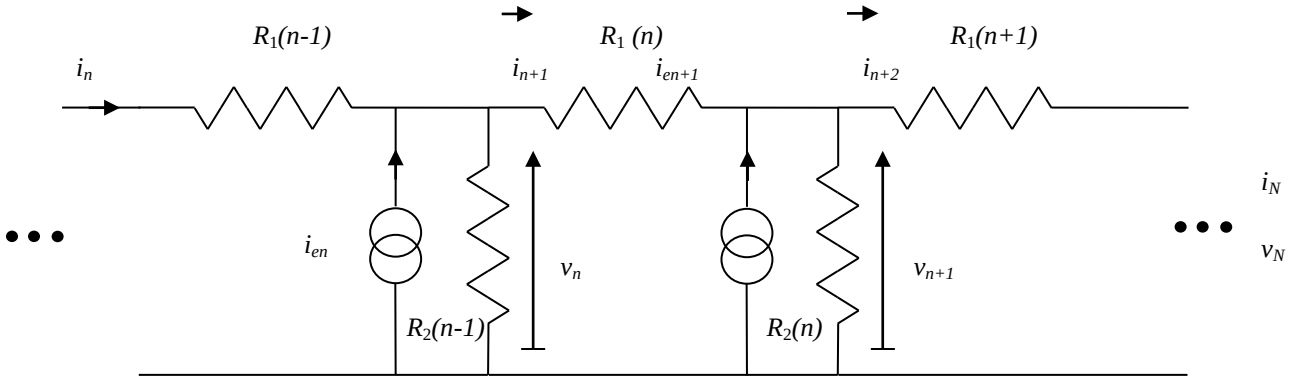

Figure A. 1: A detailed outline of the circuit components where R_1 is the resistance between an active electrode and the return electrode via the tissue in between, R_2 is the resistance between active electrodes, and N is the total number of electrodes

R_2 in that part of the circuit is as follow:

$$v_n = \left(i_n - i_{n+1} + i_{en}\right) R_2 \tag{A1}$$

where,

$$i_{n+1} = \left(v_n - v_{n+1}\right) / R_1 = G_1\left(v_n - v_{n+1}\right) \tag{A2}$$

These equations may be put in matrix form,

$$\begin{bmatrix} v_1 \\ v_2 \\ v_3 \\ \vdots \\ v_{N-1} \\ v_N \end{bmatrix} = R_2 \begin{bmatrix} 1 & -1 & 0 & 0 & \dots & 0 \\ 0 & 1 & -1 & 0 & & \\ 0 & 0 & 1 & -1 & & \\ \vdots & & & \ddots & & \\ & & & & & \\ 0 & & & & & 1 \end{bmatrix} \begin{bmatrix} i_1 \\ i_2 \\ i_3 \\ \vdots \\ i_{N-1} \\ i_N \end{bmatrix} + R_2 \begin{bmatrix} i_{e1} \\ i_{e2} \\ i_{e3} \\ \vdots \\ i_{eN-1} \\ i_{eN} \end{bmatrix} \rightarrow \boldsymbol{v} = \boldsymbol{R i} + R_2 \boldsymbol{i_{en}} \tag{A3}$$

$$\begin{bmatrix} i_1 \\ i_2 \\ i_3 \\ \vdots \\ i_{N-1} \\ i_N \end{bmatrix} = G_1 \begin{bmatrix} 0 & 0 & 0 & 0 & \dots & 0 \\ 1 & -1 & 0 & 0 & & \\ 0 & 1 & -1 & 0 & & \\ 0 & 0 & 1 & -1 & & \\ \vdots & & & \ddots & & \\ 0 & & & & 1 & -1 \end{bmatrix} \begin{bmatrix} v_1 \\ v_2 \\ v_3 \\ \vdots \\ v_{N-1} \\ v_N \end{bmatrix} \rightarrow \boldsymbol{i} = \boldsymbol{G}\boldsymbol{v} \tag{A4}$$

$$\boldsymbol{v} = \boldsymbol{R}\boldsymbol{G}\boldsymbol{V} + R_2 i_{en} \rightarrow \boldsymbol{v} = R_2 \left[\boldsymbol{I} - \boldsymbol{R}\boldsymbol{G}\right]^{-1} \boldsymbol{i}_{\boldsymbol{en}} \tag{A5}$$

Where $R_2 \left[\boldsymbol{I} - \boldsymbol{R}\boldsymbol{G}\right]^{-1} \boldsymbol{i}_{\boldsymbol{en}}$ is the overall impedance matrix that is used to calculate the resultant voltage due to an input current at i_e.

The voltage output due to excitation at a single electrode can be calculated as one column of the matrix in equation (A5). This dictates how the spread of the current throughout the system occurs and is plotted in the main text in Figure 2.3 of Chapter 2. A correction is required to get a uniform output for all the peaks in the plot. This correction is applied by simply extending the array by one element on either side to represent the tissue on either side as an infinite resistance to get a more uniform spread as shown by the middle section of Figure 2.3. These two extra elements are not excited by a current. The result is shown in Figure A.2.

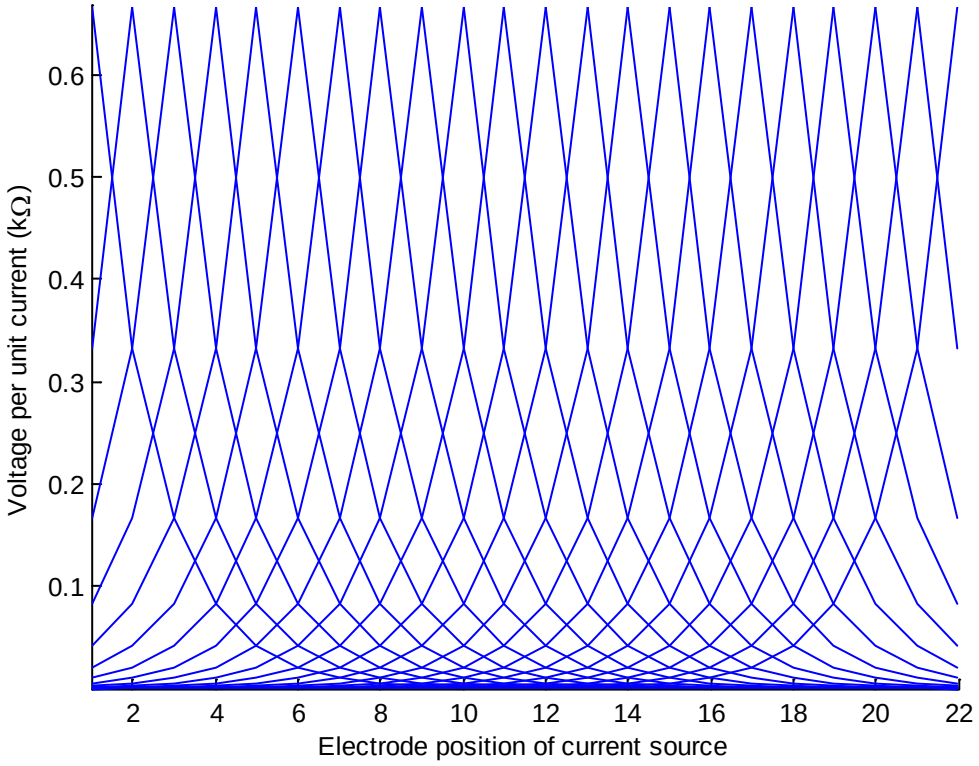

Figure A. 2: Improved cable model voltage spread against position of current source

It is also worth investigating the effect of the resistances on the shape and peak of each spread. Four combinations were calculated:

R_1 = 1 kΩ and R_2 = 1 kΩ

R_1 = 1 kΩ and R_2 = 1.5 kΩ

R_1 = 1 kΩ and R_2 = 2 kΩ

R_1 = 1 kΩ and R_2 = 10 kΩ

R_1 was kept constant and R_2 was increased in the steps outlined above and were also performed vice versa with R_1 increasing. This is not realistic in reverse because R_2 is in reality considerable greater than R_1 due to the high resistivity of the tissue in between the active and return electrode. Results are shown below in Figure A.3 and Figure A.4.

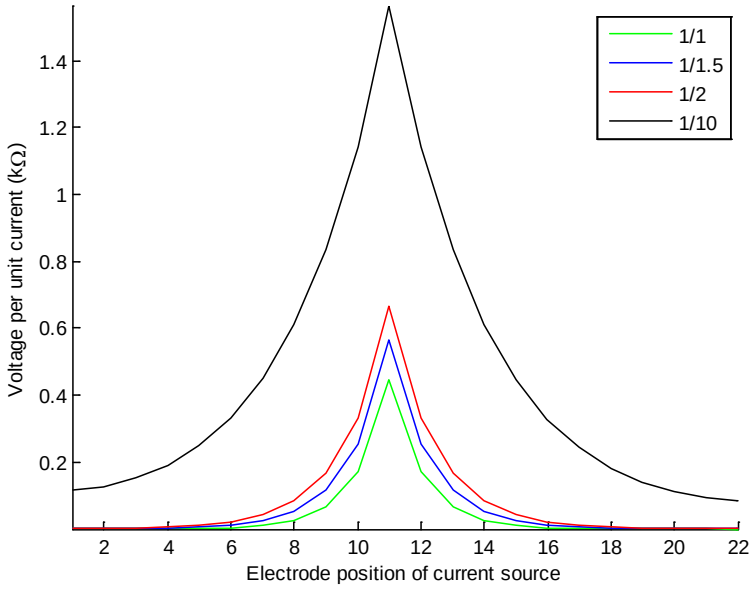

Figure A. 3: Effect of ratio of resistances R_1 / R_2 on the peak and spread of the voltage

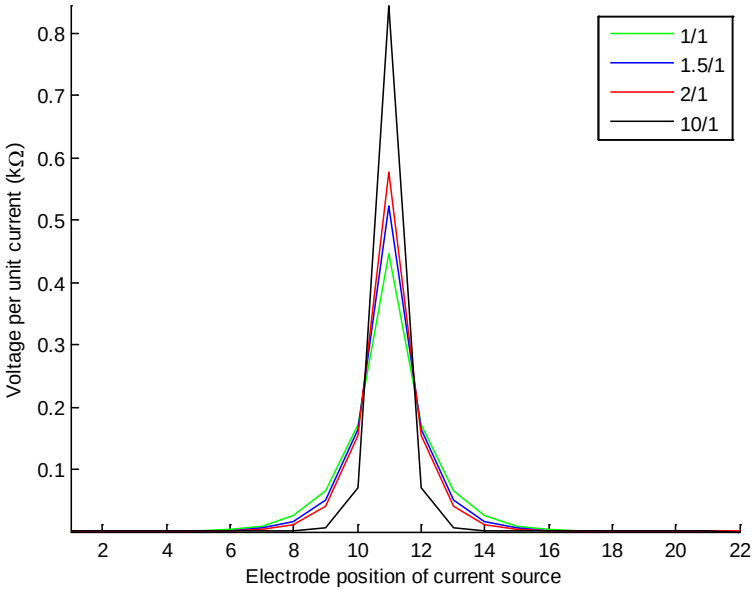

Figure A. 4: Effect of ratio of resistances R_1 / R_2 on the peak and spread of the voltage in reverse

In the main text, the attenuation change along the length of the array is defined and plotted when stimulating with one electrode in the centre for a specific resistance ratio.

This is also calculated for several resistance ratios of R_1/R_2 and an average attenuation is obtained for each. This is plotted against a theoretical prediction of the attenuation with changing resistance ratio R_1/R_2, as shown in Figure A.5. The theoretical attenuation rate is defined as the ratio of the voltage at the $(n+1)^{th}$ stage to the n^{th} stage, and can be calculated for an infinite array from the cable model as:

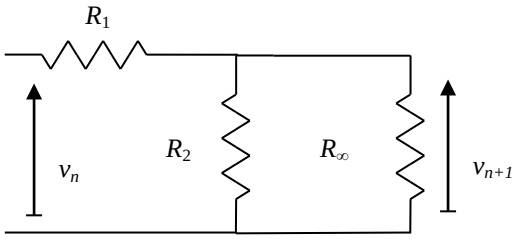

$$\frac{v_{n+1}}{v_n} = \frac{R_2 // R_\infty}{R_1 + R_2 // R_\infty} = \frac{R_2 R_\infty}{R_1(R_2 + R_\infty) + R_2 R_\infty}$$

$$Attenuation = \frac{R_2 R_\infty}{R_1 R_2 + R_1 R_\infty + R_2 R_\infty} \tag{A6}$$

Where $R_\infty = R_1\left(1+\sqrt{1+\frac{4R_2}{R_1}}\right)$ is the impedance looking into an infinite array, so that,

$$Attenuation = \frac{1}{2\left(\frac{1}{\sqrt{1+\frac{4R_2}{R_1}}+1}\right)+\frac{R_1}{R_2}+1} \tag{A7}$$

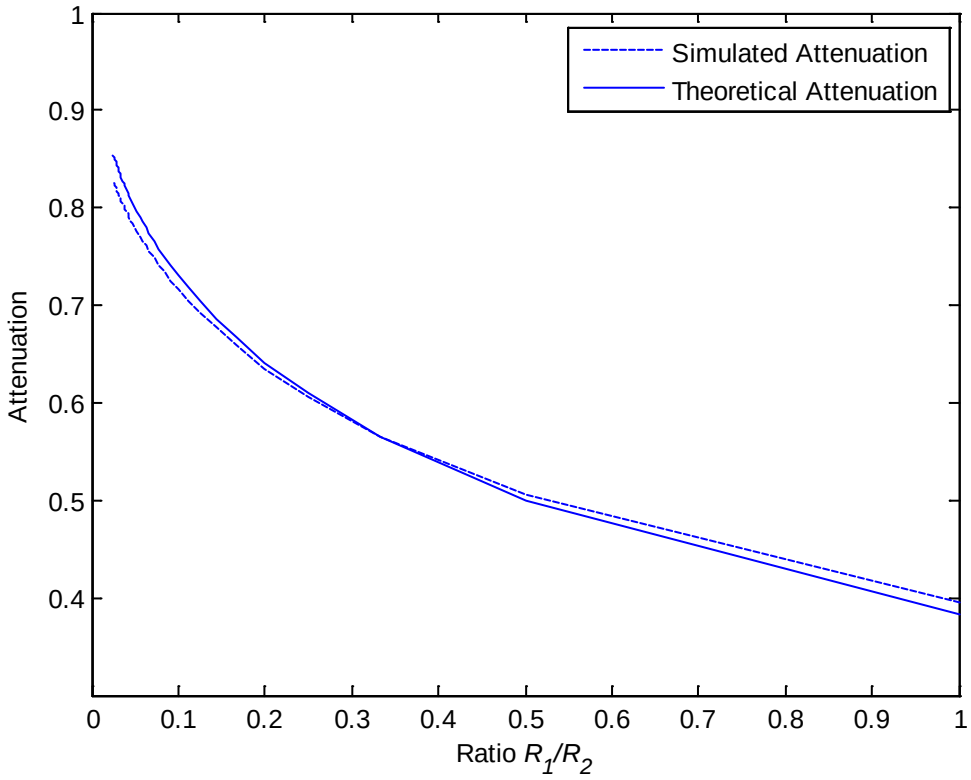

Figure A. 5: Simulated and theoretical attenuation rate against R_1 / R_2

Discussion:

To begin with, the estimated impedance matrix is based on a network of resistors where all the impedances in between the active electrodes are identical and the impedance between each active electrode and the return electrode are also all identical, defined as R_1 and R_2 respectively. The measured matrix is more complicated and takes into account resistance changes across the entire array. The potential spread due to the measured matrix in Figure 2.1 shows the complicated nature of the patient's electrical characteristics and gives a maximum resistance in the middle at electrodes 6 and 7 where it jumps considerably higher in voltage than the others. This was initially thought to be due to a characteristic of how the electrode is placed in the scala tympani, as well as representing how far the electrode array is usually placed from the return electrode at different position in such an operation. For another patient shown in Figure 2.1 this has a maximum elsewhere and produces a different shape altogether thus proving that, at this preliminary stage, there is no pattern in the spread of the electric potential that is common to all patients.

The resistance ratio tests carried out in Figure A.4 and A.5 confirm that as the resistance R_2 in between the active and return electrode increases, the peak voltage at the electrode carrying the current increases and the width of the voltage spread also increases. With the knowledge that R_2 is considerably higher than R_1 it is confirmed in Figure A.4 that when the ratio is 1 to 10 the spread is comparable to that of the measured matrix.

Figure A.5 compares the attenuation rate for different resistance ratios in the simulated case. This is also compared to the theoretical calculation described above for an infinite array. The simulated and theoretical attenuation for a changing resistance ratio follows the same pattern and are similar in magnitude. Therefore, it is possible to model to an approximation the spread of excitation potential along an electrode array using the simple cable model described above, but the model lacks the variation in the resistances that gives rise to the variations seen in the voltage distribution above.

Appendix B: Software List

Modelling complicated structures involves a lot of preparation, careful planning and full understanding of all the software being used.

In the case of the cochlear structure and electrode implants modelled in this project, software is required to measure dimensions, perform further calculation, build three dimensional models and finally to solve the resultant geometry with relation to a particular type of physics.

The function and purpose of each program is listed below however the specific procedures involved in building the model will be outlined in the relevant sections later on in this chapter.

Corel Paint Shop Pro X2

This software is used for picture editing at a high degree of accuracy. This program is used to import a image of the cochlear cross-section from a journal paper. This program is chosen over others for its higher resolution format once the picture is imported and saved.

Autocad LT 2010:

AutoCAD is a Computer Aided Design program that is used for drafting and designing two and three dimensional sketches. In this project, it is used to measure the dimensions of certain cochlear structures by importing the image taken from a journal paper in the Corel Draw format, scaling it to size and measuring the structures of interest.

Excel 2007:

This is a spreadsheet program which is part of the Office package from Microsoft. This is used to collect all the measured data from Autocad. The data can then be easily exported to Matlab for further calculation.

Matlab R2010b:

Matlab is a numerical computing program based on its own high performance programming language. This is used to calculate further dimensions on the cochlear structures based on the previously measured data. The calculated data from this program is used to build the three dimensional models in Solidworks.

Soldworks 2010/2011 Education Edition:

Solidworks is a three dimensional CAD modelling package that is used to construct the three dimensional models of the cochlea and electrode implants. Dimensions from Matlab are used in this program. The structures are built using a sequence of planes, sketches, curves, surfaces and solids. This program is perhaps the most heavily used in this project and careful planning is required in order to reduce future workload and prevent errors from occurring. Once the models are constructed, the geometry is exported to Comsol for solving.

Comsol 4.2a:

This is the final program in the procedure chain. Comsol is a finite element simulation and solver package. It is used to mesh and solve a model numerically for a specified physics problem. It is a multi-physics package enabling the coupling of various types of physics with relative ease. This program is used to import the geometry of the cochlea from Solidworks, create domains, assign materials, specify boundary conditions and configure a solver to find a solution to an electric conductive media problem.

Appendix C: Calculation of circular segment of a given area

The problem is to define the circle radius to produce a given area for a fixed chord length l. Geometry is shown in Figure C.1.

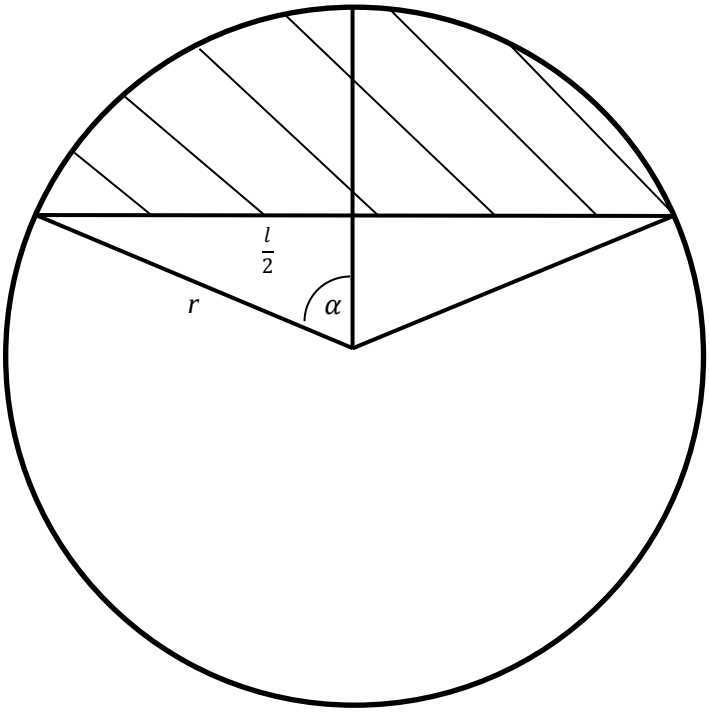

Figure C. 1: Geometry of segment

Take the geometry above as an example. The area of the segment is:

$$\text{Segment area} = \pi r^2 \left(\frac{\alpha}{180} \right) \tag{C1}$$

When r is the radius of the circle and α is half the subtended angle in degrees.

$$\text{Area of triangle } = \frac{l^2}{4tan\alpha} \tag{C2}$$

Therefore the area of the section required, shown as shaded above, is:

$$\text{Section} = \pi r^2 \left(\frac{\alpha}{180} \right) - \frac{l^2}{4\tan\alpha} \tag{C3}$$

$$r = \frac{l}{2sin\alpha} \tag{C4}$$

Substitute (C4) into (C3)

$$\text{Area} = \pi \frac{l^2}{4(sin\alpha)^2} \left(\frac{\alpha}{180} \right) - \frac{l^2}{4tan\alpha} \tag{C5}$$

Since the area and length *l* is known, the above equation is solved using the FZero function in Matlab to give the angle α. This programme tries to find a zero of function. In this case, equation (C5) is made equal to zero and solved in this way.

$$f(\alpha) = \pi \frac{l^2}{4(sin\alpha)^2} \left(\frac{\alpha}{180} \right) - \left(\frac{l^2 sin\alpha}{4cos\alpha} \right) - Area = 0 \tag{C6}$$

The range for α can vary from 0^0 to 180^o and so the resultant section of a circle that will represent the required area can be larger or smaller than a semicircle. In the case that α is larger than the midpoint of the range at 90^0, the equation above (C6) is slightly altered to take into account that the area will be larger than a semi-circle. The altered equation is shown below:

$$f(\alpha) = \pi \frac{l^2}{4(sin\alpha)^2} \left(\frac{180 - \alpha}{180} \right) - \frac{l^2 sin\alpha}{4(-cos\alpha)} - Area = 0 \tag{C7}$$

The choice of equation is governed by the definition below:

If $Area < \frac{\pi l^2}{2}$, then equation (C6) is used. If $Area > \frac{\pi l^2}{2}$, then equation (C7) is used.

Appendix D: Spline Calculation

The spline function was used in three different ways in chapter 2. One use of the spline function was to trace the outline of individual chambers of the cochlea in order to estimate cross-section areas of these chambers. This is demonstrated in Figure 2.7 of section 2.4.1. The second use was to estimate these cross-sectional areas for every quarter of a turn of the spiral, shown in Figure 2.8 of 2.4.1. The third use was to generate the spiral curve that was used to loft the spiral structure of the cochlea in Solidworks. This appendix will explain the use of the spline function to estimate cross-sectional areas at every quarter turn and generate the spiral curve.

Once the cross-section areas of the chambers were estimated in Autocad on a single plane, it was necessary to estimate these areas for every quarter of a turn of the spiral. This resulted in an estimate of these areas for 4 planes giving 8 cross-sections per turn. This estimate allows for the generation of a smooth curvature for the spiral solids. The spiral curve cannot be estimated using just one plane (2 cross-sections), as the direction for the curvature of the spiral cannot be established, and in the case of two perpendicular planes with 4 cross-sections per turn, the spline function used to generate a curve in Solidworks, would not be able to sufficiently represent the curvature. In the case of 4 planes, giving 8 cross-sections, the spline function is able to represent the curve accurately. This is demonstrated for the estimation of a circle using the spline curve function using 4 and 8 reference points, as shown in Figure D.1.

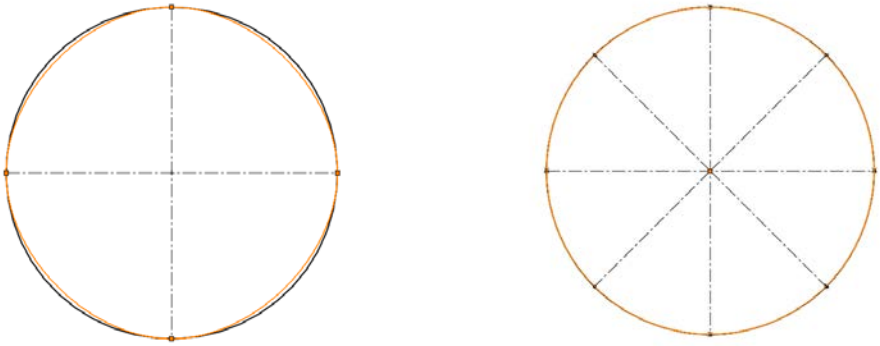

4 point estimate 8 point estimate

Figure D. 1: Spline function to estimate a circle

The estimate of the cross-section areas for every quarter turn was performed using Matlab. This estimate was calculated by the built-in spline function,

$$YY = SPLINE(X,Y,XX)$$

Where X is the original vector of positions along the cochlea, Y is the original vector of cross-section areas at the corresponding positions along the cochlea and XX is the vector of positions including both the original positions and those corresponding to every quarter turn of the spiral. The spline function generates vector YY, representing the cross-section areas corresponding to the positions in vector XX. An example of the result of the estimate is shown in Figure D2.

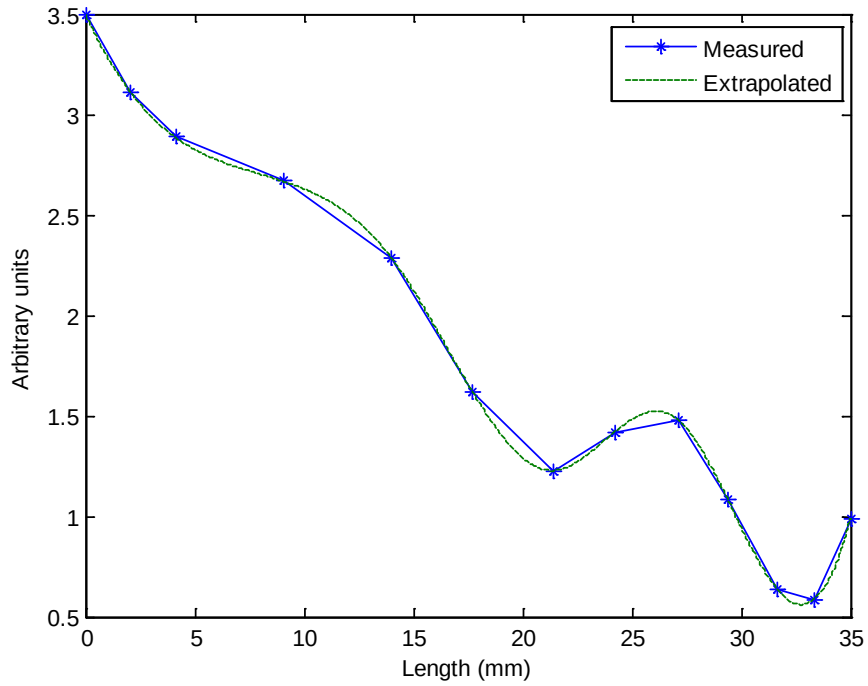

Figure D. 2: Spline calculation estimate in comparison to measured data

This spline calculation was used to extrapolate estimates for every quarter of a turn of the cochlea for a number of parameters describing the cross-section areas of the chambers as well as their position and distance horizontally and vertically from the centre of the modiolus.

Appendix E: Resistivity Review

When solving an electrical model, the parameters usually taken into consideration include the resistivity (or conductivity) and permittivity of the different materials in the structure. In the case of the cochlea, the resistivity or impedance values of cochlear structures do not vary within the frequency range of around 8Hz - 12.5 kHz according to Spelman (1987). Therefore, the model becomes purely resistive and is solved using only the electrical resistivities of the structures in the cochlea. The electrical resistivities of the cochlear structures are prone to great variability. This variability is also present in an individual. After implantation, the resistivities of the cochlear structures change considerably over time and will affect the stimulation process. It is therefore necessary to get representative numbers for these resistivities that will describe the majority of cases.

These electrical parameters can be classified as the following:

Non-Biological (Implant):

- Electrode
- Silicon carrier

Biological:

- Perilymph (The fluid in the scala tympani and scala vestibuli chambers)
- Endolymph (The fluid in the scala media chamber)
- Basilar Membrane (This separates the scala media and the scala tympani)
- Reissners Membrane (This separates the scala media and the scala vestibuli)
- Spiral Ganglion (Groups of nerve cells within the spiral lamina of the cochlea)
- Organ of Corti (This consists of the inner and outer hair cells used in normal hearing)
- Stria Vascularis (Situated on the upper portion of the spiral ligament)
- Nerve Tissue

Determination of parameter values

As previously mentioned, these electrical resistivity parameters can vary significantly from person to person, and also in an individual over time. It is difficult to measure the

electrical properties of cochlear tissue accurately and so variability also exists between authors who used these parameters in their models to simulate the excitation spread in the cochlea. It is therefore necessary to compile these parameters for comparison and establish a representative set of resistivity values to be used in the cochlear model discussed briefly in this appendix.

Table E.1 below shows a direct comparison of the resistivity values used by other authors. All resistivity values have been converted into the standard resistivity unit Ωm. Volume resistivity is given in Ωm because the equation defining the resistance of the material in the model, which in turn depends on the geometry of the model, is defined as the following:

$$R = \rho \frac{length}{area} \frac{dy}{dx} \tag{E1}$$

Where ρ is the resistivity of the material.

Source	(Hanekom, 2001)	(Briaire and Frijns, 2000)	(Rattay et al., 2001)	(Finley et al., 1990)
Electrodes	0.001		0.001	0.001
Silicon	1.01			$1x10^7$
Endolymph	0.600	0.599	0.600	0.600
Perilymph	0.700	0.699	0.700	0.700
Basilar membrane	4	16	30*	18
Reissner's membrane	340	1020	100	605
Bone	6.410	6.410	64	6.300
Organ of Corti	83.3	83.3	30*	
Stria vascularis	126	189		

* This value is for the basilar membrane and the organ of Corti together.

Table E. 1: Resistivity values from papers by other authors

Electrode contacts and Silicon carrier

The authors mentioned in Table E.1 all agree on using the same resistivity value for the electrode contacts, specified as 0.001 Ωm. Cochlear, a cochlear implant manufacturer, have reported that their electrode arrays use 99.95% pure platinum and the date sheets for this material specify a resistivity of $1x10^{-7}$ Ωm. The material library in Comsol Multiphysics, agrees with the data sheets. The value used by other authors is not referenced.

Similarily, the authors specify, but do not backup, the value used for the insulating silicon carrier. The manufacturer reports that liquid silicon rubber, durometer 60 (LSR 60), is used for the insulating carrier, specifying a material label as MED-4860. Data sheets for this material do not specify electrical properties, but a similar material, labelled as HT-1260 (also liquid silicon rubber with durometer 60) specifies a resistivity of 1×10^{12} Ωm. This value was tested in the model and it was found that there was not much of an effect when the silicon was increased beyond 10 Ωm and so this is the value that will be used in the model presented here.

Fluid chambers and Organ of Corti

The fluid chambers, perilymph and endolymph, have no data sheet to refer to, but the authors agree on the value for resistivity. This is also the case for the Organ of Corti.

Basilar membrane, Reissner's Membrane and the Stria Vascularis

The structures with the most discrepancies include the Basilar and Reissner's membranes, the Stria Vascularis and the bone tissue. Some authors have adapted the resistivity values of the membranes in order to compensate for increasing the thickness of the membranes in their models to achieve better shaped structures but keeping the total resistivity the same. It is not anticipated that this adaptation will be a requirement in the model presented here. Hanekom (2001) scales the basilar membrane and Reissner's membrane and the Stria Vascularis down by a factor of 20 and 30 and 1.5 respectively giving the above mentioned values in Table E.1. Reversing this by scaling back up gives the correct resistivity values for these structures. The correct values are 80, 10203.9 and 188.685 respectively. Briaire and Frijns (2000) lists the values as conductivities. He scales these values up for the Basilar and Reissner's membrane but does not alter the Stria valcularis. These conductivities are scaled up by a factor of 10 and 5 respectively. Therefore scaling

these conductivities back down and converting them into a resistivity in Ωm gives 160 and 5102 respectively. Therefore the comparison for these structures after conversion is shown in table 2.

Finley et al. (1990) and Rattay et al. (2001) also adapt their Basilar and Resiner's membrane resistivities to improve their models but do not make it clear by what factor these resistivities are adapted from the original.

Table E.2 shows the resistivity values after conversion from the adapted to the real values.

Source	(Hanekom, 2001)	(Briaire and Frijns, 2000)
Basilar Membrane	80	160
Reissner's Membrane	10200	5102
Stria Vascularis	189	189

Table E. 2: Resistivity values after conversion

This shows that the values for the Stria vascularis are in agreement and can be used in the model mentioned in this paper. The values for the membranes seem to still disagree by a factor of 2. In lieu of this discrepancy, it is better to calculate the resistivity based on measurements from (Strelioff, 1973). The basilar membrane was therefore calculated in the same way as Finley, using estimated resistance to calculate a resistivity based on the geometry of the model. The calculation was done for two average thicknesses, $2x10^{-5}$ and $1.3x10^{-5}$. The first is the average thickness according to (Skrodzka, 2005a, Skrodzka, 2005b) and the second is based on measurements from the image traced above. This gives a basilar membrane resistivity of 30 and 45 respectively. Similarly, the resistivity of Reissner's membrane was calculated according to the average thickness based on the measurements from the image giving a resistivity of 500. The values for both basilar and Reissner's membrane are within the order magnitude reported by other authors post adaptation and are therefore valid. An average based on the two adapted numbers was taken for the basilar membrane resulting in a resistivity of 37.5.

Bony tissue

The authors agree to the resistivity of the bone structure expect for one. They use the resistivity value measured by Spelman (1987), who used a technique that allows in vivo measurements of bony tissue impedances within the cochlea of seven anesthetized guinea pigs. The value is specified as 6.4 Ωm.

Rattay (2001) chose a different value, adapted from Kosterich et al. (1983) resulting in a difference of a factor of ten compared to the other authors. Kosterich gives measured conductivity values for fluid saturated bone at 37^0C as a function of frequency. He uses bone samples that were excised from the femoral bone of a rat. These conductivities do not vary significantly within the range of 8Hz to 12.5 kHz and an average conductivity for this range is approximately 12.9 ms/m. This gives a resistivity of around 77 Ωm. Therefore, it can be deduced that Rattay et al. (2001) used a value that is ten times that which is quoted by other authors in order to match the order of magnitude predicted by Kosterich.

Since (Spelman, 1987) measurements were closer to the realistic case in that it was measured in a live animal, it is their resistivity that will be used in the model.

Final parameters

Therefore the final list of resistivities for the model presented will be as follows in Table E.3:

Material	Resistivity (Ωm)
Electrodes	1e-7
Silicon	10
Endolymph	0.600
Perilymph	0.700
Basilar membrane	37.5
Reissner's membrane	500
Bone	6.41
Organ of corti	83
Stria Vascularis	188

Table E. 3: Final parameters to be used in the cochlear model

Appendix F: Cochlear implant data sheet

Nucleus® 24 Contour® & Contour Advance® (Freedom™) Electrodes

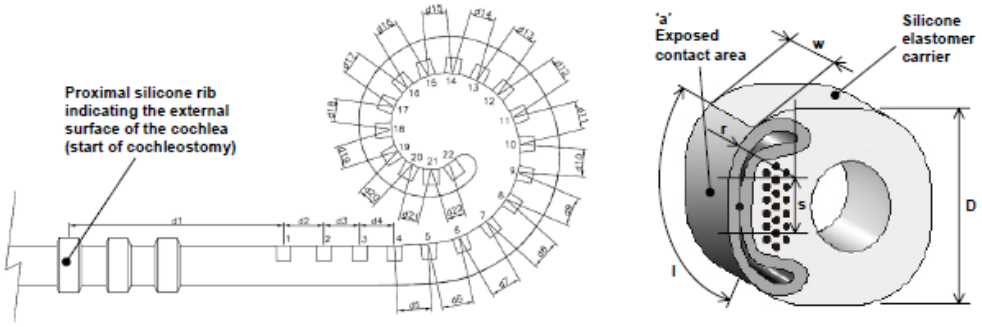

# Electrode contact no. (1-22)	d Electrode spacing along inner surface (i.e., modiolar wall); see d1-d22 [mm]	a Approximate exposed contact area [mm²]	D Overall electrode diameter [mm]	w Width of exposed contact area [mm]	l Length of exposed contact area [mm]	s Length of flat section [mm]	r Radius of curved section [mm]
1	4.36	0.306	0.800	0.3	1.02	0.25	0.3
2	0.81	0.306	0.800	0.3	1.02	0.25	0.3
3	0.73	0.306	0.800	0.3	1.02	0.25	0.3
4	0.70	0.306	0.800	0.3	1.02	0.25	0.3
5	0.69	0.306	0.800	0.3	1.02	0.25	0.3
6	0.65	0.306	0.800	0.3	1.02	0.25	0.3
7	0.63	0.306	0.800	0.3	1.02	0.25	0.3
8	0.61	0.306	0.800	0.3	1.02	0.25	0.3
9	0.59	0.306	0.800	0.3	1.02	0.25	0.3
10	0.57	0.306	0.800	0.3	1.02	0.25	0.3
11	0.57	0.297	0.796	0.3	0.99	0.25	0.298
12	0.55	0.297	0.768	0.3	0.99	0.25	0.284
13	0.52	0.297	0.741	0.3	0.99	0.25	0.2705
14	0.52	0.297	0.717	0.3	0.99	0.25	0.2585
15	0.50	0.297	0.694	0.3	0.99	0.25	0.247
16	0.48	0.297	0.672	0.3	0.99	0.25	0.236
17	0.48	0.283	0.650	0.3	0.943	0.25	0.225
18	0.47	0.283	0.626	0.3	0.943	0.25	0.213
19	0.46	0.283	0.604	0.3	0.943	0.25	0.202
20	0.40	0.283	0.578	0.3	0.943	0.25	0.189
21	0.40	0.283	0.552	0.3	0.943	0.25	0.176
22	0.40	0.283	0.519	0.3	0.943	0.25	0.1595

Figure F. 1: Nucleus 24 cochlear implant data sheet

Appendix G: Software issues and suggested precautions in the modelling phase

This section will discuss some of the traps and modelling issues that arise when using Solidworks and Comsol Multiphysics to model a biological structure such as the inner ear.

One way to reduce build time is to carefully consider which parameters will be regularly varied as part of the simulation process. Equations are the best way to control those parameters. There are two sets of parameters, those which are driving, and those which are driven. The parameters which are driving will be the main parameters varied to correspond to a particular case. An example of this is varying the distance of one side of the coil from the centre of the modiolus. Changing these parameters will force other driven parameters to adapt automatically to maintain the desired specification of the cochlea, in terms of areas and lengths of the structures. The driving parameters are defined using equations which can be accessed by opening the built in spread sheet which contains all the parameters in one file, and altering them as required. This method is much faster than opening each individual sketch and altering the parameters from within. Opening each sketch individually will considerably increase the workload. The driven parameters can either be left as is or defined by equations to relate to the driving parameters. This decision will depend on the complexity of the situation of those parameters. Driven parameters are set using an equation where they will always change in a predefined manner relative to a driving parameter, for example, by setting the driven parameter to always be equal to a third of the length of a driving parameter. In this case, using an equation to relate the two will greatly reduce build time. This will also reduce the time required to modify these parameters.

Surfacing techniques are also important to take into consideration. There are several ways to build the surfaces that split the outline solid into the required sections (into the cochlear chambers as in this thesis). The surface knitting method was attempted at the early stages of the modelling the cochlea. With this method, all the surfaces that make up the geometry required could be created, and the knitting function could be used to create solids out of the surfaces by stitching them together at the edges. In earlier releases of Solidworks, the knitting function had no suitable tolerance control. This means that if you have three surfaces to be knitted together giving an edge that is thinner than the

predefined limit, that edge will be removed and the two surfaces on either side of the edge will be knitted together. This problem occurred during the build of the basilar membrane structure, as it was quite thin in general. An example of this is given in Figure G.1.

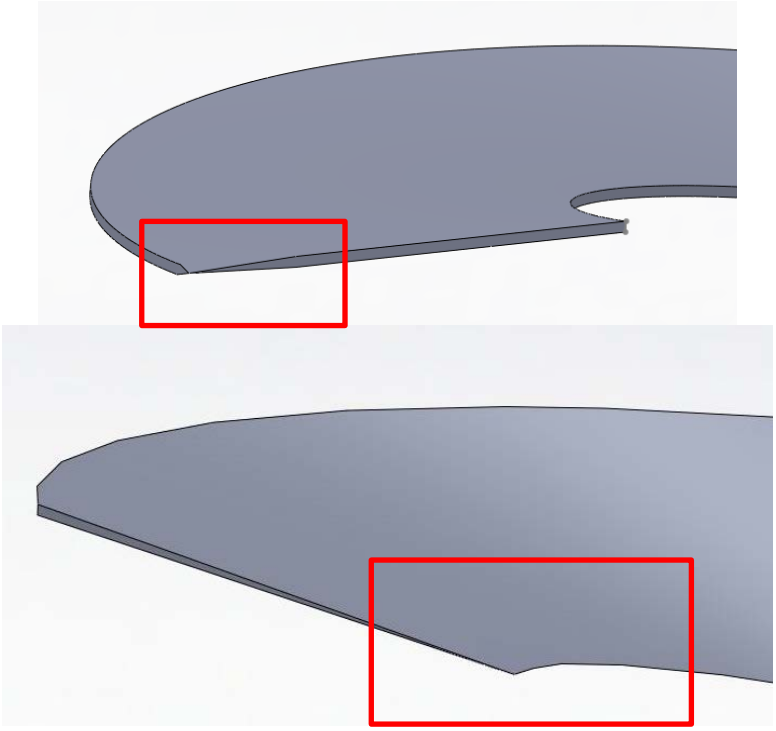

Figure G. 1: Surface knitting issues

In later releases of the software, a tolerance control was introduced giving the ability to define what the gap allowance is. Although this could potentially solve the problem, errors persisted within either Solidworks or Comsol, therefore this method was abandoned.

Similarly, when building the other structures in the model using surfaces, the common surfaces between two structures are essentially duplicated, either by using the knitting function, or by manually duplicating the surfaces first and then joining the surfaces. Either way, you cannot accurately duplicate a surface, and the slightest of differences resulted in many errors in Comsol when establishing subdomains. Comsol was not be able to recognise that the two surfaces are in fact identical and therefore cannot find a clear separation between the two structures subtended by these surfaces. It is usually recommended that the model is imported into Comsol as solids rather than a set of surfaces.

There are also limits to the degree in which geometry can be altered. If a structure takes a shape well beyond reasonable limits, for example twisting a structure, this could result in

surfaces interfering with each other. The algorithm used to generate a solid could run into problems if the solid is unsolvable.

Accurate sketch or guide curve definition is also important. In the case of the guide curve, it is explained in Appendix D that 8 reference points per turn are required as opposed to using a single plane which only gives two points, or two planes which give four points.

This explanation translates to curve generation. If you give solidworks less than 8 points per turn to specify the curvature of the cochlea, geometric errors could occur that cause problems in both Solidworks and Comsol.

In fact, several issues caused a failure when trying to use several different methods to generate the structures of the cochlea, either by using an outline and a splitting surface, or by generating the individual solids separately. Errors also occurred when establishing subdomains in the geometry. This is either by failure to successfully break the geometry into subdomains, or by allowing subdomains to be formed which contain severe geometric errors or artefacts that cannot be removed or repaired. These geometric errors include incorrect identification of surfaces, inaccurate matching of surface edges, non-smooth curvature of the cochlea and the omission of some surfaces within the geometry. These types of errors occurred in both software. All these artefacts and geometric inaccuracies lead to a complete failure of the mesh function in Comsol. An example of incorrect identification of a surface leading to incorrect matching of edges is shown in Figure G.2. Omission of a surface is shown in Figure G.3.

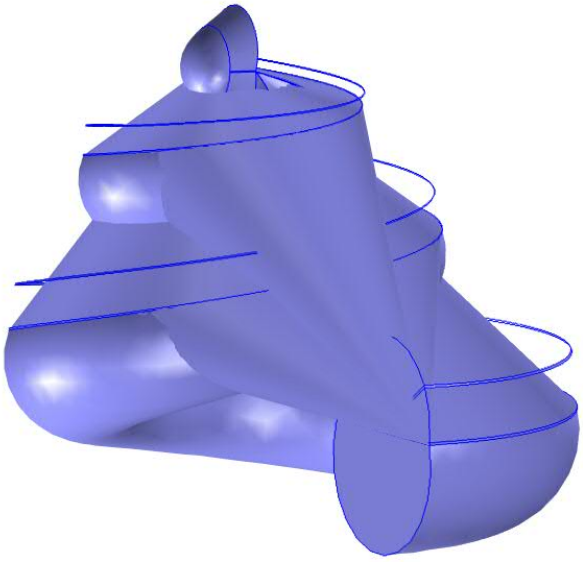

Figure G. 2: Comsol failure in recognising surfaces correctly

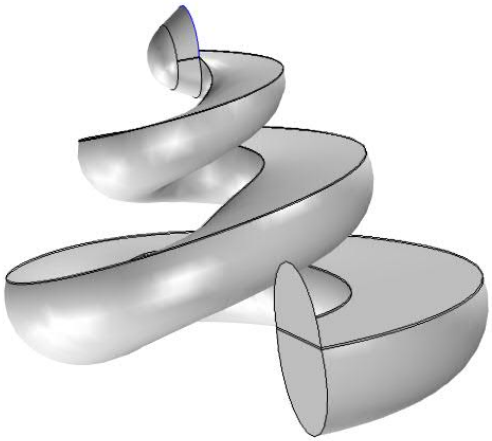

Figure G. 3: Surface omission error

In some cases, a method would work as far as the successful creation of subdomains in Comsol, and yet, errors occurred during mesh generation. Some of these errors could be repaired by manually adjusting mesh settings for narrow regions, but the majority of failures were due to inaccurate surface curvature representation.

This appendix discussed only some of the main issues that arose during the modelling process, but in reality, a long process of trial and error was required to generate a successful mesh of the cochlea.

Appendix H: Focussing strategy examples

Chapter 3 investigates the effect of focussing strategies on the voltage distribution in the cochlea. Figure H.1 to Figure H.8 show examples of the effect of different focussing strategies in comparison to single electrode stimulation on 8 different subjects. The threshold and comfort levels of each subject are obtained from a study by Pfingst and Xu (2004). These levels are adapted from currents to voltages by inputting the current level into the cochlear model, and measuring the resultant voltage. These examples are simulated using both the tightly coiled and loosely coiled cochlear implant models, both using a monopolar reference electrode configuration.

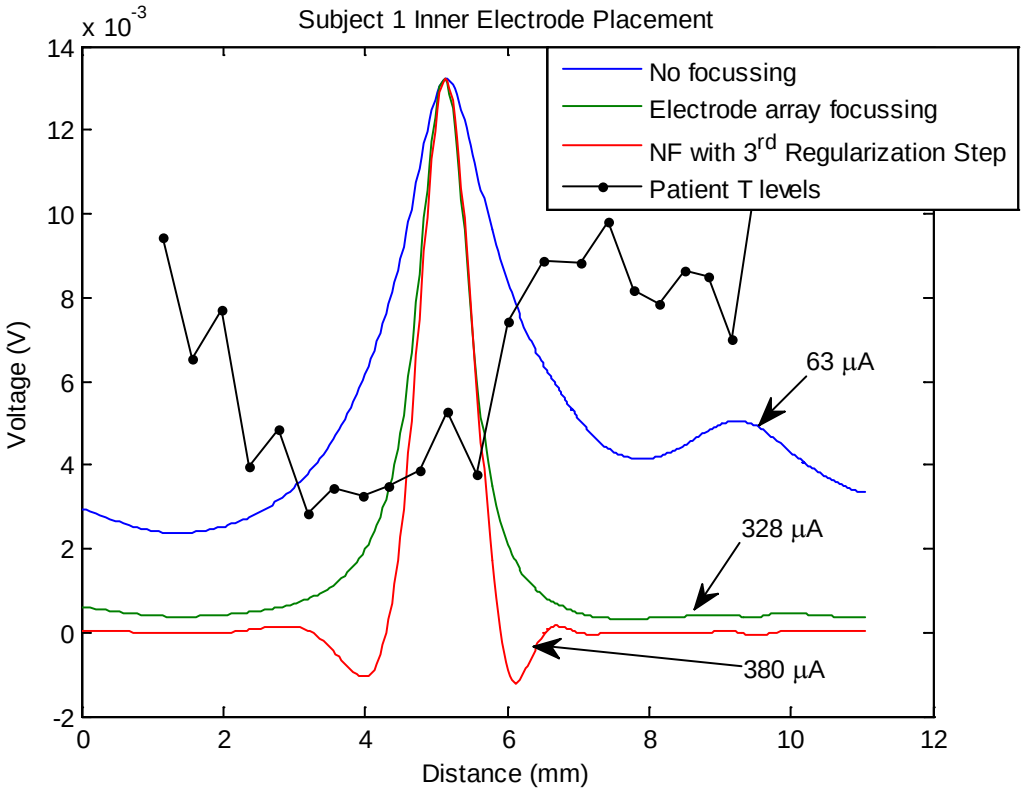

Figure H. 1: Subject 1, Inner electrode placement

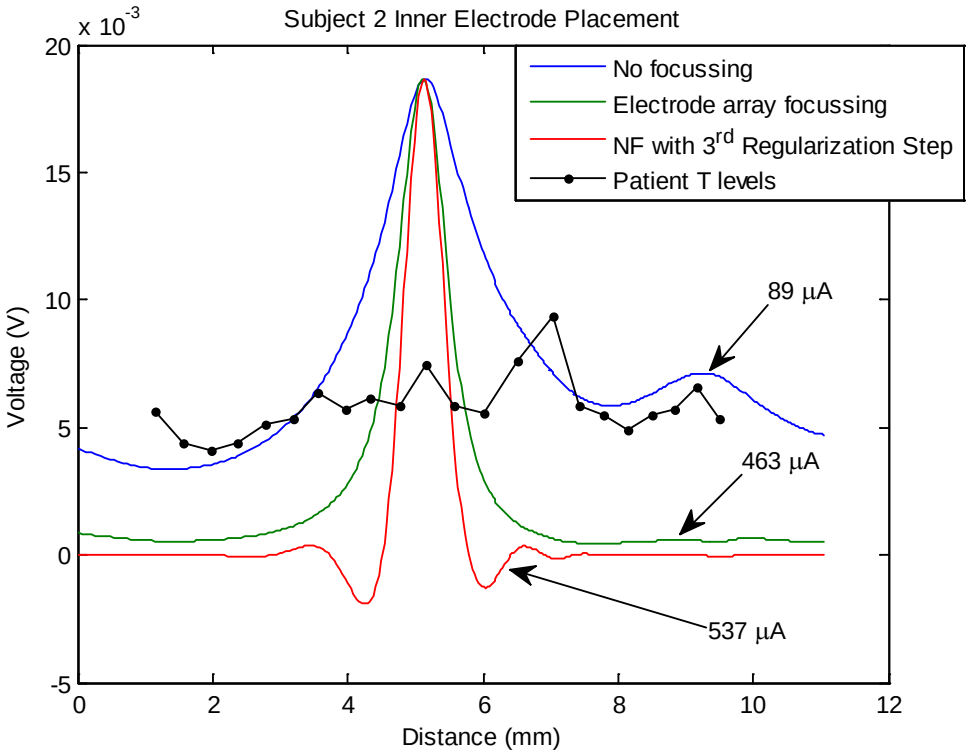

Figure H. 2: Subject 2, Inner electrode placement

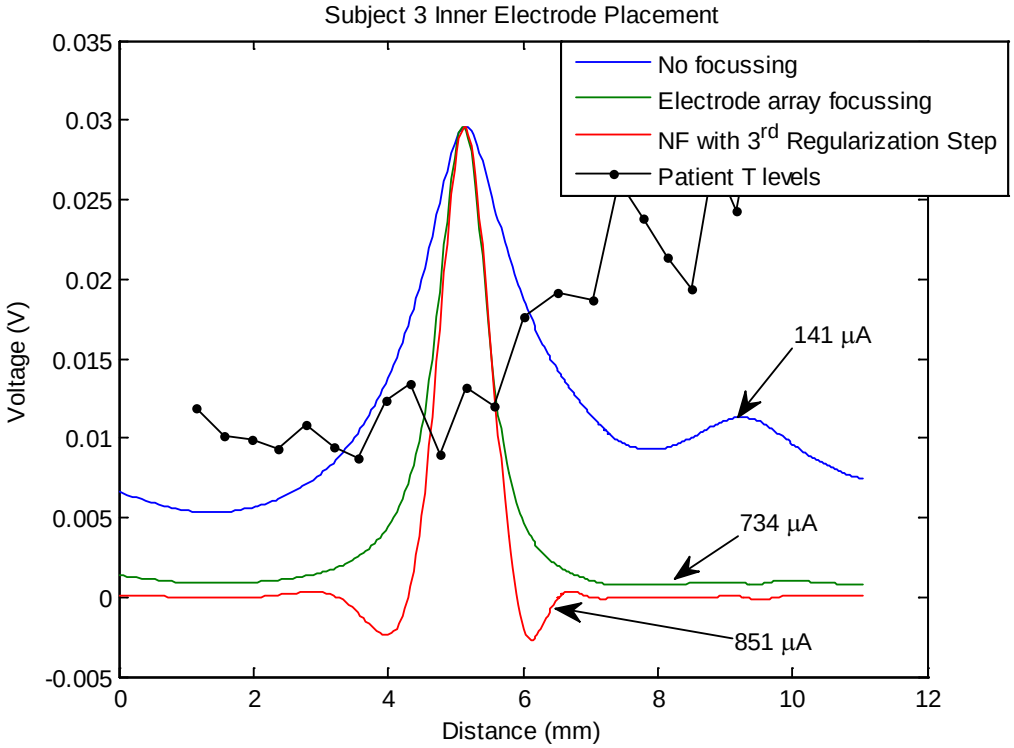

Figure H. 3: Subject 3, Inner electrode placement

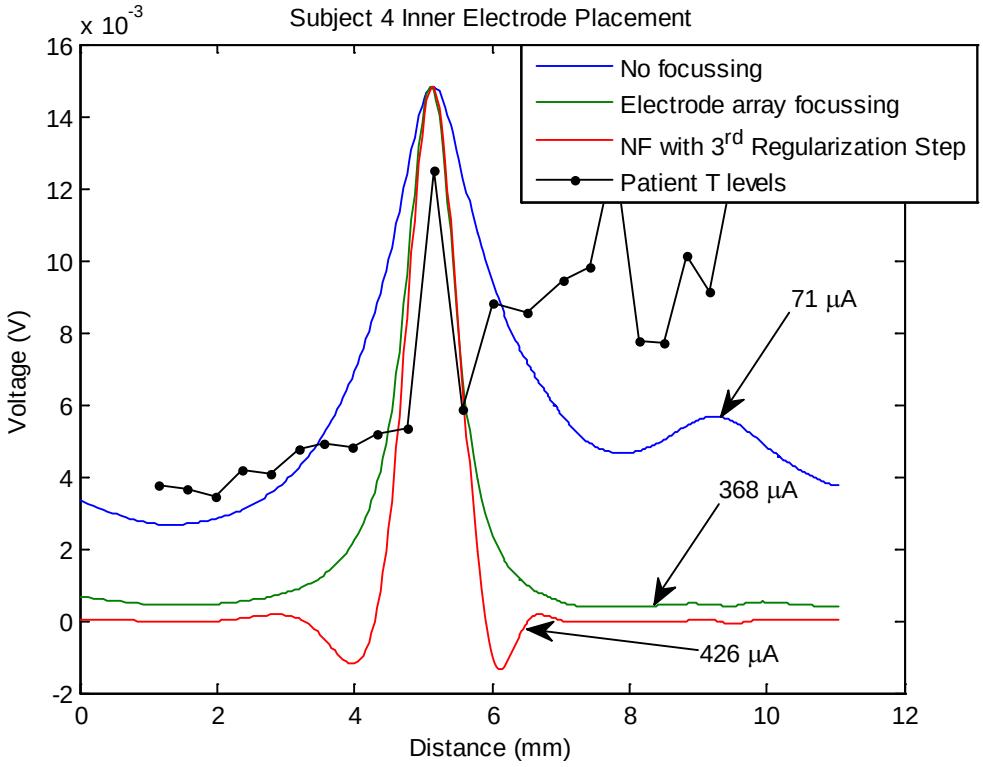

Figure H. 4: Subject 4, Inner electrode placement

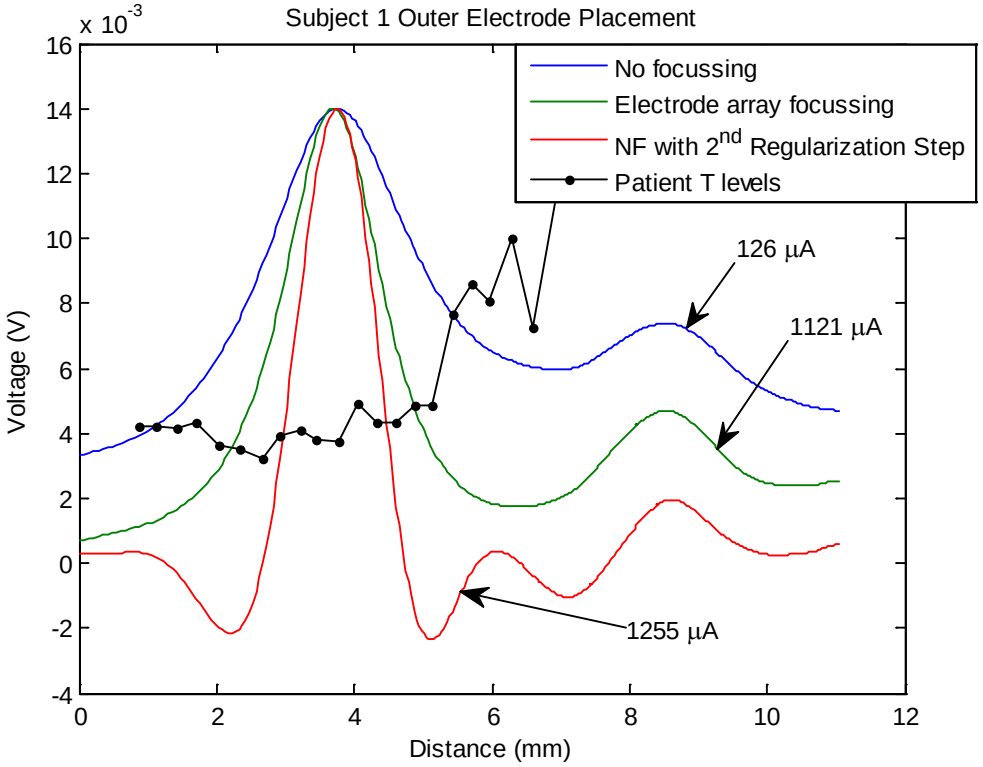

Figure H. 5: Subject 1, Outer electrode placement

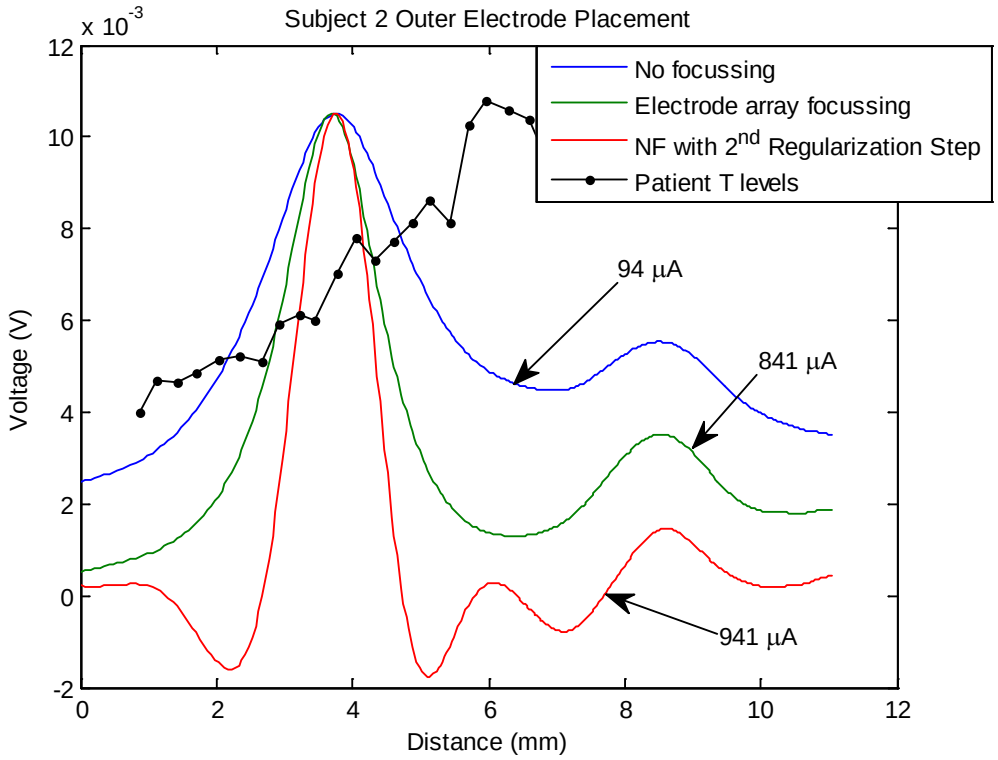

Figure H. 6: Subject 2, Outer electrode placement

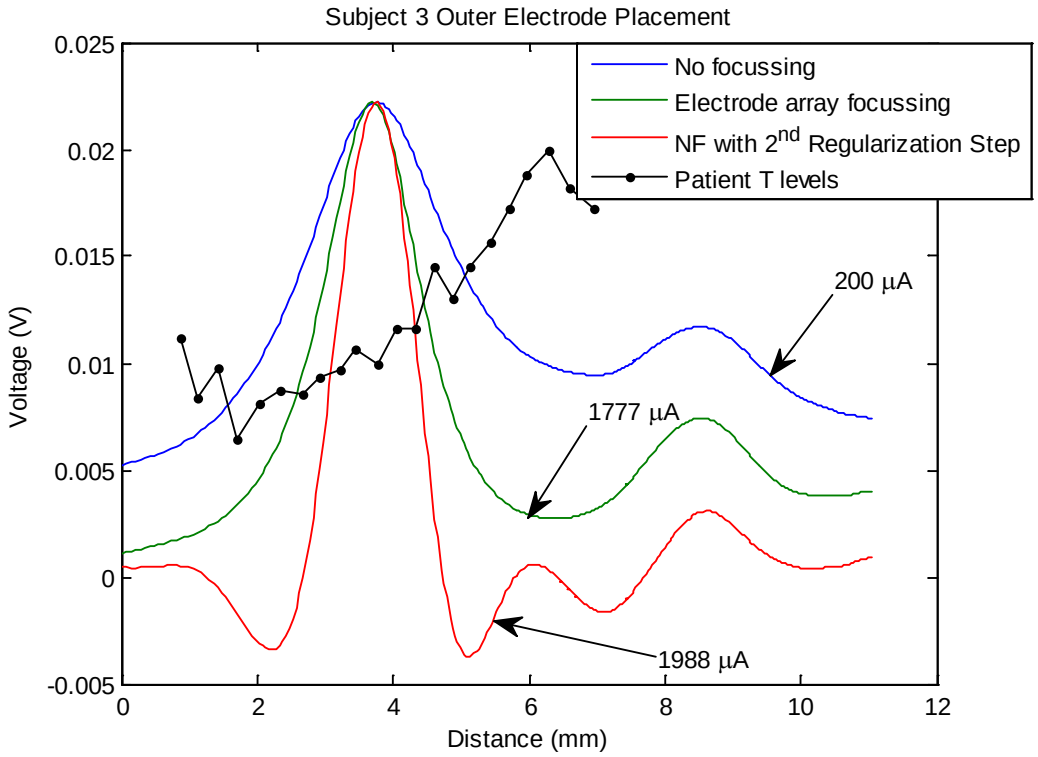

Figure H. 7: Subject 3, Outer electrode placement

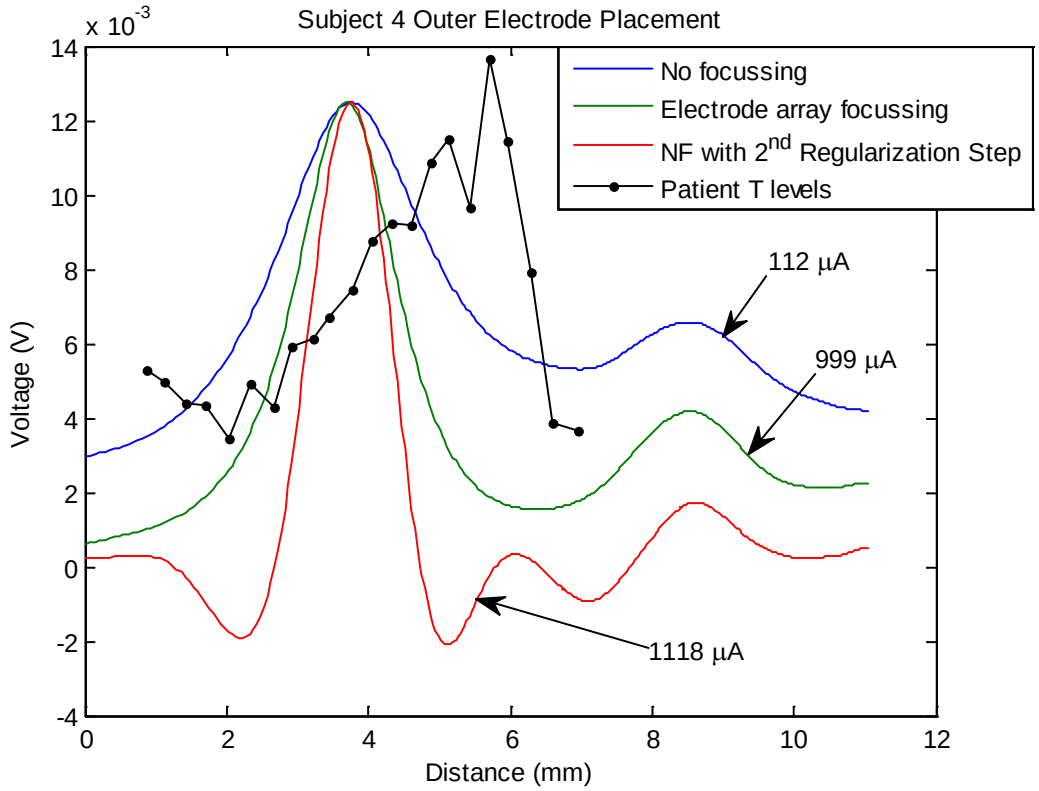

Figure H. 8: Subject 4, Outer electrode placement

When the difference between T and C levels is large, this implies that when stimulating at the C level, the threshold level is significantly lower along the spiral ganglion and so more of the spiral ganglion is excited. This therefore implies that better focussing is required to focus the voltage towards the desired target area on the spiral ganglion. If the difference between T and C levels is smaller, then less of the spiral ganglion is potentially excited and so neural focussing may not necessary.

Appendix I: A review of pulse sequence development

Several authors have investigated different aspects of cochlear implant stimulation. Tognola et al. (2005) investigated the effect of biological tissue load on the stimulation current level. The investigation was carried out by generating a stimulus using a combination of software and hardware, and this stimulus was transported in the form of a radio frequency signal to the receiver/stimulator unit by means of a coil. This in turn is delivered to the electrodes in the array where each of the electrodes is connected to probe which measures the current. The probe also presents a variable load to the electrode being measured which would simulate the varying loading conditions observed in biological tissue. Tognola reports that as you increase the load (resistance) from 1 to 10 kΩ while generating a pulse with a current level of 180 clinical units (c.u.), the corresponding current at the electrode almost remains identical. The current decreased from 434 to 415 μA giving a 4.4% reduction in output current. When this is repeated for an input current level value set to 220 c.u., the current decreased from 966 to 696 corresponding to a 27.9% reduction of the output current. It was also found that the higher the resistive load, the lower the level of saturation where increasing the specified current level no longer has an effect on the measured output current. This is because the system reaches its voltage compliance level, which is the limit of voltage supplied to the cochlea. The effect here is that as either the current or the load is increased, the voltage delivered to the cochlea will increase. If the current level is increased for a specified load, the voltage delivered at the cochlea will reach compliance level and will no longer be able to deliver the required current at the electrode beyond this compliance limit. This implies that increasing the current level for the specified resistance beyond compliance level will have no effect on the actual measured current and that the voltage requirements exceed the voltage supply of the implant is exceeded therefore the implant is said to have gone out of compliance. This therefore also implies that if the specified load is larger initially, the saturation level will be lower. Usually compliance is monitored by clinicians and corrected.

Equally as important, Tognola reports that if the phase width was increased while keeping a fixed current level and resistive load or impedance, the measured output current at the electrode was equal to that set by the operator, confirming the accuracy of the implant in portraying the time information related in the pulse.

It is suggested by van Wieringen et al. (2008) that in a biphasic pulse sequence the two opposite polarity phases can counteract each other in different ways. If the first pulse hyperpolarises the nerve, then for an action potential to occur, the second phase must repolarise the nerve and further depolarise it to reach the excitation threshold which is not possible in this case as the second phase would require a larger amplitude. If, however, the first phase depolarises the nerve fibre, the sodium channels open and the generation of the action potential is started. If the second phase is a hyperpolarising phase, it will cause quick repolarisation of the fibre and thus cancelling out any action potential. It is claimed that this could be eliminated by increasing the phase gap to 100 microseconds.

Van Wieringen also tested the effect of the inter-phase gap on the threshold and comfort level. It was found that increasing the phase gap (even up to several milliseconds) decreased the threshold levels of a biphasic pulse. An increase in the phase gap also means that the threshold of a biphasic pulse approaches that of a monophasic pulse. In a similar vein, Prado-Guitierrez et al. (2006) determined that a lower current was required for a biphasic pulse of phase gap 58 microseconds to evoke the same level of stimulation as a biphasic pulse with an 8 microsecond phase gap. They also found that this effect correlates with nerve survival by measuring these pulses in several different groups of guinea pigs that were deafened for different periods of time. He also notes that this reduction in threshold level is much larger than the difference between biphasic and monophasic thresholds.

Van Wieringen also introduces the idea of two other pulse shapes that are charge balanced. The first is a triphasic pulse that has three phase parts which are asymmetrical with alternating polarity. It was found that triphasic threshold levels were larger than those of a biphasic pulse due to one more phase reversal however this effect could mean a faster repolarisation to the resting potential to avoid simultaneous channel interactions. It was also found that triphasic pulses had significant improvement on speech perception however this strategy utilised higher stimulation rates and so it is unclear whether or not this increase in the reason for improved perception.

Van Wieringen also discusses chopped pulses. These consist of consecutive short monophasic pulses all at the same polarity followed by another series of pulses with an opposite polarity. The advantages of this type of pulse sequence include lower current amplitude requirements as well as providing a way to stimulate two electrodes simultaneously while keeping them interleaved. This has not yet been tested on humans.

Van Wieringen also investigates the sensitivity of nerve stimulation in the cochlea due to anodic stimulation in comparison with cathodic stimulation. He concluded that the anodic phase of stimulation is far more effective than cathodic stimulation in the case of the human auditory nerve. Previous studies by Hartmann et al. (1984), Rattay et al.(1989) and Miller at al. (1998) were performed on animals using monophasic stimulation and they report that nerves in the cochlea can be sensitive to either anodic or cathodic stimulation depending on the species being tested. Wieringen suggests that sensitivity also depends on the geometry and orientation of neurons. McIntyre and Grill (2002) suggest that sensitivity could be specific for different neural bundles.

Reference List

ARAN, J.-M. & ERRE, J.-P. 1977. Long-term recording of cochleo-neural potentials in the guinea pig. *In:* BEAGLEY, H. A. (ed.) *Auditory investigation: the scientific and technological basis.* Clarendon Press. Oxford.

BLACK, R. C., CLARK, G. M., TONG, Y. C. & PATRICK, J. F. 1983. CURRENT DISTRIBUTIONS IN COCHLEAR STIMULATION. *Annals of the New York Academy of Sciences,* 405**,** 137-145.

BLATRIX, S. 1999. *Promenade around the cochlea* [Online]. Available: [Accessed 25 september 2012].

BOEX, C., PELIZZONE, M. & MONTANDON, P. 1996. Speech recognition with a CIS strategy for the Ineraid multichannel cochlear implant. *American Journal of Otology,* 17**,** 61-68.

BRIAIRE, J. J. & FRIJNS, J. H. M. 2000. 3D mesh generation to solve the electrical volume conduction problem in the implanted inner ear. *Simulation Practice and Theory,* 8**,** 57-73.

CLARK, G. M., HALLWORTH, R. J. & ZDANIUS, K. 1975. A cochlear implant electrode. *The Journal of Laryngology and Otology*.

COCHLEAR. 2011. *RE: Personal communication with Paul Carter, Cochlear Corporation.*

DALLOS, P., POPPER, A. N. & FAY, R. R. 1996. *The Cochlea,* New York, Springer.

DESAUVAGE, R. C., DACOSTA, D. L., ERRE, J. P. & ARAN, J. M. 1997. Electrical and physiological changes during short-term and chronic electrical stimulation of the normal cochlea. *Hearing Research,* 110**,** 119-134.

DORMAN, M. F., SMITH, L. M., DANKOWSKI, K., MCCANDLESS, G. & PARKIN, J. L. 1992. LONG-TERM MEASURES OF ELECTRODE IMPEDANCE AND AUDITORY-THRESHOLDS FOR THE INERAID COCHLEAR IMPLANT. *Journal of Speech and Hearing Research,* 35**,** 1126-1130.

DRENNAN, W. R. & PFINGST, B. E. 2005. Current-level discrimination using bipolar and monopolar electrode configurations in cochlear implants. *Hearing Research,* 202**,** 170-179.

ELLIOTT, S. J. 2001. *Signal Processing for Active Control,* London, Academic Press.

ERIXON, E., HOGSTORP, H., WADIN, K. & RASK-ANDERSEN, H. 2009. Variational Anatomy of the Human Cochlea: Implications for Cochlear Implantation. *Otology & Neurotology,* 30**,** 14-22.

EVEREST, F. A. 2000. *Master Handbook of Acoustics,* New York, McGraw-Hill.

FINLEY, C. C., HOLDEN, T. A., HOLDEN, L. K., WHITING, B. R., CHOLE, R. A., NEELY, G. J., HULLAR, T. E. & SKINNER, M. W. 2008. Role of Electrode Placement as a Contributor to Variability in Cochlear Implant Outcomes. *Otology & Neurotology,* 29**,** 920-928.

FINLEY, C. C., WILSON, B. S. & WHITE, M. W. 1990. *MODELS OF NEURAL RESPONSIVENESS TO ELECTRICAL STIMULATION*.

FIRSZT, J. B., KOCH, D. B., DOWNING, M. & LITVAK, L. 2007. Current steering creates additional pitch percepts in adult cochlear implant recipients. *Otology & Neurotology,* 28**,** 629-636.

FRIJNS, J. H. M., KALKMAN, R. K., VANPOUCKE, F. J., BONGERS, J. S. & BRIAIRE, J. J. 2009. Simultaneous and non-simultaneous dual electrode stimulation in cochlear implants: evidence for two neural response modalities. *Acta Oto-Laryngologica,* 129**,** 433-439.

FU, Q. J. 2005. Loudness growth in cochlear implants: effect of stimulation rate and electrode configuration. *Hearing Research,* 202**,** 55-62.

GERMANOVIX, W. & TOUMAZOU, C. 2000. Design of a micropower current-mode log-domain analog cochlear implant. *IEEE Transactions on Circuits and Systems Ii-Analog and Digital Signal Processing,* 47**,** 1023-1046.

GINGGEN, A., TARDY, Y., CRIVELLI, R., BORK, T. & RENAUD, P. 2008. A telemetric pressure sensor system for biomedical applications. *Ieee Transactions on Biomedical Engineering,* 55**,** 1374-1381.

GLYNNE-JONES, P. & WHITE, N. M. 2001. Self-powered systems: A review of energy sources. *Sensor Review,* 21**,** 91-97.

GRAEME, C. 2003. *Cochlear Implants: Fundamentals & Applications,* New York, Springer.

HANEKOM, T. 2001. *Thesis - Cochlea modelling.* Thesis, University of Pretoria.

HANEKOM, T. 2005. Modelling encapsulation tissue around cochlear implant electrodes. *Medical & Biological Engineering & Computing,* 43**,** 47-55.

HARTMANN, R., TOPP, G. & KLINKE, R. 1984. DISCHARGE PATTERNS OF CAT PRIMARY AUDITORY FIBERS WITH ELECTRICAL-STIMULATION OF THE COCHLEA. *Hearing Research,* 13**,** 47-62.

HO, S. Y., WIET, R. J. & RICHTER, T. P. 2004. Modifying cochlear implant design: Advantages of placing a return electrode in the modiolus. *Otology & Neurotology,* 25**,** 497-503.

HOLDEN, L. K., SKINNER, M. W., HOLDEN, T. A. & DEMOREST, M. E. 2002. Effects of stimulation rate with the nucleus 24 ACE speech coding strategy. *Ear and Hearing,* 23**,** 463-476.

HSIAO-MAN, H. S. U., TIEN-CHEN, L. I. U. & HUNG-CHING, L. I. N. Year. The effects of varying stimulation rate on behavioural T/C-level measurements in young Nucleus 24 recipients. *In:* 4th Congress of Asia Pacific Symposium on Cochlear Implant, 2004 2004.

HUGHES, M. L. & GOULSON, A. M. 2011. Electrically Evoked Compound Action Potential Measures for Virtual Channels Versus Physical Electrodes. *Ear and Hearing,* 32**,** 323-330.

HUNT, F. V. 1954. *Electroacoustics,* New York, Wiley.

IBRAHIM, R. A. 2008. Recent advances in nonlinear passive vibration isolators. *Journal of Sound and Vibration,* 314**,** 371-452.

J.PIERS. 2001. *Design of micromechanical systems: scale laws, technologies and medical applications.* Katholieke Universiteit Leuven.

JI-JON, S. & SARPESHKAR, R. 2008. A cochlear-implant processor for encoding music and lowering stimulation power. *IEEE Pervasive Computing,* 7**,** 40-48.

KOOMEY, J. G., BERARD, S., SANCHEZ, M. & WONG, H. 2011. Implications of Historical Trends in the Electrical Efficiency of Computing. *Annals of the History of Computing, IEEE,* 33**,** 46-54.

KOSTERICH, J. D., FOSTER, K. R. & POLLACK, S. R. 1983. DIELECTRIC PERMITTIVITY AND ELECTRICAL-CONDUCTIVITY OF FLUID SATURATED BONE. *Ieee Transactions on Biomedical Engineering,* 30**,** 81-86.

LAI, W. D. & CHOI, C. T. M. 2007. Incorporating the electrode-tissue interface to cochlear implant models. *Ieee Transactions on Magnetics,* 43**,** 1721-1724.

LEE, D. S., LEE, J. S., OH, S. H., KIM, S. K., KIM, J. W., CHUNG, J. K., LEE, M. C. & KIM, C. S. 2001. Deafness - Cross-modal plasticity and cochlear implants. *Nature,* 409**,** 149-150.

LOIZOU, P. C. 1998. Mimicking the human ear. *Ieee Signal Processing Magazine,* 15**,** 101-130.

LOIZOU, P. C., POROY, O. & DORMAN, M. 2000. The effect of parametric variations of cochlear implant processors on speech understanding. *Journal of the Acoustical Society of America,* 108**,** 790-802.

MAKARY, C., SHIN, J., CARUSO, P., CURTIN, H. & MERCHANT, S. 2010. A Histological Study of Scala Communis with Radiological Implications. *Audiology and Neuro-Otology,* 15**,** 383-393.

MANLEY, G. A. & FAY, R. R. 2008. *Active Processes and Otoacoustic Emissions in Hearing,* New York, Springer.

MARIEB, E. N. 2008. *Essentials of Human Anatomy and Physiology Laboratory Manual*, Benjamin-Cummings Publishing Company.

MCINTYRE, C. C. & GRILL, W. M. 2002. Extracellular stimulation of central neurons: Influence of stimulus waveform and frequency on neuronal output. *Journal of Neurophysiology,* 88**,** 1592-1604.

MCKAY, C., FEWSTER, L. & DAWSON, P. 2004. The relationship between Neural Response Telemetry thresholds and psychophysical high-rate thresholds in cochlear implantees: a different approach. *In:* MIYAMOTO, R. T. (ed.) *Cochlear Implants.* Amsterdam: Elsevier Science Bv.

MIDDLEBROOKS, J. C. & SNYDER, R. L. 2007. Auditory prosthesis with a penetrating nerve array. *Jaro-Journal of the Association for Research in Otolaryngology,* 8**,** 258-279.

MILLER, C. A., ABBAS, P. J., HAY-MCCUTCHEON, M. J., ROBINSON, B. K., NOURSKI, K. V. & JENG, F. C. 2004. Intracochlear and extracochlear ECAPs suggest antidromic action potentials. *Hearing Research,* 198**,** 75-86.

MILLER, C. A., ABBAS, P. J., RUBINSTEIN, J. T., ROBINSON, B. K., MATSUOKA, A. J. & WOODWORTH, G. 1998. Electrically evoked compound action potentials of guinea pig and cat: responses to monopolar, monophasic stimulation. *Hearing Research,* 119**,** 142-154.

MOGILNER, A. Y., BENABID, A.-L. & REZAI, A. R. 2001. Brain stimulation: current applications and future prospects. *Thalamus & Related Systems,* 1**,** 255-267.

MONDINI, C. 1791. Anatomica hati sectio. *BONIESI,* 7**,** 28.

NAKANO, K., ELLIOTT, S. J. & RUSTIGHI, E. 2007. A unified approach to optimal conditions of power harvesting using electromagnetic and piezoelectric transducers. *Smart Materials & Structures,* 16**,** 948-958.

NMT 2008. Nucleus Matlab Toolbox

ONLINE, S. 2004. Data logger manufacturer's website.

PAPARELLA, M. M. 1980. MONDINIS DEAFNESS - A REVIEW OF HISTOPATHOLOGY. *Annals of Otology Rhinology and Laryngology,* 89**,** 1-10.

PFINGST, B. E. & XU, L. 2004. Across-site variation in detection thresholds and maximum comfortable loudness levels for cochlear implants. *Jaro-Journal of the Association for Research in Otolaryngology,* 5**,** 11-24.

POZNYAKOVSKIY, A. A., ZAHNERT, T., KALAIDZIDIS, Y., SCHMIDT, R., FISCHER, B., BAUMGART, J. & YARIN, Y. M. 2008. The creation of geometric three-dimensional models of the inner ear based on micro computer tomography data. *Hearing Research,* 243**,** 95-104.

PRADO-GUITIERREZ, P., FEWSTER, L. M., HEASMAN, J. M., MCKAY, C. M. & SHEPHERD, R. K. 2006. Effect of interphase gap and pulse duration on electrically evoked potentials is correlated with auditory nerve survival. *Hearing Research,* 215**,** 47-55.

RATTAY, F. 1989. ANALYSIS OF MODELS FOR EXTRACELLULAR FIBER STIMULATION. *IEEE Transactions on Biomedical Engineering,* 36**,** 676-682.

RATTAY, F., LEAO, R. N. & FELIX, H. 2001. A model of the electrically excited human cochlear neuron. II. Influence of the three-dimensional cochlear structure on neural excitability. *Hearing Research,* 153**,** 64-79.

RAUSCHECKER, J. P. & SHANNON, R. V. 2002. Sending Sound to the Brain. *Science,* 295**,** 1025-1029.

RISS, D., ARNOLDNER, C., BAUMGARTNER, W. D., KAIDER, A. & HAMZAVI, J. S. 2008. A new fine structure speech coding strategy: Speech perception at a reduced number of channels. *Otology & Neurotology,* 29**,** 784-788.

ROHR, R. V. 2011. *Cochlear Implant Imedance Telemetry Measurements and Model Calculations to Estimate Modiolar Currents.* MSc, Swiss Federal Institute of Technology Zurich.

SABA, R., ELLIOTT, S. J. & BAUMANN, O. N. 2008. Vibration power harvesting from head motion. *Proceedings of EURODYN 2008, 7th European Conference on Structural Dynamics***,** 12pp.

SARPESHKAR, R., SALTHOUSE, C., SIT, J. J., BAKER, M. W., ZHAK, S. M., LU, T. K. T., TURICCHIA, L. & BALSTER, S. 2005. An ultra-low-power programmable analog bionic ear processor. *Ieee Transactions on Biomedical Engineering,* 52**,** 711-727.

SAUNDERS, E., COHEN, L., ASCHENDORFF, A., SHAPIRO, W., KNIGHT, M., STECKER, M., RICHTER, B., WALTZMAN, S., TYKOCINSKI, M., ROLAND, T., LASZIG, R. & COWAN, R. 2002. Threshold, comfortable level and impedance changes as a function of electrode-modiolar distance. *Ear and Hearing,* 23**,** 28S-40S.

SHARMA, A., DORMAN, M. F. & SPAHR, A. J. 2002. Rapid development of cortical auditory evoked potentials after early cochlear implantation. *Neuroreport,* 13**,** 1365-1368.

SKRODZKA, E. B. 2005a. Mechanical passive and active models of the human basilar membrane. *Applied Acoustics,* 66**,** 1321-1338.

SKRODZKA, E. B. 2005b. Modelling of some mechanical malfunctions of the human basilar membrane. *Applied Acoustics,* 66**,** 1007-1017.

SOECIC 2011. Discussions eith the South of England Cochlear Implant Centre.

SOMEK, B., FAJT, S., DEMBITZ, A., IVKOVIC, M. & OSTOJIC, J. 2006. Coding strategies for cochlear implants. *Automatika,* 47**,** 69-7474.

SPELMAN, F. A. Year. Measurements of the resistivity of bony tissues of the cochlea. *In:* Proceedings of the Ninth Annual Conference of the IEEE Engineering in Medicine and Biology Society (Cat. No.87CH2513-0), 1987

13-16 November 1987 Boston, MA,. Ieee, 1911-12 vol.4.

STALLER, S., MENAPACE, C., DOMICO, E., MILLS, D., DOWELL, R. C., GEERS, A., PIJL, S., HASENSTAB, S., JUSTUS, M., BRUNELLI, T., ADAM, A., BORTON, T. & LEMAY, M. Year. Speech perception abilities of adult and pediatric Nucleus implant recipients using the Spectral Peak (SPEAK) coding strategy. *In:* 6th Symposium on Cochlear Implants in Children, Feb 02-03 1996 Miami Beach, Fl. Mosby-Year Book Inc, 236-242.

STEPHEN, N. G. 2006. On energy harvesting from ambient vibration. *Journal of Sound and Vibration,* 293**,** 409-425.

STRELIOFF, D. 1973. A computer simulation of the generation and distribution of cochlear potentials. *The Journal of the Acoustical Society of America,* 54**,** 620-629.

THAD, S., JOSEPH, A. P. & CHRISTIAN, P. 2004. *Human Generated Power for Mobile Electronics*, CRC Press.

THORNE, M., SALT, A. N., DEMOTT, J. E., HENSON, M. M., HENSON, O. W. & GEWALT, S. L. 1999. Cochlear fluid space dimensions for six species derived from reconstructions of three-dimensional magnetic resonance images. *Laryngoscope,* 109**,** 1661-1668.

TOGNOLA, G., BURDO, S., CAPONIO, M., NORGIA, M., PARAZZINI, M., RAVAZZANI, P., GRANDORI, F. & SVELTO, C. 2005. Measurement of electrode current pulses

from cochlear implants. *Ieee Transactions on Instrumentation and Measurement,* 54**,** 2105-2112.

TOGNOLA, G., PESATORI, A., NORGIA, M., PARAZZINI, M., DI RIENZO, L., RAVAZZANI, P., BURDO, S., GRANDORI, F. & SVELTO, C. 2007. Numerical modeling and experimental measurements of the electric potential generated by cochlear implants in physiological tissues. *Ieee Transactions on Instrumentation and Measurement,* 56**,** 187-193.

VAN DEN HONERT, C. & KELSALL, D. C. 2007. Focused intracochlear electric stimulation with phased array channels. *Journal of the Acoustical Society of America,* 121**,** 3703-3716.

VAN WIERINGEN, A., MACHEREY, O., CARLYON, R. P., DEEKS, J. M. & WOUTERS, J. 2008. Alternative pulse shapes in electrical hearing. *Hearing Research,* 242**,** 154-163.

VANDALI, A. E., WHITFORD, L. A., PLANT, K. L. & CLARKE, G. M. 2000. Speech perception as a function of electrical stimulation rate: Using the nucleus 24 cochlear implant system. *Ear and Hearing,* 21**,** 608-624.

VONDRASEK, M., SOVKA, P. & TICHY, T. 2008. ACE Strategy with Virtual Channels. *Radioengineering,* 17**,** 7.

WANG, Z. H., MAI, S. P. & ZHANG, C. Year. Power issues on circuit design for cochlear implants. *In:* OSSEIRAN, A., RENOVELL, M., AMIRA, A., PUN, K. P. & LEUNG, L. L. K., eds. 4th IEEE International Symposium on Electronic Design, Test and Applications, Jan 23-25 2008 Hong Kong, PEOPLES R CHINA. Ieee Computer Soc, 163-166.

WILLIAMS, C. B. & YATES, R. B. Year. Analysis of a micro-electric generator for microsystems. *In:* 8th International Conference on Solid-State Sensors and Actuators (Eurosensors IX), Jun 25-29 1996 Stockholm, Sweden. Elsevier Science Sa Lausanne, 8-11.

WILSON, B. S. & DORMAN, M. F. Year. Cochlear implants: A remarkable past and a brilliant future. *In:* 9th International Conference on Cochlear Implants and Related Sciences, Jun 14-17 2006 Vienna, AUSTRIA. Elsevier Science Bv, 3-21.

WILSON, B. S. & DORMAN, M. F. 2008. Cochlear implants: Current designs and future possibilities. *Journal of Rehabilitation Research and Development,* 45**,** 695-730.

WISE, K. D., NAJAFI, K. & ELECTRONIC DEVICES SOCIETY OF IEEE, E. D. S. O. I. Year. Fully-implatable auditory prostheses: Restoring hearing to the profoundly deaf. *In:* IEEE International Electron Devices Meeting, Dec 08-11 2002 San Francisco, Ca. Ieee, 499-502.

WOODMAN, P. D. & GRIFFIN, M. J. Year. Six axes of head acceleration during ambulation. *In:* HILL, F. A. & LAWRENCE, R., eds. 25th International Congress on Noise Control Engineering (Inter-Noise 96) - Noise control: The Next 25 Years, Jul 30-Aug 02 1996 Liverpool, England. Inst Acoustics, 1719-1724.

YEATMAN, E. M. 2008. Energy harvesting from motion using rotating and gyroscopic proof masses. *Proceedings of the Institution of Mechanical Engineers Part C-Journal of Mechanical Engineering Science,* 222**,** 27-36.

ZAKIS, J. & WITTE, M. 2001. Modelling of the Cochlea using Java 3D. *IEEE Engineering in Medicine and Biology Society*.

ZENG, F. G., POPPER, A. N. & FAY, R. R. 2004. *Cochlear Implants: Auditory Prostheses and Electric Hearing,* New York, Springer.